Oncolytic measles virus and mesenchymal stromal cells:

A therapeutic model and a dissection of mechanisms of action

Anna Zaiga Castleton

Thesis submitted for the degree of Doctor of Philosophy

University College London

2014

Declaration

I, Anna Zaiga Castleton, confirm that the work presented in this thesis is my own. Where information has been derived from other sources, I confirm that this has been indicated in the thesis.

Signed:

Date:

Acknowledgements

I would like to thank Dr Adele Fielding for her time, help and support with the work that has gone into this thesis. Furthermore, the mentorship and guidance that Dr Fielding has provided to me over the years has been invaluable, and has helped me progress my career as a clinical haematologist. I would like to thank my other colleagues within the Fielding laboratory, who have given me assistance, friendship, encouragement and constant support. To my parents and my sister, who have always told me that I can achieve anything that I set out to achieve - their unwavering confidence in my ability has helped me get through challenging times. To my partner Scott, who has been constantly supportive of my career choices and has never doubted me, and to our lovely boy Joseph - the best result to make it out of my PhD.

Abstract

Live, attenuated measles virus (MV) has demonstrated tumour-specific replication and anti-tumour activity in murine models of hematological and non-hematological malignancy, leading to a number of published or on-going clinical trials. However, the potentially overriding issue of how to achieve successful administration of oncolytic measles virotherapy in patients with intact humoral immunity remains.

I have examined mechanisms for optimizing delivery of oncolytic MV to acute lymphoblastic leukaemia (ALL) – a disseminated haematological malignancy. Anti MV antibody titres in adult patients with ALL were evaluated before and after leukaemia treatment regimens including high dose corticosteroids, cyclophosphamide and anti-B cell monoclonal antibodies. Antibody titres were unaffected by induction and intensification treatment protocols, suggesting the need for consideration of optimal virotherapy delivery strategies to achieve therapeutic success. Here, I demonstrate that human bone marrow-derived mesenchymal stromal cells (BM-MSCs) can be used effectively as virus delivery vehicles, permitting ex-vivo cellular virus loading and intracellular virus amplification, delivery of virus to distant sites of disease following systemic infusion, and virus hand-off to precursor B lineage ALL cell targets in the presence of pre-existing anti-MV antibodies. In vivo modelling using SCID mice bearing disseminated pre-B ALL xenografts demonstrated enhanced survival of passively immunized animals following IV treatment with BM-MSC-delivered MV versus naked MV or BM-MSCs alone.

In order for vaccine MV to be safely and rationally utilized as a novel therapeutic for ALL, a detailed mechanistic understanding of how the virus exerts its oncolytic effect is paramount. In this thesis, I have utilized a previously characterized model of cellular transformation generated using human BM-MSCs to characterize the phenomenon of relative tumour cell specificity by oncolytic MV, in terms of infectivity, productivity and cell killing. Furthermore, this thesis begins to explore some of the potential mechanisms that confer vaccine MV its tumour-tropic and anti-cancer properties.

Publications and abstracts

Publications and abstracts arising from the work described in this thesis at the time of submission:

1. Castleton A, Dey A, Beaton B, Patel B, Aucher A, Davis DM, Fielding AK. **Human mesenchymal stromal cells efficiently deliver systemic oncolytic MV to treat acute lymphoblastic leukemia in the presence of humoral immunity.** Blood. 2014 Feb 27;123(9):1327-35. doi: 10.1182/blood-2013-09-528851. Epub 2013 Dec 17.

2. Horwitz EM. **Oncolytic virotherapy for ALL: MSCs to the rescue.** Blood. 2014 Feb 27;123(9):1286-7. doi: 10.1182/blood-2014-01-546747.

3. Anna Z. Castleton and Adele K. Fielding. **Emerging Cancer Therapeutics *V2 I2*: Leukemia. Adult Acute Lymphoblastic Leukemia.** Published 08/2011. ISBN13 9781933864686

4. *American Society of Gene and Cell Therapy 17th Annual Meeting, May 21-24, 2014, Washington DC, USA.* Castleton, A; Dey, A; Patel, B; Funes, J; Boshoff, C; Capasso, M; Fielding, A. **How Does MV Kill Cancer Cells? Characterizing Oncolytic MV (OMV) Kinetics in a Mesenchymal Stromal Cell (MSC) Model of Cellular Transformation.** In: Molecular Therapy. Vol. 22(pp. S249 - S249): POSTER PRESENTATION

5. *3rd MV Minisymposium, September 9-10, 2013, Veyrier Du Lac, Haute Savoie, France.* Castleton, A; Beaton, B; Patel, B; Aucher, A; Davis, D; Fielding, A. **Human mesenchymal stromal cells deliver systemic oncolytic MV to treat acute lymphoblastic leukaemia in the presence of humoral immunity.** ORAL PRESENTATION.

6. *American Society of Gene and Cell Therapy 16th Annual Meeting, May 15-19, 2013, Salt Lake City, Utah, USA.* Castleton, A; Dey, A; Patel, B; Beaton, B;

Aucher, A; Davis, D; Fielding, A. **Human Bone Marrow-Derived Mesenchymal Stromal Cells Permit Delivery, and Enhance Efficacy of Systemically Administered Oncolytic Measles Virotherapy to Disseminated Human Pre-B ALL Murine Xenograft Models in the Presence of Humoral Immunity**. In: Molecular Therapy. Vol. 21(pp. S9 - S9). ORAL PRESENTATION. TRAVEL GRANT AWARDED.

7. *American Society of Gene and Cell Therapy 15th Annual Meeting, May 16-19, 2012, Philadelphia, Pennsylvania, USA.* Castleton, A; Ghorani, E; Zhang, C; Dey, A; Patel, B; Rai, L; ... Fielding, A. **Mesenchymal Stromal Cells Are Promising Candidates as Delivery Vehicles for Systemic Oncolytic Measles Virotherapy in Models of Acute Lymphoblastic Leukaemia.** In: Molecular Therapy. Vol. 22(pp. S211 - S211). ORAL PRESENTATION.

Statement of work undertaken

Cloning of the human *CXCR4* gene into the MV genome was performed by MSc student, Dr Ehsan Ghorani. Enzyme-linked immunosorbent assay (ELISA) of MV IgG in patient serum samples was performed by Dr Brendan Beaton. All other work was carried out by the author.

Table of contents

List of figures

List of tables

List of abbreviations

ADAR-I	Double stranded RNA-specific adenosine deaminase
ADEM	Acute demyelinating encephalomyelitis
ALL	Acute lymphoblastic leukaemia
ATM	Ataxia telangiectasia mutated
ATP	Adenosine triphosphate
BBB	Blood brain barrier
BCA	Bicinchoninic acid
BFP	Blue fluorescent protein
bhCG	human chorionic gonadotropin
BM	Bone marrow
BM-MSC	Bone marrow-derived mesenchymal stromal cells
BSA	Bovine serum albumin
CARD	Caspase activation and recruitment domain
CDV	Canine distemper virus
CEA	Carcino embryonic antigen
CML	Chronic myloid leukaemia
CNS	Central nervous system
CPA	Cyclophosphamide
CXCR4	C-X-C motif receptor 4
DC	Dendritic cell
DIRNA	Defective interfering RNA
DMEM	Dulbecco's modified eagle medium
DMSO	Dimethyl sulfoxide
DNA	Deoxyribonucleac acid
dsRNA	Double stranded RNA
ECAR	Extracellular acidification rate
EGF	Epidermal-derived growth factor
ELISA	Enzyme-linked immunosorbent assay
EPR	Enhanced permeability and retention
FBS	Foetal bovine serum
FDA	Food & Drug Administration

FGF	Fibroblast growth factor
FGF2	Fibroblast growth factor
FIP	Fusion inhibitory peptide
GAPDH	Glyceraldehyde 3-phosphate dehydrogenase
GBM	Glioblastoma multiforme
GCSF	Granulocyte colony stimulating factor
GFP	Green fluorescent protein
GM-CSF	Granulocyte-monocyte colony stimulating factor
GMP	Good manufacturing practice
HBSS	Hanks balanced salt solution
HCC	Hepatocellular carcinoma
HGF	Hepatocyte growth factor
HIV	Human immunodeficiency virus
Hpi	Hours post infection
HRP	Horseradish peroxidase
HSP	Heat shock protein
HSV-1	Herpes simplex virus
IBM	Intra bone marrow
IFN	Interferon
Ig	Immunoglobulin
IGF-1	Insulin-like growth factor
IL	Interleukin
IP	Intraperitoneal
IPS-1	(VISA – virus-induced signalling adapter)
IRF	IFN response factor
ISCT	International society for cellular therapy
ISFG3	IFN-stimulated gene factor 3
ISGs	IFN-stimulated genes
ISRE	IFN-stimulated response element
IV	Intravenous
JAK	Janus kinase
Le	Leader
LGP-2	Laboratory of genetics and physiology 2
MAVS	Mitochondrial antiviral signalling protein

MCP1	Monocyte chemotactic protein 1
MDA-5	Melanoma differentiation-associated protein 5
MFI	Mean fluorescent intensity
MHC	Major histo-compatibility
MIBE	Measles inclusion body encephalitis
MMP	Matrix metalloproteinase
MOI	Multiplicity of infection
MPS	Mononuclear phagocytic system
MRD	Minimal residual disease
MSC	Mesenchymal stromal cells
MV	MV
NDV	Newcastle disease virus
NF-kB	Nuclear factor kappa beta
NIS	Sodium iodide symporter
NK	Natural killer cell
NLS	Nuclear localisation signal
NOD/SCID	Non obese diabetic/severe combined immunodeficiency
OCR	Oxygen consumption rate
OD	Optical density
PAMP	Pathogen associated molecular patterns
PBS	Phosphate buffered saline
PCR	Polymerase chain reaction
PEG	Polyethylene glycol
PFU	Plaque forming unit
PI	Propidium iodide
Prdx	Peroxyredoxin
PRR	Pattern recognition receptors
PVRL4	Poliovirus receptor-related 4
RdRp	RNA-dependent RNA polymerase
RIG-I	Retinoic acid-inducible gene 1
RLRs	RIG-I-like receptors
RNA	Ribonucleic acid
RNP	Ribonucleoprotein complex
ROS	Reactive oxygen species

RT	Room temperature
SCCHN	Squamous cell carcinoma of the head and neck
ScFV	Short chain fragment variable
SCID	Severe combined immunodeficiency
SCR	Short consensus repeat
ScTCR	Single chain T cell receptor
SDF1a	Stromal derived growth factor 1a
SEM	Standard error of the mean
SLAM	Signalling lymphocyte activation molecule
SSPE	Subacute sclerosing pan-encephalitis
ssRNA	Single stranded RNA
STAT	Signal transduction & activator of transcription
STING	Stimulator of IFN genes
STP	Serine-threonine-proline-rich domain
T-VEC	Talimogene Laherparepvec
$TCID_{50}$	50% Tissue culture infectious dose
TKI	Tyrosine kinase inhibitor
TLRs	Toll-like receptors
Tr	Trailer
TyK	Tyrosine kinase
VEGF	Vascular endothelial growth factor
VSV	Vesicular stomatitis virus

Chapter 1: Introduction

1.1 Cancer therapy landscape

1.1.1 Conventional therapies

Since early attempts at chemotherapy over half a century ago, the progress that has been made in the development of chemotherapy drugs and cancer treatment protocols cannot be denied. Whilst this fact remains, chemotherapy regimens are frequently accompanied by unavoidable toxicities, and initial successes can be hampered by the development of potential chemoresistance and subsequent disease relapse. In the last 2 decades, heralded by the successes of the tyrosine kinase inhibitor (TKI) imatinib as an effective targeted treatment for chronic myeloid leukaemia (CML), the advances in our understanding of the molecular basis of cancer biology has paved the way for the development of other rationally designed targeted cancer therapies. However, the revolutionary successes of imatinib and CML treatment have not been replicated in other diseases. Although targeted therapies have shown modest responses in certain diseases, efficacy is often hampered by the complexity of molecular cancer biology pathways in the majority of both haematological and non-haematological malignancies, and the ability of tumours to evolve and develop resistance to highly specific anti-cancer mechanisms. The developments of monoclonal antibodies - such as the anti-CD20 targeted compound Rituximab – has led to improvements in cancer outcomes for a number of haematological diseases when used in combination with existing chemotherapies, but despite such successes, there undoubtedly remains a need to develop novel non-cross reactive cytotoxic treatments showing multi-pronged mechanisms of action, efficacy in a number of different cancer types, amenability to administration by desired routes, and favourable side effect profiles when used either alone or in combination with existing treatments.

1.1.2 Oncolytic virotherapies

Using viruses to treat cancer is not a novel concept. Viruses have attracted interest as anti-cancer therapeutics since the beginning of the 20th century, when cases of viruses causing spontaneous tumour regressions were first reported[1,2]. Remissions were most often seen in the context of haematological malignancies, but were usually short-

lived. Interest in using different live viruses to treat cancer patients waned in the 1970-80's following safety concerns regarding the use of wild-type viruses in the clinical setting[3], the anticipation of potential technical limitations to virus manufacture, and the prioritization of the development of other treatment strategies such as monoclonal antibodies or molecularly targeted treatments[4]. However, the last 30 years has seen a resurgence of interest in cancer virotherapy paralleling our increased understanding of the nature of viruses, their mechanisms of oncolytic activity, and their potential for genetic manipulation and exploitation in order to achieve desired aims.

Oncolytic viruses are characterized by their ability to preferentially infect and lyse transformed cells whilst leaving normal cells relatively unharmed. Their attraction as novel therapeutics is several-fold and includes their lack of cross resistance with existing therapies, their likely multi-pronged mechanisms of action, and their relative specificity for target cells, lending them favourable side effect profiles. Whilst considerable academic progress has been made in the field of cancer virotherapy, the pace of clinical progress has been dictated by an initial paucity of activity in early phase clinical trials. The complex biological interactions between viruses and humans, and difficulties in modeling such interactions in pre-clinical studies, have provided challenges to the rapid development of virotherapy agents. Despite these challenges, the recent years have seen a concerted effort by the oncolytic virotherapy community to push promising pre-clinical products through phase I and early phase II clinical trials, with a shortlist of candidates - having demonstrated safety and efficacy - being taken forward by biotherapeutic companies into pivotal phase III trials.

Table 1-1: Overview of oncolytic virotherapy clinical trial activity.

Virus	Trial phase	Tumour type
Adenovirus	1-3	Squamous cell carcinoma of head and neck (SCCHN); Lung metastases; glioma; sarcoma; ovarian/pancreatic/colorectal/hepatobiliary cancers
Coxsackie	1-2	Melanoma; SCCHN; solid tumours
Herpes simplex virus	1-3	Solid tumours; melanoma; SCCHN; glioma; melanoma; mesothelioma; breast cancer; colorectal cancer + liver metastases
Measles virus (Edmonston strain)	1	Cutaneous T-cell lymphoma; ovarian cancer; glioma; myeloma; mesothelioma; SCCHN
Newcastle disease virus	1-2	Glioma; solid tumours
Parvovirus	1-2	Glioma
Poliovirus	1	Glioma
Reovirus	1-3	Glioma; peritoneal cancer; solid tumours; colorectal cancer; sarcoma; melanoma; SCCHN; pancreatic cancer; lung cancer
Seneca valley virus	2	Small cell lung cancer
Retrovirus	1-2	Glioma
Vaccinia virus	1-3	Colorectal cancer; hepatocellular carcinoma; melanoma
Vesicular stomatitis virus	1-2	Solid tumours; SCCHN; hepatocellular carcinoma

1.1.2.1 Advanced phase clinical trial activity

A handful of promising oncolytic virotherapy candidates have now reached advanced phase clinical trial status. Talimogene laherparepvec (T-VEC) was the first oncolytic virus to demonstrate proven efficacy in a phase III clinical trial. Based on a strain of herpes simplex virus 1 (HSV-1), T-VEC has been modified to enhance tumour specificity, and promote anti-tumour immune responses (by insertion of the human granulocyte/monocyte – colony stimulating factor (GM-CSF) gene). In a phase II trial, using intralesional T-VEC in a cohort of heavily pre-treated patients with advanced malignant melanoma, overall response rates of 26% (with 16% complete responses) were seen, with survival rates of 52% at 2 years (medial overall survival 16 months)[5]. Following on from this success, the US Food and Drug Administration (FDA) approved a special protocol assessment using this drug for patients with stage III and IV malignant melanoma. Interim phase III trial data in over 400 patients has showed a significant improvement in objective response and durable response rates over the control arm (GM-CSF alone), with a trend toward improved overall survival[6]. Reolysin – an oncolytic agent based on wild-type Reovirus (serotype 3 Dearing strain) is being developed as a novel treatment for a number of different cancers. Published phase II data using intravenously administered Reolysin in patients with metastatic melanoma showed good tolerability. Whilst no objective responses were seen, 75-90% tumour necrosis – consistent with clinical effect – was seen in one patient with lesions surgically removed, and future phase II trials in this disease are targeted towards combination therapy with virus and standard cytotoxic compounds[7]. Phase II trials have also shown efficacy in head and neck cancers, and as with T-VEC, Reolysin has a US FDA special protocol assessment for an ongoing phase III clinical trial of intravenously delivered Reolysin in combination with paclitaxel and carboplatin for head and neck cancer. JX-594 (Pexa-Vec) is another promising oncolytic agent based on a Vaccinia poxvirus with a deleted thymidine kinase gene (improving tumour cell targeting), and modulated to express the human GM-CSF gene (improving anti-tumour immune responses). Published phase I data in primary hepatocellular carcinoma (HCC) demonstrated safety and tolerability. Early phase II trial results showing enhanced survival benefit for patients with heavily pre-treated, advanced HCC when treated with high doses of intratumoural Pexa-Vec[8] have paved

the way for a phase III trial in this disease, and have led to Pexa-Vec being assigned 'orphan drug' designation by the US FDA in 2013 for the treatment of HCC.

1.1.2.2 Measles virus (MV) clinical trial activity

The first case reports alluding to the oncolytic potential of MV were published in 1971 and detailed transient tumour regressions in patients with leukaemia, Hodgkin lymphoma or Burkitt's lymphoma[9-13]. Since this time, there has been considerable academic progress in the field of oncolytic measles virotherapy, but as with many other oncolytics, clinical trial activity has lagged behind. Despite vaccine MV showing tumour-specific replication and anti-tumour activity in pre-clinical models of lymphoma[14-16], myeloma[17,18], acute lymphoblastic leukaemia (ALL)[19], ovarian cancer[20,21], glioma[22-25] and breast cancer[26,27], the early challenges in ensuring the appropriateness of pre-clinical animal models for a virus with humans as its only natural host, and our relatively limited mechanistic understanding of what confers vaccine MV its oncolytic capabilities, have undoubtedly contributed to the slow pace of clinical development for this complex biological agent. Despite these challenges, early phase clinical trial data shows great promise. As well as demonstrating little in the way of toxicity, published phase I data has demonstrated efficacy of intratumourally-injected vaccine MV in patients with cutaneous T cell lymphoma[28], and favourable median survival rates (12.15 months compared to expected 6 months) following intraperitoneal injection of MV (modified to express the marker peptide carcinoembryonic antigen (CEA) to aid real-time monitoring of viral gene expression) to patients with recurrent ovarian cancer[29]. More recently, systemically administered MV (engineered to express the human iodide symporter gene (MV-NIS) - to allow for noninvasive radioiodine imaging) has been used in a phase I clinical trial to treat patients with relapsed, drug-refractory multiple myeloma. Early reports detail clinical responses with a reduction in paraprotein and resolution of bone marrow (BM) plasmacytosis in 2 patients treated at the highest dose of 10^{11} $TCID_{50}$ (50% tissue culture infectious dose) infectious units of MV-NIS, with one patient showing durable complete remission at all disease sites. Toxicities were mild and self-limiting, and tumour targeting was elegantly demonstrated by NIS-mediated radioiodine uptake in virally infected tumours. Of note in this study, the initial 2 responders were measles-seronegative, alluding to the potential role of anti-measles antibodies in abrogating efficacy of this otherwise promising new therapeutic[30].

Table 1-2: MV clinical trials.

Author/year	Trial design	No. of patients	Patient population	Protocol	Side effects	Efficacy
Galanis et al. 2010	Phase I	21	Platinum refractory recurrent ovarian cancer; normal CEA.	MV-CEA (derived from MV-NSe) (intraperitoneal) every 4 weeks; max. 6 cycles; (10^3 to 10^9 $TCID_{50}$).	Grade 1-2 only.	Median survival: 2.15 months (1.3-38.4).
Heinzerling et al. 2005	Phase I	5 (6 lesions)	Histologically demonstrated cutaneous T cell lymphoma stage IIb or higher; resistant or relapsed after conventional treatment; pre-existing MV immunity.	MV- Edmonston-Zagreb x16 injections (intratumoural) upto 2 cycles (10^2 to 10^3 $TCID_{50}$); pre-treatment with Interferon alpha.	Grade 1 only.	5/6 lesions treated showed clear regressions within 28 days of initial treatment; one disappearance; distant non-injected lesions improved in 2 patients.

NCT00390299	Phase I	Recruiting	Patients with recurrent glioblastoma multiforme (GBM), pre-existing immunity to MV and candidates for gross total or subtotal tumour resection.	MV-CEA (derived from MV-NSe) (10^5 to $2x10^7$ $TCID_{50}$). Group A: direct MV-CEA into resection cavity; Group B: direct tumour admin. followed by resection and second intra-cavity dose.	No dose limiting toxicities observed thus far.	Awaited.
NCT00450814 **Interim report:** **Russell et al. 2014**	Phase I	Recruiting	Patients with recurrent or refractory multiple myeloma.	MV-NIS (derived from MV-NSe) (10^6 to 10^{11} $TCID_{50}$). Group A: Single intravenous injection. Group B: Pre-treatment with cyclophosphamide 10mg/kg 2 days prior to intravenous MV-NIS single dose.	Systemic response to virus infusion at highest dose, resolving within 1 week of treatment.	2 x good responses, one being a complete response at highest dose.

1.2 MV overview

MV is a highly pathogenic morbillivirus from the Paramyxoviridae family. Predominantly a childhood infection (although occurring at any age), cases in general are rare in the UK as a result of immunization programmes. However, vaccination rates in the UK were severely affected after, now discredited, claims of a link between the MMR (Measles-Mumps-Rubella) vaccine and autism, with MMR uptake reaching its lowest levels in 2003-4 and subsequent outbreaks seen in England and Wales in 2012-2014. Measles infection is characterized by a period of latency (10-14 days) followed by symptoms including cough, fever, Koplik's spots and a maculopapular rash. Whilst complications are more likely in children with defects in cell mediated immunity, MV itself causes a characteristic suppression of cell-mediated immunity in the infected host that can contribute to serious secondary infections even after resolution of viraemia. Rare but serious complications of Measles involve the central nervous system and include include acute disseminated encephalomyelitis (ADEM) – an autoimmune demyelinating disease usually occurring within weeks of infection in children over the age of 4 years, Measles inclusion body encephalitis (MIBE) – a progressive infection occurring in immunocompromised individuals who cannot clear the virus, and the rare brain disease – subacute sclerosing panencephalitis (SSPE), which can occur in immunologically normal children several years after contracting wild-type measles infection.

1.2.1 MV strains

Wild-type MV was first isolated by Enders and Peebles in 1954, from a patient - David Edmonston - using cultured human embryonic kidney cells[31]. Further attenuated of this strain was achieved by serial tissue culture passage in human kidney cells, human amnion cells, embryonated hens' eggs, and chicken embryonic fibroblast cells in tissue culture. The resultant MV-Edm strain, now in widespread laboratory use, has mutated in order to replicate efficiently in cell culture, and is immunogenic without causing viraemia or clinical symptoms of disease. MV-Edm became the progenitor virus of many commonly utilized vaccine strains[32]. Naniche et al. showed that in contrast to wild type MV strains, vaccine strains induced high levels of interferon (IFN) in peripheral blood mononuclear cells, and were more sensitive to exogenous IFN[33]. Subsequently, changes primarily in the MV P/V/C (and M, H and

L) genes have been implicated in the mechanisms conferring attenuation of virus virulence[34-37]. MV remains a single serotype (monotypic), with serum samples from patients naturally infected with measles decades ago still containing antibodies that can neutralize currently circulating wild type strains[38], and vaccination conferring lifelong immunity. Despite the expected inherent error rate in RNA synthesis, and the lack of proof-reading capacity of the viral RNA-dependent RNA polymerase (RdRp), there is minimal genomic variability between existing MV strains. Sequencing of many virus strains has been accomplished, and has identified 23 different viral genotypes distributed over 8 clades[39]. Sequence analysis of genes encoding for the F, H, N and M proteins of Edmonston-derived and non-Edmonston-derived vaccine MV strains has shown remarkable sequence similarity amongst coding and non-coding regions[40].

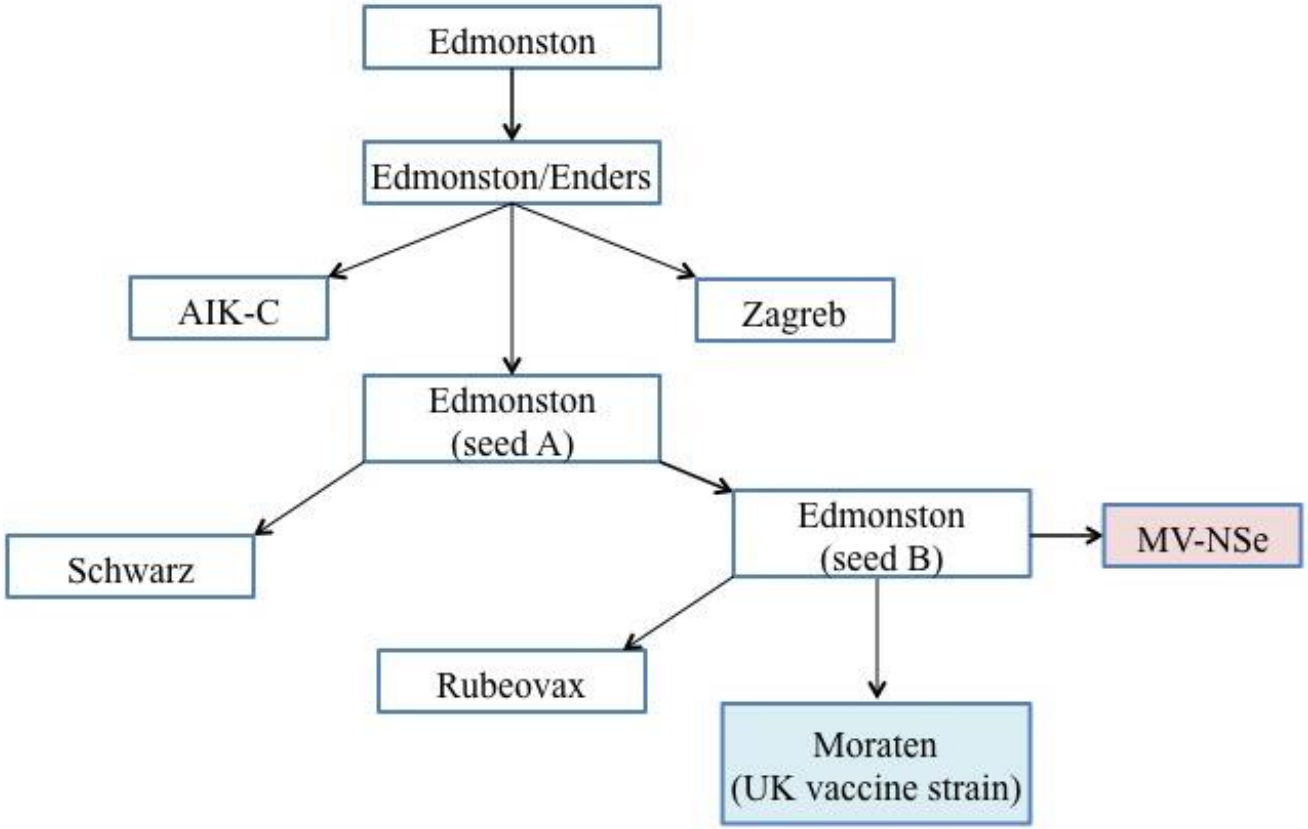

Figure 1-1: Edmonston vaccine lineage (adapted from Rota et al. 1994). Schematic representation of the Edmonston vaccine strains. Moraten (blue box) is the currently used UK vaccine strain of virus. MV-NSe (pink box) is the laboratory-adapted strain used for all experiments detailed in this thesis.

1.2.2 Virion structure

MV is a negative sense single-stranded RNA virus. Within the lipid bilayer envelope (derived from the host cell) is the viral ribonucleoprotein complex (RNP), consisting of viral proteins (N, P and L) and viral genome essential for virus propagation[41]. The viral genome is 15894 nucleotides in length, and follows the 'rule of six'[42], whereby to form a proper nucleocapsid template for efficient replication, genomic RNA must contain a total number of nucleotides which is a multiple of six, to allow complete encapsidation by the N protein. The viral genome encodes for 6 genes, separated by trinucleotide intergenic sequences. Genes are preceded by a Leader (Le) sequence at the 3' end, and a Trailer (Tr) sequence at the 5' end. The MV genome is encapsidated by the phosphorylated protein N (nucleocapsid), and is closely associated with L protein (large protein) responsible for providing the enzymatic activity of the RNA polymerase complex, and the viral protein P (phosphoprotein) - a polymerase cofactor associating with the RNP complex. The RNP complex is surrounded by the M protein (matrix protein), which serves to anchor overlying envelope proteins and regulate viral transcription. Proteins V and C are non-structural proteins encoded by the P gene. V protein prevents interferon (IFN)-induced transcriptional responses and signaling. C protein also prevents type 1 IFN transcriptional responses, acts as an infectivity factor, and plays a role in the regulation of replication and transcription. The type 2 and type 1 transmembrane glycoproteins H (haemagglutinin) and F (fusion) are responsible for virus attachment and fusion respectively.

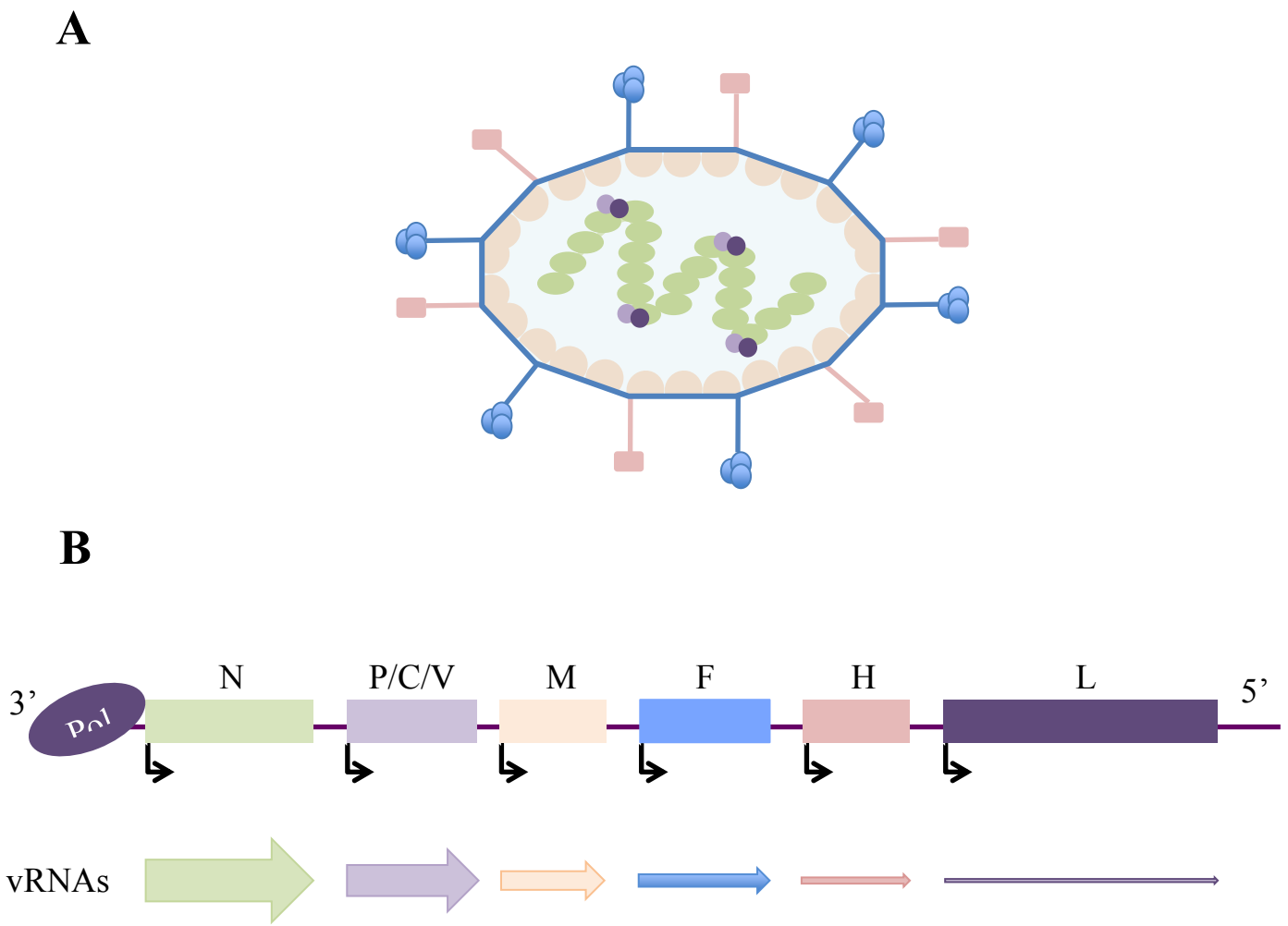

Figure 1-2: MV structure. (A) Schematic diagram of virion structure, with colours of MV genes (B) corresponding to viral proteins. MV haemagglutinin (H) and fusion (F) are embedded in the lipid envelope, anchored by the matrix protein (M). The RNA genome is encapsidated by nucleoprotein (N), with phosphoprotein (P) and large protein (L) forming the RNA dependent RNA polymerase complex (RdRp). **(B)** Organisation of the MV genome. Transcription gradient is generated by detachment of viral RdRp at the intergenic sites.

1.2.3 MV replication cycle

1.2.3.1 Entry

Target cell entry is mediated by MV cell surface glycoproteins H and F. The F glycoprotein is initially in a biologically inactive state (F_0), but becomes activated upon proteolytic cleavage by ubiquitously expressed furin-like proteases, to form an F_1-F_2 complex held together by a disulfide bridge between 2 cysteine residues (a feature of all Paramyxoviruses). The interaction between H and F leads to alterations in protein structure and creates fusion complexes[43] that permit entry of viral RNPs into the cytoplasm upon interaction with cellular receptors[44] (see below).

1.2.3.2 Viral RNA synthesis

Once viral nucleocapsid is released into the cytoplasm, primary transcription can occur. The viral polymerase transcribes the genomic template starting at the 3' end, in order to generate a positive Leader sequence, and successive capped and polyadenylated mRNAs, by stopping and starting at each intergenic region. Because of this, there exists a 'gradient of transcription', whereby mRNAs are generated in decreasing molar abundance from the N to the L position.

1.2.3.3 Genome replication

Once primary transcription (and translation) has generated sufficient viral proteins, MV-N (along with viral P) starts to assemble the nascent Leader chain. By the coordinated assembly and synthesis of the RNA, the polymerase is prompted to ignore the junctions between individual genes, with eventual yield of the full-length antigenomic nucleocapsid. The viral antigenomic structure serves as an intermediate template in genomic replication, and is also though to potentially play a role in preventing the host cell from undergoing apoptosis[45].

1.2.3.4 Virion assembly and release

MV components assemble in the cytoplasm, and virion budding takes place from sites on the plasma membrane of the host cell where viral components have accumulated. Budding and release of virions (with lipid envelopes derived from the host cell surface membrane) requires the coordination of multiple viral components is achieved via complex interactions between proteins (including MV-M protein), lipids and the host cell machinery.

For replication to be a success, RNA viruses utilize their intimate relationship with host cell and cellular machinery. A number of interactions between MV and host factors have been described that bind and influence MV replication (including heat shock protein 72 (HSP72)[46-48], casein kinase II[49], and peroxiredoxin 1 (Prdx 1))[50]. However, a comprehensive understanding of the involvement of such host factors in MV RNA synthesis is lacking.

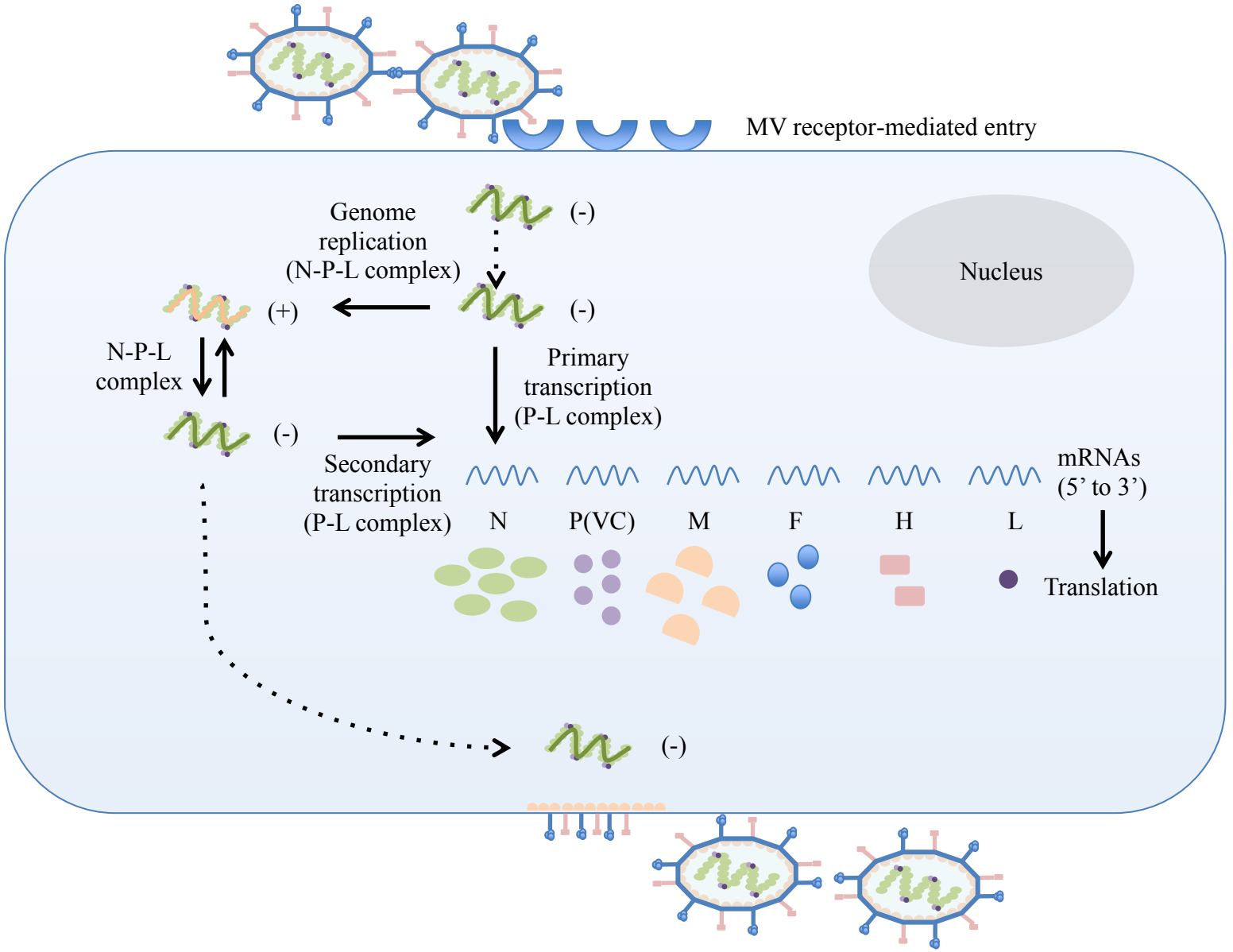

Figure 1-3: The MV replication cycle (adapted from Griffin et al. 2007).

1.2.4 MV receptors

MV causes a productive infection in humans and certain non-human primates only, with tropism and pathogenicity being determined by virus receptor specificity. Until recently, there were only two well-characterized viral receptors. Whilst signaling lymphocyte activation molecule (SLAM, or CD150) is known to act as the primary receptor for wild-type virus strains, vaccine and laboratory-adapted strains show a wider cell specificity, with the ability to utilize both SLAM and more efficiently the membrane cofactor protein, CD46[51]. The discovery of a third receptor – Nectin 4 - has led to a further advance in our understanding of MV entry and dissemination during infection.

1.2.4.1 CD46

CD46 – a C3b/C4b-binding type I transmembrane glycoprotein that acts as an inhibitor of complement-mediated lysis - is ubiquitously expressed on all human nucleated cells, and was the first receptor identified for the attenuated strain MV-Edm in 1993[52,53]. A number of different isoforms of the receptor exist, but all of the four primary isoforms of CD46 are able to serve as MV receptors - permitting infection, cell fusion, and virus cell-to-cell transmission when expressed in rodent cell lines[54]. The ability of MV strains to utilize CD46 as a cellular receptor is determined by a single amino acid substitution in the haemagglutinin (H) protein at position 481 (asparagine to tyrosine) (H481NY)[55-58]. Furthermore, serial passage of MV strains on human HEp-2 or Vero cells results in selection of viruses with tyrosine substitutions at position 481, and adaption to CD46 receptor usage[59], suggesting that this may be an in vitro phenomenon. The structure of CD46 consists of four short consensus repeats (SCR1-4), a serine-threonine-proline (STP) rich region, a transmembrane domain and a cytoplasmic tail. Binding of the MV-H glycoprotein to SCR1 and 2 is crucial for viral entry via this receptor[60,61]. Following cellular infection via CD46, vaccine and attenuated strains induce contact-mediated downregualtion of this receptor – making cells more sensitive to complement mediated lysis and potentially promoting virus clearance. This may in part explain the observation that attenuated MV strains which utilize CD46 as the primary entry receptor in vitro, do not preferentially target this receptor in vivo[62].

1.2.4.2 SLAM (CD150)

SLAM is a membrane glycoprotein expressed on immune cells, which acts as the primary cellular receptor for wild-type MV strains[55,63,64]. As a member of the immunoglobulin superfamily, SLAM was initially identified as a co-stimulatory receptor for T cells. It has a role in enhancing T cell proliferation, cytotoxicity and IFNγ production[65]. Activated T cells, immature thymocytes, memory T cells and a fraction of B cells all express high levels of SLAM[66,67] with moderate expression seen on dendritic cells (DCs)[68,69] and monocytes[70]. The tissue distribution of SLAM is in keeping with the lymphotropic nature of wild-type MV, and contributes to our understanding of measles disease progression. Wild-type H glycoprotein-expressing virus strains can enter cells through SLAM 2-3 times more efficiently than they do Vero cells expressing CD46. Conversely, virus strains possessing the H protein of attenuated MV-Edm enter CD46-expressing cells twice as efficiently as SLAM-expressing cells in vitro[58]. In addition to MV, the importance of SLAM as a virus entry receptor for morbilliviruses is evidenced by conserved usage throughout the genus, with canine distemper virus (CDV) and rinderpest using canine and bovine SLAM respectively. SLAM consists of an extracellular domain with variable (V) and constant (C2) regions, and a cytoplasmic tail with three tyrosine-based motif repeats. Three residues (I60, H61, V63) have been identified on the V domain of SLAM as being required for binding to MV-H[71], with at least ten other residues being involved in SLAM-dependent fusion, and one of these – I194, being critical for receptor binding[72]. As with CD46, receptor downregulation on host cells occurs following cellular infection, and may play a role in the suppression of cell-mediated immunity seen during active measles infection[73-75].

1.2.4.3 Nectin-4

Whilst experimental infections of non-human primates with enhanced green fluorescent protein (eGFP)-expressing strains of MV showed infection of SLAM positive lymphocytes and DCs during the peak of virus replication[76], infection of CD46 and CD150 negative cells was also evident in vitro and in vivo[77-79] . By comparing microarray data of upregulated membrane-associated genes in wild-type MV-susceptible and non-susceptible cell lines, the search for an additional MV receptor - allowing wild-type virus entry into SLAM-negative epithelial cells - led to the discovery of Nectin 4 (PVRL4) by two independent groups[80,81]. Nectin 4 is

exclusively localized on the basolateral epithelial surface, and acts as an adherens junction protein that interacts with the MV-H protein via its membrane distal domain. The location of Nectin 4 on the basolateral surface is in keeping with the observation that epithelial cells cannot be infected via their apical surface[77-79,82,83]. Discovery of this receptor has progressed our understanding of measles pathogenesis. It is now thought that initial MV infection in the respiratory tract is SLAM-dependent. MV-H attaches to alveolar macrophages or DCs[84,85] via DC-SIGN, a C-type lectin found on the surface of these cells[86,87]. Attachment subsequently results in upregulation of intracellular SLAM to the cell surface[88], and infected cells can then transmit the virus to draining lymph nodes. MV infection of activated B and T cells within the lymph nodes can occur via SLAM, leading to virus propagation and primary viraemia. Dissemination of virus to secondary lymphoid organs (including spleen, thymus and tonsils) leads to a secondary viraemia and acute immunosuppression. Spread of virus within lymphocytes or DCs to distal sites including liver, skin, gastrointestinal tract, genital and respiratory mucosal surfaces leads to virus shedding. Transmission of virus via the submucosa to epithelial cells within the respiratory tract takes place via basolateral Nectin 4[83], and virus is shed from the apical epithelial cell surface resulting in respiratory transmission to the next host[80,81,89].

1.2.4.4 Cell-to-cell spread in subacute sclerosing pan-encephalitis (SSPE)

Although MV is known to infect cells of the human central nervous system (CNS), the mechanisms utilized by MV to gain neuronal cell entry and spread from cell to cell remain unclear. It has been suggested that infection may occur via endothelial cells at the blood-brain barrier (BBB)[90], or via infected lymphocytes within the CNS[91]. Whilst strong CD46 expression can be seen on cerebral endothelial cells, weaker CD46 expression is detectible on subsets of neurons and oligodendrocytes within normal brain tissue, and is not detectible in MV-positive tissues in SSPE brains. In SSPE brains only a small subset of SLAM-positive lymphocytes can be detected, and no SLAM is found on cells commonly infected by MV[92]. Whilst the role of Nectin 4 in endothelial cell and neuronal cell infection is not clear, the possibility of an additional neuronal receptor for MV that facilitates neuronal infection remains. Non-permissive differentiated human neurons have been shown to become susceptible to MV following contact and fusion with permissive neuroepithelial cells in vitro, suggesting a requirement for contact and trans-synaptic

passage of virus[93], and a possible role for the substance P receptor neurokinin-1[94]. Attenuated transcription and translation of viral RNA within neurons is thought to allow low level virus persistence but very low levels of virus protein production[93], and may contribute to the pathogenesis of SSPE, where little infectious virus or viral antigen can be recovered, whilst viral RNA has been detected[95,96].

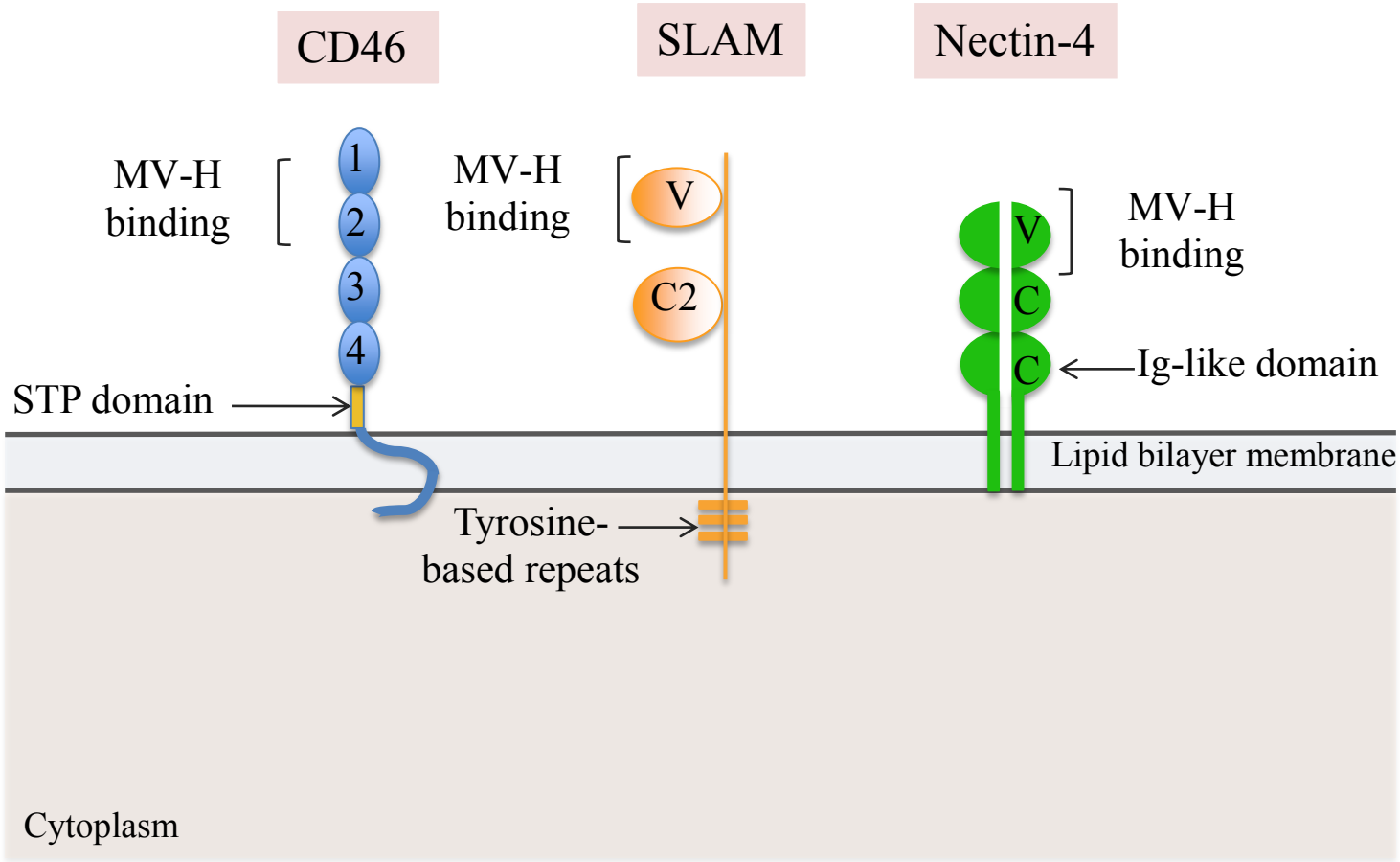

Figure 1-4: MV receptors (adapted from Dhiman et al. 2004). Schematic representation of CD46, SLAM and Nectin 4. STP domain: serine-threonine-proline-rich domain; V: variable domain; C: constant domain. Numbers 1-4 represent CD46 short consensus repeats (SCR).

1.2.5 Host immune responses to MV

1.2.5.1 Detection of RNA viruses by the host cell

Cellular antiviral innate immune responses, and counteracting virus strategies ultimately mediate the outcome of cellular MV infection. Pathogen-associated molecular patterns (PAMPs) (including the presence of viral RNA or protein) are detected by cellular pattern recognition receptors (PRRs) that influence cellular antiviral inflammatory and type 1 IFN responses. Cytosolic pattern-recognition receptors and transmembrane toll-like receptors (TLRs) are two classes of PRRs described in the detection of MV[97].

1.2.5.1.1 RIG-I like receptors

The RIG-I like receptors (RLRs) are cytosolic receptors expressed at low levels by most resting human cells, that are upregulated upon the detection of RNA viruses[98-100]. Family members of known importance in RNA viral signaling include retinoic acid-inducible gene I (RIG-I), melanoma differentiation-associated antigen 5 (MDA-5) and laboratory of genetics and physiology 2 (LGP-2). Both RIG-I and MDA-5 contribute to the recognition of MV. Whilst MDA-5 is generally thought to bind double stranded RNA (dsRNA) fragments[101], there is evidence of its involvement in the generation of IFN responses by MV[102,103]. RIG-I can detect both single-stranded (ssRNA) or short dsRNA[104]. Upon cellular entry and virus replication, viral 5'-triphosphate ssRNA structures bind to the C-terminal domain of RIG-I, triggering exposure of the caspase recruiting domain (CARDs)-like regions at the N-terminus. CARD domains are then able to interact with other CARD-containing proteins and initiate signaling via the IFN β promoter stimulator 1 (IPS-1), otherwise known as mitochondrial anti-viral signaling protein (MAVS)[105]. Signaling via IPS-1 (by both MDA-5 and RIG-I) on the outer mitochondrial membrane influences the induction of proinflammatory cytokines and type 1 IFN responses via IFN response family 3 (IRF3) and nuclear factor kappa beta (NF-κβ) activation[106], with IPS-1-deficient mice showing impaired production of proinflammatory cytokines and defective type 1 IFN responses upon RNA virus stimulation[107]. The recently identified adapter molecule – stimulator of IFN genes (STING) – also found on the mitochondrial membrane, is also thought to interact with RIG-I and IPS-1, although its role in antiviral immune signaling has yet to be fully elucidated[108]. IRF3 and NF-κβ activation lead to IFNβ

production, induction of IFN response factor 7 (IRF7) gene expression, and the subsequent enhancement of cellular type 1 IFN responses. LGP-2, another member of the RLR family, does not directly initiate antiviral gene expression, but is known to have negative regulatory functions on RIG-I signaling and cellular antiviral responses to RNA viruses[109].

1.2.5.1.2 Toll-like receptors

TLRs are transmembrane glycoproteins consisting of an extracellular N-terminal PAMP-binding region and a C-terminal intracellular signaling moiety. Of the 10 family members, TLR-2, 3, 4, 7 and 8 are known to be involved in detection of RNA viruses with TLR-2 being the best described example utilized by MV[110]. TLR-2 is known to recognize viral glycoproteins (such as the MV-H glycoprotein) rather than viral nucleic acids, and is expressed on the surface of immune cells including macrophages and DCs. Downstream signaling via this receptor ultimately leads to stimulation of a proinflammatory cytokine response[111], and potentially additional type 1 IFN responses via the transcription factor NF-κβ[112]. TLR-7 and 8, present in the endosomal compartment, are also known to be involved in the detection of ssRNA from virions internalized and digested within endosomes[113,114]. As MV enters the cell via direct membrane fusion rather than by utilizing endosomes, this pathway is likely to play less of a predominant role here.

1.2.5.2 Host innate immune responses

As described above, one of the early non-specific innate immune responses to MV infection is the induction of a type 1 IFN antiviral response. Following measles immunization, elevated levels of IFN and IFN-induced proteins can be detected in the blood[115]. IFNs act in either an autocrine or paracrine manner, binding to their cognate receptors on infected and neighbouring uninfected cells, and leading to phosphorylation and activation of signal transducers and activators of transcription 1 and 2 (STAT1 and 2) via janus kinase 1 (JAK1) and tyrosine kinase 2 (Tyk2)[116]. Phosphorylated STAT 1 and 2 heterodimers then translocate to the nucleus to form IFN-stimulated gene factor 3 (ISGF3) that binds to IFN-stimulated response elements (ISREs) and drives the expression of multiple interferon-stimulated genes (ISGs), and production of proteins with a role in establishing an antiviral state (including MxA, PKR, and ADAR1)[117-121]. Type 1 IFNs also stimulate DC maturation, natural killer (NK) cell cytotoxicity, and maturation of virus-specific cytotoxic T cells[122], reflecting

the influence that initial innate antiviral immune responses have on lasting adaptive immunity.

1.2.5.3 Host adaptive immune responses

Whilst MV infection is associated with host immunosuppression, strong and specific cellular and humoral immune responses against MV are induced that are crucial for virus clearance and longterm protection from infection respectively. The onset of the maculopapular rash in measles-infected individuals heralds the development of MV-specific CD8+ T-cell responses, and the detection of anti-MV antibodies[123,124]. Production of IFNβ has been shown to result in upregulation of MHC class I expression on infected cells in vitro[125], and is thought to contribute to the recognition of MV-infected cells by CD8+ T lymphocytes in vivo. Spontaneous proliferation of MHC class II restricted CD4+ T cells also occurs in response to MV infection, with elevated levels of soluble CD4 in the plasma of infected individuals[74]. Whilst early stages of MV infection result in the generation of a Th1 cytokine profile designed to promote clearance of virally infected cells (with production of IFNγ and IL-2 leading to activation of macrophages and proliferation of T cells respectively)[126], Th2 responses (with production of IL-4 and IL-10) that favour the generation of anti-MV antibodies and immunological memory predominate in later infection[73]. The preferential activation of type 2 CD4+ T cells in later infection is also thought to contribute to the generalized suppression of cellular immune responses seen with measles infection, with IL-4 contributing to suppressed in vitro lymphoproliferative responses to mitogens, and potentially inhibiting NK cell induction, decreasing delayed-type hypersensitivity, and decreasing macrophage activation[74]. Initial anti-MV antibody responses are in the form of IgM, but are ultimately overtaken by production of MV-specific IgG1 and IgG3 – mediators of virus neutralisation[124]. Antibodies against MV-N, H, F and M have all been detected[127], but the N protein is most abundantly expressed during infection, and therefore antibodies against MV-N predominate. Despite this, it is thought that anti-MV-N antibodies have limited biological function, and antibodies directed against the H and F glycoproteins are more important for virus neutralization[128].

1.2.6 MV mechanisms to combat host immunity

Wild-type MV strains have devised mechanisms to evade the host IFN responses, and are therefore much less efficient in their triggering of type 1 IFN production than vaccine strains[33]. MV proteins P, V and C have all been implicated in the negative regulation of viral PRRs. Wild-type V protein is known to interact with and inhibit MDA-5 signaling[129,130], and via its interaction with LGP-2, the V protein can inhibit signaling through RIG-I[131]. Downstream, the V protein has been shown to interact with IRF3 and IRF7 to inhibit their transcriptional activities[132,133], wild-type MV-C protein can accumulate in the nucleus of the host cell and directly downregulate IFNβ transcription[134], and MV proteins P, V and C have all been shown to bind and block NF-κβ signaling[135]. Virus proteins can also inhibit antiviral signaling via JAK/STAT by preventing nuclear import of activated STAT[136,137] (N and V proteins), promoting degradation of STAT1 (P protein)[138], and blocking JAK phosphorylation (V and P proteins)[139]. ADAR1 – a dsRNA-specific adenosine deaminase - was previously thought to have antiviral properties and limit MV cytotoxicity by causing mutations in the M protein gene[140]. However, recent evidence suggests that ADAR1 may also play a paradoxical role in suppressing antiviral IFN responses, and suppressing the activation of dsRNA-dependent protein kinase (PKR) triggering by MV[141]. Conversely, PKR has antiviral activity via the amplification of IFNβ induction by MV. These effects are counteracted by the MV C protein[142]. Further work is required for an elaborate understanding of how MV fights other antiviral effects.

In contrast to wild-type MV, vaccine strains have been shown to contain C proteins with disrupted nuclear localization signals (NLS), allowing triggering of more robust antiviral responses, and contributing to their attenuated pathogenicity[134]. Mutations in vaccine MV-V protein genes result in a lack of MDA-5 suppression and more robust IFN responses[143,144]. Vaccine strains of MV are also known to induce stronger IFN responses via enhanced production of defective interfering (DI) RNA particles[145].

1.3 MV as an oncolytic virotherapy agent

As previously described, evidence of the oncolytic capability of MV emerged with early case reports detailing transient but significant tumour regressions following wild-type measles infection. Whilst wild-type MV is a serious pathogen – responsible for millions of deaths worldwide[146], vaccine strains of the virus have a number of properties making them well suited to therapeutic use in anticancer strategies.

1.3.1 Vaccine MV therapeutic suitability

1.3.1.1 Specificity and efficacy in haematological malignancies

Live, attenuated Edmonston B vaccine strain MV (MV-Edm) and its derivatives are the most commonly used virus strains in experimental models of oncolysis. In haematological malignancies, MV-Edm has demonstrated selective replication in myeloma cell lines in vitro, with pre-infected cell lines showing reduced ability to form tumours in severe combined immunodeficient (SCID) mouse models in vivo, and regression of pre-formed tumours upon intratumoural injection. Partial tumour regressions were also seen when virus was administered systemically to established myeloma xenografts[147]. Successful pre-clinical modeling of MV oncolysis in myeloma led to the currently active phase I clinical trial, where promising responses are being seen. Using MV-Edm and MVlacZ (a strain of MV-Edm genetically modified by the addition of a beta-galactosidase reporter gene) in SCID mouse models of both aggressive (Raji) and indolent (DoHH2) B-cell lymphoma, tumour regressions proportional to tumour size, were seen with intratumoural virus administration (in contrast to ultraviolet inactivated (UV)-MV treated tumours) even in the presence of passively transferred anti-MV antibodies, whilst systemic administration of virus also slowed the growth of established tumours[14]. In the case of acute lymphoblastic leukaemia (ALL), large multinucleate syncytia were seen following MV-NSe infection of primary ALL cell cultures, with rapid cell death in vitro. In vivo, intratumoural MV-NSe treatment of established subcutaneous NALM-6 precursor B-ALL SCID mouse xenografts demonstrated striking antitumour activity in all cases, with antitumour activity also being evident in disseminated xenografts following intravenous virus delivery[19].

1.3.1.2 Safety

Vaccine strains of MV have been administered to more than a billion people in the last 40 years, as part of a worldwide immunization programme, and have demonstrated an excellent safety record[148]. Immunity in the majority of individuals in the developed world, and the limited tropism of MV, results in the absence of an existing human or animal reservoir for this pathogen, and reduces the likelihood of recombination events with other environmental organisms. Furthermore, the negative sense, non-segmented genomic RNA structure of MV results in a non-integrating, highly genetically stable pathogen with limited capacity for recombination between virus strains[149].

1.3.1.3 Ability to manipulate the MV genome

In addition to the above, there are a number of virus considerations that make MV a sensible choice as an oncolytic agent. In 1995, the first reverse genetics system was used to successfully rescue MV from cloned cDNA[150], and the possibility of engineering the MV genome was introduced. Methodology will be described in more detail in Chapter 4. Pleiomorphic and tolerant of manipulation, the MV genome has been extensively engineered allowing for insertion of therapeutic transgenes or traceable markers as additional transcription units, to aid efficacy and traceability. Genetic engineering has also allowed for manipulation of virus entry to specific cell types.

1.3.1.3.1 Enhancing oncolytic efficacy and virus surveillance

Oncolytic MV has been 'armed' by the expression of prodrug convertases to enhance efficacy when used in combination with chemotherapeutics[16,151]. It has been manipulated to express therapeutic proteins such as GM-CSF and G-CSF with favourable effects on therapeutic outcome being demonstrable in vivo[152]. MV has also been engineered to exploit cancer-specific proteases, by introducing proteases expressed at high levels, or preferentially expressed in cancer cells such as matrix metalloproteases (MMPs) into the virus glycoprotein cleavage domains[153]. In addition to such strategies, MV has been manipulated to express proteins such as carcinoembryonic antigen (CEA) or β-human chorionic gonadotrophin (β-hCG) upstream of MV-N to allow for measurement of concentration of virally encoded marker peptides in culture supernatants or serum[20,154]. The introduction of NIS

– the sodium iodide symporter gene – has allowed for effective tracking of virus replication, and enhancement of its therapeutic effect when administered in conjunction with radioiodine (^{131}I)[18].

1.3.1.3.2 Targeting MV tropism

The ability to target MV entry to specific cell types has meant that evermore sophisticated and specific viruses have been generated with the aim of enhancing MV oncolytic efficacy, reducing off-target side effects, and at the same time addressing some of the potential safety concerns of systemically administering a replicating virus with a ubiquitously expressed native receptor. Early targeting attempts were focused on creating viruses that could enter non-permissive cells via the creation of hybrid proteins consisting of growth factors such as epidermal-derived growth factor (EGF) or insulin-like growth factor-1 (IGF-1) linked to the extracellular (carboxyl) terminus of the MV-Edm attachment glycoprotein H. Such viruses were successfully rescued, propagated, and shown to be able to enter CD46-negative rodent cells expressing EGF or IGF-1 receptors respectively[155]. Following on from these early experiments, successful targeting was achieved by creating similar hybrid H proteins using single chain antibodies against a range of different receptors including CEA[156], CD20[157] and CD38[158], targeting tumour vasculature by the expression of disintegrin M28L echistatin[159], or targeting specific MHC ligands by the expression of high affinity single chain T-cell receptors (scTCR)[160]. With the discovery of the residues in the MV-H glycoprotein important for CD46 and SLAM receptor binding, ablation of the natural virus binding to CD46 or SLAM followed[161]. This was closely succeeded by the development of viruses blind to both CD46 and SLAM, that could gain cellular entry via non-native receptors due to additional ligands (EGF) or single chain antibodies (scFVantiCD38) on the mutated MV-H glycoprotein[162]. Such viruses could be rescued and propagated on Vero-α-His cells expressing a single chain antibody recognizing a 6-histidine peptide expressed by the receptor blind viruses at the C terminus of their ablated H protein.

1.3.2 Mechanisms of MV-mediated oncolysis

Multiple mechanisms have been proposed for the action of oncolytic viruses. Primary mechanisms inducing tumour regression (including direct viral cytolysis of tumour cells, and induction of tumour cell apoptosis) have been proposed for vaccine MV[163-

[165], alongside secondary mechanisms of action such as immune-mediated anti-tumour responses, resulting in tumour regressions in murine xenograft models in the face of limited viral intratumoural spread[14]. However, there is little evidence to suggest why vaccine MV may exert such effects in tumour cells but not in healthy normal cells. Cellular differences between malignant and non-malignant cells exploited by vaccine MV have historically extended only as far as differences in CD46 receptor density. CD46 was shown to be overexpressed in certain malignant cells, as compared to their non-transformed counterparts[166], with cell-cell fusion being minimal at low receptor densities, and increasing significantly above a threshold in vitro[167]. Whist undoubtedly of influence upon experimental in vitro and pre-clinical modeling systems, the role of tumour cell CD46 upregulation in the clinical successes seen in early phase trials is unclear. As previously described, attenuated MV strains known to utilize CD46 as the primary entry receptor in vitro, do not preferentially target this receptor in vivo[62]. An additional potential mechanism for the tumour cell-selectivity of MV vaccine strains results from defective type 1 IFN pathways in neoplastic cells. A recent study examining antiviral responses in MV susceptible and non-susceptible sarcoma cell lines, demonstrated an inhibition of viral replication and strong upregulation of the cytoplasmic PRR molecule RIG-I, and the IFN-stimulated gene (ISG) IFIT1, with enhanced and persistent phosphorylation of IFN-stimulated STAT1 in the MV-resistant cell lines. In contrast, MV-susceptible cell lines demonstrated weaker, delayed, or absent expression of IFIT1 and phosphorylation of STAT1, that was corrected with exogenous IFNβ administration, suggesting that differences in innate immune responses (cytoplasmic pathogen receptors and ISGs) may account for differential susceptibility of cells to vaccine MV-mediated killing in this model[168].

In contrast to vaccine MV, cellular mechanisms exploited by other oncolytic viruses are better characterized. Studies of Reovirus and HSV1 have revealed target specificity for cells with activated RAS signaling pathways[169,170], a feature in up to 30% of cancers[171]. Myxoma virus, a rabbit -specific poxvirus with oncolytic activity in humans, has been shown to exploit dysregualted Akt signaling pathways in a variety of cancer cells[172]. In addition, cellular susceptibility is thought to be further modulated by tumour suppressor pathways, with defects in *p53, ATM* and *pRB* all having being implicated in cancer cell specificity[173]. Defects in tumour suppressor function have also been linked to anti-cancer activity of the *EB1* gene knockout

oncolytic adenovirus (ONYX-015), demonstrating replication and killing in *p53* dysfunctional human tumour cells, but not cells with an intact *p53* pathway[174]. Subsequent reports have however challenged *p53*-selectivity as a mechanism, and as such the progression of this oncolytic virus through phase III clinical trials has slowed[175].

1.3.3 Immune barriers to oncolytic virotherapy

Although genetic engineering approaches have allowed sophisticated manipulations of the MV genome to be undertaken, there remains the real and potentially overriding issue of how such viruses can be delivered successfully to distant or widespread sites of tumour in patients with intact immunity. The importance of immune shielding may be underestimated when viruses are initially tested against human tumours in immunodeficient animal models. MV replication is specific to primates, with its only natural host being humans. Studies using human tumour xenografts established in immune deficient rodents are limited to looking at MV distribution or replication within the tumour tissue itself. Although CD46 transgenic rodent models have been generated, vaccine strains of MV only replicate well in such models if another immune defect (such as defects in the IFN receptor[176], or *RAG-1* knockout[177]) is also present. Hence accurate evaluation of the impact of the immune system on systemic virotherapy delivery is a challenge.

1.3.3.1 Reticuloendothelial system

Off-target binding or sequestration is likely to limit the efficacy of systemically administered oncolytic virotherapy, by reducing the circulatory half-life (t/2) and bioavailability of the virus concerned. In a recent publication, intravenously delivered oncolytic MV was sequestered by the mononuclear phagocytic system (MPS) of the liver and the spleen in vaccine MV-receptor CD46-positive and CD46-negative mice. Virus elimination from the systemic circulation was rapid, with a t/2 of only 1 minute[178]. With respect to another oncolytic virus, the administration of vesicular stomatitis virus (VSV) via the intravenous route to immunocompetent, virus naïve mice with hind flank tumours led to successful tumour cell delivery and intratumoural virus amplification. However, examination of virus biodistribution showed that systemic virus delivery was far from efficient, with <0.001% of virions reaching tumour, and the vast majority being taken up from the circulation by the liver and

spleen. Despite this, barriers posed by the reticuloendothelial system were overcome when virus was administered in sufficient doses[179].

1.3.3.2 T-cell immunity

As previously described, evidence of T cell activation occurs during the prodromal phase of measles infection, and full expression of the response coincides with the appearance of the classical MV exanthem. CD8+ and CD4+ MV-specific T cell responses are generated, with both playing a role in elimination of infected cells, either by class 1-restricted cytotoxic mechanisms (CD8+), or by local cytokine secretion resulting in attraction, activation or deactivation of macrophages, and in proliferation and differentiation of B and T cells (CD4+). There is evidence that replication of vaccine viruses can be prolonged in persons who are immunosuppressed or immunodeficient, with case reports linking measles vaccine virus infection to subsequent death in at least six severely immunocompromised persons. Whilst the importance of cell-mediated immunity in virus clearance has been unequivocally demonstrated[123], children infected with asymptomatic human immunodeficiency virus (HIV) have been shown to have no increase in adverse events following vaccination, as compared with controls[180], and patients with leukaemia in remission who have not received chemotherapy for at least 3 months may be vaccinated against the disease. Following vaccination with live, attenuated MV strains, cytotoxic T-cell responses elicited after re-challenge with MV are less robust than after natural infection[181], and although T cell-mediated immune responses are likely to play a role in the clearance of oncolytic measles virotherapy, these cellular defense mechanisms are often defective in the setting of malignancy. The implications of this, and the true limitations that vaccine generated, MV-specific cytotoxic T-cell responses pose to the efficacy of oncolytic measles virotherapy treatment are at present unknown, and require further elucidation. Potential mechanisms for this include adoptive transfer of T cells engineered to express MV-specific T cell receptors, into immunocompromised xenograft hosts.

1.3.3.3 Humoral immunity

Oncolytic viruses can be neutralized in the bloodstream by pre-existing antiviral antibodies. With each virus exposure, anamnestic responses result in augmentation of antibody titres, an increased likelihood of virus inactivation, and reduction in therapeutic efficacy. Anti-MV neutralising antibodies are likely to inhibit the delivery

of MV to target sites, prevent target cell infection, and prevent spread of virus within tumour cells. In pre-clinical models, SCID mice bearing disseminated KAS 6/1 myeloma xenografts showed an inferior survival following passive immunization with anti-measles antibody, before treatment with MV-NIS as compared to those without passive immunization before therapy (50 days vs. 72 days; $p<0.0001$)[182]. In athymic mice bearing established SKOV3ip.1 ovarian tumour xenografts, a significant difference in survival was seen when using naked MV-NIS in measles-naïve mice versus measles immune mice ($P<0.0001$)[183]. From these and other pre-clinical examples, it is clear that neutralizing antibodies pose a real and significant barrier to effective systemic measles virotherapy, and ways to overcome such barriers are required. One potential mechanism would be ablation of the epitopes for antibody binding. However, clinically relevant neutralizing anti-measles antibodies are directed against multiple epitopes on MV H and F – and it is therefore inconceivable that mutations could be introduced to ablate all such epitopes. Early clinical trial data regarding the significance of anti-MV antibodies is conflicting, with no correlation seen between clinical responses and humoral immune status for patients receiving intraperitoneally-delivered MV on the phase I ovarian cancer trial, but robust responses to intravenously-delivered MV seen only in seronegative phase I myeloma patients.

1.3.4 Overcoming the immune response to MV

Investigating strategies that can be employed to enable viruses to overcome the barriers posed by an intact immune system will potentially enhance their therapeutic applicability and efficacy.

1.3.4.1 Immunosuppression

Temporary immunosuppression, such as with the co-administration of virotherapy and chemotherapy, has been used in attempt to improve therapeutic efficacy of a number of oncolytic viruses, including MV[15,184]. In virus-susceptible mice, primary antibody responses to intravenously administered oncolytic MV or VSV were partially or completely suppressed by multidose regimens of oral or systemic cyclophosphamide (CPA) initiated 1 day before virus delivery. However, in the case of MV, the majority of individuals requiring treatment will have pre-existing antibodies following vaccination. It is of note therefore, that when MV-immune or

VSV-immune mice were re-challenged and concurrently treated with multiple doses of systemically delivered CPA, anamnestic antibody responses were completely suppressed, with titres falling below clinically significant levels[185]. Although such strategies may facilitate repeat virotherapy dosing, they raise issues in terms of the type, level and duration of immunosuppression that can be safely delivered whilst ensuring that viral proliferation is not allowed to proceed in an uncontrolled and potentially dangerous manner. Furthermore, there is a growing body of evidence alluding to the potential contributory role of both innate and cellular immune responses in the mechanism of viral oncolysis that may be abrogated by utilizing such strategies.

1.3.4.2 Envelope-chimeric MVs

By exchanging the MV envelope with that of the closely related virus CDV, Miest and colleagues[186] were able to generate a chimeric virus capable of escaping neutralization by sera from both MV-immunized mice and measles immune humans, whilst retaining its oncolytic efficacy. Although this strategy is appealing and appears to allow for successful virus delivery for initial injections, it is likely that neutralizing antibodies generated towards the novel virus envelope would quickly develop, and anamnestic responses would preclude repeat administration.

1.3.4.3 Carrier cell strategies

In order to circumvent humoral immunity there has been increasing interest in the use of cell-based delivery systems as a novel platform for the targeted delivery or 'chaperoning' of oncolytic viruses to sites of tumour. Success of this strategy is dependent on successful ex-vivo carrier cell loading with oncolytic virus, effective cellular targeting of tumour sites following systemic administration, and successful virus hand-off at tumour site. All of this must take place whilst evading immune attack. As well as being susceptible to viral infection, the ideal cell based vector would act as a miniature factory within which virus amplification can take place.
A number of different cell types have undergone evaluation for this purpose with varying degrees of therapeutic success. Although a number show promise in pre-clinical studies, in reality many of the potential candidates are technically difficult to isolate and either expensive or difficult to expand ex-vivo, making their use in the clinical setting logistically difficult.

Table 1-3: Cell-carrier-based systemic virotherapy (adapted from Power et al. 2007).

Cell type	Advantages	Disadvantages
PRIMARY LEUCOCYTES		
Tumour-specific CD8+ T cells	• Trafficking to tumour antigen • Activation at tumour site • Additional antitumour cell cytotoxicity	• Difficult to isolate and expand • Low infection efficiency
Activated T cells	• More readily infected than unstimulated cells • Antitumour cell cytotoxicity	• Difficult isolation and activation procedure
Cytokine-induced-killer cells (CIK)	• Traffic to tumours • Tumour cell cytotoxicity	• Difficult isolation and expansion
Dendritic cells	• Additional antitumour activity	• Difficult isolation and expansion
IMMORTALISED CELL LINES		
Solid tumour	• Easily propagated in vitro • Support productive infection	• Requires ablation of proliferative capacity due to risk of malignant growth
Haematological	• Support productive infection • Can disseminate systemically	• Requires ablation of proliferative capacity

PROGENITOR CELLS		
Outgrowth endothelial cells	• Engraftment in tumour vasculature • Easily propagated in vitro	• Requires intermittent re-isolation from clinical samples
Mesenchymal stromal cells	• Easily isolated and expanded ex-vivo • Tumour homing potential • Can engraft in tumour stroma for targeted delivery	• Intermittent re-isolation required • Infection efficiency less than that of transformed cells
Neuronal stem cells	• Targeted delivery in GBM	• Increased virus productivity and superior efficacy when compared to MSCs in glioma model

Activated T cells[188], monocytes[189], tumour associated macrophages[190], and mesenchymal stromal cells (MSCs)[183] have all been investigated as cellular vectors for oncolytic measles virotherapy. Ong et al.[188] used activated T cells to deliver oncolytic MV to NOD/SCID mice bearing myeloma xenografts. They successfully demonstrated cellular trafficking to tumour cells, cell-cell heterofusion and tumour cell infection with MV. The extent of tumour infection correlated inversely with the level of neutralizing antibody present regardless of the mode of virus delivery. However, when using cell-based delivery systems, infection of tumour cells was demonstrated over a range of antibody titres non-permissive to infection when using naked virions. Iankov et al. used MV-infected monocytic cells and outgrowth endothelial cells to demonstrate successful in-vitro transfer of infection to lymphoma, myeloma and ovarian cancer cells by cell-cell fusion even in the presence of neutralizing antibodies, whereas cell free virions were completely neutralized by antibody[189]. Furthermore, in NOD/SCID murine models they used a dual colour model to show heterofusion of intraperitoneally injected MV-infected cell carriers and tumour cells. Enhanced tumour cell infectivity and therapeutic activity was demonstrated when using MV-infected cell carriers as compared to cell free virus in the presence of neutralizing antibody.

1.4 MSCs

MSCs are an essential component of the BM microenvironment with a critical role in supporting haematopoiesis[191]. They can be isolated from a number of different sources including BM, adipose tissue[192], dental pulp[193], cord blood[194], placental tissues, fetal and amniotic tissues[195]. MSCs have several inherent characteristics that make them ideally suited to a role as delivery vehicles for the systemic administration of virotherapeutics.

1.4.1 MSC processing

MSCs can be obtained from a wide variety of tissues by simple isolation methods. They can be cultured and expanded ex-vivo in cellular therapy laboratories under good manufacturing process (GMP) conditions, and can be produced in sufficient quantities for therapy. The culture conditions employed and the source from which

MSCs are obtained is likely to have a significant impact on their biological phenotype, and needs to be taken into account.

1.4.2 MSCs in the clinic

There is a wealth of existing data for the use of MSCs in the clinical setting. The safety of administering third-party MSCs to humans via the intravenous route has been extensively demonstrated in studies using MSCs as immunomodulators in acute graft versus host disease post haematopoietic cell transplantation[196-200]. Although known to have immunomodulatory properties, thus far there is no clinical evidence to suggest that the administration of third party MSCs increases rates of disease relapse when used in the setting of haematological malignancies.

1.4.3 MSC homing

The ability of virus-loaded cells to localize to and be retained in the appropriate tissue is a pre-requisite for success in cell-based virotherapeutic delivery systems. Mechanisms implicated in tissue localization of systemically infused MSCs include MSC rolling along the endothelium in a P-selectin dependent manner[201], chemokine-mediated MSC activation and migration[202], and integrin-mediated adhesion and transendothelial migration[201]. MSC homing is most convincing in models of tissue injury[203-205], with poor localization demonstrated in the absence of tissue damage and cytokine release[206,207]. Numerous cytokines and growth factors have been implicated in MSC trafficking, including amongst others vasculoendothelial growth factor (VEGF), fibroblast growth factor 2 (FGF2), IL-6, hepatocyte growth factor (HGF), monocyte chemotactic protein 1 (MCP1), and stromal-derived growth factor 1 alpha (SDF-1α)[208]. Mechanisms of MSC homing and the role of SDF-1α will be discussed in more detail in Chapter 4.

1.4.4 MSCs as virotherapeutic cell carriers

In order for MSCs to function as effective cellular vehicles for virotherapy, their ability to support efficient and productive virus infection, retain viability, traffic to tumour sites, and effectively ‘hand-off’ virus to target cell needs to be demonstrated. Furthermore, the optimal timescale of ex-vivo loading and cellular administration post infection is likely to be a critical determinant to therapeutic success. MSCs support

productive viral infection with varying efficiencies. Komarova et al[209] successfully demonstrated the ability of BM-MSCs to support replicating adenovirus, and in vitro adenovirus-loaded MSCs caused cell killing when co-cultured with cancer cell lines. In-vivo, adenovirus-infected MSCs increased the survival of NOD/SCID mice bearing ovarian cancer xenografts as compared to cell free adenoviral injection. In relation to measles virotherapy, Mader et al[183] showed that adipose-derived MSCs could transfer MV infection to target cells via cell-cell heterofusion, and induce syncytia formation in the presence of high-titre anti-MV antibodies that completely inactivated naked virions in vitro. In athymic mice bearing ovarian cancer xenografts, they demonstrated cell-carrier trafficking and virus hand-off to peritoneal tumours, and were able to show enhanced survival of xenografted mice that were passively immunized with anti-MV antibodies when treated with MV-loaded MSCs versus those animals given treatment with naked MV or uninfected MSCs. In an orthotopically implanted SCID mouse model of human HCC, intravenously delivered MV-infected BM-MSCs were shown to home to sites of disease, transfer virus to tumour cells, and inhibit tumour growth in both measles naïve and passively immunized SCID mice[210]. In preparation for clinical use, adipose-derived MSCs obtained from healthy donors or ovarian cancer patients have been characterized for their susceptibility to virus infection, and tumour homing properties. Phenotype and doubling times of both healthy donor and patient MSCs were similar, with no tumours seen in SCID beige mice following administration of up to $1.6x10^9$ MSC/kg. Furthermore, MSCs did not promote the growth of SKOV3 human ovarian cancer cell lines. Rapid co-localisation of intraperitoneally-administered MV-infected MSCs to established ovarian tumours in athymic mice was demonstrated, with MV-infected MSC treatment, but not naked virus treatment significantly prolonging the survival of measles immune animals[211]. Such data is promising, but demonstration of the use of MSCs as cellular virotherapy delivery vehicles to treat a disseminated haematological malignancy has yet to be achieved.

1.5 Project aims

1.5.1 Improving therapeutic outcomes of systemic oncolytic measles virotherapy in pre-clinical models of ALL

This project explores the use of measles virotherapy as a novel treatment strategy for ALL. Adult ALL is an aggressive haematological malignancy with complete remission rates following initial "induction" therapy of 85-95%[212-219]. Therapy consists of combination chemotherapy with numerous immunosuppressive and myelosuppressive chemotherapeutics, in cycles. However, long-term survival is achieved in fewer than half of adults[220], and few patients with relapsed disease survive[221]. The ability to quantify and monitor minimal residual disease (MRD) in the majority of patients with ALL, provides a basis - already recognised by the regulatory authorities - for early intervention with novel therapeutics prior to overt disease relapse[222] which would be the optimal setting for novel biological therapies. With this in mind, there is a need to develop effective, non-cross resistant, rationally designed treatments in this disease that could be used alone or in combination with existing therapeutics. Using lymphotropic oncolytic MV as a novel therapy in an aggressive lymphoid malignancy should enhance tumour cell specificity. The efficacy of oncolytic MV in pre-clinical models of precursor B-lineage ALL has already been established[19], however, mechanisms to shield MV from antibody neutralization during systemic delivery need to be addressed, and this project aims to do so by investigating the use of BM-MSCs as a cell-based delivery system in this disseminated haematological malignancy. Using primary human BM-MSCs to deliver MV to a BM-based disorder is a rational choice, with such cells ideally being more likely to demonstrate desirable properties such as homing back to the BM following systemic administration. Furthermore, in ALL stromal cells are recognized as playing a significant role in maintaining leukaemia cells and affording chemoprotection[191]. Therefore, MV infection of MSCs is likely to enhance virotherapeutic success.

1.5.2 Probing mechanisms of tumour specificity and virus-initiated cell death.

As previously detailed, the oncolytic capacity of vaccine MV is unquestionable. In addition to optimizing MV delivery systems, our group has been interested in gaining

further understanding of the mechanisms that lend MV its oncolytic properties. An additional aim of this project was to probe the mechanisms conferring primary healthy cells and malignant cells their differential susceptibilities to oncolytic MV-mediated killing. To undertake this aim, I utilized a model of cellular transformation generated from primary BM-MSCs (gifted by Boshoff laboratory, UCL, UK), adapted to represent different stages of the malignant transformation process[223]. Reasons for chosing this model, and details of the model itself can be found within Chapter 5.

1.5.3 Hypotheses

The central hypothesis of this thesis, is that BM-MSCs can be effectively utilized, firstly as virotherapeutic cellular carriers - enhancing delivery and therapeutic efficacy of oncolytic MV in pre-clinical models of disseminated ALL - and secondly, as a model of cellular transformation to gain insight into the differential cellular effects of oncolytic MV in primary untransformed, and malignant cell counterparts. Specific hypotheses are detailed at the start of each data chapter, and are outlined here:

Chapter 3: Feasibility of BM-MSCs as biological delivery vehicles for systemic oncolytic measles virotherapy to ALL targets

a. A proportion of adult ALL patients will have clinically significant anti-measles antibody levels pre and post treatment that have the potential to impact on the success of systemic oncolytic measles virotherapy.
b. Human BM-MSCs will be successfully infected by oncolytic MV, sustain viral replication without cellular toxicity, target distant tumour cell niches, and hand off virus to tumour targets in the presence of anti-measles antibodies.
c. The systemic delivery of oncolytic measles virotherapy within BM-MSC cell carriers will result in enhanced therapeutic outcomes in pre-clinical models of ALL in the presence of anti-measles humoral immunity.

Chapter 4: Manipulating the MV genome to enhance localization of infected carrier cells

a. MV-infected BM-MSCs will show sub-optimal localization to tumour targets within the murine BM, due to downregulation of chemokine receptors during ex-vivo culture.
b. MSCs infected with a hCXCR4-expressing oncolytic MV may upregulate trafficking to tumour sites and enhance tumour killing.

Chapter 5: Characterising MV kinetics in a stromal cell model of transformation

a. There will be a difference in the permissiveness of fully transformed MSCs to oncolytic MV versus that of primary MSCs.
b. Differences in infectivity, productivity, and cytotoxicity will not be accounted for solely by MV receptor expression profile.
c. Transformation of BM-MSCs will result in cellular functional defects in innate immune signaling or translational regulation in response to MV infection, which may contribute to differential viral kinetics.

Chapter 2: Methods

Except where indicated in the Statement of work undertaken, I myself performed all experiments. Specific materials and methods are described in the relevant results chapters.

2.1 General cell line culture

Unless otherwise stated, suspension cells were grown in RPMI-1640 medium supplemented with 10% foetal bovine serum (FBS), penicillin-streptomycin (100u/ml and 100µg/ml respectively) and L-glutamine (2mM) in a humidified incubator with 5% CO_2 at 37°C (HERAcell, ThermoScientific, Surrey, UK). The MCF-7 cell line was further supplemented with 10mg/ml human insulin. Vero cells were grown in Dulbecco's Modified Eagle Medium (DMEM) supplemented with 10% FBS, penicillin-streptomycin and L-glutamine under the same conditions. Vero-Slam cells required the addition of 0.5mg/ml Geneticin® G418. The 293T cell line and PhoenixAMPHO cell line required 10% FBS. In general, cell lines were passaged at sub-confluency. All the cell lines used were growth factor independent. Specific techniques used for the isolation and culture of primary human BM-MSCs are given later in this chapter.

2.1.1 Cell lines

- 293T – human embryonal kidney cell line, adherent (CRL-11268; ATCC)
- Jurkat – human T-cell ALL cell line, non-adherent (TIB-152; ATCC)
- MCF-7 – human breast adenocarcinoma cell line, adherent (ACC-128; DSMZ)
- NALM-6 – human B-cell acute lymphoblastic leukaemia cell line, non-adherent (ACC-128; DSMZ)
- Phoenix AMPHO – human embryonic kidney cell line, adherent (CRL-3213; ATCC)
- Vero – african green monkey kidney cell line, adherent (CLL-81; ATCC)
- Vero-Slam – Vero cells expressing the SLAM receptor, adherent (gifted by Mayo Clinic, MN, USA)

2.1.2 Cell culture reagents

- Bovine serum albumin (BSA) (Sigma Aldrich, Poole, UK)
- Dimethyl sulfoxide (DMSO) (Sigma Aldrich, Poole, UK)
- Dulbecco's Modified Eagle Medium (DMEM) – high glucose 4.5g/l (Invitrogen, Paisley, UK)
- Foetal bovine serum (FBS), heat inactivated (Invitrogen, Paisley, UK)
- Geneticin® G418, used at 0.5mg/ml (Invitrogen, Paisley, UK)
- HBSS (Invitrogen, Paisley, UK)
- Human insulin, added at 10mg/ml (RFH Pharmacy)
- L-glutamine 200mM, added to media to achieve 2mM concentration (Invitrogen, Paisley, UK)
- OptiMEM® medium (Invitrogen, Paisley, UK)
- Penicillin-Streptomycin containing 10,000units/ml penicillin and 10,000µg/ml streptomycin, used at 100units/ml and 100µg/ml respectively (Sigma Aldrich, Poole, UK)
- Phosphate buffered saline (PBS) (Invitrogen, Paisley, UK)
- RPMI-1640 medium (Invitrogen, Paisley, UK)
- TrypLE™ Express (Invitrogen, Paisley, UK)

2.1.3 Cell culture plastics

- 1.8ml cryovials (VWR International, Merck, UK)
- 24-well transwell plates, polycarbonate membrane 8.0mm (Corning, UK)
- 0.4µm cell strainer for 50ml BD Falcon (Becton Dickinson LTD, UK)
- 6, 12, 24 and 96 well tissue culture plates (Nunc, NY, USA)
- Sterile syringe filters 25mm SFCA membrane, 0.2µm pore (VWR International, Merck, UK)
- T25, T75 and T175 flasks (VWR International, Merck, UK)
- 10cm and 14cm petri dishes (Nunc, NY, USA)

2.1.4 Active compounds used in cell culture

- AMD3100 (Sigma Aldrich, Poole, UK)
- SDF-1α, recombinant human (Peprotech, London, UK)

- Z-D-Phe-Phe-Gly-OH - fusion inhibitory peptide (FIP), used at 40μg/ml (Bachem, Swizerland)

2.1.5 Cell counts and viability

Cells were enumerated utilizing a haematocytometer. Cell viability was measured by Trypan blue (Sigma Aldrich, Poole, UK) dye exclusion and viability of cell lines maintained at >95%.

2.1.6 MTS colorimetric assay

The CellTiter 96® AQueous One Solution Cell Proliferation Assay (Promega,UK) is a colorimetric assay for determining viable cells in proliferation, or cytotoxicity. Cells cultured in 96 well plates were infected with MV-NSe at the appropriate multiplicity of infection (MOI) under standard conditions for the desired duration before performing the assay. For each well, 20μl of MTS (3-(4,5-dimethylthiazol-2-yl)-5-(3-carboxymethoxyphenyl)-2-(4-sulfophenyl)-2H-tetrazolium) reagent was added and the plate incubated at 37°C for 4 hours. The resulting absorbance was read at 490nm on a Tecan Sunrise absorbance reader (Jencons-PLS, UK).

2.2 Human BM-MSCs

The study received ethical approval from the National Research Ethics Committee (NREC number: 11/NW/0216). Healthy BM donors recruited during admission for BM harvesting gave written consent for participation in this project. The patient information leaflet, consent form and ethics approval can be found in the Appendix section of this document.

2.2.1 Primary MSC isolation and expansion

BM samples were filtered through a 40μM cell strainer (Becton Dickinson LTD, UK) and BM mononuclear cells were isolated by density gradient centrifugation using Ficoll-Paque™ (Amersham Biosciences, Bucks, UK). The resultant cell population was resuspended in MesenCult® MSC basal medium supplemented with MesenCult® stimulatory supplements (StemCell technologies, Grenoble, France), 100u/ml penicillin, 100μg/ml streptomycin, 2mM L-glutamine, and 1ng/ml recombinant basic human FGF (bFGF) (R&D systems, MN, USA). Cells were plated in T175 tissue culture flasks at a concentration of $1x10^7$ per 25ml of medium and

cultured in a 37°C, 5% CO_2 incubator. After 1-2 days, non-adherent cells were removed and adherent cells were washed using phosphate buffer saline (PBS) (Invitrogen, Paisley, UK) and fresh medium was added. Medium was replaced every 5-7 days thereafter. Following approximately 14 days in culture, cells were washed with PBS and incubated at 37°C with 5ml TrypLE™ Express (Invitrogen, Paisley, UK) for 3-5 minutes. The detached cells were collected in 10mls of fresh medium, centrifuged at 1200rpm for 5 minutes, enumerated in a haemocytometer chamber, and either frozen as described below for future propagation, or passaged into new T75 tissue culture flasks at a concentration of $3x10^5$ cells per 10mls of medium. Cells were passaged when they reached sub-confluency (80-90%). Passage 3-5 MSCs were used for experiments. For immortalized MSCs (hTERT, 3H, 4+V and 5H), cells were cultured in MesenCult® MSC basal medium supplemented with MesenCult® stimulatory supplements, 100u/ml penicillin, 100μg/ml streptomycin, 2mM L-glutamine, and 1ng/ml recombinant basic human FGF (bFGF). Cell culture passage was performed when reaching sub-confluency (80-90%).

2.2.2 MSC cryopreservation

MSCs were cryopreserved by resuspending the live cell pellet in a freezing mix consisting of 10% dimethyl sulfoxide (DMSO) (Sigma Aldrich, Poole, UK) and 90% FBS to a concentration of $1x10^6$ cells/ml. The cell suspension was aliquoted into polypropylene cryogenic vials and placed at -80ºC overnight in a freezing container (Nelgene, Rochester, US) filled with 100% isopropyl alcohol to achieve a cooling rate of 1ºC/minute. On the following day, the frozen cells were transferred to liquid nitrogen for long-term storage. When required, cells were thawed in a 37ºC water bath for 2~3 minutes. As soon as the cells were thawed, 10 ml of pre-warmed FBS was added dropwise to resuspend them. After centrifugation at 1200rpm for 5 minutes without brake, the cell pellet obtained was washed again with the appropriate cell medium supplemented with 50% FBS to remove any residual DMSO. Finally, cells were resuspended in supplemented medium and kept initially in a T25 flask at 37ºC, passaging to a T75 flask when reaching sub-confluency, at concentrations as before.

2.2.3 MSC characterization

Cells were assessed at the time of tissue culture passage (P1-3) to confirm success of the isolation procedure, and purity of the product obtained. Criteria set out by the International Society for Cellular Therapy (ISCT) were used to guide the definition of MSCs[224].

Table 2-1: Minimal criteria for human MSC definition (ISCT).

Adherent to tissue culture plastic when maintained in standard tissue culture conditions.
Cell surface positivity (>90%) for CD105, CD73 and CD90 expression.
Lack of (<2%) cell surface CD45, CD34, CD14 or CD11b, CD79a or CD19 and HLA-DR.
Multipotent differentiation in vitro: osteoblasts, adipocytes, chondroblasts.

2.2.3.1 Microscopic evaluation

Cells were monitored microscopically and identified by their adherence to tissue culture plastic and their distinctive spindle-shaped appearance in vitro.

2.2.3.2 Flow cytometric classification

For immunophenotypic characterization, MSCs were analyzed for the appropriate markers either in combinations or as single stains after harvesting by trypsinisation, resuspending in PBS and incubating with the appropriate primary antibody/antibodies at 4°C in the dark for 30 minutes before being washed and re-suspended in PBS. Corresponding isotype controls were used to account for non-specific background staining. Live cells were gated according to their forward scatter (FSC)/side scatter (SSC) characteristics or identified by using TO-PRO®-3 (Invitrogen, Paisley, UK) or Propidium Iodide (PI) (Invitrogen, Paisley, UK) to exclude dead cell population. Ten thousand live events were collected on a BD FACSAria instrument (Becton

Dickinson, Oxford, UK). Data was analyzed using FlowJo (Tree Star) (software version 7.4.1). A full list of antibodies is provided in the flow cytometry section of these methods.

2.2.3.3 Multipotent differentiation

Adipogenic and osteogenic differentiation of primary MSCs was demonstrated using the Human Mesenchymal Stem Cell Functional Identification Kit (R&D Systems, MN, USA). In addition, differentiation was further confirmed using Oil Red O and Alizaran red staining techniques on fixed cells. Briefly, MSCs plated into 24 well tissue culture plates were fixed at room temperature (RT) for 30-60 minutes with 2 mls of 10% formalin after being washed with PBS. Three parts Oil Red O stock solution (gifted by RFH histopathology department) was mixed with 2 parts distilled (DI) water and incubated at RT for 10 minutes. The working solution was then filtered through fine filter paper. Formalin was removed from each well and cells were gently rinsed with 2ml DI water, followed by incubation with 2mls 60% isopropyl alcohol for 5 minutes. Isopropanol was then removed and 2mls of Oil Red O working solution was added to each well, and left at RT for a further 5 minutes. The stain was then removed and cells were rinsed with DI water until the water was rinsing clear, then counterstained for 1 minute at RT with 2mls Carrazi's haematoxylin stain (gifted by RFH histopathology department) and visualized under a light microscope (Nikon Eclipse TS100). For the Alizarin Red staining, cells were fixed in ice cold 70% ethanol for 1 hour at RT. Alcohol was then aspirated and cells were rinsed twice with 2mls DI water per well. 2mls Alizarin Red S (Sigma Aldrich, Poole, UK) working stock was then added to each well and cells incubated for 30 minutes at RT before being washed with DI water and visualizing under a light microscope.

2.3 Flow cytometry

2.3.1 General flow cytometry method

Monoclonal antibodies were used as direct conjugates with fluorescein isothiocyanate (FITC), phycoerythrin (PE), phycoerythrin-Cy7 (PE-Cy7), peridinin-chlorophyll-protein complex (PerCP), allophycocyanin (APC), allophycocyanin-H7 (APC-H7), and Alexafluor® V450. 1-10x10^5 cells per aliquot were incubated at 4°C in the dark

with the designated panel of antibodies for 30mins before being washed and re-suspended in PBS. Samples were acquired on a BD FACSAria or LSR II flow cytometer (Becton Dickinson, Oxford, UK) with 5000-10 000 events being recorded and analysed with FlowJo (Tree Star) (software version 7.4.1).

Table 2-2: Antibodies used in flow cytometry

Target	Reactivity	Species	Ig class	Product code	Company	Clone	Conjugate
CD73	Human	Mouse	IgG1, k	550257	BD	AD2	PE
CD73	Human	Mouse	IgG1, k	561258	BD	AD2	PE-Cy7
CD105	Human	Mouse	IgG1, k	MCA1557	AbD Serotec	SN6	FITC
CD105	Human	Mouse	IgG1, k	561447	BD	266	V450
CD105	Human	Mouse	IgG1, k	9811-11	SouthernBiotech	SN6	APC
CD90	Human	Mouse	IgG1, k	555595	BD	5E10	FITC
CD34	Human	Mouse	IgG1, k	555824	BD	581	APC
CD45	Human	Mouse	IgG1, k	641399	BD		APC-H7
CD45	Human	Mouse	IgG1, k	555482	BD	H130	FITC
CD150	Human	Mouse	IgG1, k	559592	BD	A12	PE
Nectin 4	Human	Mouse	IgG2b, k	FAB2659P	R&D systems	337516	PE
CD147	Human	Mouse	IgG1, k	555962	BD	HIM6	FITC
CD46	Human	Mouse	IgG2a, k	555949	BD	E4.3	FITC
CD184	Human	Rat	IgG2a, k	551413	BD	1D9	
CD10	Human	Mouse	IgG1, k	MCA1556F	AbD Serotec	SN5c	FITC
CD10	Human	Mouse	IgG2a, k	347503	BD	W8E7	FITC
CD19	Human	Mouse	IgG1, k	345777	BD	4G7	PE

2.3.2 Fluorescent activated cell sorting

Cell sorting was performed on a MoFlo XDP (Beckman Coulter, Fullerton, Ca, USA) fitted with three lasers: 350, 488, and 647 nm. The enhanced blue fluorescent protein (eBFP) marker was excited by the 350 UV laser (100mW) and its emission was collected using a 450/65 filter. The GFP and mCherry markers were excited using the 488 blue laser. GFP emission was collected using a 653/40 filter, and mCherry using

a 613/20 filter.

2.4 Measles virus

2.4.1 MV strains

For the purposes of all experiments, the Edmonston strain vaccine virus, MV-NSe, was used unless otherwise stated. To visualize MV infection and aid infected cell tracking, MV-NSe-GFP or MV-NSe-Luc were utilized. For both of these modified vaccine strains, reporter genes were cloned into the MV genome upstream of the MV-N gene.

2.4.2 MV propagation

Attenuated vaccine strain virus - MV-NSe (or the derivatives MV-NSe-GFP, MV-NSe-Luc or MV-NSe-hCXCR4) - was used for the purposes of the experiments outlined in this document. MV strains were generated from the infectious cDNA of the Edmonston vaccine lineage Seed B. MV was propagated on Vero cells by inoculating with virus in OptiMEM® at a multiplicity of infection (MOI) of 0.01, and incubating at 37°C, 5% CO_2 for 2 hours. Following this the inoculum was removed and replaced with DMEM medium, supplemented with 5% FBS, 100 units/ml penicillin G + 100µg/ml streptomycin and 2mM L-glutamine. When the maximum cytopathic effect was observed, cells were scraped into small volumes of OptiMEM®, and exposed to two freeze-thaw cycles to release cell associated viral particles. The titer of propagated MV was determined by an end-point infectivity assay. Approximately 5×10^3 Vero cells were seeded in each well of a 96-well tissue culture plate. Ten-fold serial dilutions of MV stock were made and for each dilution, 50µl was dispensed per well for the 8 wells in one column of the 96-well plate. The plate was incubated at 37 °C, 5% CO_2 and read on day 4 post inoculation. The 50% tissue culture infectious dose ($TCID_{50}$) of MV stock was calculated using the modified Kärber formula[225] as shown below:

$$\text{Log}_{10}\,\text{TCID}_{50} = -\,[\text{Log}_{10}x - d\,(p - 0.5)] + \text{Log}_{10}\,(1/v)$$

x = highest dilution that gives 100% of wells positive for infection

d = Log_{10} of dilution interval (e.g. for 10-fold dilution, d=1)
p = sum of values of the proportion of wells positive for infection at all dilutions
v = volume of viral inoculum for each well in milliliters.

The plaque forming units (pfu) in 1ml of viral stock was estimated by multiplying $TCID_{50}$ value with 0.7 (a factor derived from Poisson distribution).

All viral stocks were frozen in small aliquots at -80°C. Repeated freeze and thaw cycles were avoided.

2.4.3 Cellular infection

MV stocks were thawed briskly in a water bath at 37°C and placed on ice before use. For MV infection of adherent human tumour cell lines or MSCs, cells were washed once with PBS and inoculated with virus in OptiMEM® at the required multiplicity of infection (MOI) for that particular experiment. Mock-infected cells were washed and 'inoculated' with OptiMEM® only. Cells were incubated at 37°C in 5% CO_2 for 2 hours before removal of the inoculum and replacement with fresh medium. For cells cultured in the presence of FIP, 40μg/ml was added to the fresh medium at this stage.

2.5 Molecular biology

2.5.1 Reagents for molecular biology

- 0.1M DTT (Invitrogen, Paisley, UK)
- 10mM dNTPs (Promega, Southampton, UK)
- 5 x first strand buffer (Invitrogen, Paisley, UK)
- Agar (Calbiochem, UK)
- Chloroform (VWR International, Lutterworth, UK)
- DNase/RNase free water (Invitrogen, Paisley, UK)
- Ethanol 100% (VWR International, Lutterworth, UK)
- Glycerol (VWR International, Lutterworth, UK)
- HiSpeed Plasmid Midi Kit (Qiagen, Crawley, UK)
- Isopropanol (VWR International, Lutterworth, UK)
- LB broth (Invitrogen, Paisley, UK)

- One Shot® TOP10 competent cells (Invitrogen, Paisley, UK)
- pCRII-TOPO TA cloning kit (Invitrogen, Paisley, UK)
- QIAex II gel purification kit (Qiagen, Crawley, UK)
- Random hexamers (Promega, Southampton, UK)
- Restriction enzymes (New England Biolabs, Hitchin, UK)
- RNasin® Plus RNase Inhibitor (Promega, Southampton, UK)
- SuperScript™ III reverse transcriptase (Invitrogen, Paisley, UK)
- T4 DNA Ligase (New England Biolabs, Hitchin, UK)
- TRIzol® (Invitrogen, Paisley, UK)

2.5.2 DNA extraction

DNA extraction was performed using the HiSpeed Plasmid Midi Kit. Resultant DNA concentration and purity was determined by measuring UV-light absorbance of samples at 260nm (A260) and 280nm (A280) with NanoDrop™1000 spectrophotometer (Thermo Scientific, Essex, UK). Samples with A260/A280 ratio of 1.75~2.0 were used for the purposes of the experiments outlined. DNA was stored at -20°C until use.

2.5.3 RNA extraction

Total RNA was extracted from cells at the appropriate time points using TRIzol®. Cell pellets (typically 1.5×10^5 cells) were lysed in 500µl TRIzol®. After five minutes incubation at RT, 100µl of chloroform was added to each sample, mixed well and incubated at RT for a further 2 minutes before being centrifuged at 12,000g for 15 minutes at 4°C. The aqueous layer was removed and mixed with 250µl of isopropanol to encourage RNA precipitation, before pelleting the RNA by centrifugation at 12,000g for 10 minutes. The RNA pellet was washed once with 75% ethanol, air-dried, and re-suspended in 20µl of RNase/DNase-free water. Concentration and purity of RNA was determined by measuring UV-light absorbance of the samples at 260nm (A260) and 280nm (A280) with NanoDrop™1000 spectrophotometer (Thermo Scientific, Essex, UK). Samples with A260/A280 ratio of 1.75~2.0 were used for the purposes of the experiments outlined. RNA stocks were stored at -80°C in aliquots of 10~15µl. Once thawed, any un-used RNA in an aliquot was not re-frozen. A fresh aliquot was taken from -80°C if any other use was required.

2.5.4 First-strand cDNA synthesis

To each 0.4-1µg sample of total RNA, 2µl (334ng) of random hexamer, 1µl of 0.1M DTT and 2µl of 10mM dNTPs were added and mixed. Samples were then heat blocked at 65°C for 5 minutes and then incubated on ice for a further 10-15 minutes. Following this 4µl of 5 × first strand buffer, 1µl (40 units) of RNasin® Plus RNase Inhibitor and 1µl (200 units) of SuperScript™ III reverse transcriptase were added to each sample, and the reaction mixtures were incubated at 25°C for 10 minutes, 50°C for 50 minutes and 70°C for 15 minutes. The product containing 1st strand cDNA was then used for PCR immediately or stored at -20°C for future use.

2.5.5 MV-nucleocapsid (MV-N) mRNA relative quantification

Expression of MV-N mRNA was quantified by a customized TaqMan gene expression Real-time PCR assay (Applied Biosystems, California, US) in reactions of 25µl volume. cDNA was mixed with 0.9mM forward and reverse primers and 0.25 mM TaqMan® probe labelled with FAM™ reporter dye. To each reaction, 12.5µl of TaqMan® Universal Master Mix (Applied Biosystems, California, US) was added, and the remaining volume was made up with RNase/DNase-free water. The PCR conditions for the assay are as follows:

- Step 1: 50°C for 2 mins
- Step 2: 95°C for 10 mins
- Step 3: 40 cycles of 95°C for 15 seconds, 60°C for 1 minute
- (Data collection was performed during step 3, stage 2)

Primer sequences for MV-N are shown below:

MV-N s 5′-GTATCCTGCTCTTGGACTGCAT-3′

MV-N a 5′-GTTCATCAAGGACTCAAGTGTGGAT-3′

Glyceraldehyde 3-phosphate dehydrogenase (*GAPDH*) was used as the housekeeping gene for all assays. All PCR reactions were carried out on an ABI 7500 system (Applied Biosystems, California, US). Samples were run in triplicates for each gene. Non-template controls (NTC) using RNase/DNase-free water instead of cDNA were

included in each plate. PCR cycle number at threshold is represented as Ct. Relative expression level of genes of interest was calculated using the following formula[226]:

$\Delta Ct = Ct_{(experiment)} - Ct_{(GAPDH)}$

$\Delta\Delta Ct = \Delta Ct - Ct_{(calibrator)}$

$RQ = 2^{(-\Delta\Delta Ct)}$

2.5.6 Plasmid preparation

Plasmid preparation for lentiviral and retroviral vectors used 5-20ng plasmid DNA was added directly to a vial of One shot® TOP10 competent cells and incubated on ice for 30 minutes, heat-shocked at 42°C for 30 seconds before adding 250µl of pre-warmed SOC medium. Vials were then placed in a shaking incubator at 37°C for 1 hour at 225 rpm. LB agar plates containing 100µg/ml ampicillin were spread with 20-200µl of each transformation reaction, inverted and stored in a bacterial incubator at 37°C overnight. One colony was picked with a sterile pipette tip and transferred to 2mls LB broth containing 100µg/ml ampicillin to form a starter culture, and placed in the shaking incubator at 37°C for 3-4 hours, before being transferred to 50mls of media and leaving in the shaking incubator overnight. The following morning, glycerol stocks were made from the culture by mixing 500µl bacterial culture with 500µl 50% sterile glycerol, and freezing at -80C. The remaining liquid culture medium was decanted and centrifuged at 4000rpm for 20 minutes at 4°C (no brake). Supernatant was discarded and bacterial pellet was used for DNA extraction using the HiSpeed Plasmid Midi Kit according to manufacturer's instructions. Plasmid DNA concentration was quantified using a NanoDrop™1000 spectrophotometer (Thermo Scientific, Essex, UK). Samples with A260/A280 ratio of 1.75~2.0 were used for the purposes of the experiments outlined. DNA was stored at -20°C until use.

2.6 Immunostaining

2.6.1 MV-H glycoprotein

For MV-H glycoprotein staining, cells were grown at appropriate density in 12 or 24 well tissue culture plates. At the desired time points post infection, medium was removed and cells were fixed at RT for 30-60 minutes with 10% formalin. After washing with DI water, cells were then incubated with anti-H antibody (clone MS-X;

1:100 dilution, Chemicon, Merck, UK) or mouse IgG1 κ (clone MOPC21; 1µg/ml; Sigma Aldrich, Poole, UK) for 45 minutes, washed x 2, incubated with polyclonal goat anti-mouse biotin IgG (1:400 dilution; Dako, Cambridgeshire, UK) for 30 minutes, washed again x 2, and then incubated with Streptavidin/HRP (1:500 dilution; Dako, Cambridgeshire, UK) for 30 minutes. Following this, cells were incubated with AEC+ High Sensitivity Substrate Chromogen (Dako, Cambridgeshire, UK) for 5 minutes, washed with DI water x 3 and counterstained with Carrazi's haematoxylin for 30 seconds. After a final wash step with DI water, cells were visualized under a light microscope (Nikon Eclipse TS100).

2.6.2 Human CXCR4 (hCXCR4)

Cells were grown at appropriate density in 12 or 24 well tissue culture plates. At the desired time points post MV-NSe-hCXCR4 infection, medium was removed and cells were fixed at RT for 30-60 minutes with 10% formalin. After washing with DI water, cells were incubated with human CXCR4 monoclonal antibody (clone 44716; 15µg/ml; R&D systems, UK) overnight at 4°C. Cells were stained with the anti-mouse HRP-AEC Cell and Tissue Staining Kit (R&D systems, UK) according to manufacturer's instructions, and counterstained with Carrazi's haematoxylin for 30 seconds. After a final wash step with DI water, cells were visualized under a light microscope (Nikon Eclipse TS100).

2.7 Enzyme-linked immunosorbent assay (ELISA)

MV IgG antibody quantification was performed using solid phase ELISA based on the sandwich principle (IBL international, Hamburg, Germany). Patient ALL serum samples were obtained and preserved at -80 °C at the time of specimen collection. Each sample was undiluted and analyzed in duplicate alongside standard samples and controls. Optical density (OD) was measured at 450 nm (reference wavelength 650 nm) using Tecan Sunrise absorbance reader (Jencons-PLS, UK). OD of standards was plotted against their concentration (x-axis; logarithmic) and concentration of samples was determined directly from the standard curve. Titers of 200mIU/ml or higher were deemed MV immune

2.8 Animal methods

2.8.1 Murine strains

Six to eight week old CB17 severe combined immunodeficient (SCID) mice (Charles River Laboratories, Margate, UK) were housed in a barrier facility and cared for in accordance with UK home office approved protocol.

2.8.2 Xenograft models

To establish disseminated ALL xenografts, $1x10^6$ viable NALM-6 cells (either un-manipulated (MV-NSe) or firefly luciferase-expressing (MV-NSe-Luc) (see chapter specific methods)) were injected intravenously in a volume of 200µl via the lateral tail vein. Mice were regularly observed and euthanized when pre-defined humane endpoints were reached. MSC localization experiments and MV-loaded carrier cell therapeutic experiments are described in chapter-specific methods (Chapter 3).

2.8.3 Bioluminescent imaging

Bioluminescent imaging was performed using an IVIS® 100 Lumina (Caliper Life Sciences, Cheshire, UK). Prior to imaging, shaved animals were given 200µl D-Luciferin (Caliper Life Sciences, Cheshire, UK) intraperitoneally and then anaesthetized using 1.5-2% isofluorane. Data was analysed using Living Image® 3.2 software.

2.9 Statistical analysis

Graphs were plotted using Prism 5.0 (GraphPad software) and Microsoft Excel. Data are presented as mean ± SEM (standard error mean) where appropriate. Statistical analysis was performed by unpaired student's *t* test or Mann Whitney U test as appropriate. For pre-clinical virotherapy animal experiments, Kaplan-Meier curves were used to assess survival, and differences between groups were compared using the log-rank test. P value ≤ 0.05 is considered statistically significant. All p values quoted are two-sided.

Chapter 3: Feasibility of BM-MSCs as biological delivery vehicles for systemic oncolytic measles virotherapy to ALL targets

3.1 Background

3.1.1 Cellular carriers as systemic virotherapy delivery units

Although standard chemotherapy regimes would be presumed to have an impact on levels of antibodies against vaccine-preventable diseases, in unselected cohorts of children treated with intensive chemotherapy regimes for a range of malignancies, a decline in anti-measles antibody levels below the clinically protective level was seen in only 6%-25% of cases with established pre-treatment immunity[227,228]. Furthermore, in successfully treated paediatric ALL cases, only 35-40% of children were deemed non-measles immune on completion of therapy[229,230]. It is therefore reasonable to presume that even in heavily treated adults with ALL, a proportion of patients will have clinically significant anti-measles antibodies that will prevent successful systemic delivery of naked measles virotherapy. It is worth noting however, that the effect upon neutralizing antibody levels, of the recent introduction of the targeted anti-CD20 monoclonal antibody treatment (Rituximab) to induction regimes for adult ALL patients on the UKALL14 trial, is unknown, but it would be expected to ablate memory B cells tasked with the production of anti-measles antibodies on rechallenge. In order to circumvent humoral immunity, cell-based delivery systems have been developed for the 'chaperoning' of oncolytic viruses to sites of tumour. Success requires ex-vivo carrier cell loading with oncolytic virus, cellular targeting of tumour sites following systemic administration, and virus hand-off by carrier cells to the tumour site, whilst going unnoticed by the immune system. The advantages and disadvantages of the commonly utilized cell carriers have been detailed in Chapter 1 (see Table 1-3).

3.1.2 MSC carriers

I chose to investigate the potential of human BM-MSCs to act as virotherapeutic delivery vehicles in this study for a number of reasons. Firstly, as outlined in the

introduction, MSCs are a highly clinically relevant commodity, with a wealth of data detailing the safe use of intravenously delivered allogeneic or autologous BM-MSCs as a therapeutic strategy in several diseases including acute graft-versus-host disease following hematopoietic cell transplantation for hematological malignancy[196,197,200]. Secondly, MSCs are hypoimmunogenic[231], permitting safe administration without pre-conditioning. Thus, allogeneic, donor-mismatched BM-MSCs can potentially be an "off the shelf" commodity, allowing their use as virotherapeutic delivery vehicles but without themselves representing a target for elimination of the therapeutic element. Thirdly, evidence suggests that MSCs co-locate and interact with ALL in the BM microenvironment[191]. Finally, based on preclinical studies investigating the migratory capacity of MSCs[232], I hypothesized that BM-MSCs would be likely to 'home' to BM targets upon systemic infusion. It is worth mentioning, however, that there is ongoing debate about the use of allogeneic versus autologous MSCs. The majority of in vivo studies of MSC therapies have utilized allogeneic or syngeneic donor cells because of the difficulty of extracting cells in a survival surgery in small animals. It has been proposed, that each individuals MSCs and the specific responses that they elicit, are determined by their genotype. Minor differences between host and donor cells may therefore have an impact on trophic (and other) effects. Furthermore, although MSCs are generally considered immune-privileged, they do express detectable levels of HLA class I antigens, and if allowed to differentiate in vivo, their HLA expression will be altered, making them potentially more recognizable by the host. In a mouse study comparing immune response with syngeneic versus allogeneic MSCs, allogeneic cells triggered a significant increase in CD8+, natural killer, and natural killer T cells compared with animals receiving syngeneic cells[233], and in clinical trials, anti-HLA antibody responses have been detected against allogeneic MSCs[234].

In vivo studies have shown both BM-derived and adipose-derived MSCs to be effectively utilized as MV carriers in pre-clinical models of ovarian carcinoma, and HCC respectively[183,210]. Whilst the ovarian carcinoma model required delivery of cellular virotherapy units via the intraperitoneal route, localization at sites of HCC was seen when BM-MSCs were delivered intravenously. In both studies, therapeutic outcomes demonstrated superiority when using MSCs as cellular virotherapy units as compared to delivery of naked virus in the presence of anti-measles humoral

immunity. So far, there has been no pre-clinical demonstration of the success of this approach following intravenous cell carrier delivery to a disseminated model of haematological malignancy.

MSCs can be isolated from a number of alternative sources in addition to BM, and subtle differences in their in vitro immunophenotype, differentiation capacity and gene expression profile have been seen. However, the extent to which these features lead to biological differences in vivo remains unknown but MSC lineage needs to be carefully and rationally considered for each particular tumor type. On this point it is noteworthy to mention, that authors have drawn our attention to the consistency and reproducibility of gene expression profiles for MSCs derived from different donors using the same culture procedure, in contrast to the diversity of gene expression seen when comparing MSCs from different ontogenetic sources, or grown using different culture conditions[110]. Using intravenously administered BM-MSCs for the targeted delivery of an oncolytic virus to a BM-based malignancy such as ALL is rapidly translatable, since it is fully compatible with current investigational and therapeutic approaches.

3.2 Purpose of this chapter

In this chapter, I initially investigated the existing MV immune status in a cohort of heavily treated adult patients with ALL. Following this, the potential of human BM-MSCs to be successfully infected by oncolytic MV, and the feasibility of utilizing such cells as viable virus producing units will be addressed. A prerequisite to therapeutic success is the ability of biological carriers to target and 'off-load' virus to tumour cells upon systemic infusion. In addition to investigating the ability of human BM-MSCs to target and hand off virus to distant tumour targets, this chapter also explores therapeutic outcomes of this approach to virotherapy delivery in pre-clinical models of ALL.

3.3 Hypotheses

a. A proportion of adult ALL patients will have clinically significant anti-measles antibody levels pre and post treatment, which have the potential to impact on the success of systemic oncolytic measles virotherapy.

b. Human BM-MSCs will be successfully infected by oncolytic MV, sustain viral replication without cellular toxicity, target distant tumour cell niches, and hand off virus to tumour targets in the presence of anti-measles antibodies.
c. The systemic delivery of oncolytic measles virotherapy within BM-MSC cell carriers will result in enhanced therapeutic outcomes in pre-clinical models of ALL in the presence of anti-measles humoral immunity.

3.4 Methods

3.4.1 Lentiviral vector production

For the preparation of lentiviral particles, 293T cells were co-transfected with the appropriate plasmids using a Fugene® high-density transfection reagent (Roche, Sussex, UK) method. Briefly, on the day of transfection, 4 x confluent T75 tissue culture flasks of 293T cells were passaged 1:2 into 8 x T75 flasks. The cells were transfected in suspension. Plasmids used (per 2 flasks) were as follows:

- 3µg gal-pol expressor plasmid (pCMV-ΔRp8.91)
- 3µg envelope plasmid (pCAGGS-VSV-G; gifted by Dr Martin Pule, UCL, UK) or for MV-pseudotyped vectors truncated H and F constructs were used (pCGHcΔ18 and pCGFcΔ30) at a ratio of 1:7 totaling 3µg DNA.[235]
- 5µg vector construct (pSIN-GFP or pSIN-mCherry; gifted by Dr Eric Poeshla, Mayo Clinic, MN, USA).

A final volume of 100µl was made with H_20, and the DNA mix was incubated at 55ºC for 5 minutes to sterilize. Fugene® was diluted in a cryotube by adding 40µl to 200µl OptiMEM. DNA mix was then added to the Fugene® solution (ratio 1:3.6 (DNA (µg):Fugene®(µl)), mixed by gentle pipetting and then incubated at room temperature for 15 mins. The liposomal complexes were then divided between and directly added to 2 x T75 tissue culture flasks (150µl/flask) of 293T cells that had been previously trypsinised, washed and resuspended in 10mls fresh medium to obtain a cell suspension. Lentiviral vector supernatant was collected after 24, 48 and 72 hours and

stored at 4°C. When all supernatants were obtained they were pooled and frozen with 10% glycerol (filter sterilized) at -80, or concentrated immediately.

3.4.2 Lentiviral vector titration

For lentiviral vector titration, healthy 293T cells growing in log phase were harvested using TrypLE™ express as before, washed, resuspended and enumerated. Subsequently $2x10^5$ cells were plated per well of a 6 well culture plate on the first morning of the procedure. On the same afternoon, serial dilutions of virus supernatant were made in a 24 well plate according to the anticipated viral titres. Medium was aspirated from the plated target cells and 5 dilutions of supernatant were added to the wells (plain medium in the first well; 1ml per well). Additional medium was made with 8µg/ml Polybrene (Millipore, Hertfordshire, UK) and a further 1ml of this medium was added to each well. Plates were then incubated at 37°C at 5% CO_2 until day 3 when the cells were harvested by trypsinisation, washed, resuspended and transferred to flow cytometry tubes for analysis on the BD FACSAria for detectable marker expression. Virus titrations were calculated as follows:

Transducing units/ml = [$2x10^5$ seeded cells x % positive cells x 1000]/µl of vector

3.4.3 Lentiviral vector ultracentrifugation

Where required, lentiviral vector supernatants were concentration by ultracentrifugation through a 20% sucrose cushion (20% sucrose in HBSS (Invitrogen, Paisley, UK), filter sterilized). Three mls of the sucrose solution was placed at the bottom of a Beckmann centrifuge tube (Beckmann Coulter, High Wycombe, UK), and the lentiviral vector supernatant was carefully layered on top. Tubes were then placed in the ultracentrifuge buckets, positioned on the rotor and spun at 25000g for 2 hours. Supernatant was then discarded and the lentiviral vector pellet was resuspended in HBSS with 10% glycerol (filter sterilized) at a volume according to the anticipated titre. Virus was then aliquoted and stored at -80°C. A 10µl aliquot was reserved for virus titration on 293T cells.

3.4.4 Retroviral vector production

For the preparation of retroviral vector particles, Phoenix AMPHO cell line (CRL-

3213; ATCC) was co-transfected with the appropriate plasmids using a Fugene® high-density transfection reagent (Roche, Sussex, UK) method. Briefly, on the day of the procedure (day 1), Phoenix AMPHO cells were harvested by trypsinisation, washed, resuspended and enumerated. A cell suspension was made with $2x10^6$ cells in 8mls of fresh medium and cells were plated into 10cm petri dishes and incubated at 37°C and 5% CO_2 overnight. On day 2 the transfection mix was prepared as follows:

Solution A
10µl Fugene®
150µl OptiMEM®

Solution B
1.5µg pCL-ampho retrovirus packaging vector (Imgenex, CA, USA)
2.6µg vector construct (SFG.Fluc_opt_2A_eBFP2; gifted by Dr Martin Pule, UCL, UK)
Adjust volume to 50µl with H_20

The DNA mix was then added to the Fugene® solution, mixed by gentle pipetting, and incubated at room temperature for 15-20 minutes. The liposomal complexes were added directly to the Phoenix AMPHO cells and then returned to the incubator. On day 3, medium was removed from the Phoenix AMPHO cells, and replaced with 5mls of fresh RPMI (+10% FBS; 1% P/S and 1% L-glutamine). Virus supernatant was ready to be used for transduction on day 4.

3.4.5 Lentiviral/retroviral vector transduction of NALM-6 cell line

For lentiviral and retroviral vector transduction, 6 well tissue culture plates were coated with 2.5ml/well of Retronectin (Clontech, France) at a concentration of 30ng/ml, and incubated at room temperature for 2-3 hours. Retronectin was then removed and the wells were blocked for 30 minutes at room temperature with 2ml per well of 2% bovine serum albumin (BSA) (Sigma Aldrich; Poole, UK) that had been filter sterilized. The blocking solution was then removed and wells were washed twice with PBS (3mls per well). NALM-6 cells that had been kept in culture prior to this procedure were adjusted to a concentration of $1x10^6$ cells/ml in RPMI complete

medium, and 2.5mls of cell suspension was added to each well of the pre-prepared 6 well plates and incubated at 37°C for 30 minutes to allow cellular attachment. Virus supernatant was added to each well of a 6 well plate at the desired multiplicity of infection (MOI). Plates were returned to the tissue culture incubator at 37°C and 5% CO_2 overnight. The following day, viral supernatant was removed from the wells and replaced with fresh RPMI complete medium (5ml/well) and further cultured at 37°C and 5% CO_2 for 3 days, at which time cells were harvested, washed, resuspended and transferred into tubes for flow cytometric analysis to determine transgene expression. Once transgene expression was confirmed, cell sorting was performed as previously described in Chapter 2: Methods.

3.4.6 Confocal microscopy

$5x10^3$ MSCs were infected with MV-NSe-GFP (MOI 1.0) for 2 hours and cultured in Lab-Tek™ eight-well chambered borosilicate coverglasses (Nunc, NY, USA). After 48 hours, $75x10^3$ NALM-6 cells expressing mCherry were added and directly imaged by resonance laser scanning confocal microscopy (TCS SP5 RS) (Leica, UK) using excitation wavelengths of 488 and 594nm with 20x dry and 63x water immersion objectives (N.A.=1.2) and analyzed by using Volocity software (National Institutes of Health, USA).

3.4.7 Xenograft models

For assessment of MV-infected BM-MSC localization to established ALL xenografts, $1x10^6$ viable NALM-6 cells (in 200µl PBS) were injected intravenously. After 3 weeks, intra-BM (IBM) sampling was performed to confirm leukemia engraftment (see below). Ten days later, animals received $1x10^6$ MV-NSe-Luc-loaded BM-MSCs (or PBS control) intravenously. Fate of infected BM-MSCs was determined by bioluminescent imaging. Shaved animals were given 200µl D-Luciferin (Caliper Life Sciences, Cheshire, UK) intraperitoneally, and imaged under anaesthetic using an IVIS® 100 Lumina (Caliper Life Sciences, Cheshire, UK). Analysis was with Living Image® 3.2 software. To assess therapeutic efficacy, disseminated ALL xenografts were established by intravenous injection of $1x10^6$ viable NALM-6-Luc cells (in 200µl PBS). Weekly bioluminescent imaging was performed from week 3 onwards. As treatment, six consecutive weekly intravenous injections of either $1x10^6$ pfu MV-

NSe, $1x10^6$ BM-MSCs pre-loaded with MV-NSe at an MOI of 1.0, or $1x10^6$ BM-MSCs alone were given, starting 3 days after tumor administration. Passively immunized mice received 50IU anti-MV IgG intraperitoneally, 3 hours before each MV injection. Primary end-point was survival to humane end-point, with secondary end-point being disease burden (assessed by bioluminescence imaging or by flow cytometric quantification).

3.4.8 IBM sampling

Briefly, following isofluorane (Forene, Germany) induction, anesthesia was maintained using 1.5-2% isofluorane delivered via nose cone. The right leg/knee joint area of each animal was sprayed locally with 70% ethanol. Access to the BM cavity was obtained by flexing the right knee to 90°, drawing the proximal side of the tibia to the anterior, and inserting a 25-gauge needle into the joint surface of the tibia and into the BM cavity. BM was aspirated into a syringe containing preservative free heparin, and mononuclear preparations were assessed for human CD19 and CD10 positive populations by flow cytometry. Perioperatively, animals received buprenorphine analgesia.

3.5 Results

3.5.1 Optimization of MSC and ALL cell populations

3.5.1.1 Characterization of BM-MSCs

BM-derived MSCs were isolated from freshly obtained healthy BM donor samples as detailed in Chapter 2: Methods. Following a period of expansion, passage 1-3 MSCs underwent cellular characterization to confirm successful isolation and ensure purity of the product, prior to use in future experiments. All MSCs were shown to be adherent to tissue culture plastic under standard growth conditions. MSC samples were selected at random to undergo multipotent differentiation experiments. All samples chosen successfully demonstrated adipocytic and osteocytic differentiation under required experimental conditions. Representative photographs of multipotent differentiation are shown in Figure 3-1. Flow cytometric analysis of cell surface markers demonstrated >90% positivity for CD105, CD73 and CD90 in all cases, with <2% of cells demonstrating CD45, CD34, and CD19 positivity – confirming low

levels of haematopoietic cell contamination in the product (see Figure 3-2). MSCs were frozen in -80°C until required. Passage 3-5 MSCs were used for all experiments unless otherwise stated.

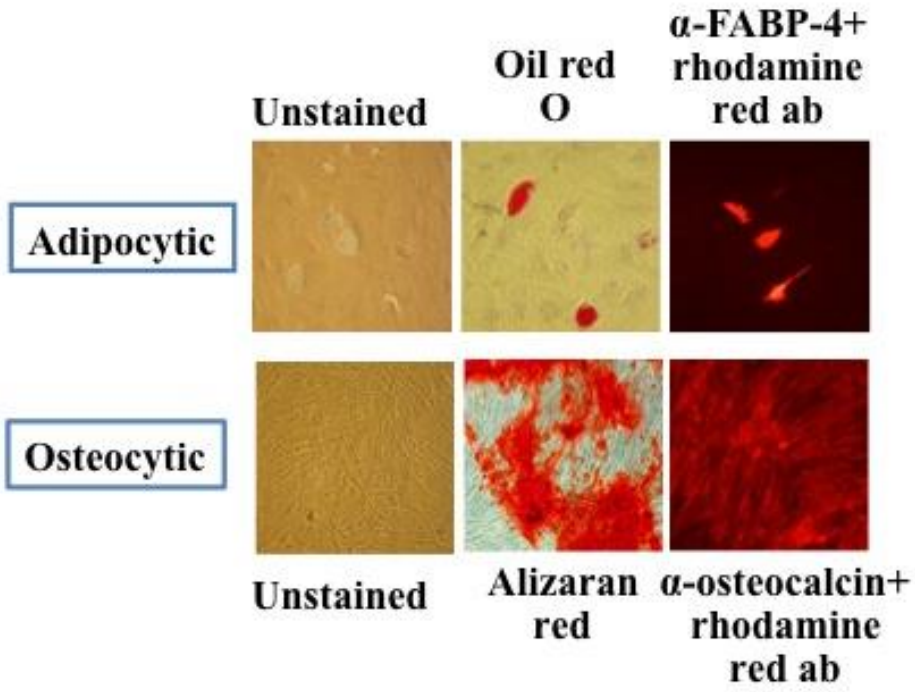

Figure 3-1: MSC differentiation. Representative photographs demonstrating adipocytic and osteocytic differentiation of BM-MSCs, using the Human Mesenchymal Stem Cell Functional Identification Kit (R&D Systems, MN, USA). In addition, Oil Red O (staining triglycerides and lipids) and Alizarin Red (staining free calcium and calcium compounds) techniques were performed on fixed cells to demonstrate adipocytic and osteogenic differentiation respectively. α-FABP-4: alpha-fatty acid binding protein 4.

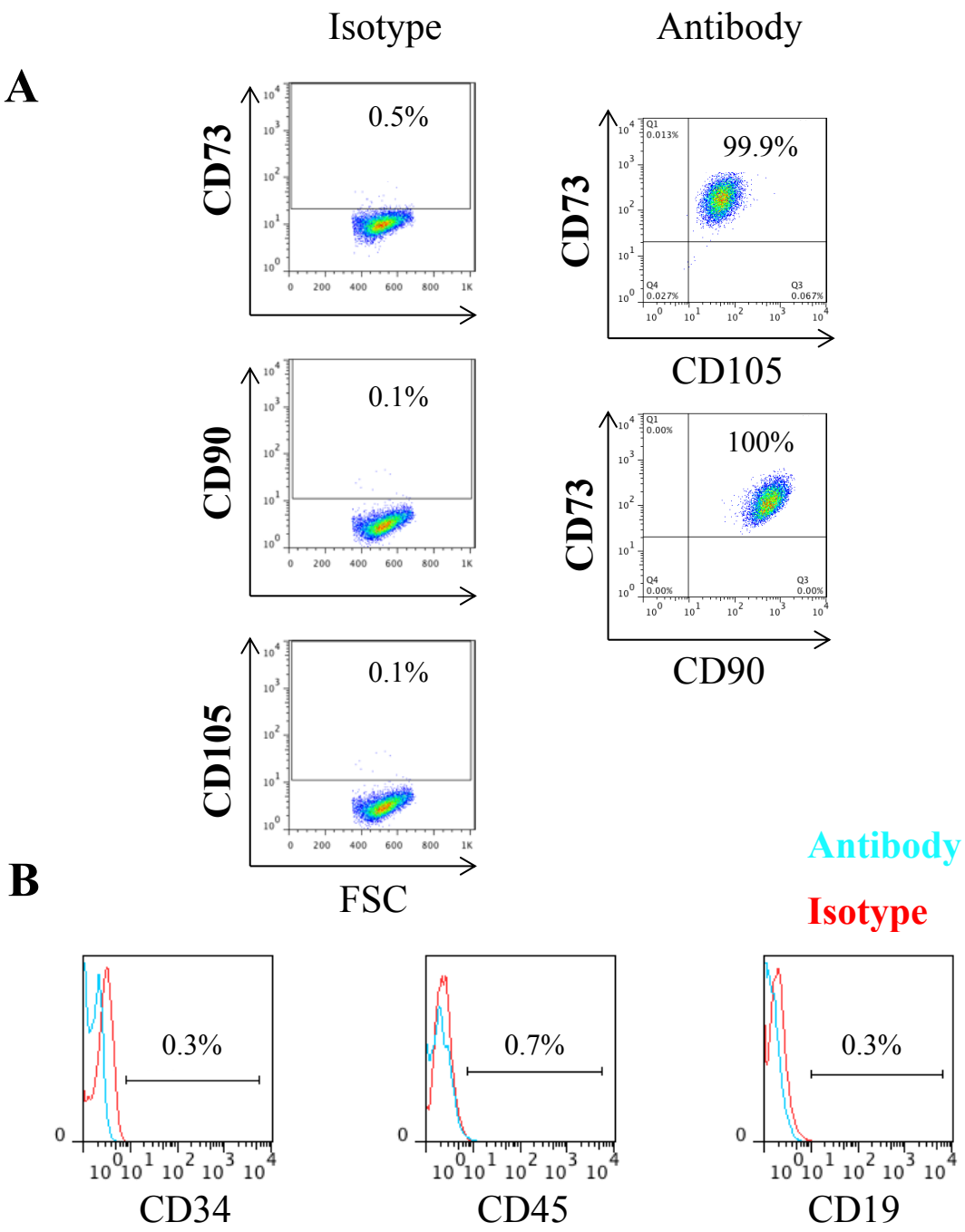

Figure 3-2: MSC phenotype. (A) Live MSC populations were gated according to their FSC and SSC characteristics, or using PI staining where required. MSC populations were shown to co-express CD73, CD105 and CD90 in >95% of cells. Corresponding isotypes were used as negative controls. **(B)** On the same cell populations, haematopoietic markers (CD34, CD45) and B cell markers (CD19) were demonstrated to be negative in >95% of cells.

3.5.1.2 ALL cell labeling

In order to aid both in vitro ALL cell imaging, and in vivo tumour burden monitoring, NALM-6 cells were used to generate stably labeled pre-B ALL cell lines by two methods. Firstly, lentiviral vector transduction of NALM-6 cells was performed to obtain cells stably expressing mCherry or GFP, and secondly retroviral vector transduction of NALM-6 cells was performed to obtain cells stably expressing both eBFP and firefly luciferase.

3.5.1.2.1 Lentiviral transduction

For initial labeling of NALM-6 with mCherry or eGFP, lentiviral vectors expressing the chosen traceable marker gene were generated as detailed in the chapter-specific methods. Vectors were pseudotyped with the VSV-G envelope, to confer broad cellular tropism, or vaccine strain MV envelope glycoproteins. In the context of SSPE, truncations of the cytoplasmic F protein domains have been shown to allow measles virus to spread more rapidly[236]. It is interesting therefore, that efficient retargeting of lentiviral vector entry using MV pseudotyping has been shown to require truncation of both cytoplasmic tails[235]. Representative photographs of 293T cells co-transfected with lentiviral vector constructs, the appropriate envelope plasmid, and p8.91 carrying the accessory proteins required for viral particle assembly are shown in Figure 3-3. Where cytoplasmic tail-truncated MV-H and F envelope glycoproteins were used, 293T cells show the presence of giant multinucleate syncytia – the cytopathological hallmark for MV infection. VSV-G-pseudotyped vector particles generated were concentrated by ultracentrifugation. Attempted ultracentrifugation of MV-pseudotyped lentiviral particles was undertaken (see Table 3-1), however inadequate titres were obtained after concentration, suggesting particle fragility and sensitivity to rapid high velocity ultracentrifugation protocols. For this reason, VSV-G-pseudotyped vectors were used for NALM-6 transduction. Post transduction, cells were FACS-sorted according to their traceable marker, obtaining a population of cells with post-sort purity of >95% in all cases. Following this, cells were either propagated in tissue culture, or frozen in aliquots for use in future experiments. Only short-term co-culture experiments were performed using mCherry transduced NALM-6 cells (maximum co-culture period 48 hours), and for this reason long-term stability of transgene expression was not determined here.

3.5.1.2.2 Retroviral vector transduction

NALM-6 cells stably transduced to express firefly luciferase were generated for the purposes of in vivo tumour burden monitoring. Vector particles were generated, and NALM-6 cells transduced and FACS-sorted as detailed in chapter-specific methods. As luciferase-expressing NALM-6 cells (NALM-6-Luc) were to be used to for pre-B ALL murine xenograft modeling, stability of transgene expression was characterized over a 6-week period (the timescale over which unmanipulated NALM-6 disseminated murine xenografts will succumb to leukaemia if left untreated). A shows in vitro characterization of eBFP expression (and corresponding mean fluorescent intensity (MFI)) in transduced NALM-6 cells as compared to mock-transduced cells over time. Both the percentage expression and MFI remain relatively stable over a 6-week period. Correlation between amount of luciferase activity and number of transduced NALM-6 cells is shown in Figure 3-4C, whilst Figure 3-4D shows luciferase activity in transduced NALM-6 cells (minus background luminescence) over 6 weeks. In order to evaluate the ability of the NALM-6-Luc cell line to be used for tumour burden monitoring in vivo, 6-8 week old SCID mice were injected with $1x10^6$ NALM-6-Luc cells via the lateral tail vein (or PBS control) and underwent weekly bioluminescent imaging to assess relative tumour burden. Tumour engraftment was evidenced by a steady increase in the amount of luminescence activity detectable in all mice receiving the NALM-6-Luc cell line. Luminescent activity was generally detectable from week 3 post-inoculation onwards, with all animals (except control) succumbing to their humane endpoint at 6 weeks post-inoculation (see Figure 3-5).

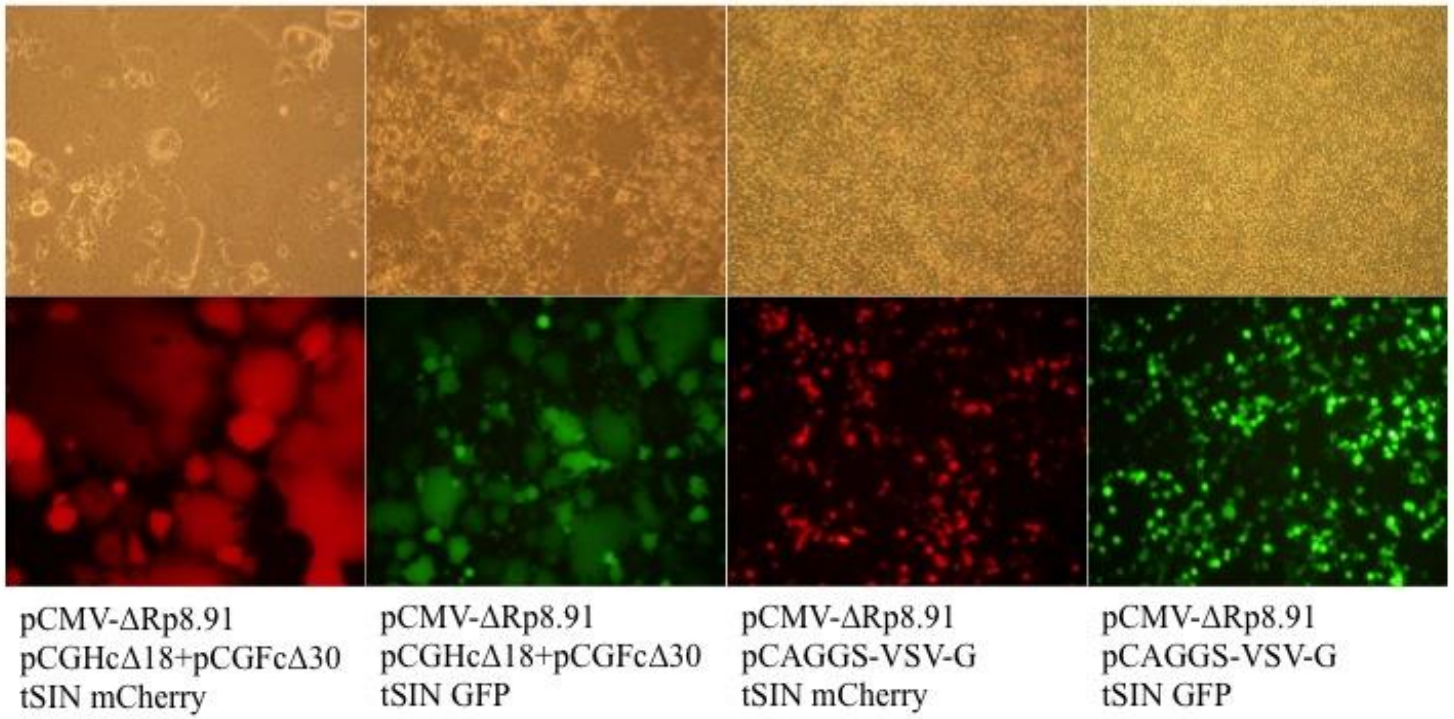

Figure 3-3: mCherry and eGFP lentiviral vector generation on 293T cells. Representative photographs of 293T cells at 24 hours post-transfection with SIN lentiviral vectors carrying mCherry and eGFP and the gag/pol expressor plasmid pCMV-ΔRp8.91. Lentiviral vector particles are pseudotyped with either tail-truncated MV-H and F glycoproteins (pCGHcΔ18+pCGFcΔ30) or VSV-G envelope glycoprotein (pCAGGS-VSV-G).

Table 3-1: Lentiviral vector titration.

Lentiviral vector particles	Lentiviral vector titration (transducing units per ml)
VSV-G-pseudotyped lentivirus expressing eGFP	$5.9x10^8$ (post ultracentrifugation)
VSV-G-pseudotyped lentivirus expressing mCherry	$1.4x10^8$ (post ultracentrifugation)
MV-pseudotyped lentivirus expressing eGFP	$3.2x10^6$
MV-pseudotyped lentivirus expressing mCherry	$6.4x10^5$

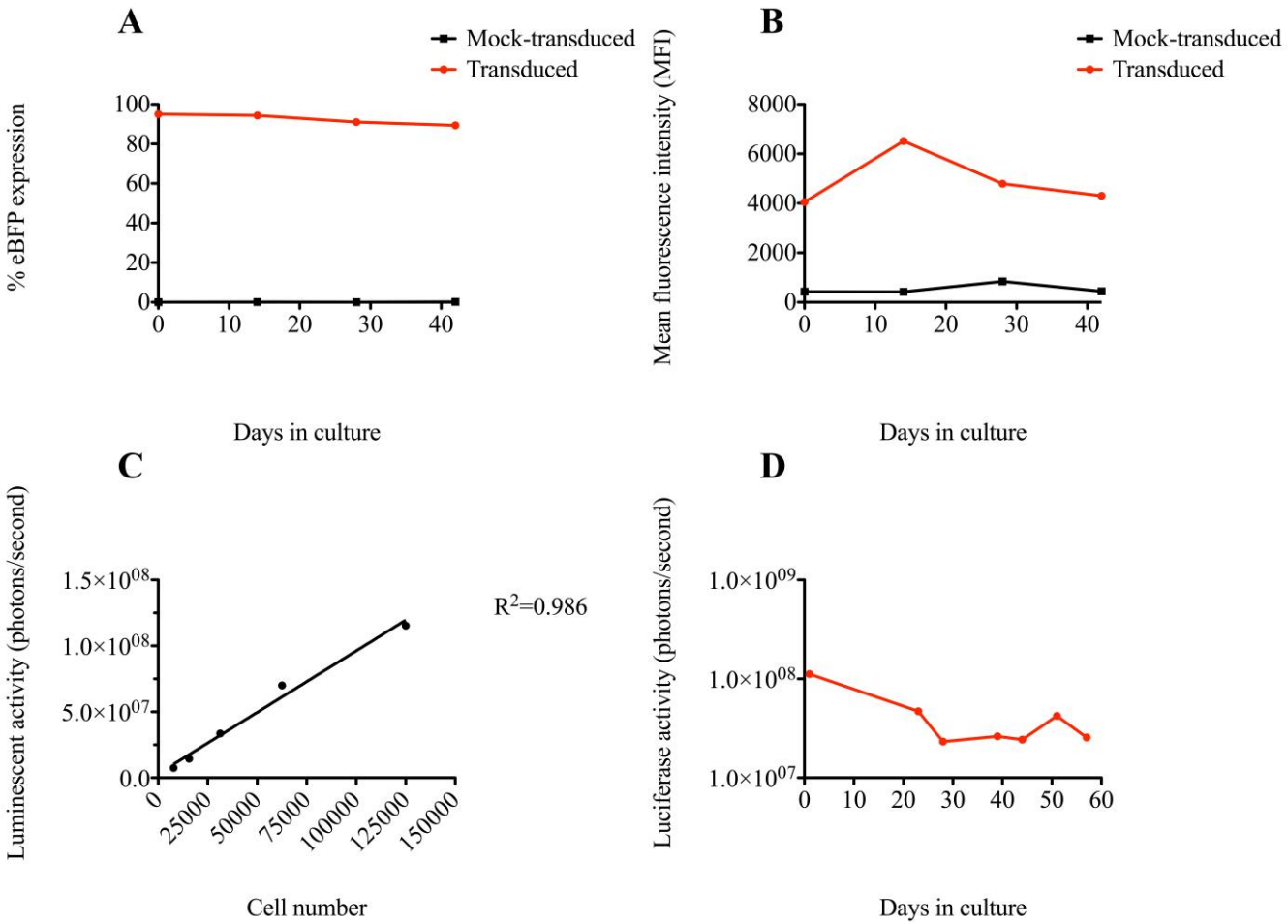

Figure 3-4: NALM-6-Luc characterisation. (A) % eBFP cell surface expression for transduced and mock-transduced NALM-6 cells as assessed by flow cytometry. Live cell population was gated according to FSC and SSC characteristics. **(B)** Corresponding MFI of transduced and mock-transduced cells. **(C)** Linear regression of luminescent activity (photons/second) for NALM-6-Luc cells at differing concentrations, performed immediately post sorting. **(D)** Luciferase activity (photons/second) for equivalent numbers of NALM-6-Luc cells kept in continuous cell culture for the duration of the experiment.

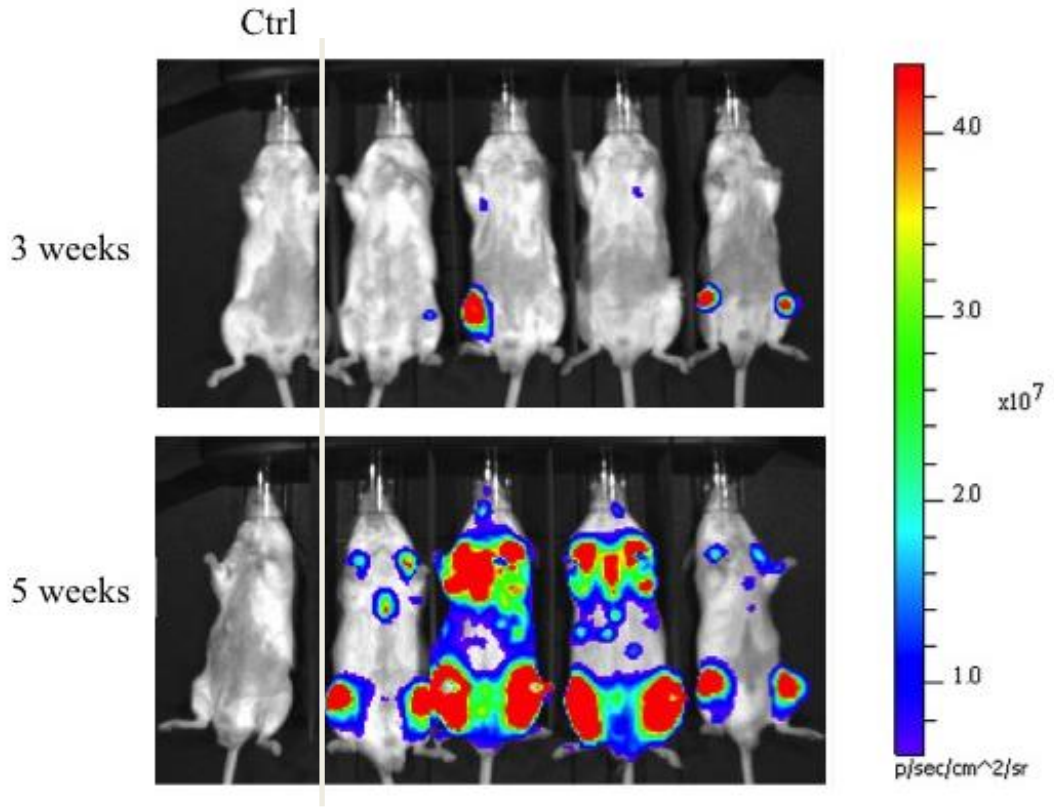

Figure 3-5: NALM-6-Luc disseminated xenograft model. SCID mice were injected with $1x10^6$ NALM-6-Luc cells via the lateral tail vein, or PBS as a control. Bioluminescent imaging was performed on a weekly basis. Representative images are shown at 3 and 5 weeks post tumour inoculation.

3.5.2 Anti-measles antibody titres persist in ALL patients following treatment

In order to contextualize the issue of humoral immunity and systemic measles virotherapy in ALL, quantification of anti-MV IgG antibody levels was performed in a cohort of 16 adult patients undergoing intensive immunosuppressive chemotherapy as participants in the UKALL14 trial (NCT01085617) – an international randomized trial for newly diagnosed adult ALL patients. Biobanked sera samples used for the purposes of this study were prior obtained following informed consent, in accordance with the UKALL14 ethically approved study protocol (REC reference: 09/H0711/90). All patients had been treated according to an intensive chemotherapy regime including high dose steroids, vincristine, daunorubicin, L-asparaginase, anti-B cell monoclonal antibodies, 6-mercaptopurine, cytarabine and cyclophosphamide. Day 3 of phase 1 induction is the earliest timepoint that sera was obtained following treatment initiation, with post-intensification samples being obtained following a minimum of 3 months of almost continuous, potentially immunosuppressive chemotherapy. Paired sera samples taken at a minimum of 2 different time points during phase 1 induction and post intensification were examined initially. A single patient had anti-MV IgG titres deemed insufficient for protective immunity against MV at the start of induction treatment, with sub-optimal titres persisting post intensification. One further patient had IgG titres just above the level at which they would be deemed MV immune at the start of treatment, which fell to just below MV-immune levels (<200mIU/ml, IBL international) post-intensification. All other patients with paired samples from phase 1 induction and post intensification showed anti-MV IgG titres persisting at clinically significant levels during this time, despite the immunosuppressive chemotherapy that they received, with no significant difference between titres at these timepoints (D3 phase 1 induction: 2340 +/- 360.8 IU/ml; D18 phase 1 induction: 2531 +/- 71.50 IU/ml; D2 post-intensification: 2293 +/- 415.0 IU/ml; D16 post-intensification: 2046 +/- 516.6 IU/ml) (see Figure 3-6A and B). This data clearly demonstrates the potential significance of anti-measles antibody levels in adult ALL patients when systemic measles virotherapy is being considered as a novel treatment strategy, and suggests that innovative ways in which humoral immunity can be overcome to promote therapeutic success of this approach need to be closely considered.

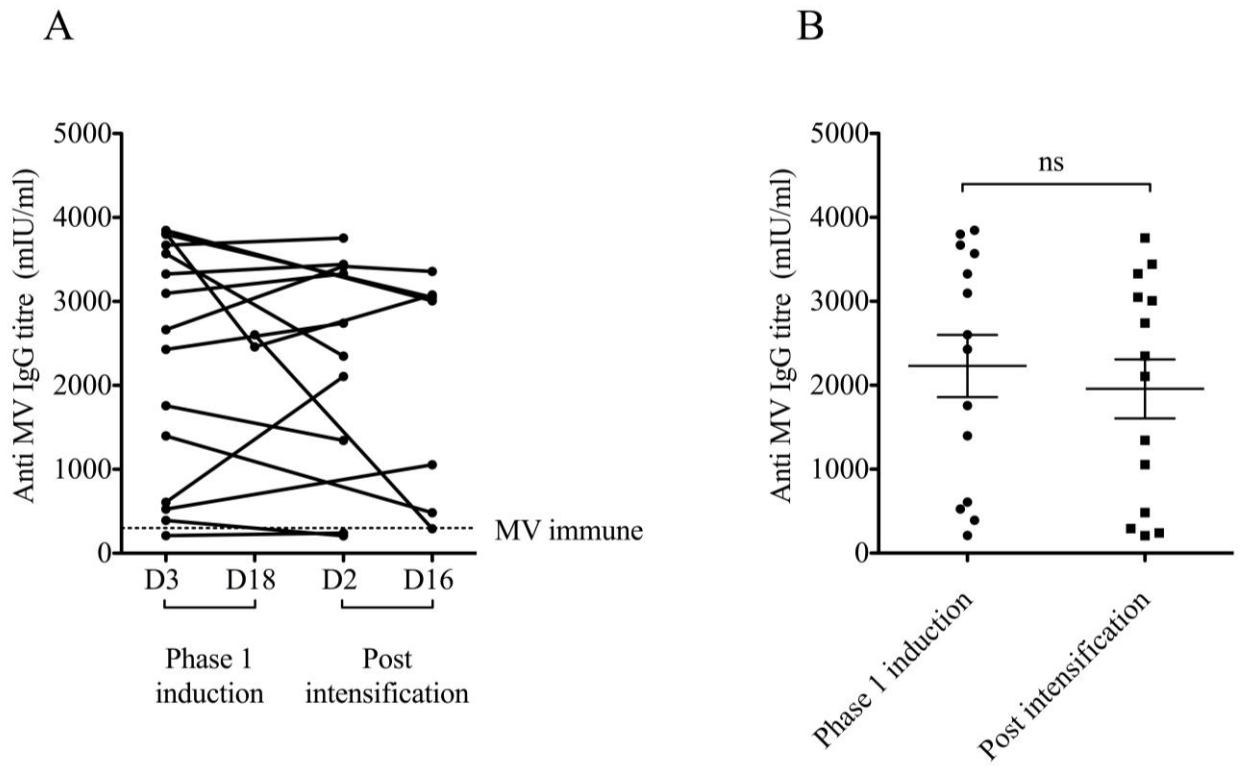

Figure 3-6: Intensive immunosuppressive therapy for ALL does not suppress anti-MV IgG production in patients on the UKALL14 trial. (A) Graph showing anti-MV IgG titres as quantified by ELISA. Paired sera from 16 patients participating in the UKALL14 trial were evaluated at a minimum of 2 time points (x-axis). Each dot represents a value, with a line connecting each patient's individual values. The dotted line represents the level at which a human is considered immune to MV infection. **(B)** Graph showing individual values with mean (horizontal line) and SEM of anti-MV IgG for the 12 patients with samples from the earliest (day 3 phase 1 induction) and latest time points (post intensification). There is no statistical difference between the two time points.

3.5.3 BM-MSCs support MV infection ex-vivo

Next, MSCs were prepared from normal human BM and their appropriate characteristics were demonstrated. To confirm the susceptibility of BM-MSCs to MV infection ex-vivo, we evaluated cell surface expression of the known MV receptors CD46, SLAM and Nectin 4 by flow cytometry (see Figure 3-7A-D). Positive controls for CD46, SLAM and Nectin 4 were Raji, Vero-SLAM and MCF7 cell lines respectively. BM-MSCs consistently expressed CD46 – the receptor for oncolytic vaccine strain MV, whilst the MV wild-type receptor SLAM, and the epithelial receptor Nectin 4 were negative.

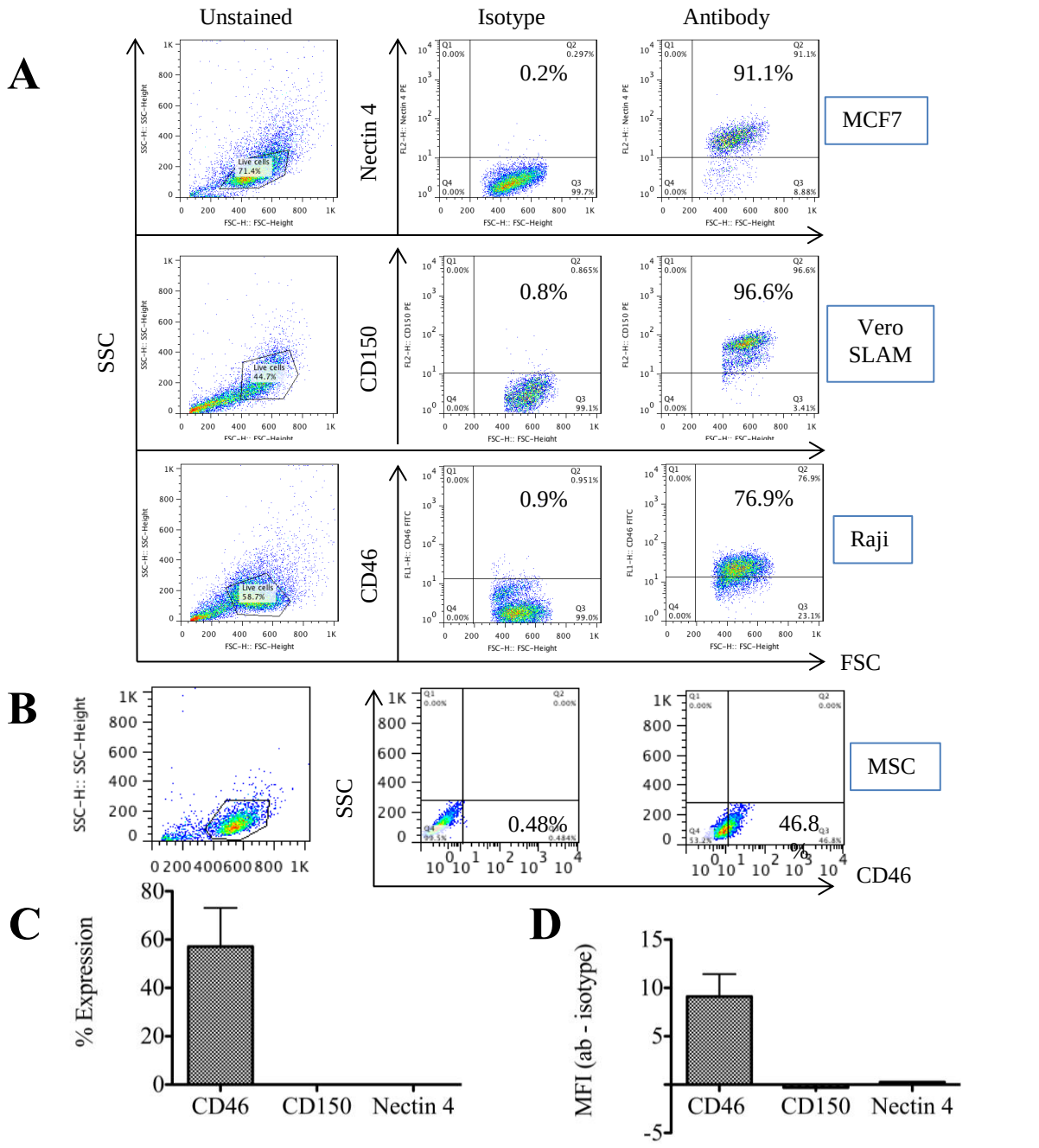

Figure 3-7: MV receptor expression profile of BM-MSCs. **(A)** Representative plots showing negative (isotype) and positive controls for Nectin 4, CD150/SLAM and CD46 using MCF7, Vero-SLAM and Raji cells respectively**. (B)** Representative plots showing MSCs stained with IgG1 FITC or CD46 FITC. (**C**) Bar chart showing mean percentage MV receptor expression on BM-MSCs and (**D**) mean fluorescent intensity (MFI) of antibody stained cells (minus isotype MFI). For CD46 N=5 and data is shown as mean +/- SEM. For CD150 and Nectin 4, N=1.

3.5.4 BM-MSCs can act as viable MV producing units

Next, I determined the optimum multiplicity of infection (MOI) and time-point post-infection, at which maximal virus productivity occurs with minimum BM-MSC death. BM-MSCs were infected with MV-NSe-GFP at MOI 0.1, 1.0, 2.0, and 5.0 and visually compared for the extent of GFP positivity in cells at 24-hourly timepoints post infection. GFP positivity consistently showed a peak in intensity at 48 hours post infection (hpi). In addition, MV-H glycoprotein immunostaining was performed to demonstrate cell surface MV-H envelope glycoprotein expression. Cell surface MV-H glycoprotein expression correlated closely with cellular GFP expression, reaching maximal intensity at 48 hpi. Photomicrographs of representative experiments at 48 hpi with MOI 1.0 are shown in Figure 3-8 demonstrating MV cytopathy, with widespread multinucleate syncytia formation and GFP expression. After 48 hours, morphological evidence of cell death ensued. The viability of BM-MSCs was formally assessed by MTS assay. Figure 3-9A shows cell proliferation (relative to uninfected control cells) at each timepoint for each MOI. At MOI of 1.0 there was no significant difference in cell viability between timepoints, with relative cell proliferation remaining above 100%.

Assessment of viral genome, by RQ-PCR for MV-N mRNA was also performed using RNA extracted from MSCs infected with a range of MOIs, at 24-hourly timepoints post infection. Whilst there was a clear increase in MV-N mRNA with MOI 1.0 versus MOI 0.1 (see Figure 3-9B), increasing the MOI beyond this provides no additional benefit. Using MOI 1.0, there was a demonstrable peak in MV-N mRNA productivity at 48 hours post infection (see Figure 3-9C), which does not improve at later timepoints.

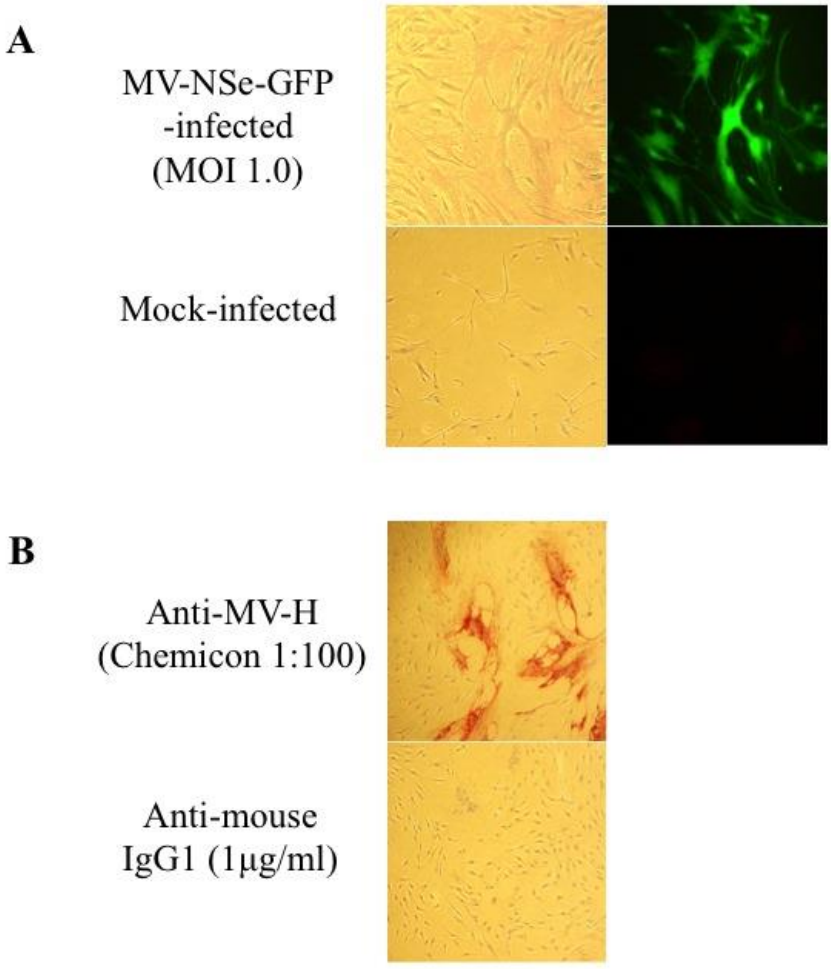

Figure 3-8: MV infectivity of BM-MSCs. (A) Representative photographs (standard and fluorescent) of MSCs infected with MV-NSe-GFP at an MOI of 1.0, taken at 48 hours post infection. Corresponding photographs for mock-infected cells are shown below. **(B)** Representative photographs of MSCs infected with MV-NSe at MOI 1.0 (48 hours post infection) and stained for MV-H glycoprotein. To account for non-specific staining, infected cells stained with isotype only are represented below.

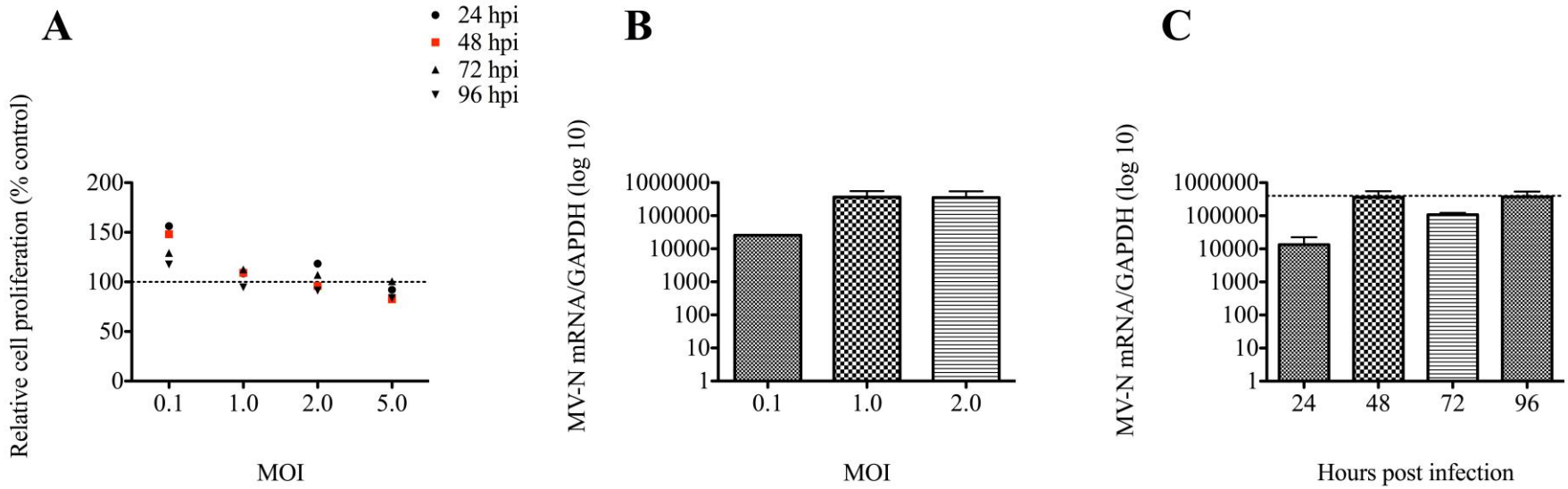

Figure 3-9: MSC viability and MV-N mRNA productivity post infection. (A) MSCs were infected, or mock-infected, at a range of multiplicities of infection (MOI) and cell proliferation of infected cells relative to their mock-infected counterparts was assessed using MTS assay, at 24-hourly intervals post infection. **(B)** MV-N mRNA levels were assessed by RQ-PCR performed using RNA extracted from MV-infected MSCs for a range of MOIs (data shown is for 48 hours post infection) and **(C)** at 24-hourly intervals post infection (data shown is for MOI 1.0). N=3 independent experiments performed in triplicate. GAPDH was used as the housekeeping gene in all cases, with equivalent mock-infected cells used as the calibrator. Data shown is mean +/- SEM.

For further assessment of MSC virus productivity, cell-associated and supernatant virus output was quantified on MSCs infected using MV-NSe at MOI 1.0, by $TCID_{50}$. In line with previous data, virus titrations confirmed a peak in cell-associated virus productivity at 48 hpi (see Figure 3-10A). Notably, there was almost no virus shed into the supernatant. Finally, I demonstrated that upon reducing virus-mediated cell-cell fusion and multinucleate syncytia formation by the post-infection addition of FIP to cell culture medium, cell-associated virus titres were higher at all timepoints post infection (Figure 3-10B), with a trend towards statistical significance at later timepoints. Trypan blue viability assay confirmed a reduction in MV-specific cell death for cells cultured with FIP as compared to those cultured without (Figure 3-11). Taken together, these data confirmed optimal conditions for ex-vivo BM-MSC loading using an MOI of 1.0 for cellular MV infection, and utilizing the post-infection addition of FIP to tissue culture media to improve cell viability and productivity. For in vivo experiments, cellular harvest was performed at 24 hours post ex-vivo loading, prior to optimal virus production at the 48 hour time point.

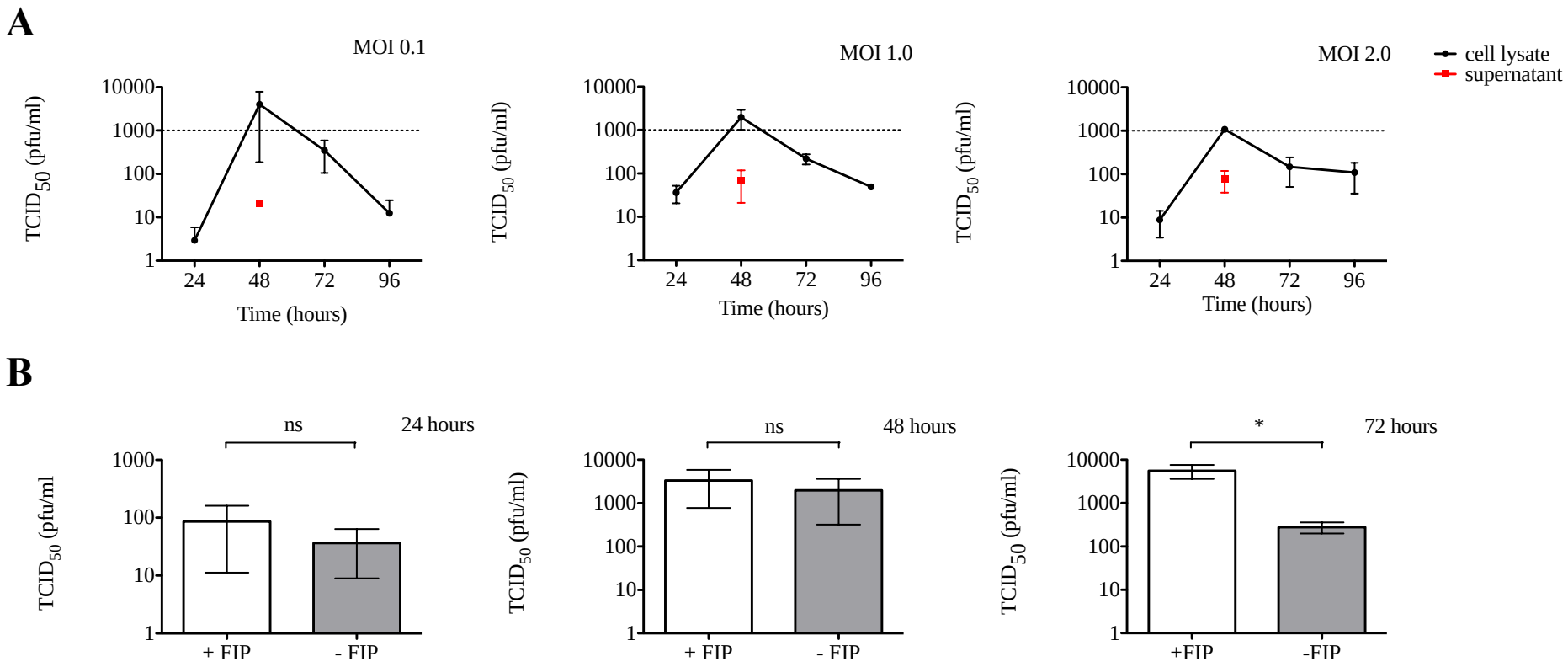

Figure 3-10: MSC cell-associated and released virus titres. (A) At 24-hourly timepoints, $TCID_{50}$ virus titrations were performed on MSC cell lysates (black) and tissue culture supernatants (red) from cells infected using a range of MOIs. **(B)** The effect of FIP on cell-associated $TCID_{50}$ virus titrations is shown using cells infected with MOI 1.0, taken at 48 hours post infection. N=3 independent experiments performed in duplicate. Mean +/- SEM are shown. The effect of FIP has been analyzed using an unpaired t-test. For 72 hpi *p=0.05.

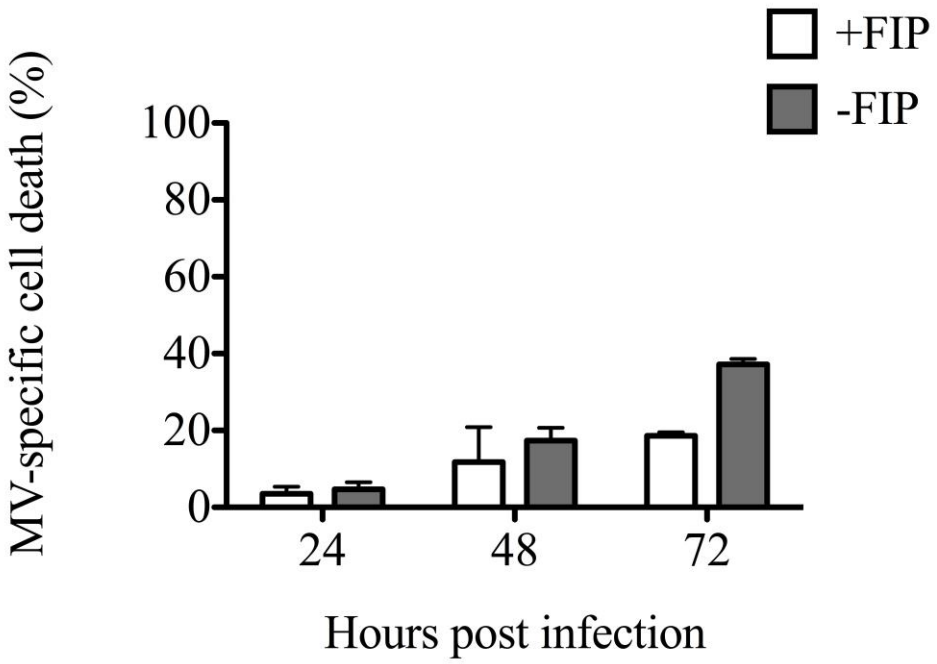

Figure 3-11: The effect of FIP on viability of MV-infected MSCs. MSCs were infected at MOI 1.0 and trypan blue viability assessment was performed every 24 hours for 3 days. Mock-infected cells were also assessed and data is expressed as the amount of MV-specific cell death by subtracting the number of non-viable mock-infected cells from non-viable MV-infected cells, and expressing as a percentage of the total cell number. Data shown is mean +/- SEM. N=3 independent experiments.

3.5.5 In vivo localisation of MV-infected BM-MSCs

To evaluate the ability of ex-vivo loaded BM-MSCs to localize to established sites of ALL we used a previously characterized model of disseminated precursor B lineage ALL[19]. 6-8 week old SCID mice were injected with $1x10^6$ NALM-6 cells intravenously. After 3 weeks IBM sampling from the right femur in each animal confirmed co-expression of human CD19 and CD10, indicating tumor cell engraftment in all mice. Representative flow cytometry plots are shown in Figure 3-12A. Injection of MV-loaded carrier cells was performed 10 days later, to minimize the potentially confounding issue of BM-MSC homing towards injured tissues resultant upon the sampling method. Passage 3 BM-MSCs were loaded ex-vivo with a firefly luciferase expressing MV (MV-NSe-Luc) at MOI 1.0, and 24 hours post inoculation, cells ($1x10^6$ cells per mouse) were harvested and injected intravenously, with control mice receiving PBS alone. The fate of infected cells was tracked using bioluminescent imaging performed at 24-hourly timepoints for 10 days. Figure 3-12B shows representative images confirming early localization of MV-infected BM-MSCs to lung parenchyma, consistent with first pass entrapment as detailed by other groups[237,238]. However, by day two following BM-MSC infusion, there was re-localization of bioluminescence signal to the ALL-containing BM. As we know from previous experiments, that virus production was essentially confined to the intracellular compartment (with amounts of released virus being negligible), this data confirms the ability of MV-NSe-Luc to reach distant tumor targets when delivered intravenously within BM-MSC. Furthermore in 2/3 animals, bioluminescent activity co-localized within the contralateral BM from that used for IBM sampling, proving that homing was not solely related to bony injury resultant upon sampling methods. Attempts to directly demonstrate the presence of human MSCs within the murine BM by flow cytometry were unsuccessful, due to low input cell doses, and lack of long-term engraftment of systemically delivered MSCs as shown by others[239].

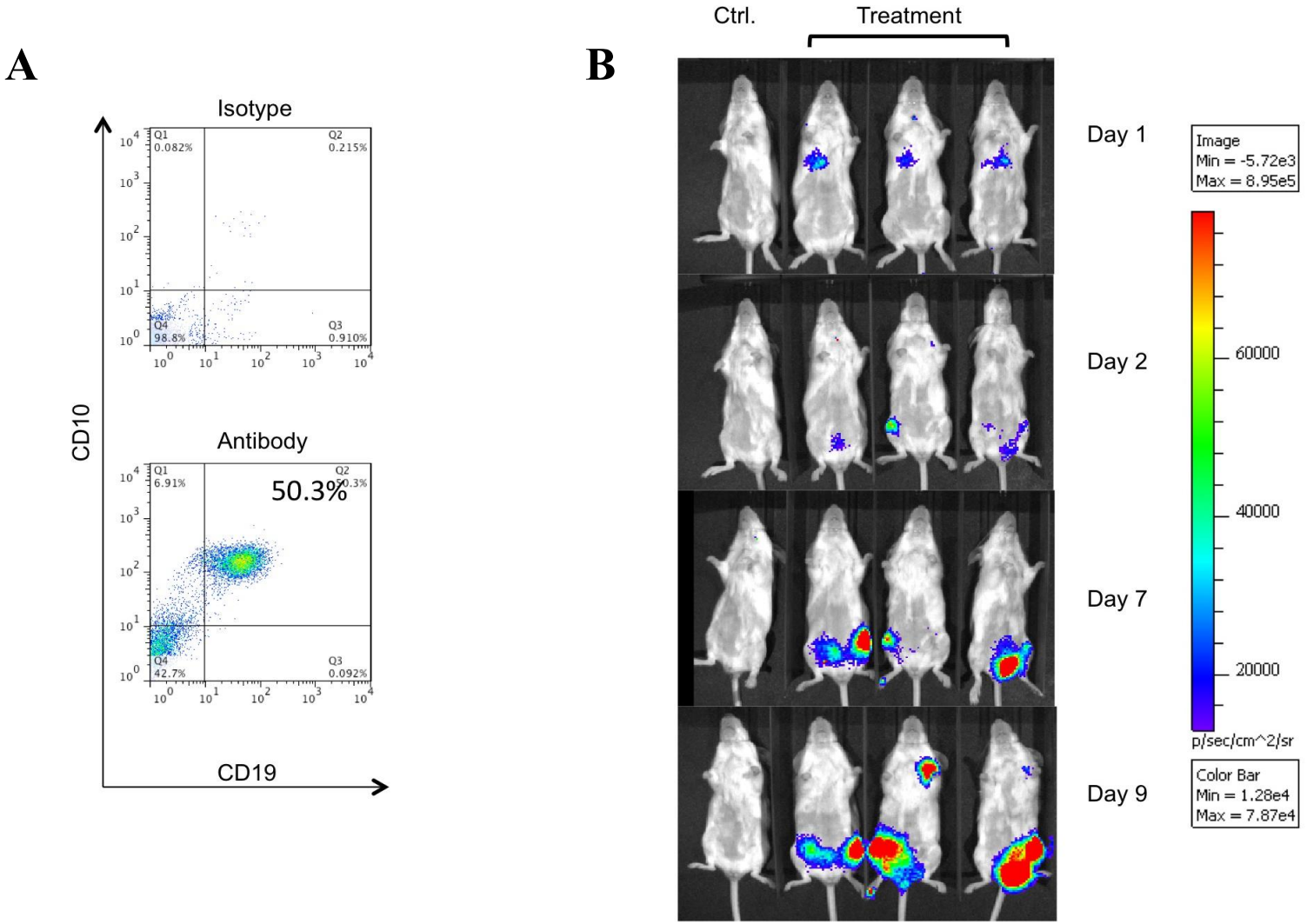

Figure 3-12: In vivo MV-NSe-Luc-infected MSC localisation. (A) Representative flow cytometry plots of murine BM confirming the presence of human CD19 (X axis) and CD10 (Y axis) - expressing leukaemia populations. Gating was of live cells based on FSC and SSC characteristics, with appropriate isotypes used as negative controls. **(B)** Representative bioluminescence images of SCID mice following systemic injection with MV-NSe-Luc-infected BM-MSCs. Mice receiving PBS only were used as controls to account for background luminescence. For treatment group N=3.

3.5.6 BM-MSCs allow successful hand-off of virus to tumour cell targets in the presence of humoral immunity

Next, the ability of BM-MSCs to deliver MV to ALL cells in the presence of pre-existing neutralising antibodies was assessed. Human anti-MV antisera (obtained from discard clinical samples identified as having high titre anti-MV antibodies present) were obtained. Anti-MV IgG was titrated in pooled, heat-inactivated sera using ELISA (see Methods – Chapter 2) and quantified at 490IU/ml. MV-loaded BM-MSCs or naked MV was treated with serial dilutions of high titre anti-MV antibody serum ex-vivo, before being overlaid onto the standard MV culture cell line, Vero. MV hand-off from BM-MSC to Vero was quantified by syncytia formation at 48 hours post overlay (Figure 3-13). Naked MV was very effectively neutralised by anti-MV IgG – with syncytia being evident only at very low concentrations of antibody (1:256 or higher dilution). When Vero cells were overlaid with MV-infected BM-MSCs, greater numbers of syncytia were seen at all antibody concentrations. Statistically significant differences were seen in numbers of syncytia for 1:256 and 1:1024 antibody dilutions. MV-infected BM-MSCs permitted MV 'hand-off', at high antibody concentrations (1:8 dilution), a five-fold higher concentration than the minimum concentration (1:256 dilution) permissive to infection when naked MV was used. These data confirm the ability of BM-MSCs to protect MV against antibody neutralisation in-vitro.

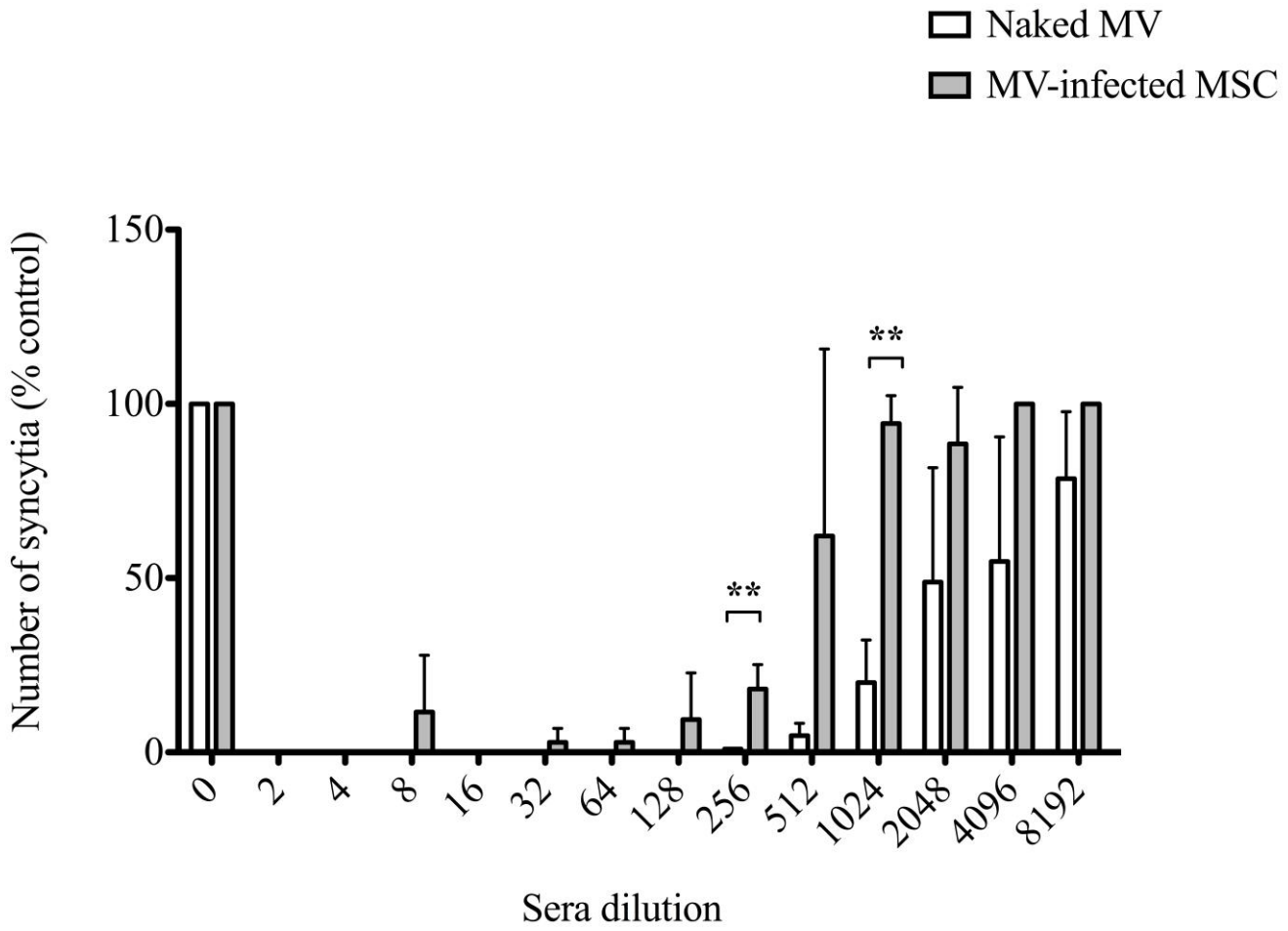

Figure 3-13: In vitro virus neutralisation in the presence of anti-MV antibody. Vero cell syncytia quantification at 48 hours post overlay with MV-NSe-loaded BM-MSCs or naked MV-NSe pre-treated with dilutions of high titre anti-MV antibody. Total numbers of syncytia from each well of a 96 well plate were counted. Data is represented as a percentage of virus control (MV or MV-infected cells with no serum pre-treatment; X axis) in relation to serum dilution (Y axis) for naked MV and MV-infected BM-MSCs, and shown as mean +/- SEM. N=6 from 3 independent experiments. Analysis uses the unpaired t-test. For 1:256 dilution, **p=0.047; for 1:1024 dilution, **p=0.0051.

Following this, I used a dual colour system to perform live-cell confocal microscopy, and allow for direct visualisation of virus 'hand-off' between NALM-6 ALL cells – stably transduced to express mCherry (see Chapter 3: Methods), and green MV-NSe-GFP-infected BM-MSCs. Representative still images are shown in Figures 3-14A and B, and demonstrate the different stages of heterofusion events between red NALM-6 cells and green MV-NSe-GFP-infected BM-MSCs. Figure 3-14A shows a series of images taking place over 20 minutes of co-culture (for full video see Appendix), with the diagrammatic representation of heterofusion shown in figure 3-14B. Figure 3-14C shows multiple episodes of the same process over a 3 minute timescale. In Figure 3-14A, a single NALM-6 cell is seen to transition from red, becoming yellow as heterofusion takes place, and subsequently green as MV-NSe-GFP hand-off occurs. Corresponding grey-scale images are shown beneath each fluorescent image here. In rare events, ALL cells were seen to turn green without evidence of fusion, and the presence of cell to cell nanotubule formation was identified. The live-cell imaging approach was used to probe the role of anti-MV antibodies in the BM-MSC-to-ALL cell fusion/hand-off process. As indicated in Figure 3-15A, cells were pre-incubated with anti-MV antibody containing serum, diluted either 1:4 (positive control, expected from data in Figure 3-13 to block fusion in both conditions) or 1:128 (the highest antibody dilution expected to clearly discriminate between the two conditions), or with FIP as an additional positive control. Figure 3-15A and B show the percentage of NALM-6 cells fusing with infected BM-MSCs, or ratio of mCherry:GFP respectively, following 80 minutes of co-culture. When anti-MV antibodies are absent, up to 40% of cells in contact demonstrated heterofusion within this time frame. Whilst fusion was predictably and significantly ablated in the presence of 1:4 serum dilution, or with FIP (positive control), no significant difference in heterofusion was observed in the presence of 1:128 serum dilution, with just over 20% of cell-cell heterofusion events remaining i.e. half the level of the negative control condition. To be certain that anti-MV antibody did not affect contact time between cells rather than prevent fusion, BM-MSC-to-ALL cell contact time in the presence of 1:128 serum dilution was quantified for at least n=125 events. The majority of heterofusion events were rapid, occurring within 20 minutes of co-culture (see Figure 3-15C) indicating that contact time between ALL and BM-MSC did not significantly change with the addition of anti-MV antibody. Taken together these data illustrate the ability of MV-infected BM-

MSCs to readily ‘hand off’ viable replicating MV to non-infected ALL cell targets, with BM-MSCs affording MV significant protection against neutralising antibodies in-vitro. A proportion of the virus ‘hand-off’ occurs via the rapid process of carrier cell-to-tumour cell heterofusion.

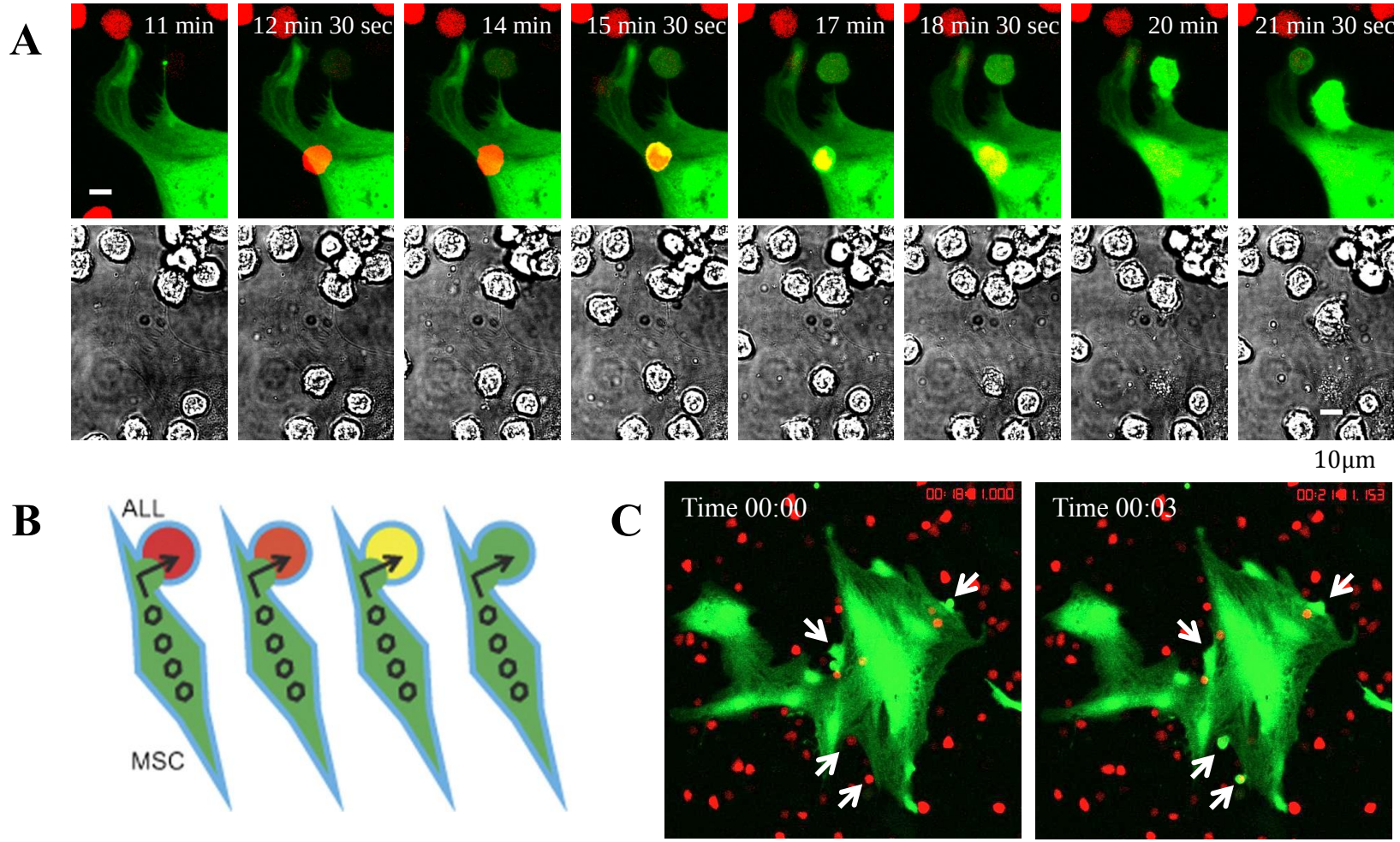

Figure 3-14: Carrier cell to tumour cell heterofusion and virus hand-off. (A) Representative live-cell confocal images of BM-MSCs at 48 hpi with MV-NSe-GFP (MOI 1.0), co-cultured with NALM-6 cells transduced with mCherry. Images show the different stages of a fusion event between a NALM-6 cell (red) and an infected BM-MSC (green). Scale bar represents 10 µm. **(B)** Representative diagram of heterofusion process (adapted from Horwiz et al. Blood 2014). (**C**) White arrows represent NALM-6 to MSC heterofusion events taking place over a 3-minute time period.

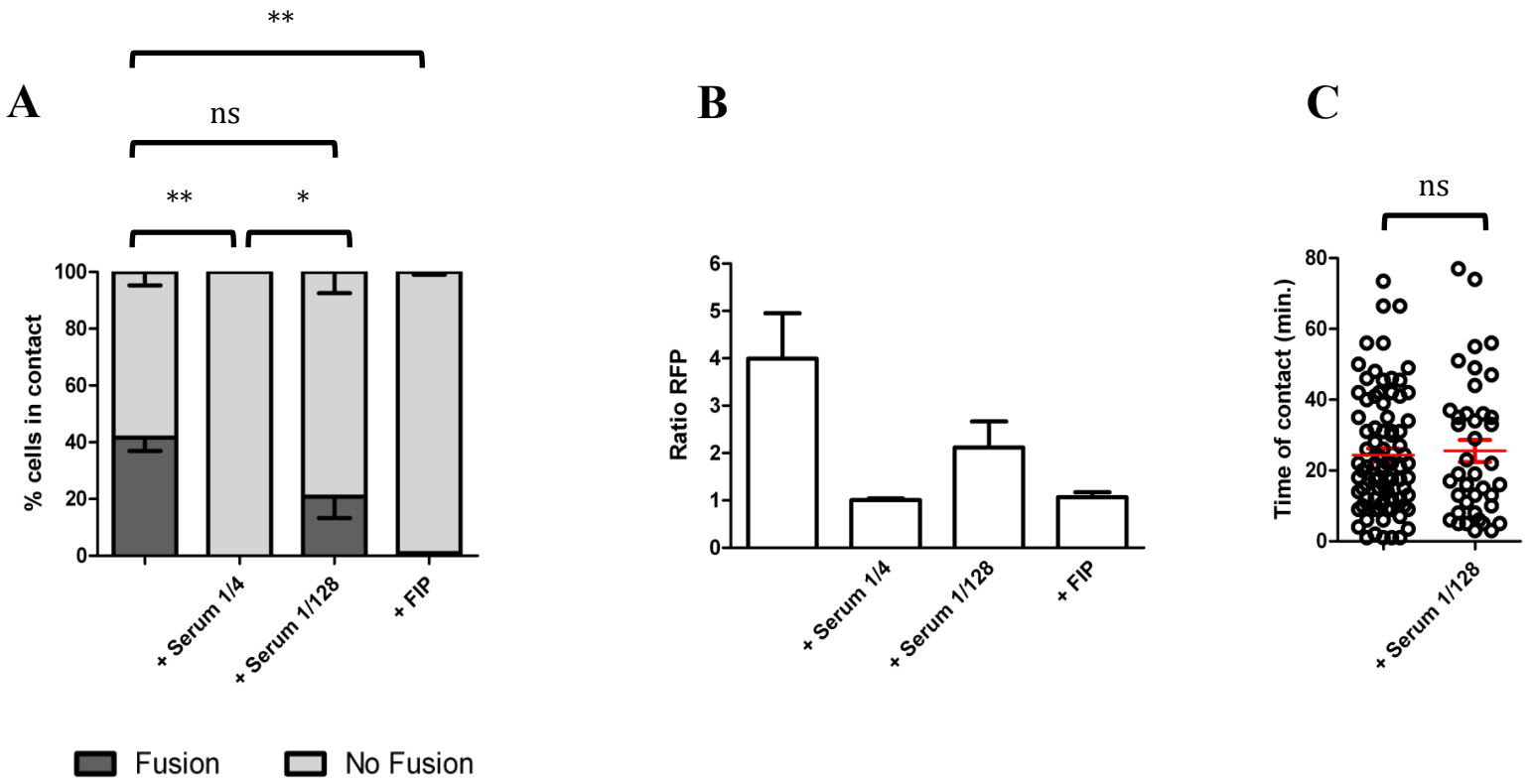

Figure 3-15: Quantification of heterofusion events. (A) Percentage of NALM-6 cells fusing (dark grey bars) or not (light grey bars) after establishing contact with infected BM-MSCs within 80 minutes of co-culture (first column). Columns 2-4 represent the test and control conditions, with dilutions of serum or FIP, as indicated. ** $p<0.01$; * $p<0.05$. **(B)** Ratio of red fluorescence in green syncytia over 80 minutes of co-culture. Columns are as for (A). **(C)** Contact time between NALM-6 cells and BM-MSC before fusion occurs, within 80 minutes of co-culture**.** When indicated, cells were also pre-incubated with anti-MV antibody serum 1:128. For each of the above conditions, n>125 cells were counted, data are from 6 independent experiments, with mean +/- SEM shown.

3.5.7 Therapeutic efficacy of BM-MSC-delivered oncolytic measles virotherapy in a disseminated precursor-B lineage ALL murine xenograft model

We then determined whether the *in vitro* findings could be translated into therapeutic efficacy in a SCID murine model of precursor B-lineage ALL. 6-8 week old SCID mice received intravenous injection with $1x10^6$ NALM-6 cells stably transduced to express firefly luciferase. On day 2, mice received intravenous injections of either $1x10^6$ plaque forming units (pfu) MV-NSe, $1x10^6$ BM-MSCs loaded ex-vivo (24 hours prior) with MV-NSe at an MOI of 1.0, or $1x10^6$ uninfected BM-MSCs. Treatments continued weekly, for a total of 6 weeks. Treatment groups were further divided into mice receiving passive immunization with 50IU anti-measles IgG, delivered intraperitoneally 3 hours before each therapy injection, or those receiving PBS as a control. Tumor burden was quantified by bioluminescent imaging. Overall survival (OS) was plotted using the method of Kaplan-Meier. Figure 3-16 shows the OS of all mice by treatment allocation. As expected, mice receiving BM-MSCs alone rapidly succumbed to ALL (median survival 53 days; range 42-62 days) Mice treated with naked MV had a significantly enhanced OS, consistent with our previously published data (median survival 91 days; range 69-96 days). When anti-MV antibody was administered to mice treated with naked MV, the therapeutic effect was abrogated (median survival 64 days; range 53-81 days). The difference between these groups was statistically significant (P=0.0013). Mice who received MV delivered within BM-MSCs had the best anti-tumor response (median survival >100 days) with all mice surviving to the end of the experiment, significantly superior to those receiving MV alone (P=0.0022). The administration of anti-MV antibody to mice receiving MV within BM-MSC did not abrogate the therapeutic effect at all.

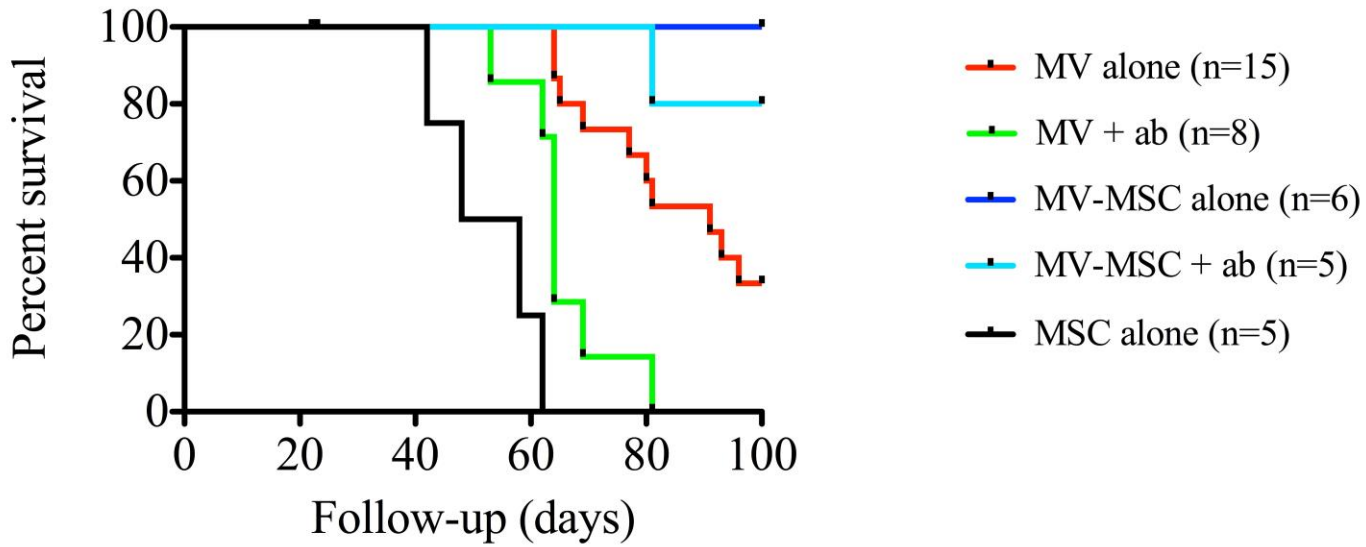

Figure 3-16: Therapeutic efficacy of cell carrier-delivered oncolytic measles virotherapy in a NALM-6 disseminated model of precursor B cell ALL. Kaplan Meier survival curves of mice bearing disseminated NALM-6 xenografts treated intravenously with a total of either $1x10^6$ pfu MV-NSe; $1x10^6$ BM-MSCs loaded with MV-NSe at MOI 1.0, or $1x10^6$ uninfected BM-MSCs. Mice in the relevant groups also received 50IU (100µl) of anti-MV IgG antibody (or 100µl PBS control) via the intraperitoneal route 3 hours before each MV injection. Data represent results from 3 independent experiments. N=2-5 per group.

Figure 3-17 shows representative bioluminescent imaging performed at equivalent timepoints, pictorially representing the relative tumor burdens for animals in the different treatment groups. Luminescent activity (relative light units (photons/second) is shown for all animals at week 6 as a scatter plot in Figure 3-18. Data for each animal is shown minus the mean average background luminescence values for control animals. The data in Figure 3-16 and Figure 3-18 confirm a statistically significant therapeutic benefit of delivering MV within BM-MSCs, in the presence of anti-MV humoral immunity. To ensure that any technical problems with ALL engraftment had not biased the results, flow cytometric evidence of ALL was sought at experiment termination in the BM of every animal in which bioluminescence did not show overt disease. Every mouse, even the long-term survivors, had some flow cytometric evidence of leukemia within the BM at termination. These data confirm our previous finding that systemically administered MV can successfully treat mice with aggressive disseminated ALL. We have shown that anti MV antibody abrogates this therapeutic potential. However, administration of MV inside BM-MSC carriers 'protects' the virus against antibody neutralization allowing an on-going therapeutic effect of systemically administered virus against disseminated tumor in the presence of high titre antibody.

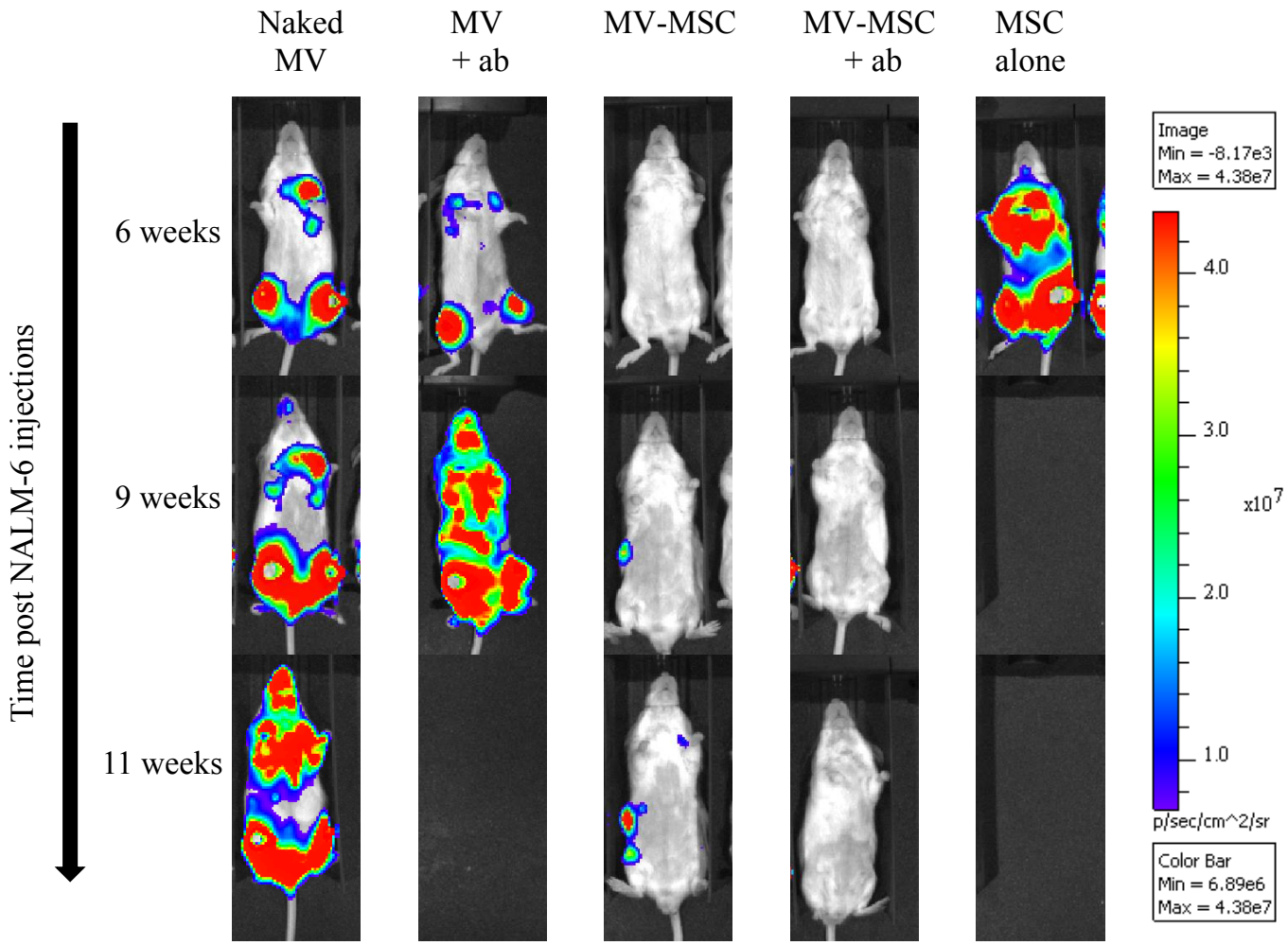

Figure 3-17: In vivo bioluminescent imaging. Representative bioluminescence images of SCID mice treated with naked MV, MV-infected BM-MSCs or BM-MSCs alone in the presence or absence of anti-measles antibody containing serum. The images demonstrate disease burden post ALL cell injection at 6, 9 and 12 weeks. Where no image is shown, this indicates that no mice remained in the relevant treatment group.

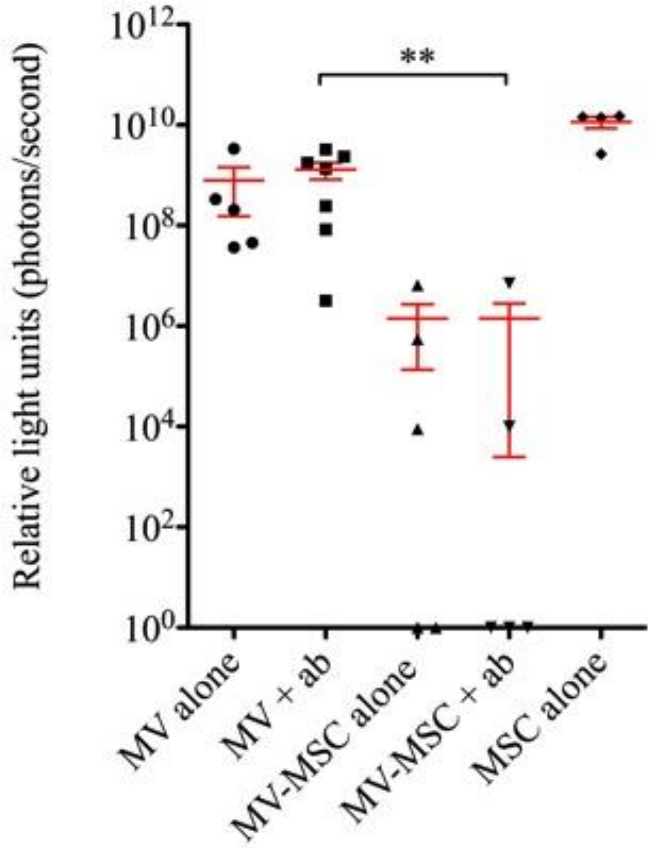

Figure 3-18: Quantification of tumour burden using bioluminescence. Scatter dot plot showing individual values for luminescence (photons/second) performed on each surviving animal in each treatment group at week 6. Values are represented minus background activity. Data shown are mean +/- SEM. To ensure data for all surviving animals could be plotted, zero or negative values were arbitrarily assigned a value of 1.0. **p=0.0051.

3.5.8 Discussion

We have previously shown that disseminated pre-B ALL xenografts in SCID mice are highly sensitive to MV-mediated oncolysis[19]. For our planned phase 1 trial in patients with relapsed ALL, the co-administration of various immunosuppressive anti-ALL agents such as cyclophosphamide, steroid or anti-B cell monoclonal antibodies alongside MV therapy is under consideration, with the aim of suppressing an anti-MV response. This rationale is based on murine data suggesting that clinically approved cyclophosphamide regimens can suppress humoral anti-MV and anti-VSV responses[185]. However, data here shows, on sera samples taken from a subset of UKALL14 trial participants before and after intensive immunosuppressive and myelosuppressive chemotherapy (including dexamethasone, anthracycline, vincristine, asparaginase, cyclophosphamide, and cytarabine) that clinically significant anti-MV antibodies persist, confirming the need for an alternative but clinically relevant strategy for circumvention. It is worth mentioning, that ELISA-based methods of detecting and quantifying anti-measles IgG levels were used here, and the neutralizing capabilities of these antibodies were assumed. However, in order to determine the neutralizing capabilities of such antibodies, functional assessment (eg. plaque reduction neutralization assay or $TCID_{50}$ assessment) would be required.

In contrast to primary ALL tumor cells, that typically die soon after MV infection[19], BM-MSCs are readily infectable by MV, retain viability at 48 hours post infection, and continue to produce virus. Attempts to accurately quantitate the level of cellular MV infection by using flow-cytometric based methods to assess extent of GFP positivity were challenging, due to autofluorescence of infected MSCs, and syncytia formation post infection (resulting in underestimation of values). Performing accurate quantification at very early timepoints post infection (in the presence of fusion inhibitory peptide to minimize syncytia effect) may be required in order to extrapolate more accurately the likely infectious burden at the time of cell harvest. Quantitative data in terms of the extent of plaque formation could also be obtained using image J (or equivalent) software. In MSC ex-vivo virus loading experiments detailed in this chapter, I used FIP to block cell-cell fusion and enhance viability and productivity of carrier cells until delivery to SCID mice. Alternatively, by introducing anti-F siRNA

into the carrier cells, MSCs could be infected with virus, but prevented from undergoing fusion before hand-off at distant tumour targets occurs.

MV-loaded BM-MSCs localized to sites of ALL in the BM of mice following intravenous infusion. Before moving to therapeutic studies in mice, I was keen to quantify the interaction between BM-MSCs and target ALL cells precisely. The timescale over which virus 'hand-off' occurs, and whether this process occurs by fusion or by cellular infection from released virus are important questions, as both parameters are likely to influence the potential success of this delivery approach in clinical trials. Live cell confocal imaging confirmed that the majority of 'hand-off' occurs via a process of cell-cell heterofusion, and occurs rapidly (within 20 minutes of co-culture), suggesting that virus delivery to tumor would take place *in vivo* long before BM-MSC viability is compromised and prior to any anamnestic response is generated. Live cell confocal imaging was also used to visualize the impact of antiviral antibodies on this process. Heterofusion events – impossible unless MV-H and F glycoproteins are both displayed at the surface of the BM-MSC - were predictably ablated in the presence of very high antibody concentrations and FIP, whilst at lower antibody concentrations heterofusion events remained plentiful. *In vivo*, passive immunization of animals prior to each MV administration was provided with injection of high titre anti-MV antiserum (50IU anti-MV IgG) – equating to an ultimate anti-MV antibody concentration several logs higher than the 300mIU/ml deemed 'high titre' in the clinical setting. This was sufficient to almost completely abrogate therapeutic responses to naked MV. However, successful delivery and therapeutic efficacy of BM-MSC-delivered oncolytic MV was demonstrated in this setting, suggesting successful MSC homing, virus hand-off, and ultimately therapeutic protection from repeated infusions of anti-MV antibody designed to model an anamnestic response. This is in contrast to the lack of abrogation of MV anti-tumor responses that we have previously described when anti-viral antibodies are delivered locally to MV-treated subcutaneous human B cell lymphoma xenografts[14], further highlighting the central importance of shielding the virus from anti-MV antibodies during systemic delivery to a disseminated malignancy. Unexpectedly, delivering MV within BM-MSC carriers also improved anti-ALL efficacy beyond that seen with naked MV. Since BM-MSCs administered alone granted no survival benefit, we hypothesize that the continuing MV replication

and production within the BM-MSCs, enhances the virus payload reaching distant tumor targets.

As previously stated, the ability to be able to detect MRD in the vast majority of patients with ALL provides a basis for early intervention with novel therapeutics such as oncolytic MV, prior to overt disease relapse. Bringing this novel delivery approach to the clinic would require clarity surrounding the virus quantification methodology, and how it can be accurately and reliably assessed so that the ultimate delivery dose of virus is reproducible. It is also worth noting that in the NALM 6 SCID mouse model of pre-B ALL, a common primary endpoint is hind limb paralysis – thought to be related to infiltration of disease within the spinal canal and CNS. Whilst the CNS was not directly examined at post-mortem to assess the presence of virus in these experiments outlined here, this would be an important finding in the context of the known MV-related CNS complications that can occur in heavily immunocompromised individuals post MV vaccination.

Chapter 4: Manipulating the MV genome to enhance localization of infected carrier cells

4.1 Background

4.1.1 MSC homing

Whilst many investigators have demonstrated that site-directed administration of MSCs can result in cellular localization, integration and engraftment – most often in injured tissues - such targeted administration is only practicable in a limited number of applications. For this strategy to be effectively utilized in the treatment of a disseminated haematological malignancy such as ALL, the localization of systemically administered MSCs to appropriate tissues such as BM and lymphoid organs should be demonstrated. Although the homing mechanisms of other cell types such as leucocytes and haematopoietic stem cells are well characterized, the mechanisms by which MSCs migrate to, engraft in, and exert local functional effects at the target tissue site are less well defined. Homing is thought to be a multi-step process involving numerous adhesion molecules and chemokines (see Figure 4-1). SDF-1α is a chemotactic cytokine that is known to play a major role in the homing and engraftment of haematopoietic stem cells and progenitor cells to the BM[240]. A number of studies have confirmed the interaction of SDF-1α and its receptor CXCR4 as central in mediating MSC homing to areas of tumour growth as well as normal BM stroma[241-243]. Levels of both SDF-1α and CXCR4 have been shown to be upregulated in stressed or injured tissues[244-246]. Whilst CXCR4 is expressed only at low levels (1-3%) on the surface of human BM-MSCs[243], in-vitro migration assays have repeatedly demonstrated the importance of this signaling pathway in the migration of MSCs, and it has been postulated that this is due to upregulation of functional intracellular CXCR4 to the cell surface in appropriate conditions[242,243,247]. Whether or not we can assume that the 'signals' provided by malignant haematopoietic cells are sufficient to stimulate the process of homing and tumour localization for MV-infected BM-MSCs remains to be determined.

4.2 Purpose of this chapter

Whilst numerous groups have demonstrated the migratory capacity of MSCs, low surface expression levels of CXCR4 on MSCs and downregulation of chemokine receptor expression during ex-vivo culture with concomitant decrease in chemotactic responses[248], present potential limitations to the therapeutic utility of these cells. Other groups have demonstrated that CXCR4 overexpression by retroviral vector transduction produces enhanced MSC homing and stromal engraftment[249]. Thus, in anticipation of potential limitations of using heavily manipulated MSCs to deliver vaccine MV to distant tumour targets, and as a means of improving the use of MSCs as vectors for viral delivery, this chapter explores the generation of a novel strain of MV expressing the human chemokine receptor *hCXCR4* gene as an additional transcription unit within the viral genome. The aim of this approach was to promote hCXCR4 surface expression on infected cell carriers, thereby enhancing trafficking, and ultimately improving therapeutic outcomes of the MSC cell carrier approach to virus delivery. As there is a high level of homology between murine and human CXCR4 (>90%), the generation of a novel strain of MV expressing the *hCXCR4* gene was thought unlikely to be a hindrance to the application of this virus in murine models of pre-B ALL. The work carried out in this chapter was performed in parallel to early ex-vivo MSC virus loading experiments detailed in Chapter 3, using standard vaccine strains of MV. Successful localization of MV-NSe-Luc-infected MSCs to the BM in pre-clinical SCID mouse models of disseminated precursor-B lineage ALL had not been demonstrated prior to commencement of the work outlined in this chapter. Furthermore, pre-clinical therapeutic efficacy of the BM-MSC carrier approach to systemic delivery of unmanipulated MV-NSe strains had not been demonstrated at the time this work was initiated.

4.3 Hypotheses

a. MV-infected BM-MSCs will show sub-optimal localization to tumour targets within the murine BM, due to downregulation of chemokine receptors during ex-vivo culture.
b. MSCs infected with a *hCXCR4*-expressing oncolytic MV may upregulate trafficking to tumour sites and enhance tumour killing.

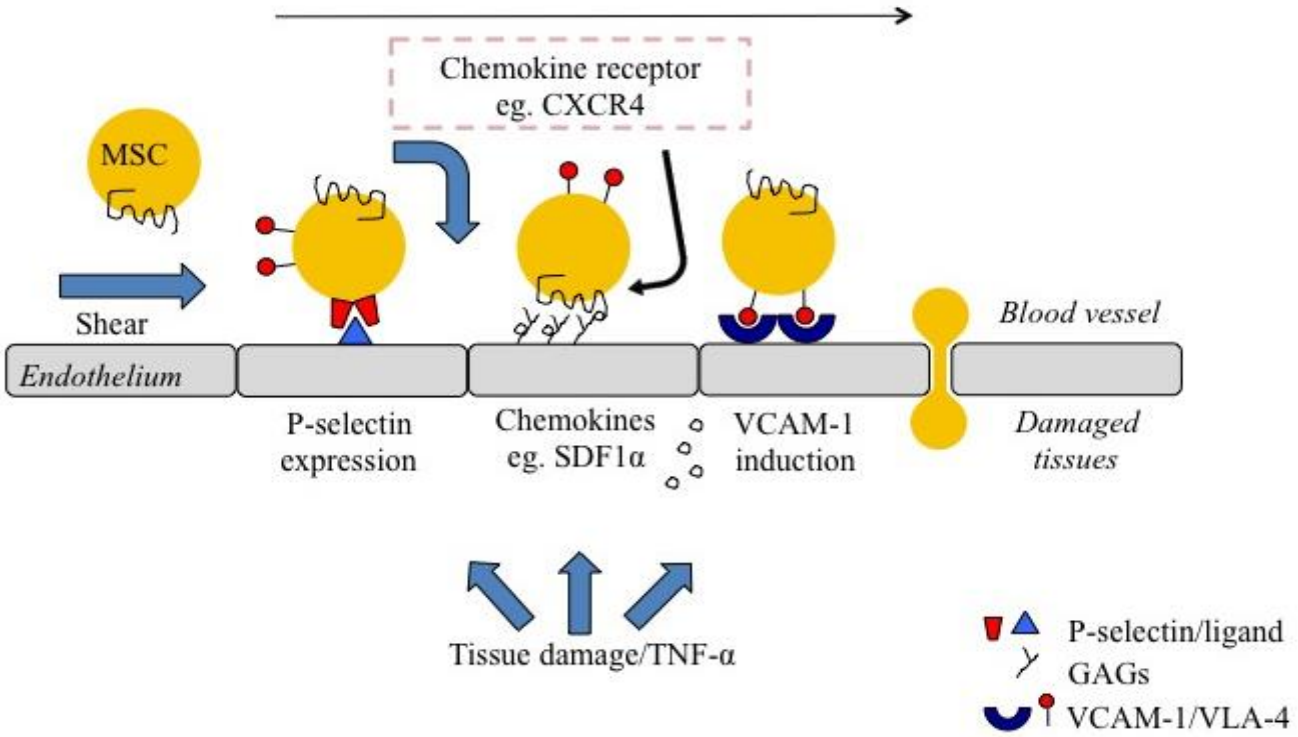

Figure 4-1: Mechanisms of MSC trafficking (adapted from Fox et al. 2007). VCAM-1: vascular cell adhesion protein 1; VLA-4: very late antigen 4 (integrin alpha4beta1); GAGs: glycosaminoglycans; TNF-α: tumour necrosis factor alpha.

4.4 Methods

4.4.1 TOPO TA cloning

The *hCXCR4* gene was PCR amplified from a human CXCR4 cDNA containing vector (Cambridge Bioscience Ltd, Cambridge, UK) using the following primers tailed with MluI and AatII restriction sites at the 5' and 3' flanks respectively (underlined):

CXCR4 s 5'-atgctgacgcgtgATGTCCATTCCTTTGCC-3'
CXCR4 a 5'-tgaccagacgtccTTAGCTGGAGTGAAAAC-3'

The PCR product was ligated into pCRII-TOPO cloning kit and the insert verified by sequence analysis. Both pCRII-TOPO-CXCR4 and a previously generated plasmid encoding a GFP expressing NSe strain of MV (p(+)MV-NSe-GFP) were restriction digested using MluI and AatII restriction enzymes, and the CXCR4 insert and MV backbone obtained by QIAex II gel purification of DNA unexposed to UV light, prior to ligation to produce p(+)MV-NSe-CXCR4. Bacterial transformation was performed using One shot® TOP10 competent cells, by adding 1 to 5ul ligation reaction directly to a vial of competent cells and incubating on ice for 30 minutes, heat-shocked at 42°C for 30 seconds, and then adding 250µl of pre-warmed SOC medium to each vial. Vials were then placed in a shaking incubator at 37°C for 1 hour at 225 rpm. LB agar plates containing 100µg/ml ampicillin were spread with 20-200µl of each transformation reaction, inverted and stored in a bacterial incubator at 37°C overnight. Colonies were picked with a sterile pipette tip and transferred to 2mls LB broth to form a starter culture, and placed in the shaking incubator at 37°C for 3-4 hours, before being transferred to 50mls of liquid culture medium and left in the shaking incubator overnight. The following morning, liquid culture medium was decanted and centrifuged at 4000rpm for 20 minutes at 4°C (no brake). Supernatant was discarded and bacterial pellet was used for DNA extraction using the HiSpeed Plasmid Midi Kit.

4.4.2 Rescue of MV from cloned cDNA

Using Lipofectamine (Invitrogen, Paisley, UK), Vero-SLAM cells infected with a T7 RNA polymerase-expressing modified vaccinia ankara virus were co-transfected with full-length cloned MV p(+) cDNA with plasmids encoding the MV polymerase complex (pCG-L, -N and -P)[150,250] in OptiMEM® GlutaMAX (Invitrogen, Paisley, UK). After 72 hours, the supernatant was overlaid onto fresh Vero-SLAM cells. Individual syncytia typical of MV mediated cytopathology were transferred to wells containing Vero cells and MV constructs were subsequently harvested in OptiMEM®.

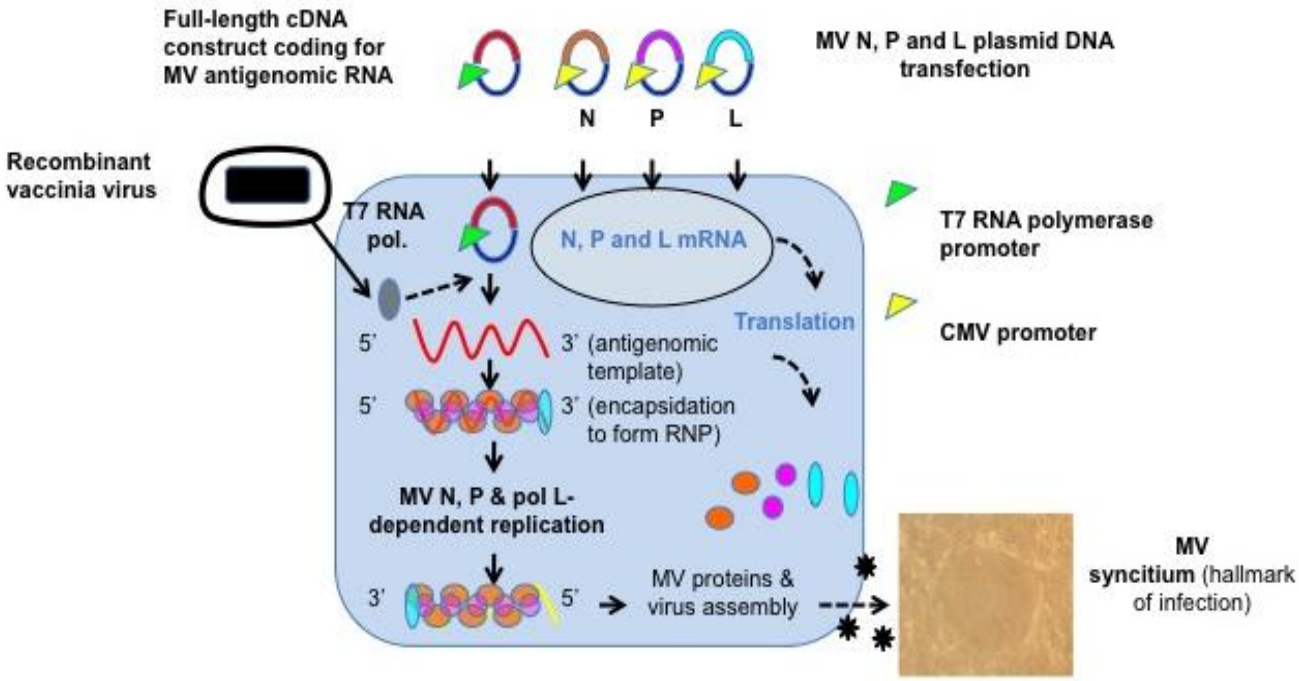

Figure 4-2: Rescue of MV from cloned cDNA. Schematic representation of methodology, using a multiple plasmid transfection approach, with recombinant Vaccinia Ankara virus to provide T7 RNA polymerase. RNP: ribonucleoprotein complex.

4.4.3 Transwell experiments

24 well Transwell® plates with polycarbonate membrane-containing inserts (8.0μm pore size; 10μm membrane thickness) (Corning, NY, USA) were used for the purposes of the transwell experiments. On day 0, inserts were pre-coated with fibronectin (R&D systems, MN, USA) at a concentration of 1μg/ml for 3 hours at 37°C. MSCs were plated on day 0 in separate tissue culture flasks. On day 1, cells were infected at MOI 1.0 with MV-NSe-GFP, MV-NSe-hCXCR4 or mock infected under standard conditions. Post infection, cells were cultured in the presence of FIP at a concentration of 40μg/ml. On day 2 (24 hours post infection), cells were harvested, washed once with serum free DMEM (+ penicillin and streptomycin as previous; + 0.1% BSA) and counted. Cell suspension was made at $4x10^5$ cells/ml, and 100μl cell suspension was aliquoted per well to the appropriate transwell insert. For CXCR4 inhibition, AMD3100/Plerixafor (Sigma Aldrich, Poole, UK) was used to pre-treat the cells where appropriate at a concentration of 100μm for 1 hour at 4°C before being added to the appropriate transwell insert. In the lower chamber of the transwell plate, 600μl of DMEM/0.1% BSA (negative control); DMEM/30% FBS (positive control) or DMEM/0.1% BSA plus SDF-1α at the desired concentration were added on day 2 prior to positioning the loaded insert. Plates were cultured in a tissue culture incubator at 37°C and 5% CO_2 for 24 hours before removing the insert and fixing cells in 70% ice cold methanol for 10 minutes. Inserts were then washed once with PBS and stained with crystal violet (Sigma Aldrich, Poole, UK) solution at a concentration of 0.5% in 20% methanol for 1 hour at room temperature. Inserts were then washed with DI H_20 until water was running clear, and un-migrated cells were gently removed from the upper surface of the transwell insert using a cotton bud. Inserts were then air-dried and membranes removed and mounted onto microscope slides before enumerating number of migrated MSCs per 5 x high-powered fields (hpf).

4.5 Results

4.5.1 Human CXCR4 can be successfully cloned into the MV genome

Efficient replication of MV requires the viral genome to have a total number of nucleotides divisible by 6 (the "rule of six")[251]. Therefore changes to the total number of nucleotides in MV-NSe-GFP during insertion of *hCXCR4* were required to be

divisible by six. Following confirmation of the gene sequence of the *hCXCR4* gene (transcript variant 1), forward and reverse primers were designed for PCR amplification of the gene and insertion of MluI and AatII restriction enzyme sites respectively. To enhance restriction enzyme efficiency, primers were designed with 6 additional nucleotides adjacent to each restriction enzyme site. Using MluI and AatII, removal of the *GFP* gene from p(+)MV-NSe-GFP (753 nucleotides), and insertion of *hCXCR4* with the addition of MluI and AatII (1081 nucleotides) requires that a further addition of 2 extra nucleotides (along with the *hCXCR4* construct) takes place in order to adhere with the 'rule of six'. As detailed in chapter specific methods, the *hCXCR4* gene was PCR amplified with the appropriate primers. Site of *hCXCR4* insertion is shown in Figure 4-3, and the success of this approach was confirmed by restriction digest of the product (see Figure 4-4) and sequence analysis.

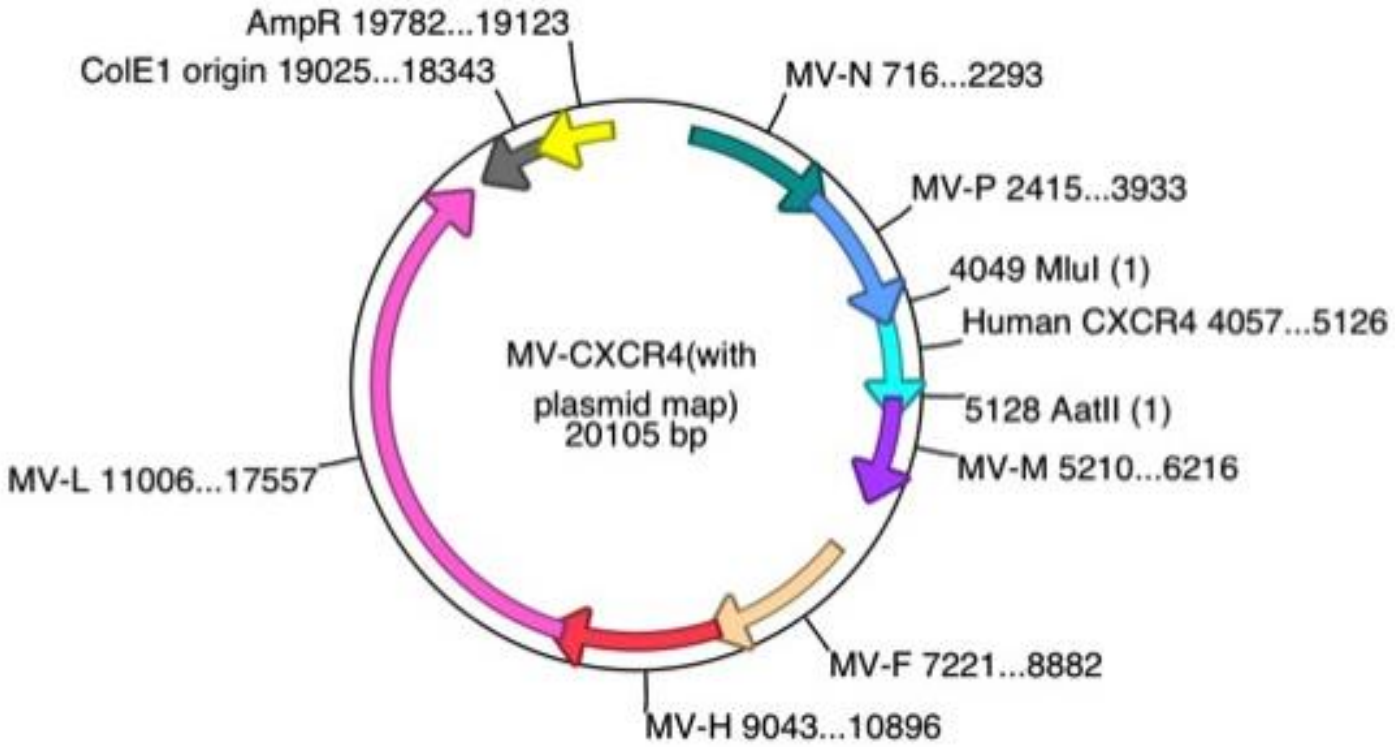

Figure 4-3: Plasmid construct of p(+)MV-NSe-hCXCR4. The *hCXCR4* gene is cloned downstream of the MV-P gene, in place of *GFP*, within the multiple cloning site (MCS) of the MV genome, using MluI and AatII restriction sites.

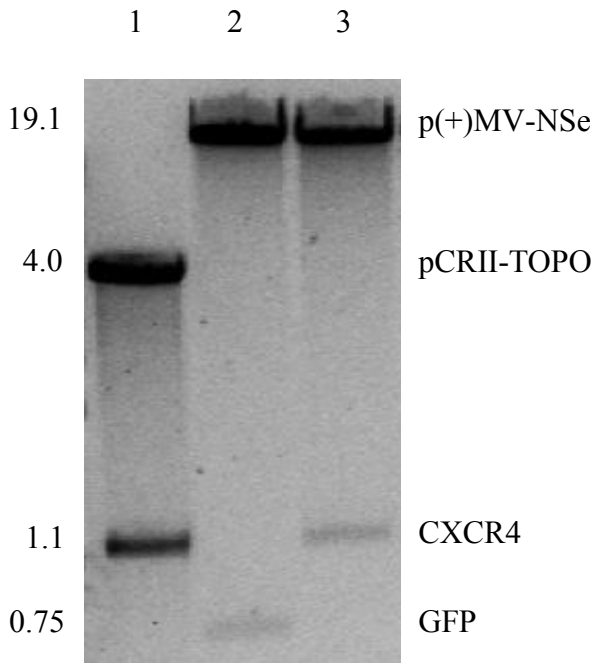

Figure 4-4: Diagnostic digest of p(+)MV-NSe-hCXCR4. hCXCR4 tailed with Mlu1 and AatII restriction sites was transferred from pCRII-TOPO-CXCR4 to p(+)MV-NSe by restriction/ligation. Successful transfer was confirmed by diagnostic digest with Mlu1/AatII of pCRII-TOPO-CXCR4 (lane 1), p(+)MV-NSe-GFP (lane 2) and p(+)MV-NSe-hCXCR4 (lane 3). The sizes of the bands obtained are represented on the left of the figure (Kb) with the identities of the bands indicated on the right.

4.5.2 MV-NSe-hCXCR4 can be rescued by reverse genetics from the full length cDNA construct

MV-NSe-hCXCR4 was rescued from p(+)MV-NSe-hCXCR4 by Lipofectamine (Invitrogen, Paisley, UK) co-transfection of Vero-SLAM cells infected with a T7 RNA polymerase expressing modified Vaccinia Ankara virus with the full length MV plasmid along with plasmids encoding the MV ribonucleoprotein complex (pCG-L, -N and -P) (see Methods Chapter 2.4.4). Three days post transfection, the supernatant was overlaid onto fresh Vero-SLAM cells, and typical cytopathic effects of MV infection were observed after 72 hours. Individual syncytia typical of MV-mediated cytopathology were transferred to wells containing Vero cells and MV-NSe-hCXCR4 was subsequently harvested in Opti-MEM (Gibco), titrated, and stored at -80°C until required.

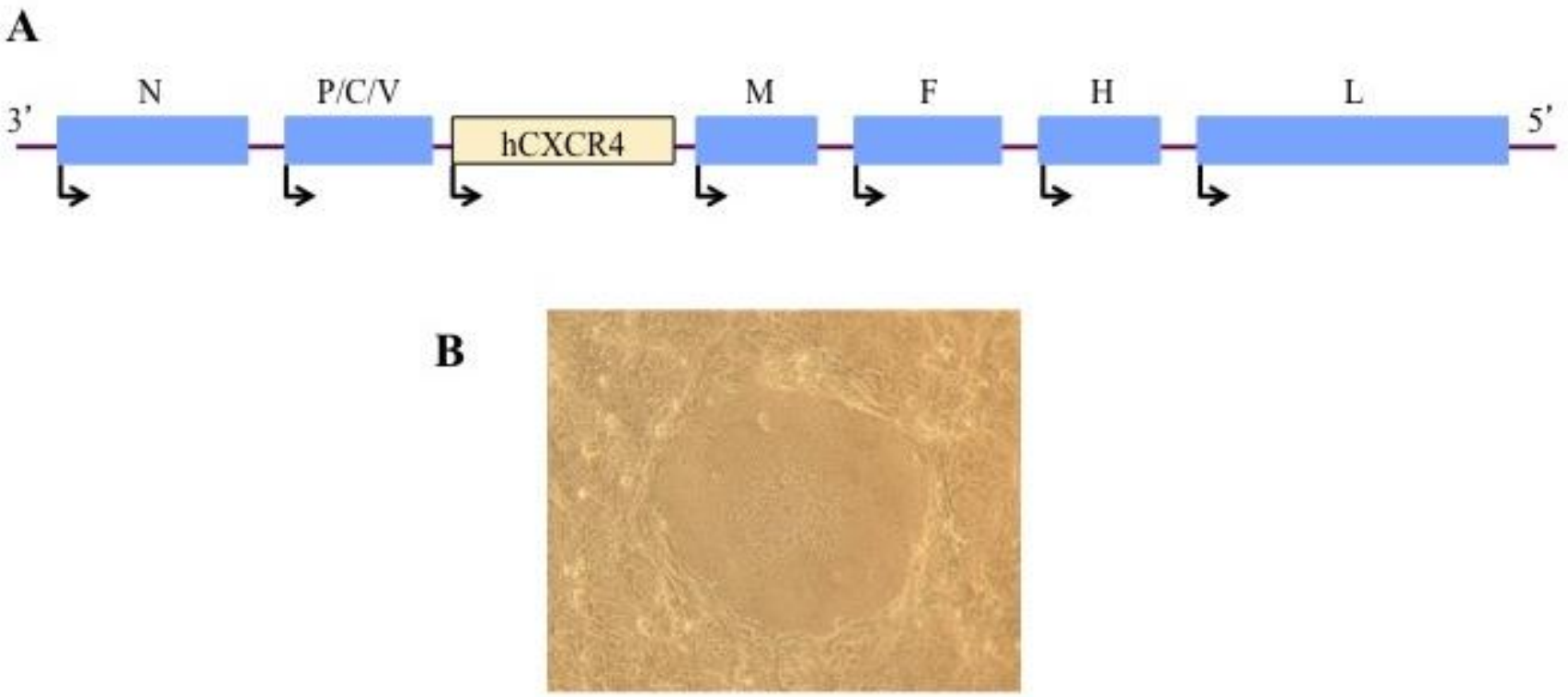

Figure 4-5: Rescue of p(+)MV-NSe-hCXCR4 from cloned cDNA. (A) Schematic representation of the p(+)MV-NSe-hCXCR4 plasmid. **(B)** Evidence of successful MV-NSe-hCXCR4 rescue from p(+)MV-NSe-hCXCR4 with giant multinucleate syncytia formation observed in Vero-SLAM cells at 72 hours.

4.5.3 Phenotypic and functional characterization of MV-NSe-hCXCR4

Following successful rescue and propagation of the hCXCR4-modified virus, one-step growth curves were performed on both Vero cells and BM-MSCs, using MV-NSe-GFP as the comparator virus. Using Vero cells, MV-NSe-hCXCR4 showed similar growth kinetics to MV-NSe-GFP. However, peak virus productivity was delayed by 24-36 hours, and viral titres were a log less than with the comparator virus – possibly as a result of the size and complexity of the transgene insert (see Figure 4-6A). Replication in BM-MSCs was retained, but again one-step growth curves confirmed a delayed and one log-reduced peak in productivity (see Figure 4-6B). Following this, confirmation of transgene expression in MV-NSe-hCXCR4-infected cells was performed. Initially, Vero cells were infected (or mock-infected) with MV-NSe-hCXCR4 at an MOI of 1.0 under standard conditions. At 48 hours post infection, cells were harvested, and stained for flow cytometric analysis. Whilst uninfected Vero cells did not express detectible hCXCR4 on the cell surface, those cells infected with the novel virus demonstrated a significant increase in the amount of cell surface hCXCR4 expression, with the chemokine receptor detectable in >85% of cells (see Figure 4-7A). For confirmation of cellular transgene expression, Vero cells and BM-MSCs were infected with MV-NSe-hCXCR4 at MOI 1.0, and chemokine receptor expression was sought by immunohistochemical staining. Whilst uninfected BM-MSCs and Vero cells showed no demonstrable hCXCR4 surface expression, both infected BM-MSCs and Vero cell populations showed syncytia formation and high levels of cell surface hCXCR4 expression localized to areas of syncytia (see Figure 4-7B).

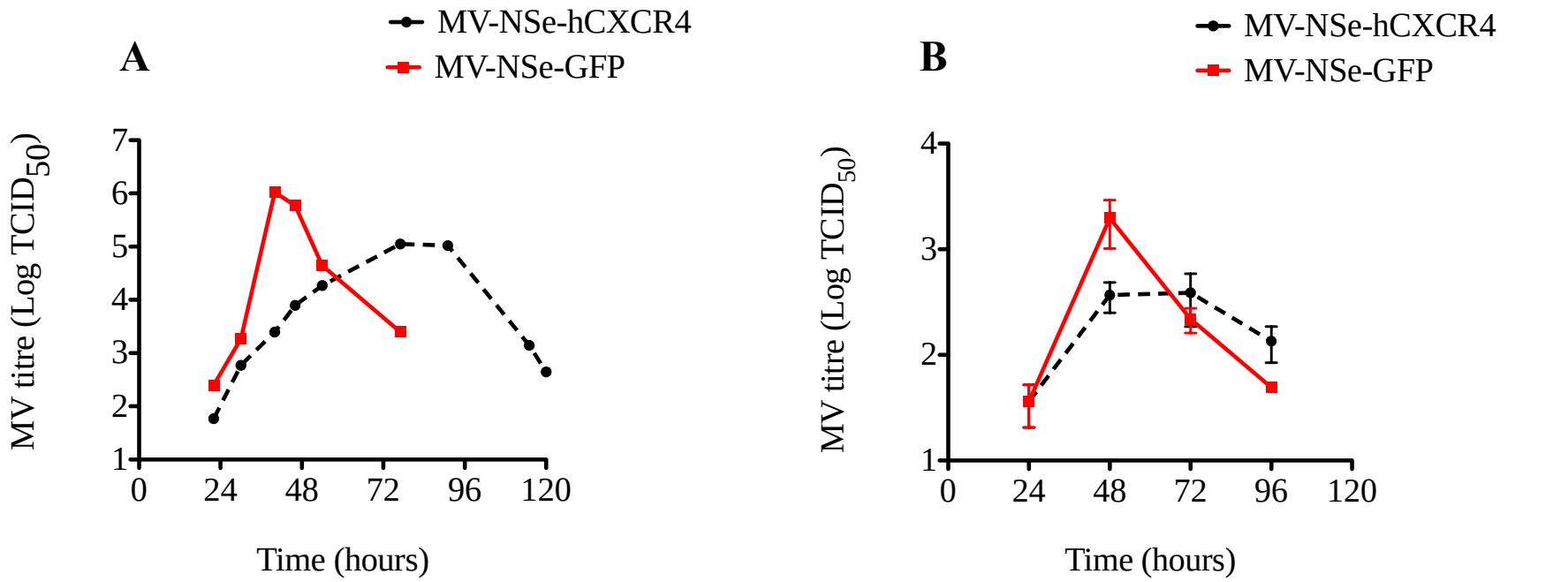

Figure 4-6: One-step growth curves for MV-NSe-hCXCR4. (A) Growth curves for MV-NSe-hCXCR4 (black) as compared to standard MV-NSe-GFP (red) on Vero cells and **(B)** BM-MSCs. In all cases, MOI 1.0 was used, and cells incubated in 37°C/5% CO_2 incubator. For Vero cells, N=1; for MSCs N=3 independent experiments. Data shown is mean +/- SEM.

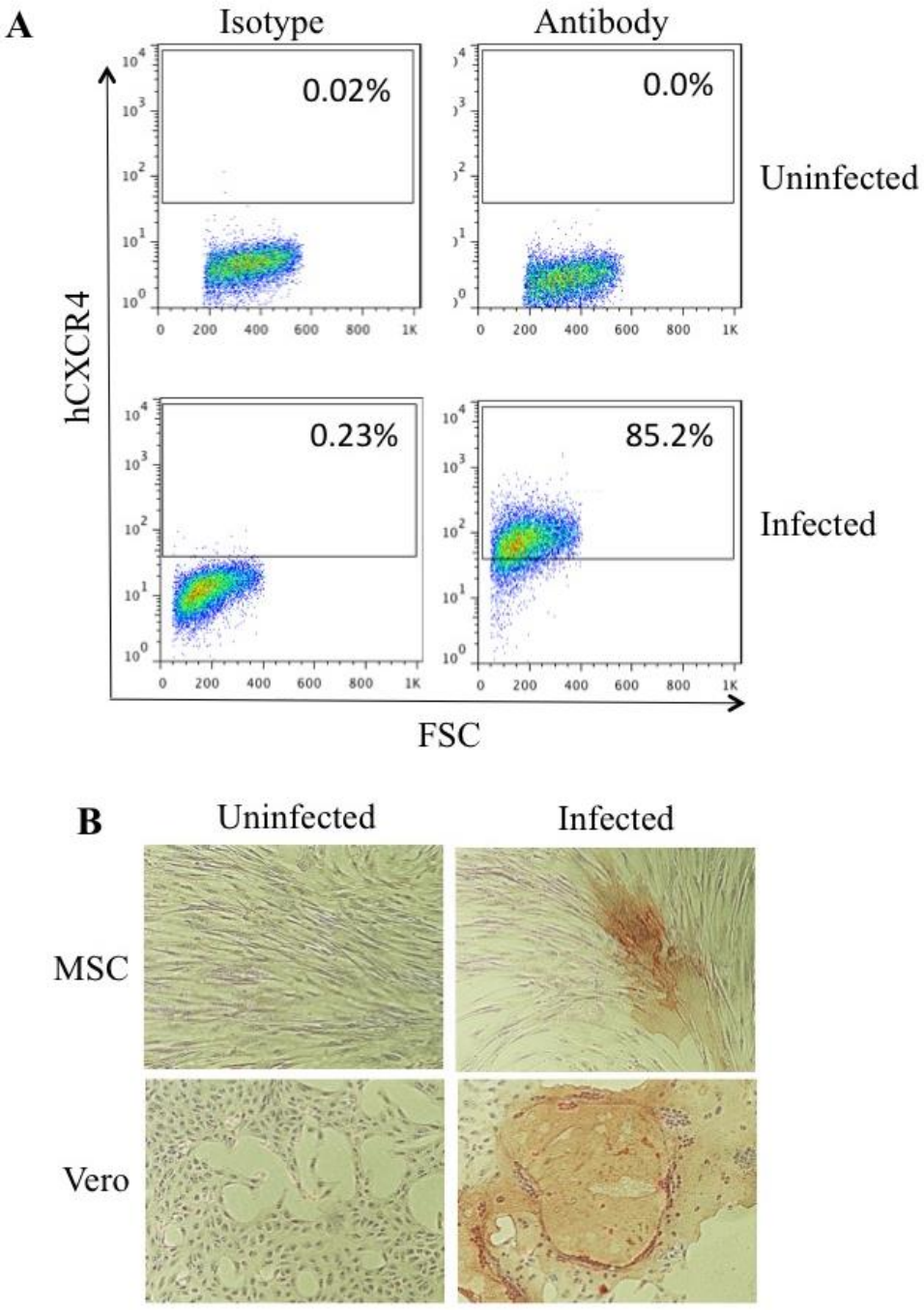

Figure 4-7: Cell surface hCXCR4 expression on MV-NSe-hCXCR4-infected cells. (A) Representative flow cytometry plots of MV-NSe-hCXCR4-infected (MOI 1.0) or uninfected Vero cells at 48 hours. Live cells were gated according to FSC and SSC characteristics. Corresponding isotypes were used as negative controls. **(B)** Representative photographs of MV-NSe-hCXCR4-infected (MOI 1.0) or uninfected BM-MSCs or Vero cells at 48 hours, following fixation and immunohistochemical staining for surface hCXCR4.

4.5.4 Migratory capacity of MV-NSe-hCXCR4-infected MSCs

To assess the effect of MV-NSe-hCXCR4 on MSC trafficking, BM-MSCs were infected with either the novel virus, or MV-NSe-GFP as a comparator at MOI 1.0, and assessment of in vitro cellular migratory capacity towards the CXCR4 ligand SDF-1α was performed using a transwell system (see Figure 4-8A-B). There was a clear enhancement in MSC migratory capacity towards an SDF-1α positive gradient, for those cells infected with the hCXCR4-expressing virus, as compared to the standard GFP-expressing virus, although for both percentage of cell migration and absolute numbers of migrated cells, differences between values failed to reach statistical significance when the two viruses were directly compared. Increasing the concentration of SDF-1α in the lower chamber promoted migration of cells infected with MV-NSe-hCXCR4, but no statistically significant difference was seen for the different chemokine concentrations. To assess the role of surface hCXCR4 expression in the migration of infected MSCs, MV-infected cells (at 24 hours) were pretreated with a non-peptide competitive antagonist of the CXCR4 receptor – AMD3100/Plerixafor, known to reversibly inhibit binding and function of SDF-1α with high affinity and potency[252-254], before being inserted into the upper transwell chamber and assessing migration towards an SDF-1α positive gradient 24 hours later (see Figure 4-9). Whilst there was no significant difference seen between the migratory capacity of MV-NSe-GFP-infected MSCs receiving pre-treatment or no pre-treatment, MSCs infected with MV-NSe-hCXCR4 showed significant abrogation in migratory capacity following pre-treatment with AMD3100, suggesting that for these cells, hCXCR4 is playing a major role in their migration towards SDF-1α in vitro (MV-NSe-GFP-MSCs with no AMD3100: 145.833+/-3.33 cells/5xhpf; with AMD3100: 113.13+/-10.67 cells/5xhpf; MV-NSe-hCXCR4-MSCs with no AMD3100: 187.50+/-11.77 cells/5xhpf; with AMD3100: 108.13+/-6.72 cells/5xhpf).

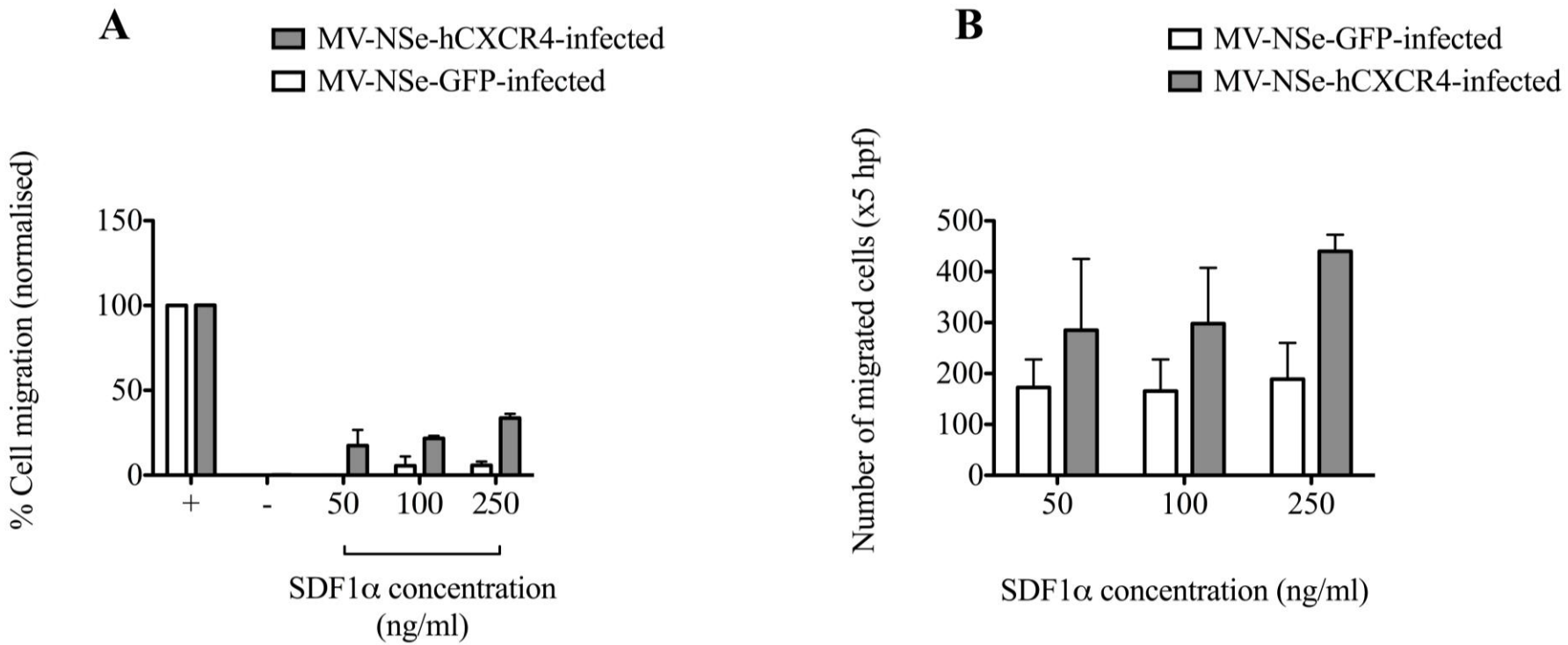

Figure 4-8: MV-NSe-hCXCR4-infected MSC migration. (A) Percentage of transwell migrated MSCs (x5 high-powered fields (hpf)) at 48 hours post infection with MV-NSe-hCXCR4 or MV-NSe-GFP (MOI 1.0). Number of migrated cells for the positive control (+) is normalized to 100%, with all other values expressed as a percentage of the positive control condition, minus background cellular migration (-). **(B)** Absolute numbers of migrated cells (x5 hpf). For each experiment, N=3. Data shown is mean +/- SEM. There is no significant difference in MSC migration between MV-NSe-GFP and MV-NSe-hCXCR4-infected cells, or between the amounts of MSC migration of MV-NSe-hCXCR4-infected cells with different concentrations of SDF-1α, using the unpaired t-test.

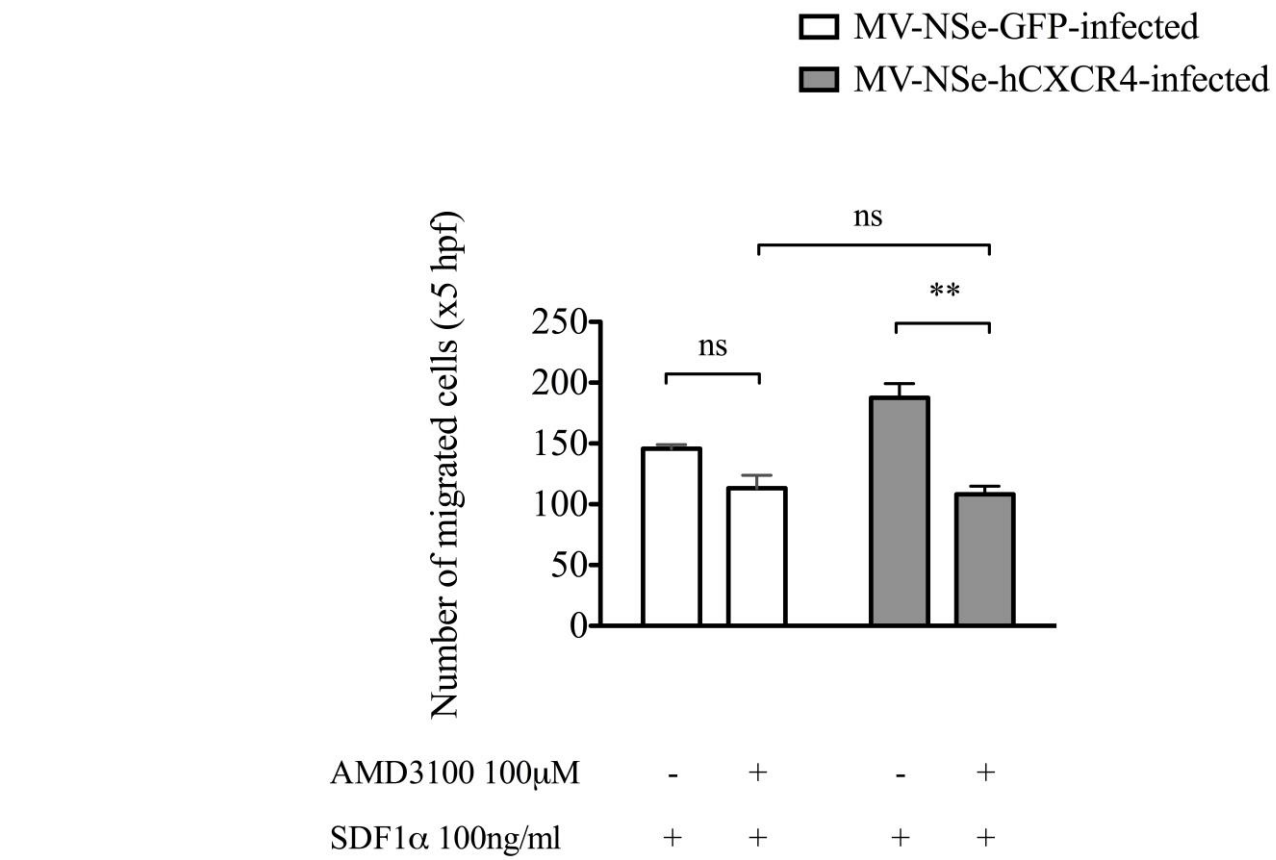

Figure 4-9: Effect of AMD3100 pre-treatment of MV-NSe-hCXCR4 infected MSCs. Absolute number of transwell migrated MSCs following pre-treatment (+) or no pre-treatment (-) with AMD3100. Data shown is mean +/- SEM for 3 independent experiments. Analysis uses the unpaired t-test. For the difference between MV-NSe-hCXCR4-infected MSCs pre-treatment versus no pre-treatment, **p=0.0011.

4.6 Discussion

Reasons for choosing BM-MSCs as biological delivery vehicles for systemically delivered oncolytic measles virotherapy have already been outlined in this chapter. Of paramount importance in the success of such approach is the ability of the chosen carrier cell to migrate to sites of tumour upon intravenous infusion. Whilst there is a plethora of data reporting the tumour-homing properties of MSCs, there is also data to suggest that following ex-vivo manipulation, MSCs downregulate surface chemokine receptors involved in the trafficking process. As a result, MSCs may be less efficient at reaching distant tumor targets. With this in mind, I set out to explore mechanisms that could be utilized to enhance the homing of BM-MSCs to tumours, whilst keeping them 'fit for purpose' as virotherapeutic delivery vehicles.

As detailed in Chapter 3, when MV-loaded MSCs were administered to SCID mice with established NALM-6 xenografts, early localization of infected carrier cells was suboptimal – with passive lung entrapment being evident. Passive lung entrapment is a well -recognized phenomenon[237], and is explained by the size of the cells administered and the animal model used. Whilst it is a phenomenon that has not been associated with the systemic delivery of MSCs to humans, it can provide an obstacle to in vivo murine modeling. Other groups have tackled this by using alternative animal models, including larger rodents or primates, or by the pre-administration of prostaglandin infusions to mice to promote vasodilatation within the pulmonary vasculature[255]. Whilst there were initial concerns here that passive lung entrapment would prevent successful carrier cell delivery to distant tumour targets in this model, there was a demonstrable re-localisation of infected MSCs to recognized sites of leukaemia within the BM of treated animals from as early as day 2 post infusion. Using a luciferase-expressing strain of MV-NSe allowed for accurate assessment of MV localization, with increasing luciferase activity over time representing MV replication within tumour tissue. As previously discussed, attempts to directly demonstrate the presence of human MSCs within the murine BM by flow cytometric analysis at the time of experiment termination were unsuccessful. This was likely to be due to the relatively low input cell doses, the reduced likelihood of MSC survival at late timepoints following virus hand-off to tumour targets, and the lack of long-

term engraftment of systemically delivered MSCs that has been demonstrated by others. Whilst bioluminescent imaging supported the finding of tumour localization of MV-NSe-Luc-infected MSCs from day 2 post infusion onwards, consideration was given to ways in which efficiency of homing mechanisms could be potentiated.

Chemokine receptors are G protein-coupled receptors that in conjunction with their ligands, regulate the migration of many cell types. CXCR4 is one of 19 known human chemokine receptors, and it is exclusively activated by the chemokine SDF-1α. SDF-1α is constitutively expressed within the BM, and can be secreted is association with tissue damage incuding infarction, ischaemia, toxic liver damage, total body irradiation, and post chemotherapy. SDF-1α is also expressed by endothelial cells and pericytes of hypoxic, injured or pathological tissues. The CXCR4/SDF-1α signaling pathway is thought to provide a number of diverse cellular functions. Of relevance to ALL is the stromal cell chemoprotection of leukaemic cells within the BM, which is in part mediated by CXCR4 and SDF-1α[256]. A major role of the CXCR4/SDF-1α axis is in the trafficking/chemotaxis of multiple cell types including MSCs. In light of this, the generation of a strain of MV-NSe expressing the hCXCR4 gene as an additional transcription unit was undertaken, with the aim of enhancing MSC surface CXCR4 receptor expression, ultimately deriving a comparison between the localization capacities, and therapeutic outcomes of standard MV-NSe loaded MSCs versus MV-NSe-hCXCR4 loaded MSCs in pre-clinical models of pre-B ALL.

MV-NSe-hCXCR4 was successfully cloned and rescued by a process of reverse genetics, and growth characteristics were similar to those of MV-NSe-GFP, from which the novel strain of MV was generated. Of note, MV-NSe-hCXCR4 reached titres that were a log lower than MV-NSe-GFP, peaking approximately 24 hours later than the original virus. It is likely that these subtle differences in growth characteristics relate to the size and the complexity of the novel insert, with the hCXCR4 gene consists of a 1071bp open reading frame (ORF), and encoding for a seven-span transmembrane receptor. Whilst both Vero cells and BM-MSCs infected with MV-NSe-hCXCR4 showed upregulation of cell surface levels of CXCR4 expression (both by flow cytometric and immunohistochemical analysis), and transwell migration studies showed improved migratory capacities of MV-NSe-hCXCR4 infected cells as compared to MV-NSe-GFP infected cells towards an SDF-

1α gradient, the migratory differences seen were not statistically significant. Interestingly, inhibition of CXCR4 by the reversible antagonist AMD3100 did result in a significant abrogation of migration for MV-NSe-hCXCR4 infected cells which was not seen for MV-NSe-GFP infected cells. It is possible that this is due to the blocking of both hCXCR4 molecules on the cell surface generated by the novel MV strain, as well as the blocking of basal cell surface hCXCR4 present on BM-MSCs prior to infection.

Ultimately, in light of the excellent therapeutic outcomes seen when standard MV-NSe was delivered within BM-MSCs to disseminated pre-B ALL xenografts (Chapter 3), the novel *hCXCR4*-expressing virus strain was not taken forward into comparative in vivo studies.

Chapter 5: Characterizing MV kinetics in a stromal cell model of transformation

5.1 Background

Whilst we have an existing understanding of the antiviral mechanisms at play within normal cells that can halt the progression of cellular MV infection, thus far we have a limited knowledge of the significance of these mechanisms in relation to the oncolytic capabilities of vaccine strain MV. In order to facilitate rational design and ultimate success of oncolytic MV in future clinical trials, a detailed understanding of the cellular mechanisms conferring this promising new virotherapeutic its tumour specificity and ultimate anticancer efficacy is required.

As discussed in Chapter 1, in vitro studies have shown that high levels of CD46 receptor density on tumour cells leads to enhanced cell fusion, viral gene expression, and ultimate virus-induced cell death by oncolytic MV[166,167], as compared to cells with low CD46 levels. Whilst widely expressed on human nucleated cells, CD46 overexpression is not a recognized feature of adult pre-B ALL (although SLAM is known to be expressed), a tumour type which we have demonstrated is exquisitely sensitive to MV-mediated oncolysis. A further hypothesis is that antiviral immune responses may be suppressed in certain cancer cells[257-259], resulting in their inability to mount an effective immune response against infection, whilst surrounding normal tissues (or virus resistant cancer cell lines) are protected by intact innate immune systems. As detailed previously, defects in cytoplasmic PRRs and ISGs have been shown to contribute to the differential susceptibility of sarcoma cell lines to vaccine MV-mediated killing[168]. Recently whole transcriptome analysis has been used to identify gene expression profiles that determine resistance to oncolytic MV in GBM models. Looking at both resistant (GBM39) and permissive (GBM12) tumour types, several ISGs were identified as being highly expressed prior to infection, in the MV-resistant relative to the MV-permissive cell line. Furthermore, in primary patient material high basal levels of ISG expression were seen in newly diagnosed GBM patient brains and correlated with resistance to MV infection when treated upon

recurrence, whereas low basal levels of ISG supported infection by oncolytic MV. These findings suggest that tumour cells can be in a pre-existing antiviral state that can limit viral infection and response to virotherapy. A subset of ISGs correlating with MV resistance were identified, and when the ISG, RSAD2 was used to transduce HEK-293T cells, inhibition of the release of MV particles was demonstrated in vitro[260]. The significance of this mechanism in relation to the efficacy of measles virotherapy remains to be determined. Although such studies provide vital mechanistic insights, studies directly comparing responses to MV infection in cancer cells and healthy normal cells are lacking.

5.1.1 A stromal cell model of oncogenesis

A broad range of both haematological and non-haematological malignancies have been shown in both pre-clinical and early clinical studies to be susceptible to the oncolytic effects of vaccine MV. However, finding appropriate models that can be effectively utilized to probe the differential cellular responses to MV between healthy and transformed cells represents a challenge. Whilst we can illustrate malignant cell permissiveness, viral replication, and ultimate MV-specific cell killing in models of pre-B ALL, we are unable to accurately compare intricate intracellular processes with those that occur when MV targets their normal healthy B cell counterparts, as we would be reliant on a comparison between cellular populations at different stages of differentiation. Furthermore, paediatric data suggests that pre-B ALL is a 'multi-hit' model of oncogenesis, with the initial cellular insult taking place in utero[261]. It is therefore impossible to conceive of ever being able to compare 'like with like' when it comes to looking at differences between healthy versus transformed cells in this disorder. With this in mind, I set out to validate a previously characterized stromal cell model of cellular transformation, as a useful biological tool with which the oncolytic mechanisms of vaccine MV could be further elucidated.

The majority of experimental models of cellular transformation utilize differentiated cells. Evidence suggests that certain types of cancer, including many haematological malignancies, are likely to be derived from mutations accumulating in normal tissue specific precursors or stem cells. In the context of lymphoid leukaemogenesis, stem cells are thought to be a target for pre-leukaemic events or leukaemic transformation,

with clonotypic leukaemia-associated chromosomal rearrangements having been identified in putative haematopoietic stem cell-enriched (CD34+CD38-) populations[262]. By their nature, stem cells already have the capacity for longevity and self-renewal. It is therefore possible, that fewer mutations or 'hits' are required for the transformation of a normal stem cell - with the effects of such transforming events being expressed downstream - than to 'turn on' the capacity to self renew in a committed progenitor or terminally differentiated cell[263]. To explore this hypothesis, Funes et al. created a model of cellular transformation using primary human BM-derived mesenchymal 'stem' cells, by the sequential disruption of a number of pathways that have been described as being involved in the in vitro transformation of differentiated cells[223]. Whilst elegantly demonstrating that disruption of the same regulatory pathways is required to generate MSCs with a fully transformed phenotype, the model of transformation generated allows the direct in vitro comparison of primary healthy untransformed MSCs alongside their malignant counterparts, and provides a potentially excellent opportunity to examine oncolytic MV kinetics.

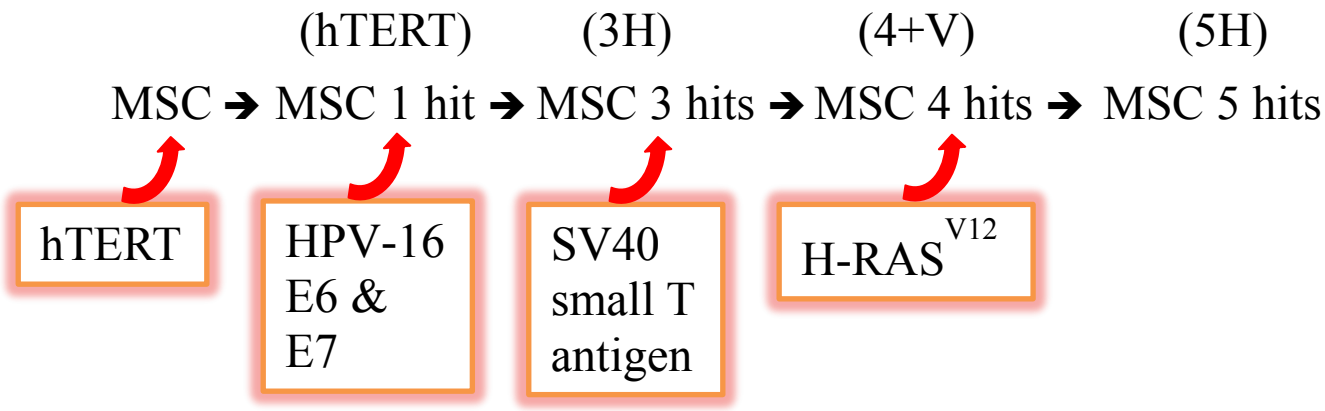

Figure 5-1: Schematic diagram of MSC stepwise transformation (adapted from Funes et al. 2007). MSCs have been named according to the oncogene, or number of oncogenes inserted by retroviral vector transduction. hTERT encodes for the catalytic subunit of human telomerase - conferring lifespan extension; HPV-16 E6 and E7 disrupt *pRB* and *p53* tumour suppressor pathways; SV40 small T antigen inactivates protein phosphatase 2A leading to *C-Myc* stabilization; *H-RAS*^{V12} provides acquisition of a constitutive mitogenic signal.

5.2 Purpose of this chapter

This chapter uses the MSC model of cellular transformation to gain insight into mechanisms of MV-mediated oncolysis. I initially set out to confirm that MV infection kinetics differed according to transformational stage. I have examined permissiveness to MV infection, determined cellular MV productivity, and investigated rates of MV-specific cell death. I also initiated preliminary studies to investigate intracellular antiviral and metabolic responses to MV infection, with the aim of generating new hypotheses by which future investigations into the mechanisms of MV-mediated oncolysis could be guided.

5.3 Hypotheses

a. There will be a difference in the permissiveness of fully transformed MSCs to oncolytic MV, versus that of primary MSCs.
b. Differences in infectivity, productivity, and cytotoxicity will not be accounted for solely by MV receptor expression profile.
c. Transformation of BM-MSCs will result in cellular functional defects in innate immune signaling or translational regulation in response to MV infection, which may contribute to differential viral kinetics.

5.4 Methods

5.4.1 IFN α/β quantification by ELISA

MSCs ($5x10^5$ cells per well) were cultured in MesenCult® MSC basal medium supplemented with MesenCult® stimulatory supplements (StemCell Technologies, Grenoble, France), 100 units/ml penicillin G + 100 μg/ml streptomycin, 2mM L-glutamine, and 1ng/ml bFGF (R&D systems, Minneapolis, MN), and infected with MV-NSe under specified experimental conditions. At 24 and 48 hours post infection, tissue culture supernatants for each experimental condition were collected and stored in separate falcon tubes at minus 80°C until all samples had been collected. Quantification of IFN α and β was performed using Verikine™ Human IFN alpha Multi-Subtype ELISA (PBL Assay Science, NJ) and VeriKine™ Human IFN Beta

ELISA (PBL Assay Science, NJ) kits respectively. 50-100µl supernatant or standard solution was added in duplicate to each well of the provided microplates pre-coated with the appropriate monoclonal antibody. After 1-hour incubation at room temperature, plates were emptied and washed 3 times with the appropriate wash buffer, and 100µl polyclonal antibody was added to each well followed by a further 1-hour incubation at room temperature. Plates were then emptied and washed x 3 before adding 100µl horseradish peroxidase (HRP) solution and incubating again for 1 hour at RT. Following a further empty and 3 x wash step, microplates were incubated for 15 minutes at room temperature in the dark with 100µl of TMB substrate before adding 100µl of stop solution to each well and reading optical absorbance using a microplate reader (Tecan, Männedorf, Switzerland). The wavelength was set according to instructions provided by the manufacturer. Background absorbance was assessed in wells using culture media alone, and average background readings were subtracted from data values. For each experiment, cubic spline analysis was performed on standard curve values, and used to interpolate experimental values.

5.4.2 RIG-I, MDA-5 and IPS-1 mRNA quantification by RQ-PCR

For RIG-I, MDA-5 and IPS-1 mRNA relative quantification, QuantiTect® Primer assay (Qiagen, Crawley, UK) was used in 25µl reactions. cDNA was mixed with 0.3µM forward and reverse primers, and 12.5µl of 2x QuantiTect® SYBR Green PCR Master Mix (Qiagen). Dissociation curves were generated for each QuantiTect® SYBR Green gene expression assay to confirm amplification of the desired product. The PCR conditions for the assay are as follows:

- 50°C for 2 minutes
- 95°C for 10 minutes

40 cycles of:

- 94°C for 15 seconds; 55°C for 30 seconds; 72°C for 35 seconds

Primer sequences are shown below:

RIG-I s 5’- ACCAGAGCACTTGTGGACGCT-3’
RIG-I a 5’- TGCCGGGAGGGTCATTCCTGT-3’
MDA-5 s 5’- GGCACCATGGGAAGTGATT-3’
MDA-5 a 5’- ATTTGGTAAGGCCTGAGCTG-3’

IPS-1 s 5’- GAGACCAGGATCGACTGCGGGC-3’

IPS-1 a 5’- AGAGGCCACTTCGTCCGCGA-3’

GAPDH was used as the housekeeping gene for all assays. PCR reactions were carried out on an ABI 7500 system (Applied Biosystems). Samples were run in triplicate for each gene. Non-template control (NTC) using RNase/DNase free water was included in each plate. PCR cycle number at threshold is represented as Ct. Relative expression of level of gene of interest was calculated using the $RQ=2^{(-\Delta\Delta Ct)}$ formula[226] (see Chapter 2: Methods)

5.4.3 ATP and cellular metabolism assays

For ATP assay, 7.5 x 10^4 cells per well were infected or mock infected under standard conditions with MV-NSe at MOI 1.0. At 24 hour intervals post infection, cells were trypsinized, washed once with PBS, and then enumerated by trypan blue. For each condition, 1 x 10^4 cells were collected and subject to 2 x freeze-thaw cycles before centrifugation at 14000 rpm for 5 mins at 4°C. Cell lysates were then re-suspended in standard reaction buffer containing luciferase and luciferin according to the manufacturer’s instructions (ATP Determination Kit; Invitrogen), and luminescence read at 560nm in a Mithras LB 940 Multimode Microplate Reader (Berthold Technologies, Germany). Protein quantification on cell lysates was performed using a Bicinchoninic Acid (BCA) Protein Assay kit (Sigma). This is based on the method of Lowry[264] and relies on the formation of a Cu^{2+}-protein complex under alkaline conditions, with subsequent reduction of Cu^{2+} to Cu^{1+}. The amount of reduction is proportional to the amount of protein present. BCA forms a purple-blue complex with Cu^{1+} under alkaline conditions with an absorbance of 560nm.

The assay was performed in a 96 well plate. A BSA standard supplied in the kit was used to construct a standard curve across the linear range of the assay (0-1000µg/ml). 25µl of test or standard samples were added to wells in duplicate. BCA working reagent was made up by mixing 1 part of 4% copper (II) sulphate pentahydrate solution with 50 parts of BCA solution (BCA, sodium carbonate, sodium tartrate and sodium bicarbonate in 0.1N NaOH, pH 11.25). 200µl of working solution was added to each sample well and the plate incubated at 37°C for 30 minutes. Absorbance was

read at 560nm and the test sample protein concentrations read off the standard curve. ATP levels were derived from ATP standard curve, and expressed per g protein.

For cellular metabolism assays, an XF24 extracellular flux analyzer (Seahorse Bioscience, MA, USA) was used to determine OCR and ECAR. Viable MSCs were seeded (5×10^4 per well) and infected with MV-NSe (MOI 1.0) for 24 or 48 hours. Before measurement, cells were changed to unbuffered XF assay media, with 5mM glucose, 2mM L-glutamine, and 0.5mM pyruvate (pH 7.4 at 37°C) for 60 minutes in a non-CO_2 incubator. The cartridge was hydrated with unbuffered XF assay media (as above) overnight. On the flux analyser, the protocol included calibration, and 4 readings to establish basal OCR/ECAR rates in both infected and uninfected cells.

5.4.4 Reactive oxygen species (ROS) production

Viable MSCs were plated out (3.75×10^4 per well) and infected (or mock infected) with MV-NSe (MOI 1.0). At 24 hours post infection, cells were trypsinised, washed and and stained with 5mM CellROX® Green reagent (LifeTechnologies) according to manufacturer's instructions, before washing x 3 with PBS and performing flow cytometric analysis. Viable cells were gated according to FSC and SSC characteristics. ROS levels in infected cells were compared to basal levels in uninfected cells.

5.4.5 Caspase 3/7 activation

Caspase 3 and 7 activation were assessed using a luciferase-based assay (Caspase-Glo® 3/7 Assay, Promega). MSCs were plated (3.75×10^4 per well) and infected with MV-NSe (MOI 0.01, 0.1, 1.0) or mock infected for 24 and 48 hours. Cells were harvested at the appropriate time point by trypsinisation, washed and enumerated using trypan blue. Following this, 5000 cells per well were plated in triplicate for each condition into a white 96-well microplate. Caspase-Glo® buffer and substrate were allowed to equilibrate to room temperature, and following mixing of buffer and substrate, 100µl of reagent was added to each well. Following 30 seconds of agitation on a plate shaker, and incubation at room temperature for 30 minutes, the plate was read on a Mithras LB 940 Multimode Microplate Reader (Berthold Technologies).

Average background values (reagent plus culture medium only) were subtracted from all data values.

5.5 Results

5.5.1 Transformed MSC in-vitro growth characteristics

In order to accurately evaluate cell-to-cell differences in MV infectivity and virus productivity between primary MSCs and serially transformed MSCs, I initially sought to characterize cell growth kinetics. Data demonstrate an increase in cellular growth rates (see Figure 5-2A), with a reciprocal decrease in doubling time (82 hours versus 22.3 hours for primary MSCs and 5H cells respectively) as MSCs become progressively transformed (see Figure 5-2B). This needs to be taken into consideration when assessing for differences in level of infection and virus propagation in vitro.

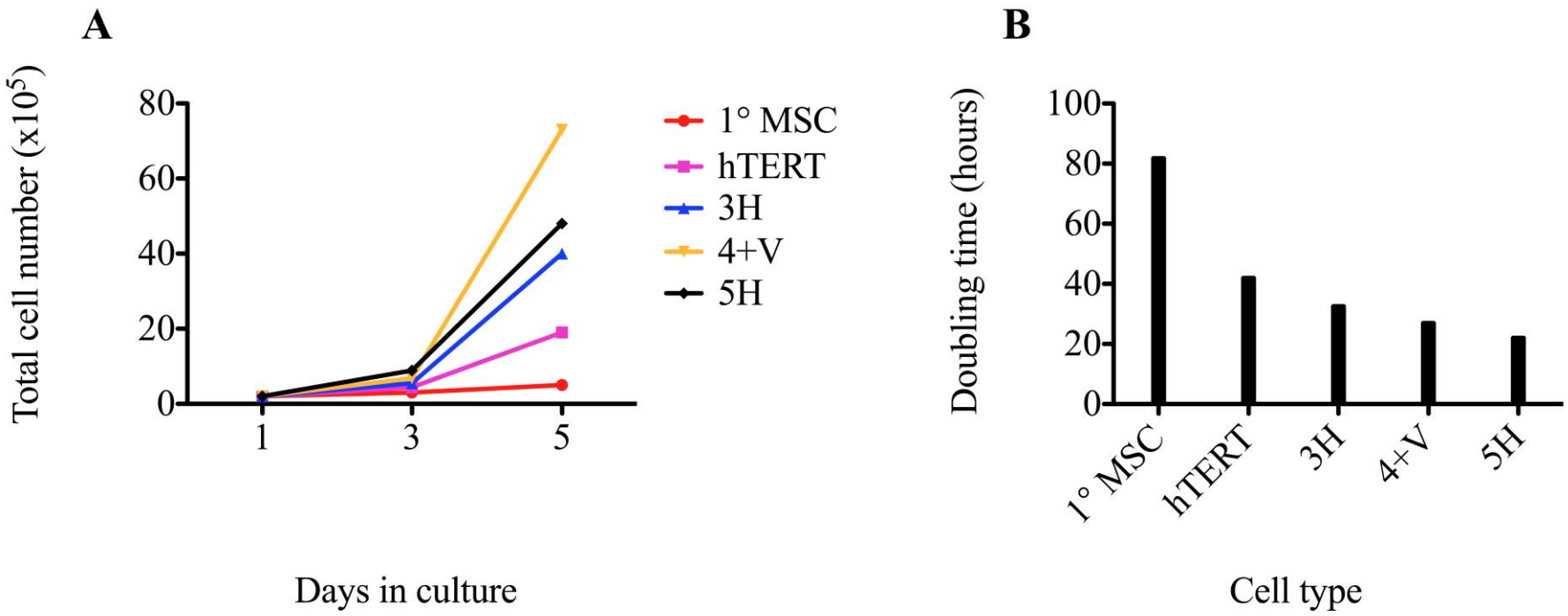

Figure 5-2: Growth characteristics of MSCs following stepwise transformation. (A) Growth curves of MSCs showing the total number of cells at 1, 3 and 5 days in culture, following initial seeding of $2x10^5$ cells. **(B)** Calculated cell doubling times.

5.5.2 Effect of transformation on MV-infectivity and virus production

Primary MSCs or sequentially transformed MSCs were infected with MV-NSe-GFP using an MOI of 1.0. Observing syncytia formation, GFP expression, and MV-H glycoprotein immunostaining at 48 hours post infection permitted assessment of the cellular permissiveness to MV infection. As demonstrated, cellular infection using a recombinant virus expressing GFP leads to increased numbers of large, multinucleate, GFP positive syncytia in 5H cells as compared to primary untransformed MSCs - where permissiveness is markedly reduced (as evidenced by smaller syncytia size and lower levels of GFP expression). Furthermore, MV-NSe infection of 5H cells results in stronger surface MV-H glycoprotein expression than is seen in primary cells – which in conjunction with surface expression of MV-F glycoprotein is likely to facilitate cell to cell fusion and virus spread.

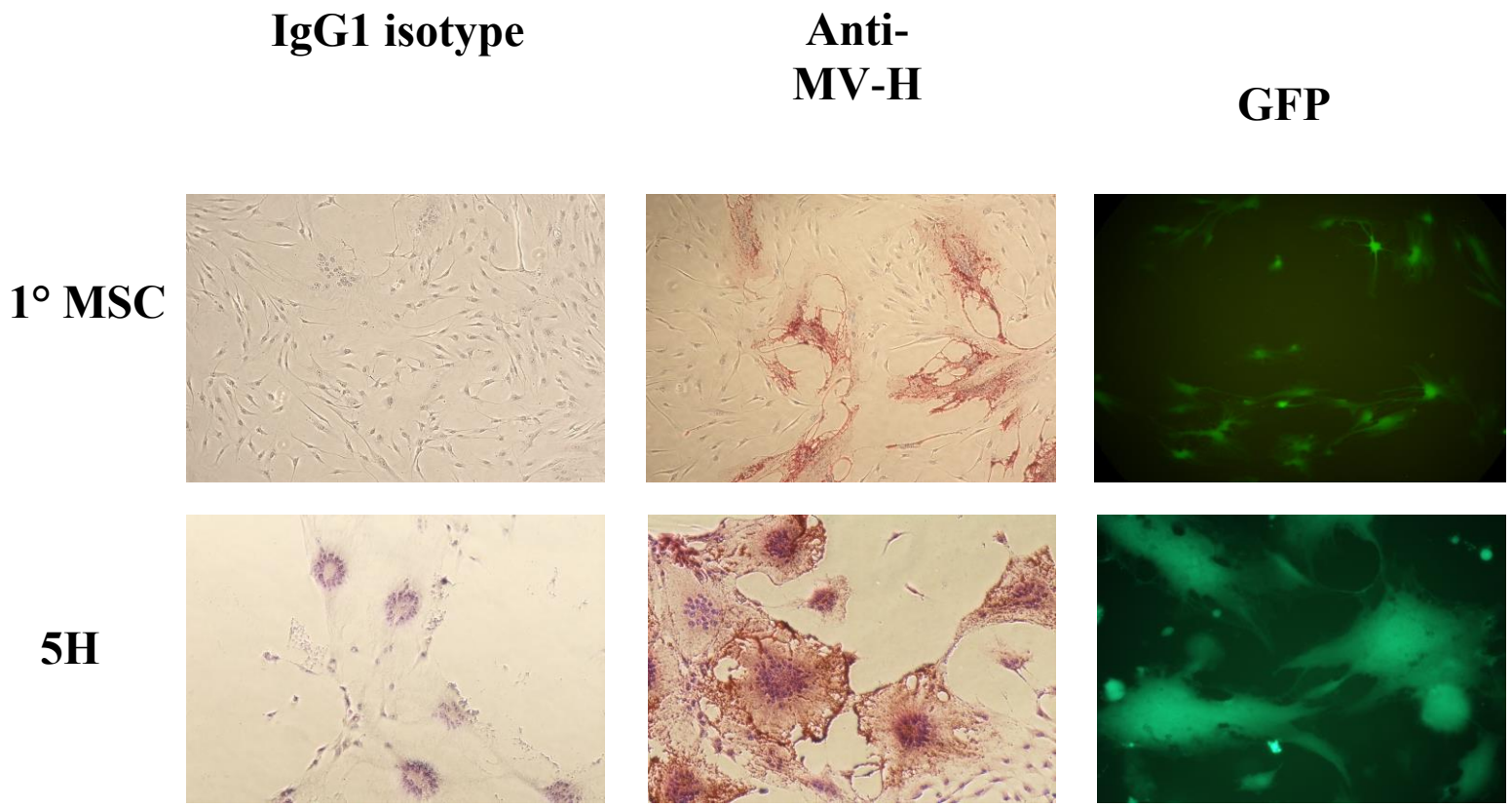

Figure 5-3: Transformation of BM-MSCs leads to enhanced cellular infectivity by MV-NSe in vitro. Primary MSCs or fully transformed MSCs (5H cells) were infected with MV-NSe-GFP using an MOI of 1.0 under standard tissue culture conditions. At 48 hours post infection, cells were assessed for the extent of MV infection as evidenced by MV-H glycoprotein expression by immunostaining, and GFP expression by fluorescence microscopy. To ensure the specificity of MV-H immunostaining, anti-human IgG1 isotype antibody was used as a negative control. All cells were counter stained with Carrazi's haematoxylin. All photographs were taken with a Nikon eclipse TS3100 using x 20 objective.

To assess MV productivity post infection, cell lysates and tissue culture supernatants were harvested and $TCID_{50}$ virus titrations were performed on hTERT, 3H, 4+V and 5H cells at 24, 48 and 72 hours post infection (see Figure 5-4) In keeping with previously generated data using primary MSCs, virus productivity in hTERT cells was only detectable intracellularly, and at low levels, peaking at 48-72 hours post infection. Similar levels of productivity were seen in 3H cells, with minimal detectable virus in culture supernatants. For 4+V and 5H MSCs there is a 2 to 3-log increase in intracellular virus productivity at 48 hours post infection, as compared to their less transformed counterparts ($2.2x10^2$ +/- 65.4 for 3H versus $1.2x10^5$ +/- $1.2x10^4$ for 4+V MSC p=0.0006; as previous for 3H versus $1.1x10^4$ +/- $1.8x10^3$ for 5H MSC p=0.004; see Figure 5-4B). Furthermore, there is a 3-log enhancement in the amount of released virus produced in 4+V MSCs when compared to cells at earlier stages of immortalization (39.3 +/- 19.7 for 3H versus $1.7x10^4$ +/- $8.7x10^3$ for 4+V MSC p=0.0432; see Figure 5-4C). Taken together, these data provide evidence that immortalization of healthy BM-MSCs can significantly enhance the ability of MSCs to support MV infection and replication.

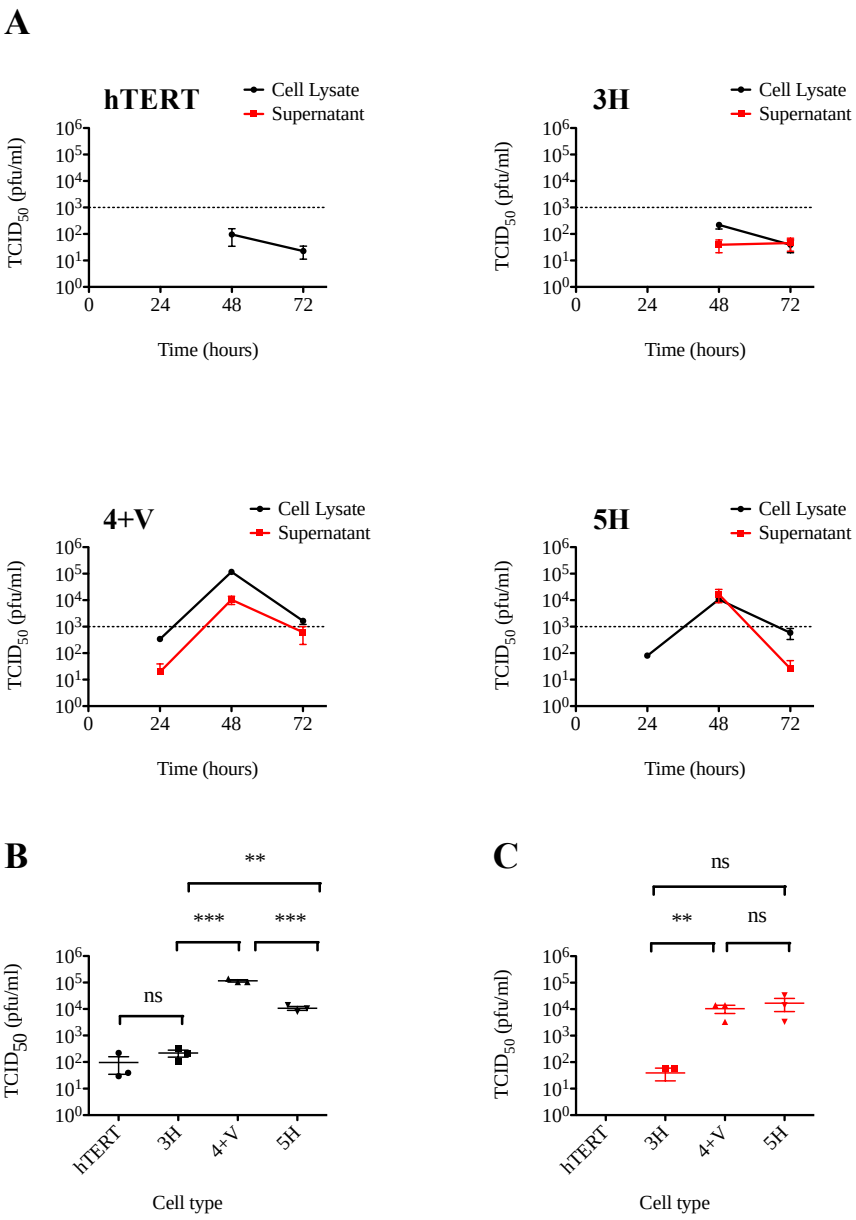

Figure 5-4: Cellular immortalisation leads to phenotypic alterations in the ability of MSCs to support and sustain productive MV infection. (A) hTERT, 3H, 4+V and 5H cells were infected with MV-NSe at MOI 1.0 under standard tissue culture conditions, and $TCID_{50}$ quantification was performed at 24, 48 and 72 hours post infection on cell lysates and tissue culture supernatants. **(B)** Titres at 48 hours post infection are shown for cell lysates and **(C)** supernatants. Data shown are mean and SEM for 3 independent experiments. Statistical analysis was performed using the unpaired t-test. For figure B, 3H vs. 5H **p=0.004; 3H vs. 4+V ***p=0.0006; 4+V vs. 5H ***p=0.0009. For figure C, 3H vs. 4+V *p=0.0432.

5.5.3 Stage of immortalization and extent of MV-specific cell death

In order to assess the consequences of MV infection and spread in the stromal cell model of transformation, hTERT-immortalised, 3H, 4+V and 5H cells were infected with MV-NSe at an MOI of 1.0 under standard conditions, and viability was assessed using trypan blue staining at 24, 48 and 72 hours post infection. The percentage of MV-specific cell death was calculated in relation to cell death in uninfected control wells. Data clearly demonstrates a progressive enhancement in the percentage of MV-specific cell death that parallels the development of a fully immortalized cellular phenotype. Whilst the earlier stages of transformation (hTERT-immortalisation, and abrogation of tumour suppressor genes *p53* and *pRB*) have little significant effect on the extent of cell killing here, there is a 3-fold increase in MV-mediated cell killing at both 48 and 72 hours post infection with stabilization of the *c-Myc* oncogene (48 hpi: 15.865 +/- 2.795% for 3H versus 44.867 +/- 14.675% for 4+V; 72 hpi: 17.290 +/- 4.266% for 3H versus 58.2 +/- 12.9% for 4+V), and a further ~1.5-fold increase with oncogenic *H-Ras* activation (48 hpi: 67.942 +/- 5.219%; 72 hpi: 71.450 +/- 10.294% for 5H). These data clearly illustrate the relationship between immortalization stage and potential efficacy of vaccine MV-mediated cell killing (see Figure 5-5). Interestingly, the addition of FIP to cell culture media minimizes the differential effect upon cell killing that is conferred by progressive transformational stage at later timepoints (48 hpi: 7.27 +/- 2.496% for 3H; 7.8 +/- 2.485% for 4+V; 14.350 +/- 5.421% for 5H; 72 hpi: 6.793 +/- 6.503% for 3H; 12.3 +/- 1.453% for 4+V; 10.755 +/- 3.125% for 5H), with only 2-fold increases seen between 3H and 4+V cells at 72 hours, and between 3H and 5H cells at 48 and 72 hours post infection. This suggests that the formation of cell-cell syncytia plays a critical role in MV-mediated cell death in vitro.

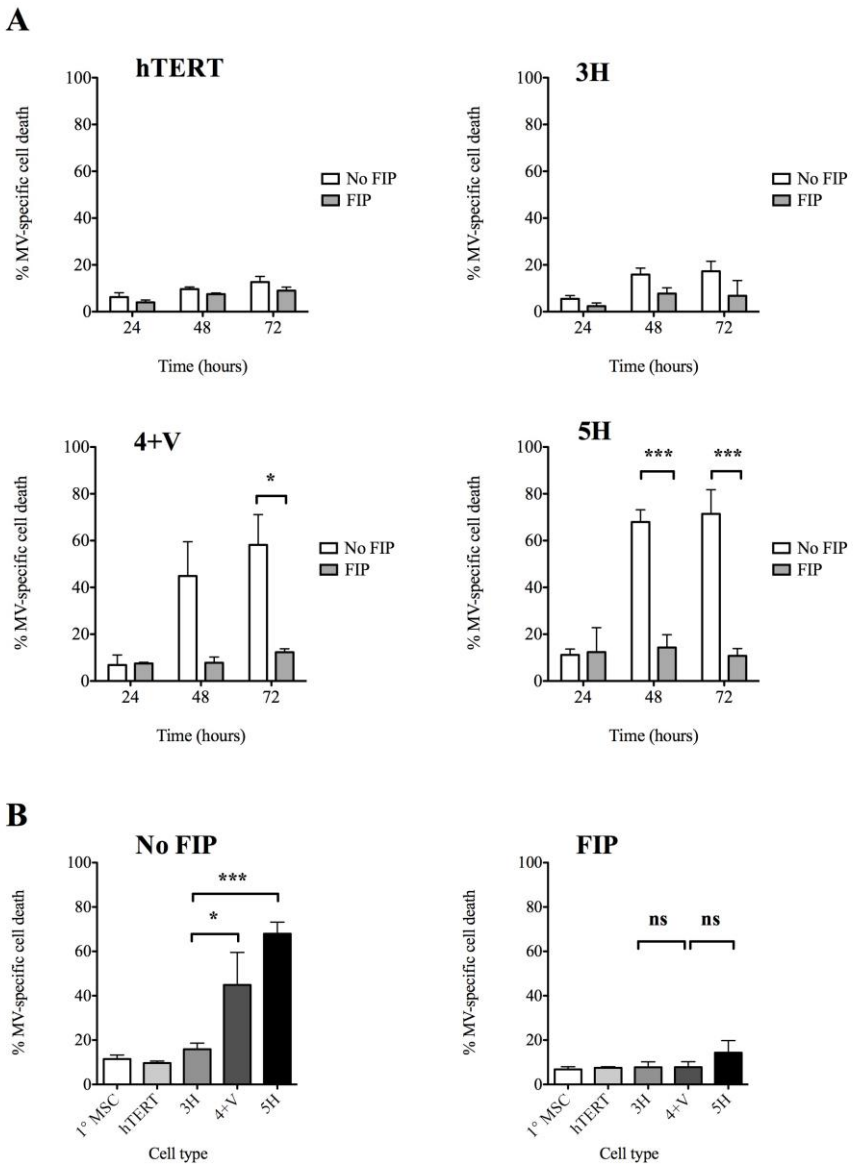

Figure 5-5: Extent of MV-mediated cell killing is proportional to stage of cellular immortalisation. (A) MSCs were infected with MV-NSe at an MOI of 1.0 under standard conditions. Cells were cultured in the presence or absence of FIP, harvested daily for 3 days post infection, and viability assessed by trypan blue assay to enumerate % cell killing by MV relative to uninfected controls. **(B)** % MV specific cell death shown for each cell type with and without FIP. Data is expressed as mean +/- SEM. N=3 independent experiments, with data collected in triplicate. Statistical analysis is performed using an unpaired t-test. For 4+V, *p=0.0242; for 5H 48 hours, ***p=0.0001; for 5H 72 hours, ***p=0.0001. Viability data at 48 hours post infection in the absence of FIP is shown in figure B. *p=0.0274; ***p<0.0001.

To further assess the effect of transformational stage on the ability of vaccine MV to induce cell death, infected or uninfected MSCs (MOI 1.0) were assessed at 48 hours to determine their differential ability to promote MTS reduction in vitro. Due to differences in cellular growth rates in vitro, MV-specific cell death appears to be offset by the metabolic activity of surviving cells, making it difficult to interpret the extent of oncolytic activity using this method (see Figure 5-6A). However, when results are corrected for cell doubling time, it is clear that primary MSCs demonstrate little metabolic consequence in relation to MV infection, but there is a stepwise decrease in the ability of cells to perform MTS reduction to formazan product paralleling the stepwise increase in cellular immortalization (see Figure 5-6B).

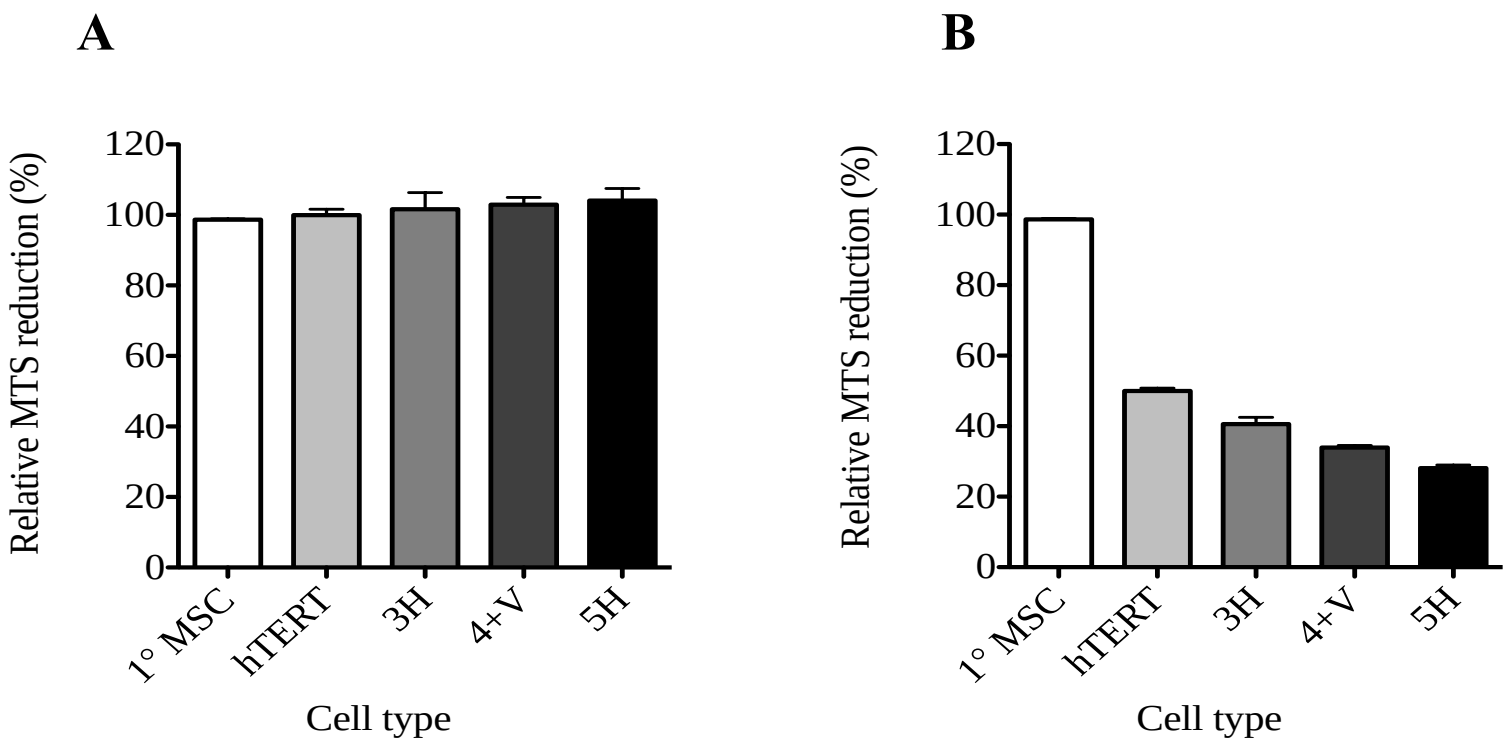

Figure 5-6: MSC transformational stage impacts on cellular proliferation and viability post-MV-NSe infection. MSCs were infected with MV-NSe (or mock infected) at MOI 1.0. At 48 hours post infection, CellTiter 96® AQueous One Solution Reagent was directly added to each of the wells, and following a 4 hour incubation, absorbance was recorded at 490nm with a 96-well plate reader. Graphs represent data uncorrected (**A**) and corrected (**B**) for cell doubling time. Data was collected in triplicate. N=2 independent experiments.

5.5.4 MV receptor expression profile

As existing literature suggests, differences in MV receptor expression profile is a potential mechanism by which MV-permissiveness could be altered. I determined cell surface expression patterns of the MV receptors CD46, SLAM and Nectin 4 for each MSC type, by flow cytometric methods (see Figure 5-7). Overall, there was no significant difference in either the level of expression (see Figure 5-7B), or the density of expression (see Figure 5-7C) of MV receptors for MSCs at all transformational stages. All cells were negative for the presence of SLAM and Nectin 4, whilst CD46 was detected in all cases. Percentage expression ranged from 82.6% +/- 4.3 for primary MSCs to a peak of 92.4% +/- 5.1 for 3H cells, with 4+V and 5H cells falling within this range despite phenotypically being the most permissive to MV infection. Similarly, MFI was highest for 3H cells (20.4 +/- 3.8) with 4+V cells exhibiting the lowest CD46 receptor densities (15.1 +/- 1.2). Taken together, these data suggest that additional mechanisms, occurring as a result of cellular immortalization, are influencing MV-permissiveness here. It is worth stating, however, that the data shown in Figure 5-7B and C demonstrates marked variability as compared to the minimal variability in expression that we would expect to see with standard MV permissive cell lines (eg. Vero). As previously detailed, cells used for these experiments were derived via the stepwise introduction of oncogenes by retroviral transduction. During the initial generation of these cells, selection was performed by culturing each sequential cell type in the appropriate antibiotics as determined by the drug resistance genes carried on the relevant retroviral vectors. It is possible, that within each cell culture, heterogenous expression of oncogenes exists, giving rise to the variability in the data seen here, and potentially reducing the sensitivity of the experiment.

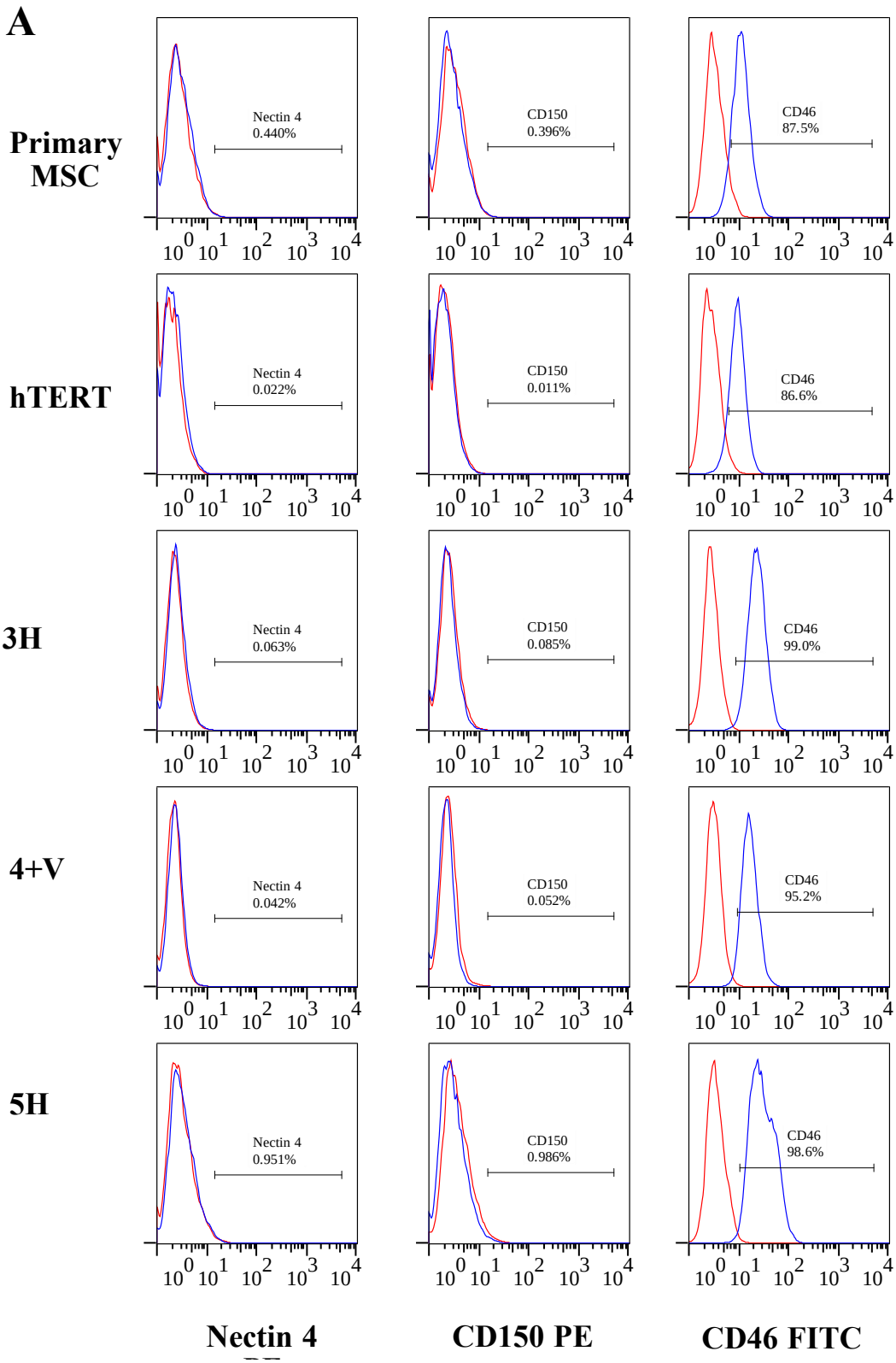
A
Primary MSC
hTERT
3H
4+V
5H
Nectin 4
0.440%
CD150
0.396%
CD46
87.5%
Nectin 4
0.022%
CD150
0.011%
CD46
86.6%
Nectin 4
0.063%
CD150
0.085%
CD46
99.0%
Nectin 4
0.042%
CD150
0.052%
CD46
95.2%
Nectin 4
0.951%
CD150
0.986%
CD46
98.6%
Nectin 4
CD150 PE
CD46 FITC

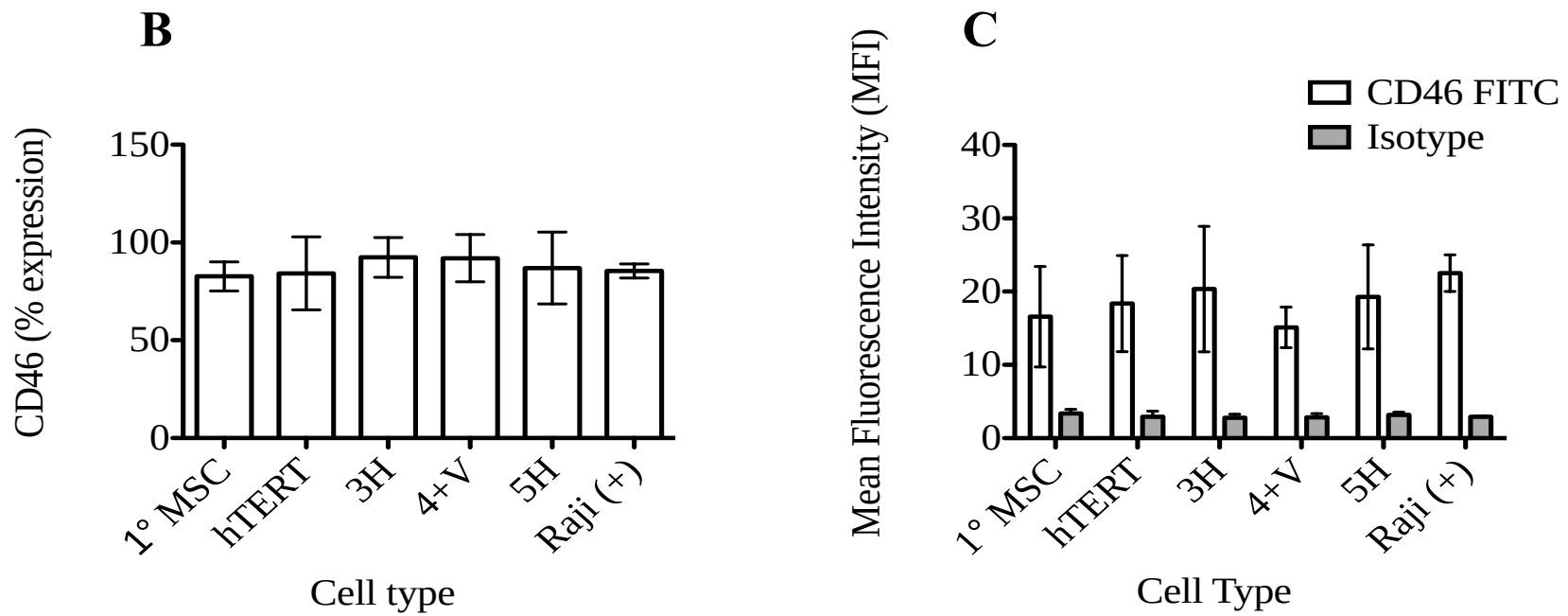

Figure 5-7: Cellular MV receptor expression profiles. (A) MSCs were subject to flow cytometric analysis of surface CD46, CD150/SLAM and Nectin 4 MV receptors. Analysis was performed on live cell population (determined according to FSC and SSC characteristics), with isotype-stained cells as negative controls. Representative flow cytometry plots are shown. **(B)** Cumulative CD46 expression data and **(C)** corresponding MFI for MSCs, with Raji cells used as CD46 positive control. Data shown is mean +/- SEM for 5 independent experiments.

Overall, there was no significant difference in either the level of expression or the density of expression of MV receptors for MSCs at all transformational stages. All cells were negative for the presence of CD150/SLAM and Nectin 4, whilst CD46 was detected in all cases. Percentage expression ranged from 82.6% +/- 4.3 for primary MSCs to a peak of 92.4% +/- 5.1 for 3H cells, with 4+V and 5H cells falling within this range despite phenotypically being the most permissive to MV infection. Similarly, MFI was highest for 3H cells (20.4 +/- 3.8) with 4+V cells exhibiting the lowest CD46 receptor densities (15.1 +/- 1.2). Taken together, these data suggest that additional mechanisms, occurring as a result of cellular immortalization, are influencing MV-permissiveness here.

5.5.5 The role of the type I IFN antiviral response pathway in MV oncolytic activity

Next I sought to examine the integrity of the type 1 IFN response pathway to MSCs following viral infection, as a potential mechanism by which cellular permissiveness to viral production is limited. The sensing of PAMPs is an essential function of the innate immune system. PRRs expressed by a variety of different cells are responsible for sensing the presence of microbial invasion and up regulating the transcription of genes involved in inflammatory responses. Production of type 1 IFNs plays a central role in the induction of antiviral responses, as the trigger for transcription of many ISGs that influence protein synthesis, growth regulation and apoptosis. RLRs were described as cytoplasmic sensors of viral RNA following early reports of TLR-independent mechanisms of viral sensing. These PRRs are now known to be integral to inducing cellular immune responses to MV, upon detection of ssRNA (or dsRNA) within the cytoplasm of an infected cell (see Figure 5-8).

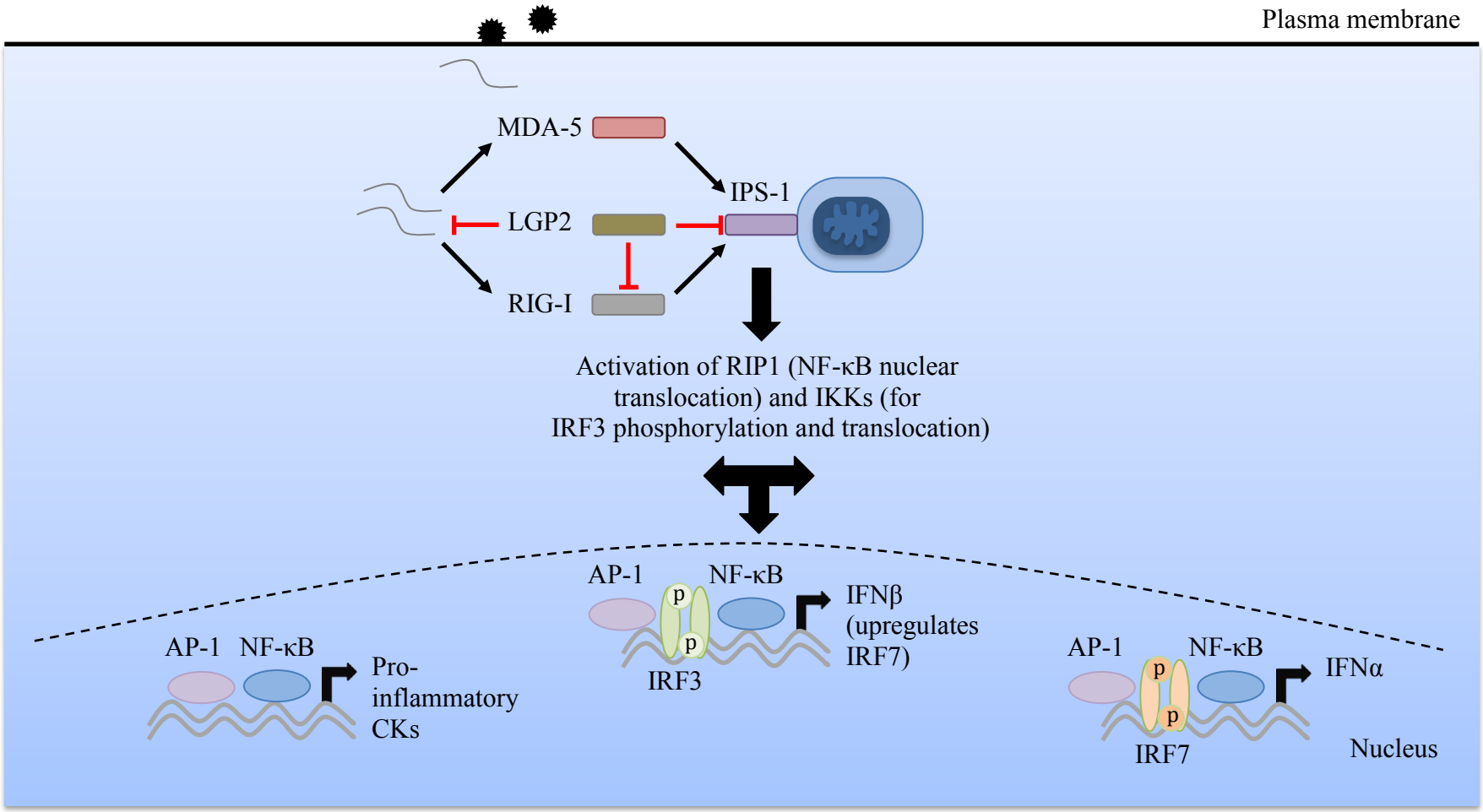

Figure 5-8: The RLR signaling pathway (adapted from Jensen et al. 2012). Schematic representation of signaling pathway following detection of viral RNA by RIG-I and MDA-5. IPS-1 serves as a platform to co-ordinate the activation of signaling pathways also utilized by the TLRs. Activation of the receptor-interacting serine-threonine kinase 1 (RIP-1) cascade results in nuclear translocation of NF-κB. Activation of inhibitors of NF- κB kinase (IKKs) leads to phosphorylation of IRF3, nuclear translocation, and the production of IFNβ, which up regulates IRF7 and subsequently leads to IFNα production.

To determine cellular production of type 1 IFNs, tissue culture supernatants taken 24 and 48 hours post cell infection by MV (MOI 1.0) were used to perform ELISA for IFNα and β. Whilst primary cells showed detectable levels of IFNα and β at 24 and 48 hours, hTERT, 3H, 4+V and 5H cells produced no detectable levels of IFNα, and IFNβ production was inversely proportional to stage of transformation, with minimal production seen in 5H cells as compared to primary untransformed cells (see Figure 5-9A-B). To assess the integrity of RLR signaling pathways, expression levels of RIG-I, MDA-5 and IPS-1 were determined upon cellular stimulation with MV by performing RNA extraction on MSCs at 24 and 48 hours post infection, and relative quantification of RIG-I, MDA-5 and IPS-1 mRNA using real-time PCR. Data was normalized to baseline levels of RIG-I, MDA-5 and IPS-1 mRNA at equivalent time points in uninfected cells. As anticipated, levels of RIG-I and MDA-5 mRNA paralleled the cellular production of IFNβ, with hTERT cells showing highest expression and 5H cells showing minimal expression levels at both 24 and 48 hours (see Figure 5-10A-B). Interestingly, this relationship is not borne out for IPS-1, where expression levels were negligible in all cell types at all time points post infection (see Figure 5-10C). Looking at earlier timepoints post infection may be informative here. Whilst there is an apparent defect in IFNβ (and IFNα) production that parallels progressive MSC immortalization, it is unclear whether or not these differences in cytokine profile, and the resultant consequences upon RLR signaling, are sufficient to induce the cellular phenotypic differences in MV permissiveness.

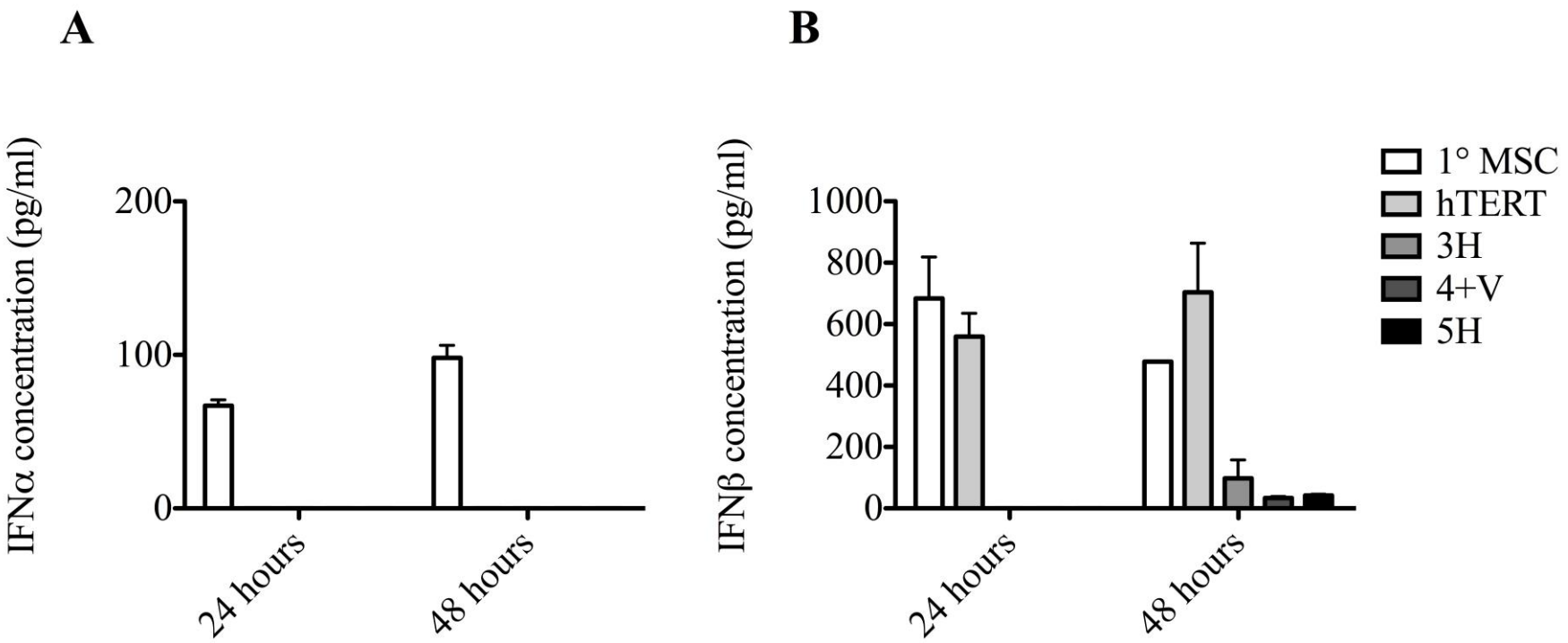

Figure 5-9: Cellular type 1 IFN responses to MV infection are influenced by stage of immortalization. (A) IFNα and **(B)** IFNβ levels as assessed by ELISA on tissue culture supernatants from infected cells at 24 hours and 48 hours post infection. N=2 independent experiments, with samples performed in duplicate. For all experiments, data shown is mean +/- SEM.

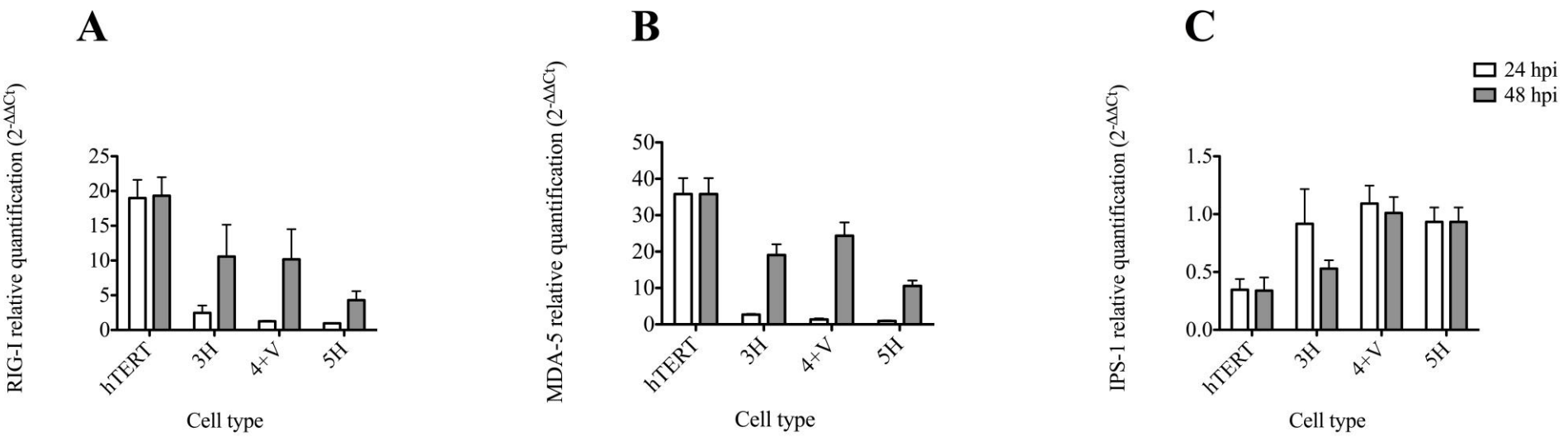

Figure 5-10: Activation of the RLR signaling pathway in response to MV infection. (A) RIG-I **(B)** MDA-5 and **(C)** IPS-1 mRNA levels as assessed by RQ-PCR for each cell type. N=3 independent experiments, with samples performed in triplicate. For all experiments, data shown are mean +/- SEM.

5.5.6 Bioenergetics of MV oncolysis and the role of syncytia formation

As data previously demonstrated, there is a significant abrogation in the amount of MV-specific cell killing in MSCs at later stages of transformation (4+V and 5H), which occurs when cells are cultured post infection in the presence of FIP (see Figure 5-5), suggesting that syncytia are playing a role in the extent of MV-mediated cell death in vitro in this model. To further assess the cellular processes occurring following MV challenge, and the role of syncytia, bioenergetics studies were performed on both hTERT and 5H MSCs, post MV infection, +/- FIP, using the Seahorse XF^e24 analyzer. There was a significant increase in the rate of oxygen consumption (OCR) at 24 hours post infection in both hTERT and 5H cells (see Figure 5-11A). Average increases in OCR seen for 5H cells were ~3-fold from baseline, whereas for hTERT cells less than 2-fold increases were seen. This is followed by a rapid fall off in OCR at 48 hours post infection, particularly for 5H cells, as cell death ensues (*0 hours*: 5H 315.6 +/- 14.08 pMoles/min and hTERT 115.6 +/- 2.66 pMoles/min; *24 hours*: 5H 871.0 +/- 79.35 pMoles/min and hTERT 174.3 +/- 8.78 pMoles/min; *48 hours*: 5H 17.75 +/- 1.81 pMoles/min and hTERT 78.3 +/- 2.82 pMoles/min). The initial increase in OCR seen post MV infection was clearly abrogated with the addition of FIP to tissue culture media (see Figure 5-11B) (*0 hours*: 5H 315.6 +/- 14.08 pMoles/min and hTERT 115.6 +/- 2.66 pMoles/min; *24 hours*: 5H 315.3 +/- 4.059 pMoles/min and hTERT 128.5 +/- 7.801 pMoles/min; *48 hours*: 5H 316.6 +/- 13.50 pMoles/min and hTERT 134.6 +/- 6.029 pMoles/min), with inhibition of syncytia formation being confirmed by direct observation using light microscopy. In contrast, the effect of MV infection on extracellular acidification rate (ECAR) in both 5H and hTERT cells in the absence of FIP is less marked (see Figure 5-12A) (0 hours: 5H 22.3 +/- 2.206 mpH/min and hTERT 3.5 +/- 0.256 mpH/min; 24 hours: 5H 24.56 +/- 2.215 mpH/min and hTERT 4.875 +/- 0.4795 mpH/min; 48 hours: 5H 2.08 +/- 0.5825 mpH/min and hTERT 4.33 +/- 0.189 mpH/min). As with OCR, the addition of FIP post infection results in a marked abrogation of the dramatic fall-off in ECAR seen at 48 hours (see Figure 5-12B) (0 hours: 5H 22.3 +/- 2.206 mpH/min and hTERT 3.5 +/- 0.258 mpH/min; 24 hours: 5H 26.27 +/- 0.58 mpH/min and hTERT 4.857 +/- 0.595 mpH/min; 48 hours: 5H 26.86 +/- 1.725 mpH/min and hTERT 4.64 +/- 0.364 mpH/min). These data suggest that MV infection is impacting on cellular bioenergetics, in particular on mitochondrial

respiration. The extent of impact parallels stage of immortalization, and is not evident when syncytia formation is inhibited.

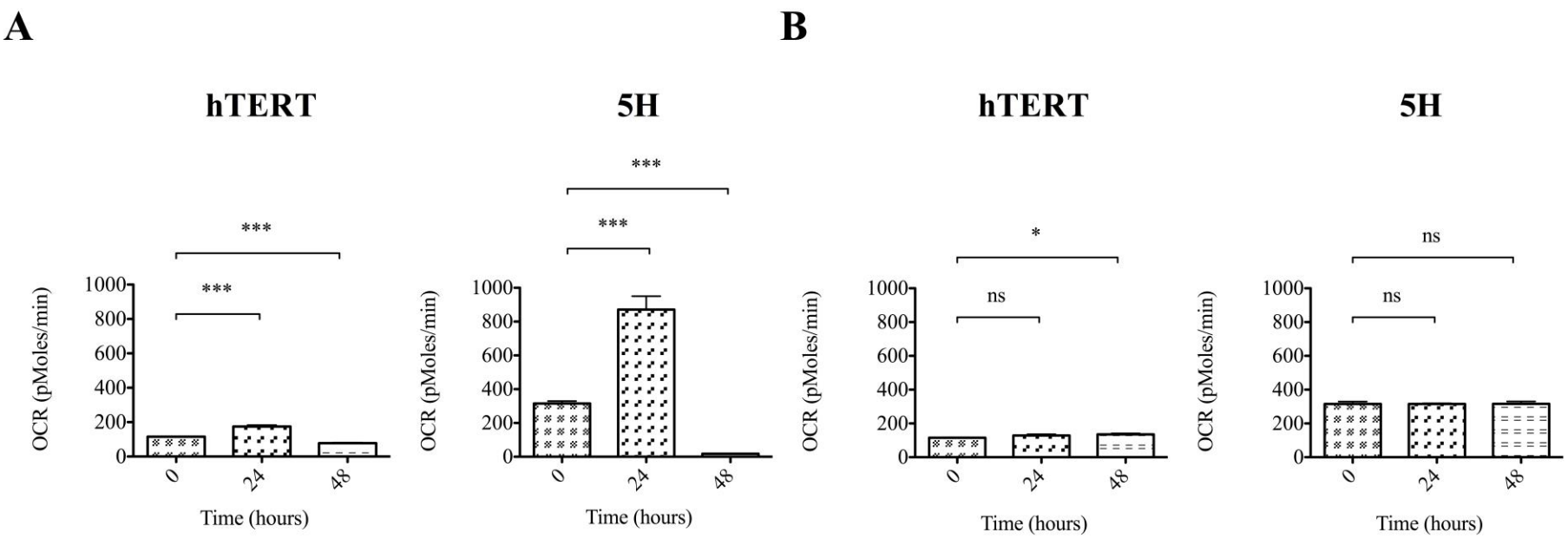

Figure 5-11: Cellular mitochondrial respiration post MV infection. (A) Seahorse XF^{e} 24 analyzer was used to assess oxygen consumption rate (OCR) of hTERT and 5H cells at 0, 24 and 48 hours post infection with MV-NSe in the absence of and **(B)** in the presence of FIP. Data shown is mean +/- SEM of 3 independent experiments, with 5 replicates for each data point. Statistical analysis is performed using an unpaired t test. For hTERT and 5H minus FIP ***p<0.0001. For hTERT plus FIP *p=0.0127.

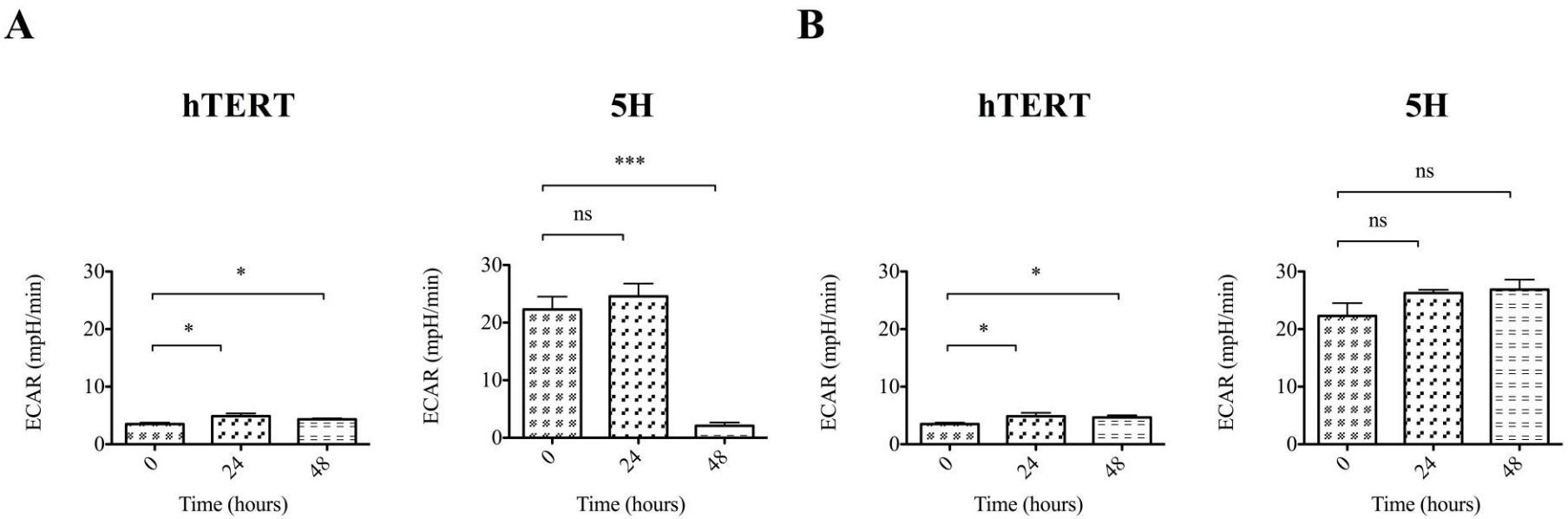

Figure 5-12: Cellular glycolytic activity post MV infection. (A) Seahorse XF^{e} 24 analyzer was used to assess extracellular acidification rate (ECAR) of hTERT and 5H cells at 0, 24 and 48 hours post infection with MV-NSe in the absence of and **(B)** in the presence of FIP. Data shown is mean +/- SEM of 3 independent experiments, with 5 replicates for each data point. Statistical analysis is performed using an unpaired t test. For hTERT minus FIP 24 hours *p0.0111 and 48 hours *p=0.0150; for 5H minus FIP 48 hours ***p<0.0001. For hTERT plus FIP 24 hours *p=0.0221 and 48 hours *p=0.0146.

In light of the dramatic differences in OCR post MV infection, cellular ATP quantification and oxygen radical quantification were performed at 24 hourly intervals post infection. Preliminary data shows a ~3-fold increase in the amount of ATP production primarily in 4+V and 5H cells at 24 hours post infection (see Figure 5-13), coinciding with the increase in OCR demonstrated with bioenergetics studies in 5H cells. ATP production is dramatically reduced at 48 hours, correlating with the fall-off in OCR and ECAR seen in bioenergetics studies. Furthermore, flow cytometric analysis of ROS production in hTERT and 5H cells demonstrates a ~10 fold increase in the amount of ROS production by fully transformed cells at 24 hours post infection in comparison to ROS production in minimally transformed cells (see Figure 5-14).

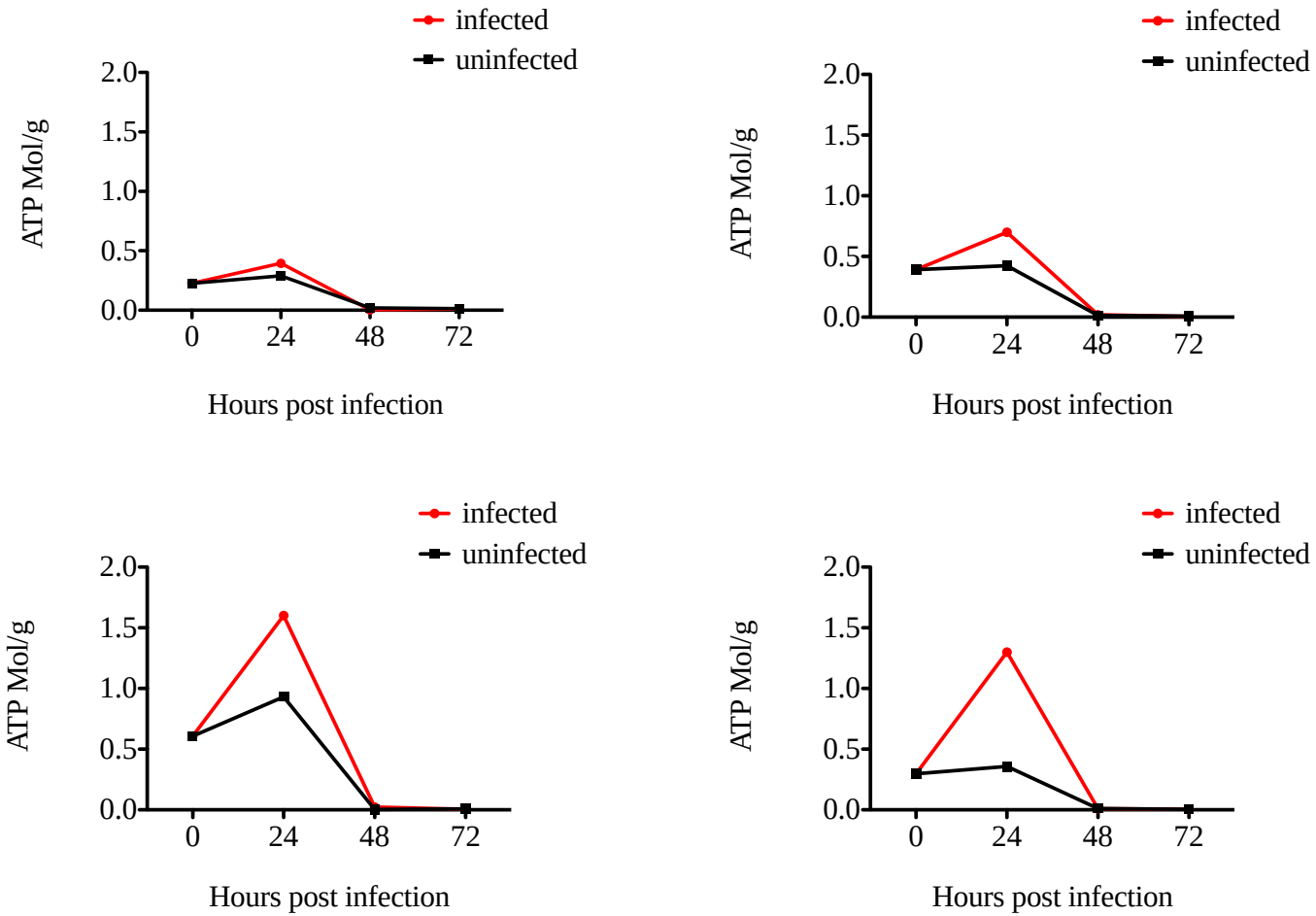

Figure 5-13: Effect of MV infection on cellular ATP production. Differentially transformed MSCs, either uninfected, or post infection with MV-NSe (MOI 1.0) were assessed at 24 hourly intervals post infection for the amount of intracellular ATP production. ATP concentration was quantified using a luciferase-based assay, and represented as values per gram of protein. Data shown is for a single experiment, performed in triplicate.

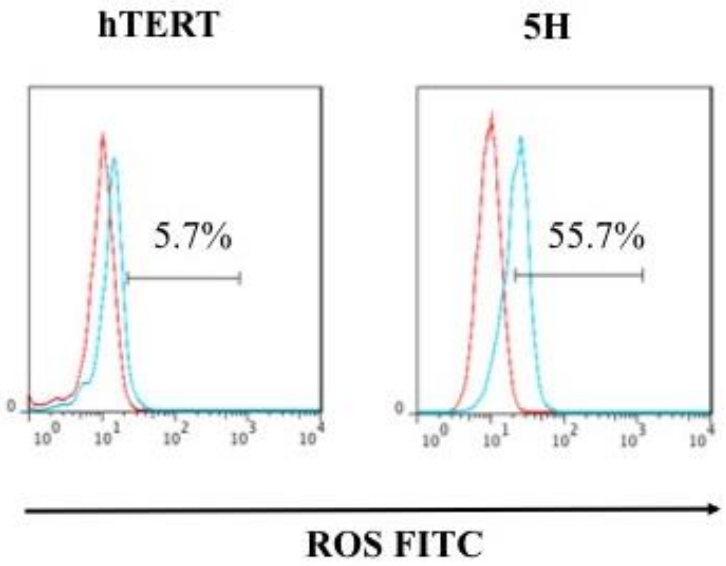

Figure 5-14: Assessment of cellular ROS production following MV infection. hTERT and 5H cells were infected (or mock infected) with MV-NSe at MOI 1.0 under standard tissue culture conditions. At 24 hours, cells were harvested and subject to flow cytometric analysis for the amount of ROS production. Representative plots from a single experiment are shown. Viable cells were gated according to FSC and SSC characteristics. Red line: baseline ROS expression in uninfected cells. Blue line: ROS expression in infected cells.

To investigate apoptosis triggering following MV infection, caspase 3/7 activation was assessed in hTERT and 5H cells at 24 and 48 hours post MV-NSe infection for a range of MOIs, using a luciferase based assay (see Figure 5-15). Whilst caspase 3/7 activation is minimal in hTERT cells post MV-infection (hTERT 48 hrs uninfected 5208.5 +/- 222.5; MOI 0.01 3167.0 +/- 69.0; MOI 0.1 2750.0 +/- 82.0; MOI 1.0 3957.0 +/- 65.0), there is a marked increase in caspase 3/7 activation for 5H cells at 48 hours post infection, which increases in parallel with an increasing MOI (5H 48 hrs uninfected 3362.5 +/- 1028.5; MOI 0.01 2355.0 +/- 166; MOI 0.1 9866.0 +/- 1225; MOI 1.0 50034.0 +/- 2054.0).

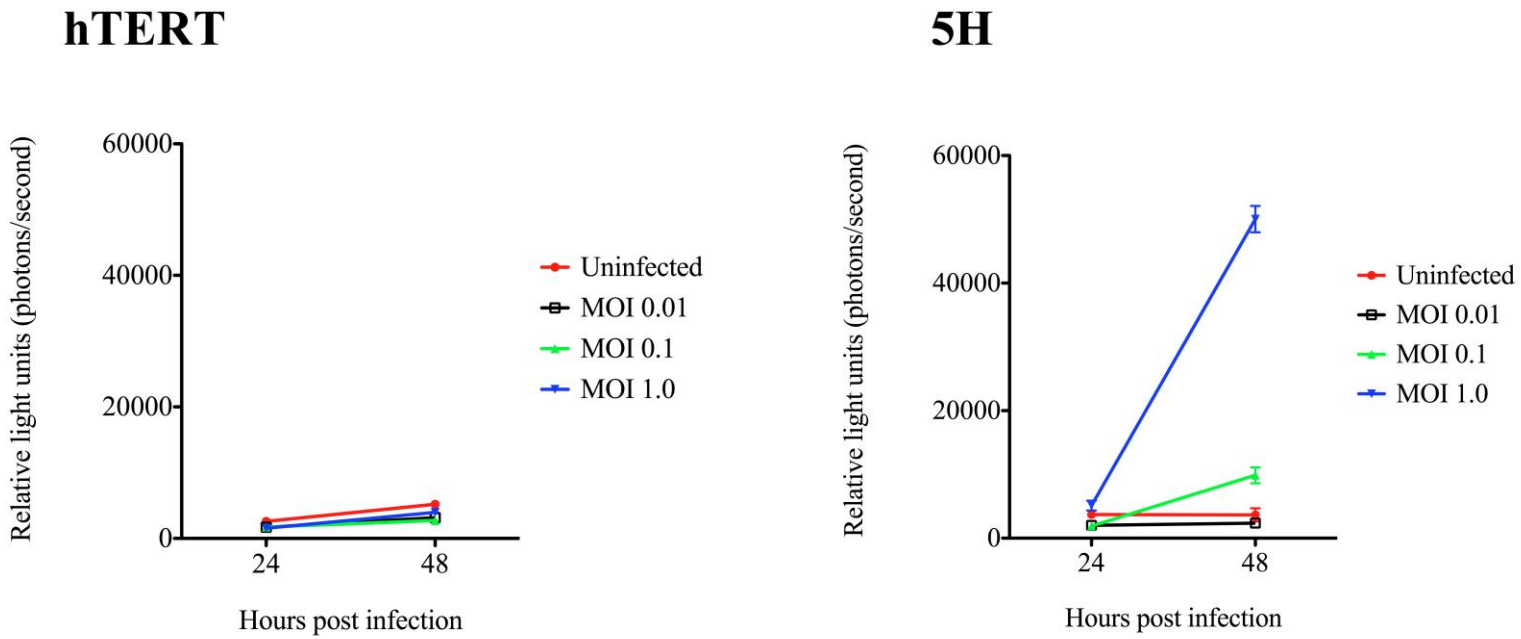

Figure 5-15: Caspase 3/7 activation following cellular infection by MV. Levels of caspase 3/7 activation post MV-NSe infection at a range of MOIs was performed on hTERT and 5H cells using a luciferase based assay. Data represented is mean +/- SEM from 2 independent experiments performed in triplicate.

5.6 Discussion

Tumorigenesis is a multistep process involving the combined accumulation of oncogenic pathway activations and the inactivation of tumor suppressor genes. Whilst a handful of studies have attempted to investigate the mechanisms underlying tumour specificity demonstrated by live, attenuated vaccine MV strains by looking at MV-permissive versus resistant models of the same tumour type, no studies have been performed directly comparing cellular responses of transformed and untransformed cells for this virus. Wang et al. used an alternative oncolytic virus – myxoma virus – to look at the effect of immortalization on permissiveness and susceptibility to killing of mouse embryonic fibroblasts (MEFs). Whilst primary MEFs were non-permissive to myxoma virus replication, corresponding immortalized MEFs supported a highly productive viral infection, with permissiveness being related to an immortalization-associated selective block to the cellular αβ IFN induction machinery normally triggered in response to virus infection[265].

Here, a stromal cell model of oncogenesis was utilized to probe mechanisms of tumour selectivity known to be a defining feature of oncolytic MV. Proof of principle was achieved, with demonstration of enhanced infectivity, improved virus productivity (both intracellular and released virus) and improved rates of MV-specific cell death with progressive cellular transformation, that was not solely related to enhanced cell turnover. Whilst hTERT-immortalised MSCs, or MSCs with additional disruption of tumour suppressor gene pathways showed limited MV cytopathy, those cells with disrupted proto-oncogenes such as *c-Myc* and *H-Ras* were highly susceptible to MV-mediated killing, (even following experimental correction for cellular doubling time). Whilst examination of cellular MV receptor profiles did not demonstrate significant differences that would suggest virus discrimination between normal versus cancer cells on a cell entry level, there was marked variability in the receptor profile data. The possibility remains that subtle but significant differences in receptor profile could be influencing virus entry into normal versus transformed cells, and this requires clarification. Cell-to-cell spread via fusion mechanisms appears to be vital to dissemination of virus and propagation of cell killing in vitro. This interesting finding is in contrast to in vivo pre-clinical models, where therapeutic effect of

oncolytic MV is evident with little MV cytopathy demonstrable within treated tumours[14]. It is likely that anti-MV or anti-tumour immune responses are involved in perpetuating or amplifying anti-tumour efficacy in vivo.

Examination of cellular type 1 IFN responses to MV stimulation in this model demonstrated a robust induction of IFNβ (and to a lesser extent IFNα) in primary MSCs, that was lost with progressive cellular transformation, suggesting that IFN response pathways are affected by immortalization, and potentially implicating this as a mechanism for the enhanced MV permissiveness seen here. This could be further confirmed by the pre-treatment of fully immortalized MSCs with exogenous IFNβ with subsequent re-evalualtion of the extent of cellular virus productivity, and induced cell death.

As cytoplasmic RLR signaling mechanisms are known to play a significant role in the triggering of IFN responses by MV, activation of RLRs was investigated by examining relative levels of RIG-I, MDA-5 and their common signaling adapter IPS-1 mRNA post MV-infection. Along with the blunted type 1 IFN responses seen in fully immortalized, MV permissive MSCs, reduced levels of RIG-I and MDA-5 mRNA are seen in these cells, suggesting that defective RLR-mediated signaling may result from immortalization, and contribute to the impaired antiviral responses seen. However, whilst RIG-I and MDA-5 levels parallel those of the type 1 IFNs, it is interesting to note that levels of IPS-1 mRNA were negligible, being effectively indistinguishable at different stages of transformation. It would be expected that IPS-1 mRNA levels would reflect those of the upstream RLR family members, with signaling via IPS-1 being intact in untransformed/normal MSCs and impaired in immortalized MSCs. Whether or not defects in RLR-mediated signaling are responsible for abrogating the antiviral responses in MV permissive cells is unclear from this data. It is possible that additional interacting pathways, known to play a role in IFN-mediated cellular responses (such as STING signaling or TLR-mediated signaling) may be contributing to the altered type 1 IFN profile, and the phenotypic differences in MV-permissiveness seen in here. It is worth noting, however, that TLR-2 (the well recognized TLR utilized by MV) has been shown only to be activated by wild-type but not vaccine virus strains[110].

In addition to examining innate immune responses of MV-stimulated healthy and transformed MSCs, to gain understanding of how MV can discriminate between these conditions, I was interested to examine the metabolic consequences resultant upon cellular MV infection, with the aim of understanding the specific bioenergetic processes and cell death mechanisms consequent upon MV infection. When considering mode of cell death implicated in models of MV oncolysis, mechanisms usually refer to the observation of apoptotic phenomena[25,266], although this has recently been contested. In relation to another oncolytic virus, Whilding et al.[267] evaluated cell death pathways following thymidine kinase-deleted (dTK) vaccinia virus infection of ovarian cancer cells. They were able to demonstrate a significant increase after 24 hours of infection, in both OCR and ECAR, followed by a steep decline to below baseline. In addition there was a reduction in intracellular ATP levels in all cell lines infected with dTK vaccinia strain. These bioenergetics events were ultimately linked to the occurance of necrotic cell death mediated through a programmed series of events. Recent work looking at the effect of MV-Edm infection on cell death mechanisms in non-small cell lung cancer (NSCLC) cell lines demonstrated an induction of autophagy and sequestosome 1-mediated mitophagy (intracellular degradation of mitochondria) leading to decreased cytochrome c release, and early blocking of the pro-apoptotic cascade in order to favour viral replication, before ultimate necrotic cell death due to ATP depletion. When autophagy was impaired, MV-Edm-induced cell death was abrogated despite increased induction of apoptotic pathways[268]. Furthermore, the same group was able to demonstrate in this model, that MV-Edm exploits autophagy to mitigate the innate immune response mediated by RLRs, by the mitophagy-targeted reduction of IPS-1[269].

Data presented here suggests a role for syncytia formation in the potentiation of MV-mediated cell killing in vitro. Previous studies have demonstrated mitochondrial dysfunction in gibbon ape leukaemia virus hyperfusogenic envelope protein (GALV-FMG) induced syncytia, prior to loss of mitochondrial membrane potential and syncytial viability, cellular ATP depletion and cell death with necrosis[270]. Preliminary bioenergetics data here shows a marked increase in OCR (with less of an effect on ECAR) in response to MV infection that is clearly abrogated in the presence of FIP. Increases in OCR were reflected by modest increases in ATP levels at early timepoints post infection in 4+V and 5H transformed MSCs, with ATP levels

subsequently demonstrating a dramatic fall off at 48 hours post infection. It is possible therefore, that the increases in OCR seen in MV-permissive fully transformed MSCs post infection are not related to increased ATP generation, but relate to mitochondrial dysfunction and production of oxygen radicals post MV infection. Flow cytometric analysis of ROS production in the less-permissive hTERT cells versus the fully permissive 5H cells demonstrated an increase in ROS production in transformed cells at 24 hours post infection that supports this theory, however further evaluation of the effect of antioxidants on cell killing is warranted, along with investigation of the direct effects of MV-infection on cellular mitochondria (including mitochondrial stress tests, evalualtion of mitochondrial mass and mitochondrial membrane potential studies pre and post infection with MV).

The presence of oxygen radicals has been implicated in several aspects of RNA virus disease pathogenesis including triggering of apoptosis pathways[271], and it is notable therefore, that post-MV infection there is clear activation of caspases 3 and 7 in the MV-permissive MSCs here. Activation of caspases seen in this model is in keeping with existing literature, where both vaccine and (to a greater extent) wild-type MV have been shown to induce caspase 3 activation and widespread apoptosis via induction of tumour necrosis factor-related apoptosis-inducing ligand (TRAIL)[272]. Further confirmation of the role of apoptosis pathways in cell death mechanisms in this model should be sought (including examination of the effect of the pan-caspase inhibitor, Z-VAD-fmk, on extent of cell death, and by seeking evidence of poly ADP ribose polymerase (PARP) cleavage). In addition, evaluation of the potential roles of autophagy and primary necrosis in MV-mediated killing in this model is warranted. Although it is clear that apoptosis pathways are being triggered here, it is likely that mechanisms of cell death may not be universal for all pre-clinical models. It is also probable that mechanisms of virally-mediated cell killing in vitro may be distinct from those seen in vivo.

Chapter 6: General discussion

Whilst the appropriateness of using oncolytic measles virotherapy as a novel treatment strategy in precursor B-lineage ALL has previously been addressed, this project has established the importance of understanding the intricate interactions that take place between oncolytic virus and host. Understanding host responses to mode of virotherapy delivery and the impact that this will have on therapeutic outcomes, and furthermore understanding cellular factors that allow MV to discriminate between host healthy and cancer cells are of paramount importance if MV is to be taken forward into rationally designed, safe and effective clinical trials. This chapter will address the overall findings of the project in the broader context of research in the oncolytic virotherapy field, discussing new insights into the complex biological interactions between MV and host, and considering future investigative directions, whilst also taking into account the limitations of methodological approaches.

6.1 Criteria for selection of oncolytic viruses for cancer therapy

In order for successful oncolytic application, viruses have to meet stringent selection criteria for safety and efficacy. As previously discussed (Chapter 1), vaccine strain MV has demonstrated selectivity and specificity for cancer cells in a range of malignancies. The negative sense, single stranded unsegmented viral RNA genome does not lend itself to recombination, limiting the possibility of the vaccine virus regaining pathogenicity. Safety of live, attenuated MV strains has been demonstrated in worldwide vaccination programmes, with only select cases of atypical measles infection occurring in severely immunocompromised individuals (CD4 <200)[273,274]. There have been no cases of transmission of measles infection following vaccination, to healthy individuals, and early phase clinical trials have demonstrated little in the way of virus shedding. Furthermore, early phase trial data shows minimal undesirable side effects, with the recent myeloma trial detailing only transient and reversible systemic symptoms upon infusion of the highest doses of product (10^{11} $TCID_{50}$)[30]. Whilst these features make MV a sensible choice as an oncolytic agent, there are two significant issues harbouring uptake of this promising virus into advanced phase trials. Firstly, pre-existing immunity to MV in vaccinated individuals has been shown in pre-clinical studies to harbor the systemic delivery of virus to tumour targets, limit

intratumoural spread and have an adverse impact on therapeutic efficacy. Secondly, we have a limited mechanistic understanding of the factors that confer MV the ability to be able to preferentially target malignant cells over healthy cells.

6.2 Using BM-MSCs as biological delivery vehicles for oncolytic MV

Whilst pre-existing neutralizing anti-MV antibodies are implicated as a likely mechanism that will limit the ultimate clinical applicability of this virus as an oncotherapeutic agent, the scope of the problem has not previously been defined for patients with ALL. Data in Chapter 3 demonstrates the issue with clarity, with the significant majority of a cohort of adult ALL patients having clinically significant levels of anti-measles antibodies present despite prior treatment with extensive immunosuppressive chemotherapeutic regimens. In relation to another haematological disorder, the ongoing phase 1 clinical trial using MV in heavily pre-treated myeloma patients has provisional data suggesting that responders at the highest dose level were restricted to those patients who were deemed measles non-immune by their low or undetectable levels of anti-MV antibody prior to therapy. Furthermore, single intravenously delivered doses of oncolytic MV administered to patients triggered strong anamnestic responses[30]. Enhancing efficacy of oncolytic measles virotherapy by developing strategies for efficient virus delivery in the face of host antiviral immune mechanisms is clearly required. Here, BM-MSCs were utilized as effective cellular delivery vehicles for oncolytic MV to distant pre-B ALL cell targets. The initial rational for choosing MSCs for this purpose has been discussed elsewhere in this document. Chapter 3 demonstrates the ability of BM-MSCs to be infected by MV, act as miniature virus producing units (retaining virus intracellularly), retain viability long enough to be delivered intravenously to distant tumour targets within the murine BM, and hand-off virus to ALL cell targets in the presence of passive immunity. Furthermore, enhanced therapeutic outcomes were achieved by using this approach to MV-delivery, as compared to control groups where naked MV was administered. This is the first demonstration of the use of cellular carriers such as BM-MSCs to effectively deliver oncolytic MV to a disseminated malignancy such as ALL in the presence of humoral immunity. It is of interest that survival data demonstrated enhanced therapeutic outcomes for animals treated with MSC-delivered MV as compared to controls even in the absence of humoral immunity. It is likely that

MSCs are acting as biological factories within which MV can be amplified, enhancing the oncolytic payload delivered to distant tumour targets. It may also be the case that MSCs are enhancing targeting of MV to ALL, potentially due to their lack of immune recognition. On a more general level, the data firmly establishes the concept of targeting distant leukaemia sites using MSCs, which could be extrapolated to the delivery of novel treatments other than oncolytic viruses.

6.3 Enhancing MSC tumour trafficking

Whilst both DNA and RNA viruses have been used in oncolytic virotherapy, DNA viruses were initially thought to be more amenable to genetic manipulation. However, the advent of a robust reverse genetics system for the rescue of negative sense RNA viruses from cDNA has opened the doors to genetic engineering of MV in order to improve cellular targeting, virus traceability and therapeutic efficacy. Chapter 4 demonstrates the successful cloning and rescue of a novel strain of MV-NSe encoding for the human chemokine receptor gene *hCXCR4* as an additional transcription unit within the MV genome. Whilst proof of principle was established with enhanced MSC cell surface expression of hCXCR4 detectable post infection, and improved migratory capacity towards a SDF-1α gradient demonstrable in vitro, the migratory benefit gained from using this novel virus strain was not significantly superior to use of the standard MV-NSe strain for MSC infection. Furthermore, in light of the excellent therapeutic responses seen in this project when standard MV-NSe was delivered to distant ALL cell targets in vivo, use of the hCXCR4-expressing vaccine MV strain was not taken forward into animal modeling.

6.4 Differentiating between normal and cancer cells

Whilst other investigators have used MV-permissive and non-permissive cancer cell lines to probe mechanisms of virus specificity, this study is the first to utilize a model of progressive transformation, allowing the direct comparison of cellular processes resultant upon MV infection, in primary normal cells alongside their malignant counterparts. Whilst an artificially induced model of cellular immortalisation, MSCs deemed ‘fully transformed’ here have previously been shown to possess phenotypic characteristics of transformation including anchorage-independent growth and tumourigenicity in vivo[223]. Chapter 5 demonstrates enhanced permissiveness,

productivity, and susceptibility to MV-mediated killing of fully immortalized, tumorigenic MSCs in comparison to healthy MSCs, that is not resultant upon MV receptor-mediated entry. In response to MV infection, an upregulation of the intracellular sensing molecules RIG-I and MDA-5 was identified in MSCs at earlier stages of transformation (previously shown to be less permissive to MV infection and replication) indicating a potential role of the innate immune system in preventing MV-induced oncolysis in this model. Whilst levels of IPS-1 mRNA did not appear to follow the same pattern, it is notable that levels of cellular type 1 IFN production were enhanced in primary and hTERT MSCs, with a progressive decline in stimulation of IFN responses as MSCs become immortalized. It is likely that defects in innate immune responses in immortalized cells are playing a role in MV-permissiveness here. In addition to looking at other PRRs known to be involved in induction of type 1 IFN responses (including TLRs), examining modulation of STAT1 phosphorylation and profiling of ISGs in permissive and 'resistant' stromal cells before and after infection with MV will help to identify downstream candidates that may potentially inhibit or enhance cellular virus infectivity[275,276].

6.5 MV-induced modes of cell death

Whilst bioenergetics studies were able to demonstrate a marked effect of MV-infection on cellular OCR, only subtle differences in intracellular levels of ATP were seen in the MV-permissive MSCs. The detection of ROS in infected 5H cells could provide an explanation for the increased oxygen requirements seen. Whilst triggering of caspases 3 and 7 was evident in transformed MSCs post infection, whether or not oxygen radical production is playing a role in the triggering of apoptosis pathways requires further investigation. Induction of apoptosis provides a mechanism whereby viruses can evade host cell immune responses. During apoptosis, progeny virions along with the cellular contents of a cell are packaged into membrane enclosed vesicles, which are rapidly taken up by neighbouring cells and allow for undetected virus propagation in the host. Apoptotic pathways utilized, and the targets that viruses strike, are varied between different viruses and between different cell types. An example of this is with adenovirus. Whilst *E1A* gene of adenovirus associates with the pRB/p300 family of histone acetyltransferases and induces *p53* dependent apoptosis in many cancer cells[277], adenovirus early region 4 open reading frame (E4orf4)

induced apoptosis is *p53* independent in mouse embryo fibroblast derived cells[278]. A recent study examining cell death processes in melanoma cell cultures infected with oncolytic Newcastle-disease-virus (NDV), demonstrated the ability of this oncolytic virus to overcome cellular resistance to apoptosis by triggering the activation of caspases that can cleave the inhibitor of apoptosis protein (IAP) family member Livin (highly expressed in melanoma cells) to create a truncated pro-apoptotic protein[279] and potentiate NDV-induced oncolysis. Data in Chapter 5 demonstrates triggering of caspases 3 and 7 in 5H transformed MSCs post MV infection, despite lack of functional p53 in these cells. Like the related avian Paramyxovirus NDV, the possiblity that MV can overcome resistance to apoptosis by modulating inhibitors of apoptotic pathways remains.

6.6 Study limitations

6.6.1 Using MV in murine xenografts models

As previously discussed, humans are the only natural host for sustaining MV transmission. Historically, the lack of suitable animal models has greatly hindered the progress of oncolytic MV research. Whilst transgenic animal models have been developed in order to humanize mice and allow for cellular MV infection and the study of virus-host interaction, these models are not without limitation. In order to mimic the cellular distribution and amount of CD46 found in humans, several transgenic models have been generated. In addition to generating murine models where CD46 gene expression levels are comparable to that found in humans, additional immune defects are required to overcome intracellular factors in murine cells that limit MV replication. Resultant murine strains (eg. CD46Ge x *IFNAR*-KO[176]; YAC-CD46 x *RAG-1*[280]) although useful as models of pathogenicity, cannot sustain human tumour xenografts. Therefore in order to study the therapeutic effects of oncolytic MV in vivo, immunocompromised SCID mice engrafted with human xenografts are utilized. Whilst helpful in demonstrating tumour susceptibilities, virus replication is limited in these models to human tumour cells, and therefore questions regarding virus toxicity or off-target effects cannot be addressed. As immunocompromised models are required, modeling the immune responses to virus administration is challenging, and humoral immune responses must be re-capitulated by passive immunization of animals. Mader et al. demonstrated that at 3 hours post

intraperitoneal injection of human serum containing 80EU of anti-measles antibody to immunocompromised mice, animals were confirmed to be measles immune with a gradual decrease in plaque reduction neutralization (PRN) titres over the following week, and an anti-MV antibody t/2 of 19.2 hours[183]. Whilst passive immunization allows for effective modeling of pre-existing humoral immune responses, anamnestic responses cannot be assessed, nor does this model address the impact of cell-mediated immunity on systemic delivery of oncolytic measles virus. Looking at novel ways to model the impact of cell-mediated immune responses (eg. by adoptive transfer of anti-MV specific T cells) could be informative here, and should be explored.

6.6.2 Models of transformation

As previously addressed, the stromal cell model of transformation utilized here allows for the direct in vitro comparison of primary healthy untransformed MSCs alongside their malignant counterparts, and provides a potentially excellent opportunity to examine oncolytic MV kinetics. However, it is important to note that although providing insight into potential mechanisms of cellular virus sensitivity or resistance, and modes of cell killing, the findings here may be specific to the model in question. Whether or not similar results can be re-capitulated in other cell-types remains to be determined.

6.7 Conclusions and future research areas

Whilst, in general it is fair to say that efforts of the oncolytic virotherapy community have been directed more towards the use of viruses in the treatment of solid tumours, than in disseminated haematological malignancies, the work presented in this project has cemented the case for using oncolytic MV as a novel treatment strategy for disseminated leukaemias such as pre-B ALL. Furthermore, this work has addressed the important issue of how treatment can be delivered successfully in the face of pre-existing immunity in order to maximize therapeutic benefit. Clinical validation of the use of oncolytic MV in ALL is now required. An initial phase I trial of oncolytic MV in adult ALL is planned. Alongside efforts to determine the safety of intravenously administered oncolytic MV in this disease, secondary goals will include the careful monitoring of humoral and cellular responses to injected virus, to set a baseline for evaluation of ‘immune shielding’ approaches.

In addition, the work presented here has begun to explore the mechanisms that MV can exploit to differentiate between healthy and transformed cells. Future work will be focused on probing antiviral response pathways further, where possible in a range of tissue types, to gain a comprehensive mechanistic understanding of how MV acts to kill cancer cells whilst leaving normal cells unharmed. Such work is essential to the future progression of this promising novel anticancer agent in the clinical arena.

References

1. Dock G. The influence of complicating diseases upon leukemia. *Am J Med Sci.* 1904(127):563-592.
2. Bierman HR, Crile DM, Dod KS, Kelly KH, Petrakis NL, White LP, Shimkin MB. Remissions in leukemia of childhood following acute infectious disease: staphylococcus and streptococcus, varicella, and feline panleukopenia. *Cancer.* May 1953;6(3):591-605.
3. Kelly E, Russell SJ. History of oncolytic viruses: genesis to genetic engineering. *Mol Ther.* Apr 2007;15(4):651-659.
4. Breitbach CJ, Reid T, Burke J, Bell JC, Kirn DH. Navigating the clinical development landscape for oncolytic viruses and other cancer therapeutics: no shortcuts on the road to approval. *Cytokine Growth Factor Rev.* Apr-Jun 2010;21(2-3):85-89.
5. Senzer NN, Kaufman HL, Amatruda T, Nemunaitis M, Reid T, Daniels G, Gonzalez R, Glaspy J, Whitman E, Harrington K, Goldsweig H, Marshall T, Love C, Coffin R, Nemunaitis JJ. Phase II clinical trial of a granulocyte-macrophage colony-stimulating factor-encoding, second-generation oncolytic herpesvirus in patients with unresectable metastatic melanoma. *J Clin Oncol.* Dec 1 2009;27(34):5763-5771.
6. Andtbacka FAC RHI, Amatruda T, Senzer N, al. e. OPTiM: a randomized phase III trial of talimogene laherparepvec (T-VEC) versus subcutaneous (SC) granulocyte-macrophage colony-stimulating factor (GM-CSF) for the treatment (tx) of unresected stage IIIB/C and IV melanoma. American Society of Clinical Oncology; 2013.
7. Galanis E, Markovic SN, Suman VJ, Nuovo GJ, Vile RG, Kottke TJ, Nevala WK, Thompson MA, Lewis JE, Rumilla KM, Roulstone V, Harrington K, Linette GP, Maples WJ, Coffey M, Zwiebel J, Kendra K. Phase II trial of intravenous administration of Reolysin(®) (Reovirus Serotype-3-dearing Strain) in patients with metastatic melanoma. *Mol Ther.* Oct 2012;20(10):1998-2003.
8. Heo J. A randomized, controlled phase II trial of JX-594, a targeted, multimechanistic oncolytic poxvirus, in patients with advanced hepatocellular carcinoma, final results. American Association for the Study of Liver Diseases; 2011.
9. Pasquinucci G. Possible effect of measles on leukaemia. *Lancet.* Jan 16 1971;1(7690):136.
10. Gross S. Measles and leukaemia. *Lancet.* Feb 20 1971;1(7695):397-398.
11. Zygiert Z. Hodgkin's disease: remissions after measles. *Lancet.* Mar 20 1971;1(7699):593.
12. Taqi AM, Abdurrahman MB, Yakubu AM, Fleming AF. Regression of Hodgkin's disease after measles. *Lancet.* May 16 1981;1(8229):1112.
13. Bluming AZ, Ziegler JL. Regression of Burkitt's lymphoma in association with measles infection. *Lancet.* Jul 10 1971;2(7715):105-106.
14. Grote D, Russell SJ, Cornu TI, Cattaneo R, Vile R, Poland GA, Fielding AK. Live attenuated measles virus induces regression of human lymphoma xenografts in immunodeficient mice. *Blood.* Jun 15 2001;97(12):3746-3754.
15. Ungerechts G, Frenzke ME, Yaiw KC, Miest T, Johnston PB, Cattaneo R. Mantle cell lymphoma salvage regimen: synergy between a reprogrammed

oncolytic virus and two chemotherapeutics. *Gene Ther.* Dec 2010;17(12):1506-1516.
16. Ungerechts G, Springfeld C, Frenzke ME, Lampe J, Johnston PB, Parker WB, Sorscher EJ, Cattaneo R. Lymphoma chemovirotherapy: CD20-targeted and convertase-armed measles virus can synergize with fludarabine. *Cancer Res.* Nov 15 2007;67(22):10939-10947.
17. Dingli D, Offord C, Myers R, Peng KW, Carr TW, Josic K, Russell SJ, Bajzer Z. Dynamics of multiple myeloma tumor therapy with a recombinant measles virus. *Cancer Gene Ther.* Dec 2009;16(12):873-882.
18. Dingli D, Peng KW, Harvey ME, Greipp PR, O'Connor MK, Cattaneo R, Morris JC, Russell SJ. Image-guided radiovirotherapy for multiple myeloma using a recombinant measles virus expressing the thyroidal sodium iodide symporter. *Blood.* Mar 1 2004;103(5):1641-1646.
19. Patel B, Dey A, Ghorani E, Kumar S, Malam Y, Rai L, Steele AJ, Thomson J, Wickremasinghe RG, Zhang Y, Castleton AZ, Fielding AK. Differential cytopathology and kinetics of measles oncolysis in two primary B-cell malignancies provides mechanistic insights. *Mol Ther.* Jun 2011;19(6):1034-1040.
20. Peng KW, TenEyck CJ, Galanis E, Kalli KR, Hartmann LC, Russell SJ. Intraperitoneal therapy of ovarian cancer using an engineered measles virus. *Cancer Res.* Aug 15 2002;62(16):4656-4662.
21. Peng KW, Hadac EM, Anderson BD, Myers R, Harvey M, Greiner SM, Soeffker D, Federspiel MJ, Russell SJ. Pharmacokinetics of oncolytic measles virotherapy: eventual equilibrium between virus and tumor in an ovarian cancer xenograft model. *Cancer Gene Ther.* Aug 2006;13(8):732-738.
22. Allen C, Paraskevakou G, Liu C, Iankov ID, Msaouel P, Zollman P, Myers R, Peng KW, Russell SJ, Galanis E. Oncolytic measles virus strains in the treatment of gliomas. *Expert Opin Biol Ther.* Feb 2008;8(2):213-220.
23. Allen C, Vongpunsawad S, Nakamura T, James CD, Schroeder M, Cattaneo R, Giannini C, Krempski J, Peng KW, Goble JM, Uhm JH, Russell SJ, Galanis E. Retargeted oncolytic measles strains entering via the EGFRvIII receptor maintain significant antitumor activity against gliomas with increased tumor specificity. *Cancer Res.* Dec 15 2006;66(24):11840-11850.
24. Studebaker AW, Kreofsky CR, Pierson CR, Russell SJ, Galanis E, Raffel C. Treatment of medulloblastoma with a modified measles virus. *Neuro Oncol.* Oct 2010;12(10):1034-1042.
25. Liu C, Sarkaria JN, Petell CA, Paraskevakou G, Zollman PJ, Schroeder M, Carlson B, Decker PA, Wu W, James CD, Russell SJ, Galanis E. Combination of measles virus virotherapy and radiation therapy has synergistic activity in the treatment of glioblastoma multiforme. *Clin Cancer Res.* Dec 2007;13(23):7155-7165.
26. McDonald CJ, Erlichman C, Ingle JN, Rosales GA, Allen C, Greiner SM, Harvey ME, Zollman PJ, Russell SJ, Galanis E. A measles virus vaccine strain derivative as a novel oncolytic agent against breast cancer. *Breast Cancer Res Treat.* Sep 2006;99(2):177-184.
27. Iankov ID, Msaouel P, Allen C, Federspiel MJ, Bulur PA, Dietz AB, Gastineau D, Ikeda Y, Ingle JN, Russell SJ, Galanis E. Demonstration of anti-tumor activity of oncolytic measles virus strains in a malignant pleural effusion breast cancer model. *Breast Cancer Res Treat.* Aug 2010;122(3):745-754.

28. Heinzerling L, Kunzi V, Oberholzer PA, Kundig T, Naim H, Dummer R. Oncolytic measles virus in cutaneous T-cell lymphomas mounts antitumor immune responses in vivo and targets interferon-resistant tumor cells. *Blood.* Oct 1 2005;106(7):2287-2294.
29. Galanis E, Hartmann LC, Cliby WA, Long HJ, Peethambaram PP, Barrette BA, Kaur JS, Haluska PJ, Jr., Aderca I, Zollman PJ, Sloan JA, Keeney G, Atherton PJ, Podratz KC, Dowdy SC, Stanhope CR, Wilson TO, Federspiel MJ, Peng KW, Russell SJ. Phase I trial of intraperitoneal administration of an oncolytic measles virus strain engineered to express carcinoembryonic antigen for recurrent ovarian cancer. *Cancer Res.* Feb 1 2010;70(3):875-882.
30. Russell SJ, Federspiel MJ, Peng KW, Tong C, Dingli D, Morice WG, Lowe V, O'Connor MK, Kyle RA, Leung N, Buadi FK, Rajkumar SV, Gertz MA, Lacy MQ, Dispenzieri A. Remission of disseminated cancer after systemic oncolytic virotherapy. *Mayo Clin Proc.* Jul 2014;89(7):926-933.
31. ENDERS JF, PEEBLES TC. Propagation in tissue cultures of cytopathogenic agents from patients with measles. *Proc Soc Exp Biol Med.* Jun 1954;86(2):277-286.
32. Katz SL. John F. Enders and measles virus vaccine--a reminiscence. *Curr Top Microbiol Immunol.* 2009;329:3-11.
33. Naniche D, Yeh A, Eto D, Manchester M, Friedman RM, Oldstone MB. Evasion of host defenses by measles virus: wild-type measles virus infection interferes with induction of Alpha/Beta interferon production. *J Virol.* Aug 2000;74(16):7478-7484.
34. Takeda M, Kato A, Kobune F, Sakata H, Li Y, Shioda T, Sakai Y, Asakawa M, Nagai Y. Measles virus attenuation associated with transcriptional impediment and a few amino acid changes in the polymerase and accessory proteins. *J Virol.* Nov 1998;72(11):8690-8696.
35. Takeuchi K, Miyajima N, Kobune F, Tashiro M. Comparative nucleotide sequence analyses of the entire genomes of B95a cell-isolated and vero cell-isolated measles viruses from the same patient. *Virus Genes.* 2000;20(3):253-257.
36. Tahara M, Takeda M, Yanagi Y. Contributions of matrix and large protein genes of the measles virus edmonston strain to growth in cultured cells as revealed by recombinant viruses. *J Virol.* Dec 2005;79(24):15218-15225.
37. Tahara M, Takeda M, Yanagi Y. Altered interaction of the matrix protein with the cytoplasmic tail of hemagglutinin modulates measles virus growth by affecting virus assembly and cell-cell fusion. *J Virol.* Jul 2007;81(13):6827-6836.
38. Bellini WJ, Rota JS, Rota PA. Virology of measles virus. *J Infect Dis.* Nov 1994;170 Suppl 1:S15-23.
39. Rota PA, Brown K, Mankertz A, Santibanez S, Shulga S, Muller CP, Hübschen JM, Siqueira M, Beirnes J, Ahmed H, Triki H, Al-Busaidy S, Dosseh A, Byabamazima C, Smit S, Akoua-Koffi C, Bwogi J, Bukenya H, Wairagkar N, Ramamurty N, Incomserb P, Pattamadilok S, Jee Y, Lim W, Xu W, Komase K, Takeda M, Tran T, Castillo-Solorzano C, Chenoweth P, Brown D, Mulders MN, Bellini WJ, Featherstone D. Global distribution of measles genotypes and measles molecular epidemiology. *J Infect Dis.* Jul 2011;204 Suppl 1:S514-523.

40. Rota JS, Wang ZD, Rota PA, Bellini WJ. Comparison of sequences of the H, F, and N coding genes of measles virus vaccine strains. *Virus Res.* Mar 1994;31(3):317-330.
41. Lamb RA. Paramyxovirus fusion: a hypothesis for changes. *Virology.* Nov 1993;197(1):1-11.
42. Calain P, Roux L. The rule of six, a basic feature for efficient replication of Sendai virus defective interfering RNA. *J Virol.* Aug 1993;67(8):4822-4830.
43. Mühlebach MD, Leonard VH, Cattaneo R. The measles virus fusion protein transmembrane region modulates availability of an active glycoprotein complex and fusion efficiency. *J Virol.* Nov 2008;82(22):11437-11445.
44. Hashiguchi T, Ose T, Kubota M, Maita N, Kamishikiryo J, Maenaka K, Yanagi Y. Structure of the measles virus hemagglutinin bound to its cellular receptor SLAM. *Nat Struct Mol Biol.* Feb 2011;18(2):135-141.
45. Iseni F, Garcin D, Nishio M, Kedersha N, Anderson P, Kolakofsky D. Sendai virus trailer RNA binds TIAR, a cellular protein involved in virus-induced apoptosis. *EMBO J.* Oct 2002;21(19):5141-5150.
46. Zhang X, Oglesbee M. Use of surface plasmon resonance for the measurement of low affinity binding interactions between HSP72 and measles virus nucleocapsid protein. *Biol Proced Online.* 2003;5:170-181.
47. Carsillo T, Carsillo M, Niewiesk S, Vasconcelos D, Oglesbee M. Hyperthermic pre-conditioning promotes measles virus clearance from brain in a mouse model of persistent infection. *Brain research.* Apr 2004;1004(1-2):73-82.
48. Carsillo T, Traylor Z, Choi C, Niewiesk S, Oglesbee M. hsp72, a host determinant of measles virus neurovirulence. *J Virol.* Nov 2006;80(22):11031-11039.
49. Das T, Schuster A, Schneider-Schaulies S, Banerjee AK. Involvement of cellular casein kinase II in the phosphorylation of measles virus P protein: identification of phosphorylation sites. *Virology.* Aug 1995;211(1):218-226.
50. Watanabe A, Yoneda M, Ikeda F, Sugai A, Sato H, Kai C. Peroxiredoxin 1 is required for efficient transcription and replication of measles virus. *J Virol.* Mar 2011;85(5):2247-2253.
51. Dhiman N, Jacobson RM, Poland GA. Measles virus receptors: SLAM and CD46. *Rev Med Virol.* 2004 Jul-Aug 2004;14(4):217-229.
52. Dörig RE, Marcil A, Chopra A, Richardson CD. The human CD46 molecule is a receptor for measles virus (Edmonston strain). *Cell.* Oct 1993;75(2):295-305.
53. Naniche D, Varior-Krishnan G, Cervoni F, Wild TF, Rossi B, Rabourdin-Combe C, Gerlier D. Human membrane cofactor protein (CD46) acts as a cellular receptor for measles virus. *J Virol.* Oct 1993;67(10):6025-6032.
54. Manchester M, Liszewski MK, Atkinson JP, Oldstone MB. Multiple isoforms of CD46 (membrane cofactor protein) serve as receptors for measles virus. *Proc Natl Acad Sci U S A.* Mar 1994;91(6):2161-2165.
55. Erlenhöfer C, Duprex WP, Rima BK, ter Meulen V, Schneider-Schaulies J. Analysis of receptor (CD46, CD150) usage by measles virus. *J Gen Virol.* Jun 2002;83(Pt 6):1431-1436.
56. Lecouturier V, Fayolle J, Caballero M, Carabaña J, Celma ML, Fernandez-Muñoz R, Wild TF, Buckland R. Identification of two amino acids in the hemagglutinin glycoprotein of measles virus (MV) that govern hemadsorption, HeLa cell fusion, and CD46 downregulation: phenotypic markers that

differentiate vaccine and wild-type MV strains. *J Virol.* Jul 1996;70(7):4200-4204.
57. Hsu EC, Sarangi F, Iorio C, Sidhu MS, Udem SA, Dillehay DL, Xu W, Rota PA, Bellini WJ, Richardson CD. A single amino acid change in the hemagglutinin protein of measles virus determines its ability to bind CD46 and reveals another receptor on marmoset B cells. *J Virol.* Apr 1998;72(4):2905-2916.
58. Schneider U, von Messling V, Devaux P, Cattaneo R. Efficiency of measles virus entry and dissemination through different receptors. *J Virol.* Aug 2002;76(15):7460-7467.
59. Nielsen L, Blixenkrone-Møller M, Thylstrup M, Hansen NJ, Bolt G. Adaptation of wild-type measles virus to CD46 receptor usage. *Arch Virol.* 2001;146(2):197-208.
60. Manchester M, Valsamakis A, Kaufman R, Liszewski MK, Alvarez J, Atkinson JP, Lublin DM, Oldstone MB. Measles virus and C3 binding sites are distinct on membrane cofactor protein (CD46). *Proc Natl Acad Sci U S A.* Mar 1995;92(6):2303-2307.
61. Manchester M, Gairin JE, Patterson JB, Alvarez J, Liszewski MK, Eto DS, Atkinson JP, Oldstone MB. Measles virus recognizes its receptor, CD46, via two distinct binding domains within SCR1-2. *Virology.* Jun 1997;233(1):174-184.
62. Takeuchi K, Nagata N, Kato SI, Ami Y, Suzaki Y, Suzuki T, Sato Y, Tsunetsugu-Yokota Y, Mori K, Van Nguyen N, Kimura H, Nagata K. Wild-type measles virus with the hemagglutinin protein of the edmonston vaccine strain retains wild-type tropism in macaques. *J Virol.* Mar 2012;86(6):3027-3037.
63. Tatsuo H, Ono N, Tanaka K, Yanagi Y. SLAM (CDw150) is a cellular receptor for measles virus. *Nature.* Aug 24 2000;406(6798):893-897.
64. Hsu EC, Iorio C, Sarangi F, Khine AA, Richardson CD. CDw150(SLAM) is a receptor for a lymphotropic strain of measles virus and may account for the immunosuppressive properties of this virus. *Virology.* Jan 2001;279(1):9-21.
65. Henning G, Kraft MS, Derfuss T, Pirzer R, de Saint-Basile G, Aversa G, Fleckenstein B, Meinl E. Signaling lymphocytic activation molecule (SLAM) regulates T cellular cytotoxicity. *Eur J Immunol.* Sep 2001;31(9):2741-2750.
66. Cocks BG, Chang CC, Carballido JM, Yssel H, de Vries JE, Aversa G. A novel receptor involved in T-cell activation. *Nature.* Jul 1995;376(6537):260-263.
67. Sidorenko SP, Clark EA. Characterization of a cell surface glycoprotein IPO-3, expressed on activated human B and T lymphocytes. *J Immunol.* Nov 1993;151(9):4614-4624.
68. Ohgimoto S, Ohgimoto K, Niewiesk S, Klagge IM, Pfeuffer J, Johnston IC, Schneider-Schaulies J, Weidmann A, ter Meulen V, Schneider-Schaulies S. The haemagglutinin protein is an important determinant of measles virus tropism for dendritic cells in vitro. *J Gen Virol.* Aug 2001;82(Pt 8):1835-1844.
69. Polacino PS, Pinchuk LM, Sidorenko SP, Clark EA. Immunodeficiency virus cDNA synthesis in resting T lymphocytes is regulated by T cell activation signals and dendritic cells. *J Med Primatol.* Jun 1996;25(3):201-209.
70. Minagawa H, Tanaka K, Ono N, Tatsuo H, Yanagi Y. Induction of the measles virus receptor SLAM (CD150) on monocytes. *J Gen Virol.* Dec 2001;82(Pt 12):2913-2917.

71. Ohno S, Seki F, Ono N, Yanagi Y. Histidine at position 61 and its adjacent amino acid residues are critical for the ability of SLAM (CD150) to act as a cellular receptor for measles virus. *J Gen Virol.* Sep 2003;84(Pt 9):2381-2388.
72. Navaratnarajah CK, Vongpunsawad S, Oezguen N, Stehle T, Braun W, Hashiguchi T, Maenaka K, Yanagi Y, Cattaneo R. Dynamic interaction of the measles virus hemagglutinin with its receptor signaling lymphocytic activation molecule (SLAM, CD150). *J Biol Chem.* Apr 2008;283(17):11763-11771.
73. Ward BJ, Griffin DE. Changes in cytokine production after measles virus vaccination: predominant production of IL-4 suggests induction of a Th2 response. *Clin Immunol Immunopathol.* May 1993;67(2):171-177.
74. Griffin DE, Ward BJ. Differential CD4 T cell activation in measles. *J Infect Dis.* Aug 1993;168(2):275-281.
75. Tanaka K, Minagawa H, Xie MF, Yanagi Y. The measles virus hemagglutinin downregulates the cellular receptor SLAM (CD150). *Arch Virol.* 2002;147(1):195-203.
76. de Swart RL, Ludlow M, de Witte L, Yanagi Y, van Amerongen G, McQuaid S, Yüksel S, Geijtenbeek TB, Duprex WP, Osterhaus AD. Predominant infection of CD150+ lymphocytes and dendritic cells during measles virus infection of macaques. *PLoS Pathog.* Nov 2007;3(11):e178.
77. Andres O, Obojes K, Kim KS, ter Meulen V, Schneider-Schaulies J. CD46- and CD150-independent endothelial cell infection with wild-type measles viruses. *J Gen Virol.* May 2003;84(Pt 5):1189-1197.
78. Takeuchi K, Miyajima N, Nagata N, Takeda M, Tashiro M. Wild-type measles virus induces large syncytium formation in primary human small airway epithelial cells by a SLAM(CD150)-independent mechanism. *Virus Res.* Jul 2003;94(1):11-16.
79. Takeda M, Tahara M, Hashiguchi T, Sato TA, Jinnouchi F, Ueki S, Ohno S, Yanagi Y. A human lung carcinoma cell line supports efficient measles virus growth and syncytium formation via a SLAM- and CD46-independent mechanism. *J Virol.* Nov 2007;81(21):12091-12096.
80. Muhlebach MD, Mateo M, Sinn PL, Prufer S, Uhlig KM, Leonard VH, Navaratnarajah CK, Frenzke M, Wong XX, Sawatsky B, Ramachandran S, McCray PB, Cichutek K, von Messling V, Lopez M, Cattaneo R. Adherens junction protein nectin-4 is the epithelial receptor for measles virus. *Nature.* Nov 2 2011.
81. Noyce RS, Bondre DG, Ha MN, Lin LT, Sisson G, Tsao MS, Richardson CD. Tumor cell marker PVRL4 (nectin 4) is an epithelial cell receptor for measles virus. *PLoS Pathog.* Aug 2011;7(8):e1002240.
82. Tahara M, Takeda M, Shirogane Y, Hashiguchi T, Ohno S, Yanagi Y. Measles virus infects both polarized epithelial and immune cells by using distinctive receptor-binding sites on its hemagglutinin. *J Virol.* May 2008;82(9):4630-4637.
83. Ludlow M, Rennick LJ, Sarlang S, Skibinski G, McQuaid S, Moore T, de Swart RL, Duprex WP. Wild-type measles virus infection of primary epithelial cells occurs via the basolateral surface without syncytium formation or release of infectious virus. *J Gen Virol.* Apr 2010;91(Pt 4):971-979.
84. Lemon K, de Vries RD, Mesman AW, McQuaid S, van Amerongen G, Yüksel S, Ludlow M, Rennick LJ, Kuiken T, Rima BK, Geijtenbeek TB, Osterhaus AD, Duprex WP, de Swart RL. Early target cells of measles virus after aerosol infection of non-human primates. *PLoS Pathog.* 2011;7(1):e1001263.

85. Ferreira CS, Frenzke M, Leonard VH, Welstead GG, Richardson CD, Cattaneo R. Measles virus infection of alveolar macrophages and dendritic cells precedes spread to lymphatic organs in transgenic mice expressing human signaling lymphocytic activation molecule (SLAM, CD150). *J Virol.* Mar 2010;84(6):3033-3042.
86. de Witte L, Abt M, Schneider-Schaulies S, van Kooyk Y, Geijtenbeek TB. Measles virus targets DC-SIGN to enhance dendritic cell infection. *J Virol.* Apr 2006;80(7):3477-3486.
87. de Witte L, de Vries RD, van der Vlist M, Yüksel S, Litjens M, de Swart RL, Geijtenbeek TB. DC-SIGN and CD150 have distinct roles in transmission of measles virus from dendritic cells to T-lymphocytes. *PLoS Pathog.* Apr 2008;4(4):e1000049.
88. Avota E, Gulbins E, Schneider-Schaulies S. DC-SIGN mediated sphingomyelinase-activation and ceramide generation is essential for enhancement of viral uptake in dendritic cells. *PLoS Pathog.* Feb 2011;7(2):e1001290.
89. Racaniello V. Virology. An exit strategy for measles virus. *Science.* Dec 2011;334(6063):1650-1651.
90. Esolen LM, Takahashi K, Johnson RT, Vaisberg A, Moench TR, Wesselingh SL, Griffin DE. Brain endothelial cell infection in children with acute fatal measles. *J Clin Invest.* Nov 1995;96(5):2478-2481.
91. Dittmar S, Harms H, Runkler N, Maisner A, Kim KS, Schneider-Schaulies J. Measles virus-induced block of transendothelial migration of T lymphocytes and infection-mediated virus spread across endothelial cell barriers. *J Virol.* Nov 2008;82(22):11273-11282.
92. McQuaid S, Cosby SL. An immunohistochemical study of the distribution of the measles virus receptors, CD46 and SLAM, in normal human tissues and subacute sclerosing panencephalitis. *Lab Invest.* Apr 2002;82(4):403-409.
93. McQuaid S, Campbell S, Wallace IJ, Kirk J, Cosby SL. Measles virus infection and replication in undifferentiated and differentiated human neuronal cells in culture. *J Virol.* Jun 1998;72(6):5245-5250.
94. Makhortova NR, Askovich P, Patterson CE, Gechman LA, Gerard NP, Rall GF. Neurokinin-1 enables measles virus trans-synaptic spread in neurons. *Virology.* May 2007;362(1):235-244.
95. Allen IV, McQuaid S, McMahon J, Kirk J, McConnell R. The significance of measles virus antigen and genome distribution in the CNS in SSPE for mechanisms of viral spread and demyelination. *J Neuropathol Exp Neurol.* Apr 1996;55(4):471-480.
96. Haase AT, Swoveland P, Stowring L, Ventura P, Johnson KP, Norrby E, Gibbs CJ. Measles virus genome in infections of the central nervous system. *J Infect Dis.* Aug 1981;144(2):154-160.
97. Jensen S, Thomsen AR. Sensing of RNA viruses: a review of innate immune receptors involved in recognizing RNA virus invasion. *J Virol.* Mar 2012;86(6):2900-2910.
98. Kang DC, Gopalkrishnan RV, Lin L, Randolph A, Valerie K, Pestka S, Fisher PB. Expression analysis and genomic characterization of human melanoma differentiation associated gene-5, mda-5: a novel type I interferon-responsive apoptosis-inducing gene. *Oncogene.* Mar 2004;23(9):1789-1800.
99. Yoneyama M, Kikuchi M, Natsukawa T, Shinobu N, Imaizumi T, Miyagishi M, Taira K, Akira S, Fujita T. The RNA helicase RIG-I has an essential

function in double-stranded RNA-induced innate antiviral responses. *Nat Immunol.* Jul 2004;5(7):730-737.
100. Yoneyama M, Fujita T. RIG-I family RNA helicases: cytoplasmic sensor for antiviral innate immunity. *Cytokine Growth Factor Rev.* 2007 Oct-Dec 2007;18(5-6):545-551.
101. Kang DC, Gopalkrishnan RV, Wu Q, Jankowsky E, Pyle AM, Fisher PB. mda-5: An interferon-inducible putative RNA helicase with double-stranded RNA-dependent ATPase activity and melanoma growth-suppressive properties. *Proc Natl Acad Sci U S A.* Jan 2002;99(2):637-642.
102. Ikegame S, Takeda M, Ohno S, Nakatsu Y, Nakanishi Y, Yanagi Y. Both RIG-I and MDA5 RNA helicases contribute to the induction of alpha/beta interferon in measles virus-infected human cells. *J Virol.* Jan 2010;84(1):372-379.
103. Berghäll H, Sirén J, Sarkar D, Julkunen I, Fisher PB, Vainionpää R, Matikainen S. The interferon-inducible RNA helicase, mda-5, is involved in measles virus-induced expression of antiviral cytokines. *Microbes Infect.* Jul 2006;8(8):2138-2144.
104. Kato H, Takeuchi O, Sato S, Yoneyama M, Yamamoto M, Matsui K, Uematsu S, Jung A, Kawai T, Ishii KJ, Yamaguchi O, Otsu K, Tsujimura T, Koh CS, Reis e Sousa C, Matsuura Y, Fujita T, Akira S. Differential roles of MDA5 and RIG-I helicases in the recognition of RNA viruses. *Nature.* May 2006;441(7089):101-105.
105. Kawai T, Takahashi K, Sato S, Coban C, Kumar H, Kato H, Ishii KJ, Takeuchi O, Akira S. IPS-1, an adaptor triggering RIG-I- and Mda5-mediated type I interferon induction. *Nat Immunol.* Oct 2005;6(10):981-988.
106. Plumet S, Herschke F, Bourhis JM, Valentin H, Longhi S, Gerlier D. Cytosolic 5'-triphosphate ended viral leader transcript of measles virus as activator of the RIG I-mediated interferon response. *PLoS One.* 2007;2(3):e279.
107. Kumar H, Kawai T, Kato H, Sato S, Takahashi K, Coban C, Yamamoto M, Uematsu S, Ishii KJ, Takeuchi O, Akira S. Essential role of IPS-1 in innate immune responses against RNA viruses. *J Exp Med.* Jul 2006;203(7):1795-1803.
108. Arnoult D, Carneiro L, Tattoli I, Girardin SE. The role of mitochondria in cellular defense against microbial infection. *Semin Immunol.* Aug 2009;21(4):223-232.
109. Rothenfusser S, Goutagny N, DiPerna G, Gong M, Monks BG, Schoenemeyer A, Yamamoto M, Akira S, Fitzgerald KA. The RNA helicase Lgp2 inhibits TLR-independent sensing of viral replication by retinoic acid-inducible gene-I. *J Immunol.* Oct 2005;175(8):5260-5268.
110. Bieback K, Lien E, Klagge IM, Avota E, Schneider-Schaulies J, Duprex WP, Wagner H, Kirschning CJ, Ter Meulen V, Schneider-Schaulies S. Hemagglutinin protein of wild-type measles virus activates toll-like receptor 2 signaling. *J Virol.* Sep 2002;76(17):8729-8736.
111. Wang JP, Kurt-Jones EA, Shin OS, Manchak MD, Levin MJ, Finberg RW. Varicella-zoster virus activates inflammatory cytokines in human monocytes and macrophages via Toll-like receptor 2. *J Virol.* Oct 2005;79(20):12658-12666.

112. Barbalat R, Lau L, Locksley RM, Barton GM. Toll-like receptor 2 on inflammatory monocytes induces type I interferon in response to viral but not bacterial ligands. *Nat Immunol.* Nov 2009;10(11):1200-1207.
113. Diebold SS, Kaisho T, Hemmi H, Akira S, Reis e Sousa C. Innate antiviral responses by means of TLR7-mediated recognition of single-stranded RNA. *Science.* Mar 2004;303(5663):1529-1531.
114. Heil F, Hemmi H, Hochrein H, Ampenberger F, Kirschning C, Akira S, Lipford G, Wagner H, Bauer S. Species-specific recognition of single-stranded RNA via toll-like receptor 7 and 8. *Science.* Mar 2004;303(5663):1526-1529.
115. PETRALLI JK, MERIGAN TC, WILBUR JR. CIRCULATING INTERFERON AFTER MEASLES VACCINATION. *N Engl J Med.* Jul 1965;273:198-201.
116. Stark GR, Kerr IM, Williams BR, Silverman RH, Schreiber RD. How cells respond to interferons. *Annu Rev Biochem.* 1998;67:227-264.
117. Horvath CM, Darnell JE. The antiviral state induced by alpha interferon and gamma interferon requires transcriptionally active Stat1 protein. *J Virol.* Jan 1996;70(1):647-650.
118. Pfaller CK, Li Z, George CX, Samuel CE. Protein kinase PKR and RNA adenosine deaminase ADAR1: new roles for old players as modulators of the interferon response. *Curr Opin Immunol.* Oct 2011;23(5):573-582.
119. Samuel CE. Adenosine deaminases acting on RNA (ADARs) are both antiviral and proviral. *Virology.* Mar 2011;411(2):180-193.
120. Qureshi SA, Salditt-Georgieff M, Darnell JE. Tyrosine-phosphorylated Stat1 and Stat2 plus a 48-kDa protein all contact DNA in forming interferon-stimulated-gene factor 3. *Proc Natl Acad Sci U S A.* Apr 1995;92(9):3829-3833.
121. Haller O, Kochs G. Human MxA protein: an interferon-induced dynamin-like GTPase with broad antiviral activity. *J Interferon Cytokine Res.* Jan 2011;31(1):79-87.
122. Honda K, Taniguchi T. IRFs: master regulators of signalling by Toll-like receptors and cytosolic pattern-recognition receptors. *Nat Rev Immunol.* Sep 2006;6(9):644-658.
123. Griffin DE, Ward BJ, Jauregui E, Johnson RT, Vaisberg A. Immune activation in measles. *N Engl J Med.* Jun 1989;320(25):1667-1672.
124. El Mubarak HS, Ibrahim SA, Vos HW, Mukhtar MM, Mustafa OA, Wild TF, Osterhaus AD, de Swart RL. Measles virus protein-specific IgM, IgA, and IgG subclass responses during the acute and convalescent phase of infection. *J Med Virol.* Feb 2004;72(2):290-298.
125. Dhib-Jalbut SS, Cowan EP. Direct evidence that interferon-beta mediates enhanced HLA-class I expression in measles virus-infected cells. *J Immunol.* Dec 1993;151(11):6248-6258.
126. van Binnendijk RS, Poelen MC, Kuijpers KC, Osterhaus AD, Uytdehaag FG. The predominance of CD8+ T cells after infection with measles virus suggests a role for CD8+ class I MHC-restricted cytotoxic T lymphocytes (CTL) in recovery from measles. Clonal analyses of human CD8+ class I MHC-restricted CTL. *J Immunol.* Mar 1990;144(6):2394-2399.
127. Norrby E, Orvell C, Vandvik B, Cherry JD. Antibodies against measles virus polypeptides in different disease conditions. *Infect Immun.* Dec 1981;34(3):718-724.

128. Bouche FB, Ertl OT, Muller CP. Neutralizing B cell response in measles. *Viral Immunol.* 2002;15(3):451-471.
129. Childs K, Stock N, Ross C, Andrejeva J, Hilton L, Skinner M, Randall R, Goodbourn S. mda-5, but not RIG-I, is a common target for paramyxovirus V proteins. *Virology.* Mar 2007;359(1):190-200.
130. Childs KS, Andrejeva J, Randall RE, Goodbourn S. Mechanism of mda-5 Inhibition by paramyxovirus V proteins. *J Virol.* Feb 2009;83(3):1465-1473.
131. Childs K, Randall R, Goodbourn S. Paramyxovirus V proteins interact with the RNA Helicase LGP2 to inhibit RIG-I-dependent interferon induction. *J Virol.* Apr 2012;86(7):3411-3421.
132. Pfaller CK, Conzelmann KK. Measles virus V protein is a decoy substrate for IkappaB kinase alpha and prevents Toll-like receptor 7/9-mediated interferon induction. *J Virol.* Dec 2008;82(24):12365-12373.
133. Irie T, Kiyotani K, Igarashi T, Yoshida A, Sakaguchi T. Inhibition of interferon regulatory factor 3 activation by paramyxovirus V protein. *J Virol.* Jul 2012;86(13):7136-7145.
134. Sparrer KM, Pfaller CK, Conzelmann KK. Measles virus C protein interferes with Beta interferon transcription in the nucleus. *J Virol.* Jan 2012;86(2):796-805.
135. Schuhmann KM, Pfaller CK, Conzelmann KK. The measles virus V protein binds to p65 (RelA) to suppress NF-kappaB activity. *J Virol.* Apr 2011;85(7):3162-3171.
136. Palosaari H, Parisien JP, Rodriguez JJ, Ulane CM, Horvath CM. STAT protein interference and suppression of cytokine signal transduction by measles virus V protein. *J Virol.* Jul 2003;77(13):7635-7644.
137. Takayama I, Sato H, Watanabe A, Omi-Furutani M, Sugai A, Kanki K, Yoneda M, Kai C. The nucleocapsid protein of measles virus blocks host interferon response. *Virology.* Mar 2012;424(1):45-55.
138. Devaux P, von Messling V, Songsungthong W, Springfeld C, Cattaneo R. Tyrosine 110 in the measles virus phosphoprotein is required to block STAT1 phosphorylation. *Virology.* Mar 2007;360(1):72-83.
139. Yokota S, Okabayashi T, Yokosawa N, Fujii N. Measles virus P protein suppresses Toll-like receptor signal through up-regulation of ubiquitin-modifying enzyme A20. *FASEB J.* Jan 2008;22(1):74-83.
140. Cattaneo R, Billeter MA. Mutations and A/I hypermutations in measles virus persistent infections. *Curr Top Microbiol Immunol.* 1992;176:63-74.
141. Li Z, Okonski KM, Samuel CE. Adenosine deaminase acting on RNA 1 (ADAR1) suppresses the induction of interferon by measles virus. *J Virol.* Apr 2012;86(7):3787-3794.
142. Nakatsu Y, Takeda M, Ohno S, Shirogane Y, Iwasaki M, Yanagi Y. Measles virus circumvents the host interferon response by different actions of the C and V proteins. *J Virol.* Sep 2008;82(17):8296-8306.
143. Seya T. Addendum to "Strain-to-strain difference of V protein of measles virus affects MDA5-mediated IFN-β-inducing potential" [Mol. Immunol. 48(4) (2011) 497-504]. *Mol Immunol.* Jul 2011;48(12-13):1589-1590.
144. Takaki H, Watanabe Y, Shingai M, Oshiumi H, Matsumoto M, Seya T. Strain-to-strain difference of V protein of measles virus affects MDA5-mediated IFN-β-inducing potential. *Mol Immunol.* Jan 2011;48(4):497-504.
145. Shingai M, Ebihara T, Begum NA, Kato A, Honma T, Matsumoto K, Saito H, Ogura H, Matsumoto M, Seya T. Differential type I IFN-inducing abilities of

wild-type versus vaccine strains of measles virus. *J Immunol.* Nov 2007;179(9):6123-6133.
146. Griffin DE. *Measles Virus.* Philadelphia: Lippincott Williams & Wilkins; 2007.
147. Peng KW, Ahmann GJ, Pham L, Greipp PR, Cattaneo R, Russell SJ. Systemic therapy of myeloma xenografts by an attenuated measles virus. *Blood.* Oct 1 2001;98(7):2002-2007.
148. Afzal MA, Minor PD, Schild GC. Clinical safety issues of measles, mumps and rubella vaccines. *Bull World Health Organ.* 2000;78(2):199-204.
149. Rima BK, Earle JA, Baczko K, ter Meulen V, Liebert UG, Carstens C, Carabana J, Caballero M, Celma ML, Fernandez-Munoz R. Sequence divergence of measles virus haemagglutinin during natural evolution and adaptation to cell culture. *J Gen Virol.* Jan 1997;78 (Pt 1):97-106.
150. Radecke F, Spielhofer P, Schneider H, Kaelin K, Huber M, Dotsch C, Christiansen G, Billeter MA. Rescue of measles viruses from cloned DNA. *EMBO J.* Dec 1 1995;14(23):5773-5784.
151. Ungerechts G, Springfeld C, Frenzke ME, Lampe J, Parker WB, Sorscher EJ, Cattaneo R. An immunocompetent murine model for oncolysis with an armed and targeted measles virus. *Mol Ther.* Nov 2007;15(11):1991-1997.
152. Grote D, Cattaneo R, Fielding AK. Neutrophils contribute to the measles virus-induced antitumor effect: enhancement by granulocyte macrophage colony-stimulating factor expression. *Cancer Res.* Oct 1 2003;63(19):6463-6468.
153. Springfeld C, von Messling V, Frenzke M, Ungerechts G, Buchholz CJ, Cattaneo R. Oncolytic efficacy and enhanced safety of measles virus activated by tumor-secreted matrix metalloproteinases. *Cancer Res.* Aug 1 2006;66(15):7694-7700.
154. Peng KW, Facteau S, Wegman T, O'Kane D, Russell SJ. Non-invasive in vivo monitoring of trackable viruses expressing soluble marker peptides. *Nat Med.* May 2002;8(5):527-531.
155. Schneider U, Bullough F, Vongpunsawad S, Russell SJ, Cattaneo R. Recombinant measles viruses efficiently entering cells through targeted receptors. *J Virol.* Nov 2000;74(21):9928-9936.
156. Hammond AL, Plemper RK, Zhang J, Schneider U, Russell SJ, Cattaneo R. Single-chain antibody displayed on a recombinant measles virus confers entry through the tumor-associated carcinoembryonic antigen. *J Virol.* Mar 2001;75(5):2087-2096.
157. Bucheit AD, Kumar S, Grote DM, Lin Y, von Messling V, Cattaneo RB, Fielding AK. An oncolytic measles virus engineered to enter cells through the CD20 antigen. *Mol Ther.* Jan 2003;7(1):62-72.
158. Peng KW, Donovan KA, Schneider U, Cattaneo R, Lust JA, Russell SJ. Oncolytic measles viruses displaying a single-chain antibody against CD38, a myeloma cell marker. *Blood.* Apr 1 2003;101(7):2557-2562.
159. Hallak LK, Merchan JR, Storgard CM, Loftus JC, Russell SJ. Targeted measles virus vector displaying echistatin infects endothelial cells via alpha(v)beta3 and leads to tumor regression. *Cancer Res.* Jun 15 2005;65(12):5292-5300.
160. Peng KW, Holler PD, Orr BA, Kranz DM, Russell SJ. Targeting virus entry and membrane fusion through specific peptide/MHC complexes using a high-affinity T-cell receptor. *Gene Ther.* Aug 2004;11(15):1234-1239.

161. Vongpunsawad S, Oezgun N, Braun W, Cattaneo R. Selectively receptor-blind measles viruses: Identification of residues necessary for SLAM- or CD46-induced fusion and their localization on a new hemagglutinin structural model. *J Virol.* Jan 2004;78(1):302-313.
162. Hadac EM, Peng KW, Nakamura T, Russell SJ. Reengineering paramyxovirus tropism. *Virology.* Nov 24 2004;329(2):217-225.
163. Parato KA, Senger D, Forsyth PA, Bell JC. Recent progress in the battle between oncolytic viruses and tumours. *Nat Rev Cancer.* Dec 2005;5(12):965-976.
164. Zhang SC, Wang WL, Cai WS, Jiang KL, Yuan ZW. Engineered measles virus Edmonston strain used as a novel oncolytic viral system against human hepatoblastoma. *BMC Cancer.* 2012;12:427.
165. Zhang SC, Cai WS, Zhang Y, Jiang KL, Zhang KR, Wang WL. Engineered measles virus Edmonston strain used as a novel oncolytic viral system against human neuroblastoma through a CD46 and nectin 4-independent pathway. *Cancer Lett.* Dec 2012;325(2):227-237.
166. Ong HT, Timm MM, Greipp PR, Witzig TE, Dispenzieri A, Russell SJ, Peng KW. Oncolytic measles virus targets high CD46 expression on multiple myeloma cells. *Exp Hematol.* Jun 2006;34(6):713-720.
167. Anderson BD, Nakamura T, Russell SJ, Peng KW. High CD46 receptor density determines preferential killing of tumor cells by oncolytic measles virus. *Cancer Res.* Jul 15 2004;64(14):4919-4926.
168. Berchtold S, Lampe J, Weiland T, Smirnow I, Schleicher S, Handgretinger R, Kopp HG, Reiser J, Stubenrauch F, Mayer N, Malek NP, Bitzer M, Lauer UM. Innate immune defense defines susceptibility of sarcoma cells to measles vaccine virus-based oncolysis. *J Virol.* Mar 2013;87(6):3484-3501.
169. Norman KL, Hirasawa K, Yang AD, Shields MA, Lee PW. Reovirus oncolysis: the Ras/RalGEF/p38 pathway dictates host cell permissiveness to reovirus infection. *Proc Natl Acad Sci U S A.* Jul 27 2004;101(30):11099-11104.
170. Farassati F, Yang AD, Lee PW. Oncogenes in Ras signalling pathway dictate host-cell permissiveness to herpes simplex virus 1. *Nat Cell Biol.* Aug 2001;3(8):745-750.
171. Duursma AM, Agami R. Ras interference as cancer therapy. *Semin Cancer Biol.* Aug 2003;13(4):267-273.
172. Wang G, Barrett JW, Stanford M, Werden SJ, Johnston JB, Gao X, Sun M, Cheng JQ, McFadden G. Infection of human cancer cells with myxoma virus requires Akt activation via interaction with a viral ankyrin-repeat host range factor. *Proc Natl Acad Sci U S A.* Mar 21 2006;103(12):4640-4645.
173. Kim M, Williamson CT, Prudhomme J, Bebb DG, Riabowol K, Lee PW, Lees-Miller SP, Mori Y, Rahman MM, McFadden G, Johnston RN. The viral tropism of two distinct oncolytic viruses, reovirus and myxoma virus, is modulated by cellular tumor suppressor gene status. *Oncogene.* Jul 8 2010;29(27):3990-3996.
174. McCormick F. Future prospects for oncolytic therapy. *Oncogene.* Nov 21 2005;24(52):7817-7819.
175. Crompton AM, Kirn DH. From ONYX-015 to armed vaccinia viruses: the education and evolution of oncolytic virus development. *Curr Cancer Drug Targets.* Mar 2007;7(2):133-139.

176. Mrkic B, Pavlovic J, Rulicke T, Volpe P, Buchholz CJ, Hourcade D, Atkinson JP, Aguzzi A, Cattaneo R. Measles virus spread and pathogenesis in genetically modified mice. *J Virol.* Sep 1998;72(9):7420-7427.
177. Sellin CI, Horvat B. Current animal models: transgenic animal models for the study of measles pathogenesis. *Curr Top Microbiol Immunol.* 2009;330:111-127.
178. Liu YP, Tong C, Dispenzieri A, Federspiel MJ, Russell SJ, Peng KW. Polyinosinic acid decreases sequestration and improves systemic therapy of measles virus. *Cancer Gene Ther.* Mar 2012;19(3):202-211.
179. Breitbach CJ, Paterson JM, Lemay CG, Falls TJ, McGuire A, Parato KA, Stojdl DF, Daneshmand M, Speth K, Kirn D, McCart JA, Atkins H, Bell JC. Targeted inflammation during oncolytic virus therapy severely compromises tumor blood flow. *Mol Ther.* Sep 2007;15(9):1686-1693.
180. von Reyn CF, Clements CJ, Mann JM. Human immunodeficiency virus infection and routine childhood immunisation. *Lancet.* Sep 1987;2(8560):669-672.
181. Wu VH, McFarland H, Mayo K, Hanger L, Griffin DE, Dhib-Jalbut S. Measles virus-specific cellular immunity in patients with vaccine failure. *J Clin Microbiol.* Jan 1993;31(1):118-122.
182. Liu C, Russell SJ, Peng KW. Systemic therapy of disseminated myeloma in passively immunized mice using measles virus-infected cell carriers. *Mol Ther.* Jun 2010;18(6):1155-1164.
183. Mader EK, Maeyama Y, Lin Y, Butler GW, Russell HM, Galanis E, Russell SJ, Dietz AB, Peng KW. Mesenchymal stem cell carriers protect oncolytic measles viruses from antibody neutralization in an orthotopic ovarian cancer therapy model. *Clin Cancer Res.* Dec 1 2009;15(23):7246-7255.
184. Myers RM, Greiner SM, Harvey ME, Griesmann G, Kuffel MJ, Buhrow SA, Reid JM, Federspiel M, Ames MM, Dingli D, Schweikart K, Welch A, Dispenzieri A, Peng KW, Russell SJ. Preclinical pharmacology and toxicology of intravenous MV-NIS, an oncolytic measles virus administered with or without cyclophosphamide. *Clin Pharmacol Ther.* Dec 2007;82(6):700-710.
185. Peng KW, Myers R, Greenslade A, Mader E, Greiner S, Federspiel MJ, Dispenzieri A, Russell SJ. Using clinically approved cyclophosphamide regimens to control the humoral immune response to oncolytic viruses. *Gene Ther.* Mar 2013;20(3):255-261.
186. Miest TS, Yaiw KC, Frenzke M, Lampe J, Hudacek AW, Springfeld C, von Messling V, Ungerechts G, Cattaneo R. Envelope-chimeric entry-targeted measles virus escapes neutralization and achieves oncolysis. *Mol Ther.* Oct 2011;19(10):1813-1820.
187. Power AT, Bell JC. Cell-based delivery of oncolytic viruses: a new strategic alliance for a biological strike against cancer. *Mol Ther.* Apr 2007;15(4):660-665.
188. Ong HT, Hasegawa K, Dietz AB, Russell SJ, Peng KW. Evaluation of T cells as carriers for systemic measles virotherapy in the presence of antiviral antibodies. *Gene Ther.* Feb 2007;14(4):324-333.
189. Iankov ID, Blechacz B, Liu C, Schmeckpeper JD, Tarara JE, Federspiel MJ, Caplice N, Russell SJ. Infected cell carriers: a new strategy for systemic delivery of oncolytic measles viruses in cancer virotherapy. *Mol Ther.* Jan 2007;15(1):114-122.

190. Peng KW, Dogan A, Vrana J, Liu C, Ong HT, Kumar S, Dispenzieri A, Dietz AB, Russell SJ. Tumor-associated macrophages infiltrate plasmacytomas and can serve as cell carriers for oncolytic measles virotherapy of disseminated myeloma. *Am J Hematol.* Jul 2009;84(7):401-407.
191. Iwamoto S, Mihara K, Downing JR, Pui CH, Campana D. Mesenchymal cells regulate the response of acute lymphoblastic leukemia cells to asparaginase. *J Clin Invest.* Apr 2007;117(4):1049-1057.
192. Mosna F, Sensebé L, Krampera M. Human bone marrow and adipose tissue mesenchymal stem cells: a user's guide. *Stem Cells Dev.* Oct 2010;19(10):1449-1470.
193. Huang GT, Gronthos S, Shi S. Mesenchymal stem cells derived from dental tissues vs. those from other sources: their biology and role in regenerative medicine. *J Dent Res.* Sep 2009;88(9):792-806.
194. Bieback K, Klüter H. Mesenchymal stromal cells from umbilical cord blood. *Curr Stem Cell Res Ther.* Dec 2007;2(4):310-323.
195. Sivasubramaniyan K, Lehnen D, Ghazanfari R, Sobiesiak M, Harichandan A, Mortha E, Petkova N, Grimm S, Cerabona F, de Zwart P, Abele H, Aicher WK, Faul C, Kanz L, Bühring HJ. Phenotypic and functional heterogeneity of human bone marrow- and amnion-derived MSC subsets. *Ann N Y Acad Sci.* Aug 2012;1266:94-106.
196. Le Blanc K, Frassoni F, Ball L, Locatelli F, Roelofs H, Lewis I, Lanino E, Sundberg B, Bernardo ME, Remberger M, Dini G, Egeler RM, Bacigalupo A, Fibbe W, Ringden O. Mesenchymal stem cells for treatment of steroid-resistant, severe, acute graft-versus-host disease: a phase II study. *Lancet.* May 10 2008;371(9624):1579-1586.
197. Ringden O, Uzunel M, Rasmusson I, Remberger M, Sundberg B, Lonnies H, Marschall HU, Dlugosz A, Szakos A, Hassan Z, Omazic B, Aschan J, Barkholt L, Le Blanc K. Mesenchymal stem cells for treatment of therapy-resistant graft-versus-host disease. *Transplantation.* May 27 2006;81(10):1390-1397.
198. Prasad VK, Lucas KG, Kleiner GI, Talano JA, Jacobsohn D, Broadwater G, Monroy R, Kurtzberg J. Efficacy and safety of ex vivo cultured adult human mesenchymal stem cells (Prochymal) in pediatric patients with severe refractory acute graft-versus-host disease in a compassionate use study. *Biol Blood Marrow Transplant.* Apr 2011;17(4):534-541.
199. Perez-Simon JA, Lopez-Villar O, Andreu EJ, Rifon J, Muntion S, Campelo MD, Sanchez-Guijo FM, Martinez C, Valcarcel D, Canizo CD. Mesenchymal stem cells expanded in vitro with human serum for the treatment of acute and chronic graft-versus-host disease: results of a phase I/II clinical trial. *Haematologica.* Jul 2011;96(7):1072-1076.
200. Kebriaei P, Isola L, Bahceci E, Holland K, Rowley S, McGuirk J, Devetten M, Jansen J, Herzig R, Schuster M, Monroy R, Uberti J. Adult human mesenchymal stem cells added to corticosteroid therapy for the treatment of acute graft-versus-host disease. *Biol Blood Marrow Transplant.* Jul 2009;15(7):804-811.
201. Ruster B, Gottig S, Ludwig RJ, Bistrian R, Muller S, Seifried E, Gille J, Henschler R. Mesenchymal stem cells display coordinated rolling and adhesion behavior on endothelial cells. *Blood.* Dec 1 2006;108(12):3938-3944.

202. Abbott JD, Huang Y, Liu D, Hickey R, Krause DS, Giordano FJ. Stromal cell-derived factor-1alpha plays a critical role in stem cell recruitment to the heart after myocardial infarction but is not sufficient to induce homing in the absence of injury. *Circulation.* Nov 23 2004;110(21):3300-3305.
203. Barbash IM, Chouraqui P, Baron J, Feinberg MS, Etzion S, Tessone A, Miller L, Guetta E, Zipori D, Kedes LH, Kloner RA, Leor J. Systemic delivery of bone marrow-derived mesenchymal stem cells to the infarcted myocardium: feasibility, cell migration, and body distribution. *Circulation.* Aug 19 2003;108(7):863-868.
204. Ortiz LA, Gambelli F, McBride C, Gaupp D, Baddoo M, Kaminski N, Phinney DG. Mesenchymal stem cell engraftment in lung is enhanced in response to bleomycin exposure and ameliorates its fibrotic effects. *Proc Natl Acad Sci U S A.* Jul 8 2003;100(14):8407-8411.
205. Chapel A, Bertho JM, Bensidhoum M, Fouillard L, Young RG, Frick J, Demarquay C, Cuvelier F, Mathieu E, Trompier F, Dudoignon N, Germain C, Mazurier C, Aigueperse J, Borneman J, Gorin NC, Gourmelon P, Thierry D. Mesenchymal stem cells home to injured tissues when co-infused with hematopoietic cells to treat a radiation-induced multi-organ failure syndrome. *J Gene Med.* Dec 2003;5(12):1028-1038.
206. Devine SM, Cobbs C, Jennings M, Bartholomew A, Hoffman R. Mesenchymal stem cells distribute to a wide range of tissues following systemic infusion into nonhuman primates. *Blood.* Apr 15 2003;101(8):2999-3001.
207. Bensidhoum M, Chapel A, Francois S, Demarquay C, Mazurier C, Fouillard L, Bouchet S, Bertho JM, Gourmelon P, Aigueperse J, Charbord P, Gorin NC, Thierry D, Lopez M. Homing of in vitro expanded Stro-1- or Stro-1+ human mesenchymal stem cells into the NOD/SCID mouse and their role in supporting human CD34 cell engraftment. *Blood.* May 1 2004;103(9):3313-3319.
208. Fox JM, Chamberlain G, Ashton BA, Middleton J. Recent advances into the understanding of mesenchymal stem cell trafficking. *Br J Haematol.* Jun 2007;137(6):491-502.
209. Komarova S, Kawakami Y, Stoff-Khalili MA, Curiel DT, Pereboeva L. Mesenchymal progenitor cells as cellular vehicles for delivery of oncolytic adenoviruses. *Mol Cancer Ther.* Mar 2006;5(3):755-766.
210. Ong HT, Federspiel MJ, Guo CM, Ooi LL, Russell SJ, Peng KW, Hui KM. Systemically delivered measles virus-infected mesenchymal stem cells can evade host immunity to inhibit liver cancer growth. *J Hepatol.* Nov 2013;59(5):999-1006.
211. Mader EK, Butler G, Dowdy SC, Mariani A, Knutson KL, Federspiel MJ, Russell SJ, Galanis E, Dietz AB, Peng KW. Optimizing patient derived mesenchymal stem cells as virus carriers for a phase I clinical trial in ovarian cancer. *J Transl Med.* 2013;11:20.
212. Larson RA, Dodge RK, Burns CP, Lee EJ, Stone RM, Schulman P, Duggan D, Davey FR, Sobol RE, Frankel SR, et al. A five-drug remission induction regimen with intensive consolidation for adults with acute lymphoblastic leukemia: cancer and leukemia group B study 8811. *Blood.* Apr 15 1995;85(8):2025-2037.
213. Annino L, Vegna ML, Camera A, Specchia G, Visani G, Fioritoni G, Ferrara F, Peta A, Ciolli S, Deplano W, Fabbiano F, Sica S, Di Raimondo F,

Cascavilla N, Tabilio A, Leoni P, Invernizzi R, Baccarani M, Rotoli B, Amadori S, Mandelli F, Group G. Treatment of adult acute lymphoblastic leukemia (ALL): long-term follow-up of the GIMEMA ALL 0288 randomized study. *Blood.* Feb 1 2002;99(3):863-871.

214. Hunault M, Harousseau JL, Delain M, Truchan-Graczyk M, Cahn JY, Witz F, Lamy T, Pignon B, Jouet JP, Garidi R, Caillot D, Berthou C, Guyotat D, Sadoun A, Sotto JJ, Lioure B, Casassus P, Solal-Celigny P, Stalnikiewicz L, Audhuy B, Blanchet O, Baranger L, Bene MC, Ifrah N, Group G. Better outcome of adult acute lymphoblastic leukemia after early genoidentical allogeneic bone marrow transplantation (BMT) than after late high-dose therapy and autologous BMT: a GOELAMS trial. *Blood.* Nov 15 2004;104(10):3028-3037.
215. Kantarjian H, Thomas D, O'Brien S, Cortes J, Giles F, Jeha S, Bueso-Ramos CE, Pierce S, Shan J, Koller C, Beran M, Keating M, Freireich EJ. Long-term follow-up results of hyperfractionated cyclophosphamide, vincristine, doxorubicin, and dexamethasone (Hyper-CVAD), a dose-intensive regimen, in adult acute lymphocytic leukemia. *Cancer.* Dec 15 2004;101(12):2788-2801.
216. Takeuchi J, Kyo T, Naito K, Sao H, Takahashi M, Miyawaki S, Kuriyama K, Ohtake S, Yagasaki F, Murakami H, Asou N, Ino T, Okamoto T, Usui N, Nishimura M, Shinagawa K, Fukushima T, Taguchi H, Morii T, Mizuta S, Akiyama H, Nakamura Y, Ohshima T, Ohno R. Induction therapy by frequent administration of doxorubicin with four other drugs, followed by intensive consolidation and maintenance therapy for adult acute lymphoblastic leukemia: the JALSG-ALL93 study. *Leukemia.* Jul 2002;16(7):1259-1266.
217. Thomas X, Boiron JM, Huguet F, Dombret H, Bradstock K, Vey N, Kovacsovics T, Delannoy A, Fegueux N, Fenaux P, Stamatoullas A, Vernant JP, Tournilhac O, Buzyn A, Reman O, Charrin C, Boucheix C, Gabert J, Lheritier V, Fiere D. Outcome of treatment in adults with acute lymphoblastic leukemia: analysis of the LALA-94 trial. *J Clin Oncol.* Oct 15 2004;22(20):4075-4086.
218. Linker C, Damon L, Ries C, Navarro W. Intensified and shortened cyclical chemotherapy for adult acute lymphoblastic leukemia. *J Clin Oncol.* May 15 2002;20(10):2464-2471.
219. Gokbuget N, Hoelzer D, Arnold R, Bohme A, Bartram CR, Freund M, Ganser A, Kneba M, Langer W, Lipp T, Ludwig WD, Maschmeyer G, Rieder H, Thiel E, Weiss A, Messerer D. Treatment of Adult ALL according to protocols of the German Multicenter Study Group for Adult ALL (GMALL). *Hematol Oncol Clin North Am.* Dec 2000;14(6):1307-1325, ix.
220. Pulte D, Gondos A, Brenner H. Improvement in survival in younger patients with acute lymphoblastic leukemia from the 1980s to the early 21st century. *Blood.* Feb 12 2009;113(7):1408-1411.
221. Fielding AK, Richards SM, Chopra R, Lazarus HM, Litzow MR, Buck G, Durrant IJ, Luger SM, Marks DI, Franklin IM, McMillan AK, Tallman MS, Rowe JM, Goldstone AH. Outcome of 609 adults after relapse of acute lymphoblastic leukemia (ALL); an MRC UKALL12/ECOG 2993 study. *Blood.* Feb 1 2007;109(3):944-950.
222. Topp MS, Kufer P, Gokbuget N, Goebeler M, Klinger M, Neumann S, Horst HA, Raff T, Viardot A, Schmid M, Stelljes M, Schaich M, Degenhard E, Kohne-Volland R, Bruggemann M, Ottmann O, Pfeifer H, Burmeister T, Nagorsen D, Schmidt M, Lutterbuese R, Reinhardt C, Baeuerle PA, Kneba M,

Einsele H, Riethmuller G, Hoelzer D, Zugmaier G, Bargou RC. Targeted therapy with the T-cell-engaging antibody blinatumomab of chemotherapy-refractory minimal residual disease in B-lineage acute lymphoblastic leukemia patients results in high response rate and prolonged leukemia-free survival. *Journal of clinical oncology : official journal of the American Society of Clinical Oncology.* Jun 20 2011;29(18):2493-2498.

223. Funes JM, Quintero M, Henderson S, Martinez D, Qureshi U, Westwood C, Clements MO, Bourboulia D, Pedley RB, Moncada S, Boshoff C. Transformation of human mesenchymal stem cells increases their dependency on oxidative phosphorylation for energy production. *Proc Natl Acad Sci U S A.* Apr 10 2007;104(15):6223-6228.
224. Dominici M, Le Blanc K, Mueller I, Slaper-Cortenbach I, Marini F, Krause D, Deans R, Keating A, Prockop D, Horwitz E. Minimal criteria for defining multipotent mesenchymal stromal cells. The International Society for Cellular Therapy position statement. *Cytotherapy.* 2006;8(4):315-317.
225. Karber G. 50% end point calculation. Vol 162: Arch. Exp. Pathol. Pharmakol.; 1931:480-483.
226. Pfaffl MW. A new mathematical model for relative quantification in real-time RT-PCR. *Nucleic Acids Res.* May 2001;29(9):e45.
227. Reinhardt D, Houliara K, Pekrun A, Lakomek M, Krone B. Impact of conventional chemotherapy on levels of antibodies against vaccine-preventable diseases in children treated for cancer. *Scand J Infect Dis.* 2003;35(11-12):851-857.
228. Zignol M, Peracchi M, Tridello G, Pillon M, Fregonese F, D'Elia R, Zanesco L, Cesaro S. Assessment of humoral immunity to poliomyelitis, tetanus, hepatitis B, measles, rubella, and mumps in children after chemotherapy. *Cancer.* Aug 2004;101(3):635-641.
229. Volc SM, Almeida MT, Abadi MD, Cornacchioni AL, Odone Filho V, Cristofani LM. Measles and rubella antibody status in children after treatment for acute lymphoblastic leukemia. *J Pediatr (Rio J).* 2006 Nov-Dec 2006;82(6):481-484.
230. Nilsson A, De Milito A, Engström P, Nordin M, Narita M, Grillner L, Chiodi F, Björk O. Current chemotherapy protocols for childhood acute lymphoblastic leukemia induce loss of humoral immunity to viral vaccination antigens. *Pediatrics.* Jun 2002;109(6):e91.
231. Chou SH, Lin SZ, Day CH, Kuo WW, Shen CY, Hsieh DJ, Lin JY, Tsai FJ, Tsai CH, Huang CY. Mesenchymal stem cell insights: prospects in hematological transplantation. *Cell Transplant.* 2013;22(4):711-721.
232. Dittmar T, Entschladen F. *Migratory Properties of Mesenchymal Stem Cells.* Vol 129. Advances in Biochemical Engineering/Biotechnology: Springer Link; 2012.
233. Eliopoulos N, Stagg J, Lejeune L, Pommey S, Galipeau J. Allogeneic marrow stromal cells are immune rejected by MHC class I- and class II-mismatched recipient mice. *Blood.* Dec 2005;106(13):4057-4065.
234. Perin E, Dib N, DeMaria A, Marroquin O, Huang P, Traverse J. A phase II dose-escalation study of allogenic mesenchymal precursor cells in patients with ischemic and non-ischemic heart failure. Scientific Sessions of the American Heart Association.; 2011; Orlando, FL.

235. Funke S, Maisner A, Muhlebach MD, Koehl U, Grez M, Cattaneo R, Cichutek K, Buchholz CJ. Targeted cell entry of lentiviral vectors. *Mol Ther.* Aug 2008;16(8):1427-1436.
236. Schmid A, Spielhofer P, Cattaneo R, Baczko K, ter Meulen V, Billeter MA. Subacute sclerosing panencephalitis is typically characterized by alterations in the fusion protein cytoplasmic domain of the persisting measles virus. *Virology.* Jun 1992;188(2):910-915.
237. Fischer UM, Harting MT, Jimenez F, Monzon-Posadas WO, Xue H, Savitz SI, Laine GA, Cox CS, Jr. Pulmonary passage is a major obstacle for intravenous stem cell delivery: the pulmonary first-pass effect. *Stem Cells Dev.* Jun 2009;18(5):683-692.
238. Harting MT, Jimenez F, Xue H, Fischer UM, Baumgartner J, Dash PK, Cox CS. Intravenous mesenchymal stem cell therapy for traumatic brain injury. *J Neurosurg.* Jun 2009;110(6):1189-1197.
239. Kyriakou C, Rabin N, Pizzey A, Nathwani A, Yong K. Factors that influence short-term homing of human bone marrow-derived mesenchymal stem cells in a xenogeneic animal model. *Haematologica.* Oct 2008;93(10):1457-1465.
240. Lapidot T, Petit I. Current understanding of stem cell mobilization: the roles of chemokines, proteolytic enzymes, adhesion molecules, cytokines, and stromal cells. *Exp Hematol.* Sep 2002;30(9):973-981.
241. Song C, Li G. CXCR4 and matrix metalloproteinase-2 are involved in mesenchymal stromal cell homing and engraftment to tumors. *Cytotherapy.* May 2011;13(5):549-561.
242. Son BR, Marquez-Curtis LA, Kucia M, Wysoczynski M, Turner AR, Ratajczak J, Ratajczak MZ, Janowska-Wieczorek A. Migration of bone marrow and cord blood mesenchymal stem cells in vitro is regulated by stromal-derived factor-1-CXCR4 and hepatocyte growth factor-c-met axes and involves matrix metalloproteinases. *Stem Cells.* May 2006;24(5):1254-1264.
243. Wynn RF, Hart CA, Corradi-Perini C, O'Neill L, Evans CA, Wraith JE, Fairbairn LJ, Bellantuono I. A small proportion of mesenchymal stem cells strongly expresses functionally active CXCR4 receptor capable of promoting migration to bone marrow. *Blood.* Nov 2004;104(9):2643-2645.
244. Schioppa T, Uranchimeg B, Saccani A, Biswas SK, Doni A, Rapisarda A, Bernasconi S, Saccani S, Nebuloni M, Vago L, Mantovani A, Melillo G, Sica A. Regulation of the chemokine receptor CXCR4 by hypoxia. *J Exp Med.* Nov 3 2003;198(9):1391-1402.
245. Ponomaryov T, Peled A, Petit I, Taichman RS, Habler L, Sandbank J, Arenzana-Seisdedos F, Magerus A, Caruz A, Fujii N, Nagler A, Lahav M, Szyper-Kravitz M, Zipori D, Lapidot T. Induction of the chemokine stromal-derived factor-1 following DNA damage improves human stem cell function. *J Clin Invest.* Dec 2000;106(11):1331-1339.
246. Yamaguchi J, Kusano KF, Masuo O, Kawamoto A, Silver M, Murasawa S, Bosch-Marce M, Masuda H, Losordo DW, Isner JM, Asahara T. Stromal cell-derived factor-1 effects on ex vivo expanded endothelial progenitor cell recruitment for ischemic neovascularization. *Circulation.* Mar 11 2003;107(9):1322-1328.
247. Sordi V, Malosio ML, Marchesi F, Mercalli A, Melzi R, Giordano T, Belmonte N, Ferrari G, Leone BE, Bertuzzi F, Zerbini G, Allavena P, Bonifacio E, Piemonti L. Bone marrow mesenchymal stem cells express a

restricted set of functionally active chemokine receptors capable of promoting migration to pancreatic islets. *Blood.* Jul 15 2005;106(2):419-427.
248. Honczarenko M, Le Y, Swierkowski M, Ghiran I, Glodek AM, Silberstein LE. Human bone marrow stromal cells express a distinct set of biologically functional chemokine receptors. *Stem Cells.* Apr 2006;24(4):1030-1041.
249. Bobis-Wozowicz S, Miekus K, Wybieralska E, Jarocha D, Zawisz A, Madeja Z, Majka M. Genetically modified adipose tissue-derived mesenchymal stem cells overexpressing CXCR4 display increased motility, invasiveness, and homing to bone marrow of NOD/SCID mice. *Exp Hematol.* Jun 2011;39(6):686-696.e684.
250. Takeda M, Takeuchi K, Miyajima N, Kobune F, Ami Y, Nagata N, Suzaki Y, Nagai Y, Tashiro M. Recovery of pathogenic measles virus from cloned cDNA. *J Virol.* Jul 2000;74(14):6643-6647.
251. Peeters BP, Gruijthuijsen YK, de Leeuw OS, Gielkens AL. Genome replication of Newcastle disease virus: involvement of the rule-of-six. *Arch Virol.* 2000;145(9):1829-1845.
252. Dillmann F, Veldwijk MR, Laufs S, Sperandio M, Calandra G, Wenz F, Zeller J, Fruehauf S. Plerixafor inhibits chemotaxis toward SDF-1 and CXCR4-mediated stroma contact in a dose-dependent manner resulting in increased susceptibility of BCR-ABL+ cell to Imatinib and Nilotinib. *Leuk Lymphoma.* Oct 2009;50(10):1676-1686.
253. Kalatskaya I, Berchiche YA, Gravel S, Limberg BJ, Rosenbaum JS, Heveker N. AMD3100 is a CXCR7 ligand with allosteric agonist properties. *Mol Pharmacol.* May 2009;75(5):1240-1247.
254. Heckmann D, Laufs S, Maier P, Zucknick M, Giordano FA, Veldwijk MR, Eckstein V, Wenz F, Zeller WJ, Fruehauf S, Allgayer H. A Lentiviral CXCR4 overexpression and knockdown model in colorectal cancer cell lines reveals plerixafor-dependent suppression of SDF-1α-induced migration and invasion. *Onkologie.* 2011;34(10):502-508.
255. Gao J, Dennis JE, Muzic RF, Lundberg M, Caplan AI. The dynamic in vivo distribution of bone marrow-derived mesenchymal stem cells after infusion. *Cells Tissues Organs.* 2001;169(1):12-20.
256. Peled A, Tavor S. Role of CXCR4 in the pathogenesis of acute myeloid leukemia. *Theranostics.* 2013;3(1):34-39.
257. Mullighan CG, Zhang J, Harvey RC, Collins-Underwood JR, Schulman BA, Phillips LA, Tasian SK, Loh ML, Su X, Liu W, Devidas M, Atlas SR, Chen IM, Clifford RJ, Gerhard DS, Carroll WL, Reaman GH, Smith M, Downing JR, Hunger SP, Willman CL. JAK mutations in high-risk childhood acute lymphoblastic leukemia. *Proc Natl Acad Sci U S A.* Jun 2009;106(23):9414-9418.
258. van Eyndhoven WG, Gamper CJ, Cho E, Mackus WJ, Lederman S. TRAF-3 mRNA splice-deletion variants encode isoforms that induce NF-kappaB activation. *Mol Immunol.* Jul 1999;36(10):647-658.
259. Nagel I, Bug S, Tönnies H, Ammerpohl O, Richter J, Vater I, Callet-Bauchu E, Calasanz MJ, Martinez-Climent JA, Bastard C, Salido M, Schroers E, Martin-Subero JI, Gesk S, Harder L, Majid A, Dyer MJ, Siebert R. Biallelic inactivation of TRAF3 in a subset of B-cell lymphomas with interstitial del(14)(q24.1q32.33). *Leukemia.* Nov 2009;23(11):2153-2155.
260. Kurokawa C, Iankov I, Aderca I, Petel C, Middha S, Giannini C, Parney I, Galanis E. Pre-existing antiviral state can impact oncolytic infection in

glioblastoma patients treated with oncolytic measles virus. American Society of Gene and Cellular Therapy; 2014; Washington DC.
261. Zelent A, Greaves M, Enver T. Role of the TEL-AML1 fusion gene in the molecular pathogenesis of childhood acute lymphoblastic leukaemia. *Oncogene.* May 2004;23(24):4275-4283.
262. George AA, Franklin J, Kerkof K, Shah AJ, Price M, Tsark E, Bockstoce D, Yao D, Hart N, Carcich S, Parkman R, Crooks GM, Weinberg K. Detection of leukemic cells in the CD34(+)CD38(-) bone marrow progenitor population in children with acute lymphoblastic leukemia. *Blood.* Jun 2001;97(12):3925-3930.
263. Reya T, Morrison SJ, Clarke MF, Weissman IL. Stem cells, cancer, and cancer stem cells. *Nature.* Nov 2001;414(6859):105-111.
264. LOWRY OH, ROSEBROUGH NJ, FARR AL, RANDALL RJ. Protein measurement with the Folin phenol reagent. *J Biol Chem.* Nov 1951;193(1):265-275.
265. Wang F, Barrett JW, Ma Y, Dekaban GA, McFadden G. Induction of alpha/beta interferon by myxoma virus is selectively abrogated when primary mouse embryo fibroblasts become immortalized. *J Virol.* Jun 2009;83(11):5928-5932.
266. Phuong LK, Allen C, Peng KW, Giannini C, Greiner S, TenEyck CJ, Mishra PK, Macura SI, Russell SJ, Galanis EC. Use of a vaccine strain of measles virus genetically engineered to produce carcinoembryonic antigen as a novel therapeutic agent against glioblastoma multiforme. *Cancer Res.* May 2003;63(10):2462-2469.
267. Whilding LM, Archibald KM, Kulbe H, Balkwill FR, Öberg D, McNeish IA. Vaccinia virus induces programmed necrosis in ovarian cancer cells. *Mol Ther.* Nov 2013;21(11):2074-2086.
268. Xia M, Meng G, Jiang A, Chen A, Dahlhaus M, Gonzalez P, Beltinger C, Wei J. Mitophagy switches cell death from apoptosis to necrosis in NSCLC cells treated with oncolytic measles virus. *Oncotarget.* Jun 2014;5(11):3907-3918.
269. Xia M, Gonzalez P, Li C, Meng G, Jiang A, Wang H, Gao Q, Debatin KM, Beltinger C, Wei J. Mitophagy enhances oncolytic measles virus replication by mitigating DDX58/RIG-I-like receptor signaling. *J Virol.* May 2014;88(9):5152-5164.
270. Higuchi H, Bronk SF, Bateman A, Harrington K, Vile RG, Gores GJ. Viral fusogenic membrane glycoprotein expression causes syncytia formation with bioenergetic cell death: implications for gene therapy. *Cancer Res.* Nov 2000;60(22):6396-6402.
271. Reshi ML, Su YC, Hong JR. RNA Viruses: ROS-Mediated Cell Death. *Int J Cell Biol.* 2014;2014:467452.
272. Abdullah H, Brankin B, Brady C, Cosby SL. Wild-type measles virus infection upregulates poliovirus receptor-related 4 and causes apoptosis in brain endothelial cells by induction of tumor necrosis factor-related apoptosis-inducing ligand. *J Neuropathol Exp Neurol.* Jul 2013;72(7):681-696.
273. Goon P, Cohen B, Jin L, Watkins R, Tudor-Williams G. MMR vaccine in HIV-infected children -- potential hazards? *Vaccine.* Jul 2001;19(28-29):3816-3819.
274. Angel JB, Walpita P, Lerch RA, Sidhu MS, Masurekar M, DeLellis RA, Noble JT, Snydman DR, Udem SA. Vaccine-associated measles pneumonitis in an adult with AIDS. *Ann Intern Med.* Jul 1998;129(2):104-106.

275. Schoggins JW. Interferon-stimulated genes: roles in viral pathogenesis. *Curr Opin Virol.* Jun 2014;6C:40-46.
276. Schoggins JW, MacDuff DA, Imanaka N, Gainey MD, Shrestha B, Eitson JL, Mar KB, Richardson RB, Ratushny AV, Litvak V, Dabelic R, Manicassamy B, Aitchison JD, Aderem A, Elliott RM, García-Sastre A, Racaniello V, Snijder EJ, Yokoyama WM, Diamond MS, Virgin HW, Rice CM. Pan-viral specificity of IFN-induced genes reveals new roles for cGAS in innate immunity. *Nature.* Jan 2014;505(7485):691-695.
277. Heise C, Hermiston T, Johnson L, Brooks G, Sampson-Johannes A, Williams A, Hawkins L, Kirn D. An adenovirus E1A mutant that demonstrates potent and selective systemic anti-tumoral efficacy. *Nat Med.* Oct 2000;6(10):1134-1139.
278. Marcellus RC, Teodoro JG, Wu T, Brough DE, Ketner G, Shore GC, Branton PE. Adenovirus type 5 early region 4 is responsible for E1A-induced p53-independent apoptosis. *J Virol.* Sep 1996;70(9):6207-6215.
279. Lazar I, Yaacov B, Shiloach T, Eliahoo E, Kadouri L, Lotem M, Perlman R, Zakay-Rones Z, Panet A, Ben-Yehuda D. The oncolytic activity of Newcastle disease virus NDV-HUJ on chemoresistant primary melanoma cells is dependent on the proapoptotic activity of the inhibitor of apoptosis protein Livin. *J Virol.* Jan 2010;84(1):639-646.
280. Patterson JB, Manchester M, Oldstone MB. Disease model: dissecting the pathogenesis of the measles virus. *Trends Mol Med.* Feb 2001;7(2):85-88.

Appendix 1: Ethics approval and consent form

NHS
Health Research Authority

National Research Ethics Service

NRES Committee North West - Liverpool East
HRA NRES Centre Manchester
Barlow House
3rd Floor
4 Minshull Street
Manchester
M1 3DZ

Tel: 0161 625 7832
Fax: 0161 625 7299

03 June 2013

Dr Adele Fielding
Senior Lecturer
Royal Free & UCL Medical School
Rowland Hill Street
London
NW3 2PF

Dear Dr Fielding

Study title:	**Adult Acute Lymphoblastic Leukaemia (ALL): laboratory-only studies utilising discarded or ethically approved banked tissue for the characterisation of leukaemia initiating populations, and for the evaluation of virotherapeutics.**
REC reference:	**11/NW/0216**
IRAS project ID:	**62661**

Thank you for sending the progress report for the above study dated 22 May 2013. The report will be reviewed by the Chair of the Research Ethics Committee, and I will let you know if any further information is requested.

The favourable ethical opinion for the study continues to apply for the duration of the research as described in the application and protocol agreed by the REC, taking account of any substantial amendments.

Where research involves the use of human tissue in England, Wales or Northern Ireland, legal authority to hold the tissue under the terms of the ethical approval remains in place for the duration of the approved project.

11/NW/0216:	**Please quote this number on all correspondence**

A Research Ethics Committee established by the Health Research Authority

CONFIDENTIAL

Patient Information Sheet

Title: Bone Marrow Derived Mesenchymal Stem Cells As Cellular Carriers

Investigators:

Dr Adele Fielding

Consultant in Haematology

UCL Cancer Institute

0207 7940500 x 34970

REC reference: 11/NW/0216

Dear Patient,

You are being invited to take part in a research study. Before you decide, it is important that you understand why the research is being done and what it will involve. Please take time to read the following information carefully and discuss it with others if you wish. Ask your doctor if there is anything that is not clear or if you would like more information.

What is the purpose of the study?

The bone marrow contains cells that can multiply and grow to form many different types of tissue, including blood, bone, liver, brain and blood vessels. These 'multipurpose' cells are called stem cells. Different types of stem cells can

be used for different purposes according to their nature. For instance, blood stem cells can be used for stem cell transplantation to treat cancers such as leukaemia. Other stem cells found in the bone marrow can make different types of tissues in the body. We are interested in a particular type of stem cell – the mesenchymal stem cell – that can make tissues that help support the structure of the bone marrow, and can play a role in supporting bone marrow cell growth. The purpose of our research is to learn how to grow these stem cells in the laboratory, and to see if we can use them to deliver cancer-killing viruses to the bone marrow to treat leukaemia.

Why have I been chosen?

You have been chosen because you are donating blood stem cells for transplantation, by donating your bone marrow.

Do I have to take part?

No. It is up to you whether or not to take part. If you decide to take part you will be given this information sheet to keep and be asked to sign a consent form. If you decide to take part you are still free to withdraw at any time and without giving a reason. A decision to withdraw at any time, or a decision not to take part will not affect the standard of your medical care.

What does this study involve?

If you agree to take part in this study, when you have your bone marrow harvested, a very small proportion (1-4mls, which is a teaspoon) will be set aside for this research. You will not have to undergo any additional tests or procedures.

What are the risks of this study?

There are no risks involved, over and above those related to your bone marrow harvest.

What are the possible benefits of taking part?

There are no foreseeable direct benefits to you. However, the knowledge and information gained from this research may help us to develop new therapies for patients with leukaemia in the future.

Will it affect me?

It will not have any effect on you at all.

What information about me will be held?

All bone marrow stem cell samples used in this research are anonymised. That means that any information attached to the sample you donate for research will have your name, address, date of birth and all identifiable information removed so that you cannot be recognised from it.

Will any part of my stem cell sample be retained for future research?

The sample of bone marrow that you donate as a gift may be retained for future research. An ethics committee will review any new research.

Will I be informed of the results?

The results of this research will be published in the medical literature. You will not be identified in any way in these publications or at any stage of the research.

Withdrawal from the study.

Your participation in this study is entirely voluntary. You are free to decline to enter or to withdraw from the study at any time without having to give a reason. If you chose not to enter the study, this will in no way affect your future medical care. All information regarding your medical records will be treated as strictly confidential and will only be used for medical purposes.

Who has reviewed the study?

The Multi-Centre Research Ethics Committee for Scotland and the Ethics Committee in your local area has also reviewed the study from an ethics standpoint.

Contacts for further information.

If you require any further information regarding the study, we can be contacted at the address/telephone numbers at the top of this paper.

What do I have to do if I agree to take part?

Please read and sign the accompanying consent form that goes with this sheet.

Thank you for taking the time to read this information sheet.

PATIENT CONSENT FORM

Bone Marrow Derived Mesenchymal Stem Cells as Cellular Carriers

The patient should complete this sheet him/herself. (Please circle one)

1. I confirm that I have read and understood the information contained in the information sheet version 1 dated December 2006 for the above study. YES/NO

2. I have had the opportunity to ask questions and had satisfactory answers to them YES/NO

3. I understand that my participation is voluntary and that I am free to withdraw at any time without giving any reason and without my medical care or legal rights being affected. YES/NO

4. Do you give permission for your information to be collected, stored, and used for research in a database held at the Royal Free Laboratory? YES/NO

5. Do you give permission for your left-over samples to be stored and used for future ethically approved studies? YES/NO

6. I understand that some study documentation collected during the study may be looked at by responsible individuals from the sponsor (UCL) for the purpose of monitoring or auditing for good research practice. I give permission for these individuals to have access to this data. YES/NO

7. I agree to take part in the above study. YES/NO

PATIENT

Name (block letters) ……..

Signed ……Date ……

INVESTIGATOR TAKING CONSENT (please delete)

Name (block letters) ……

Signed ……Date ……

Appendix 2: Live cell confocal imaging

Supplementary Video (CD-ROM): MV-infected BM-MSC to ALL cell heterofusion. Representative live cell confocal video demonstrating heterofusion events between NALM-6 cell (red) and MV-NSe-GFP-infected BM-MSCs (green) over 60 minutes of co-culture.